MULTI-OBJECTIVE OPTIMUM OPERATION OF V2G IN DISTRIBUTION SYSTEM

SUWIMON TECHANOK

A Thesis Submitted in Partial Fulfillment of the Requirements for
the Degree of Master of Engineering in Electrical Engineering
Suranaree University of Technology
Academic Year 2024

การดำเนินงานที่เหมาะที่สุดแบบหลายวัตถุประสงค์ของยานยนต์สู่โครงข่ายในระบบจำหน่าย

นางสาวสุวิมล เตชะนอก

วิทยานิพนธ์นี้เป็นส่วนหนึ่งของการศึกษาตามหลักสูตรปริญญาวิศวกรรมศาสตรมหาบัณฑิต
สาขาวิชาวิศวกรรมไฟฟ้า
มหาวิทยาลัยเทคโนโลยีสุรนารี
ปีการศึกษา 2567

MULTI-OBJECTIVE OPTIMUM OPERATION OF V2G IN DISTRIBUTION SYSTEM

Suranaree University of Technology has approved this thesis submitted in partial fulfillment of the requirements for a Master's Degree.

Thesis Examining Committee

.....

(Asst. Prof. Dr. Piampoom Sarikprueck)

Chairperson

.....

(Assoc. Prof. Dr. Keerati Chayakulkheeree)

Member (Thesis Advisor)

.....

(Prof. Dr. Thanatchai Kulworawanichpong)

Member

Tosaphol Ratniyomchai

.....

(Asst. Prof. Dr. Tosaphol Ratniyomchai)

Member

.....

(Assoc. Prof. Dr. Yupaporn Ruksakulpiwat)

Vice Rector for Academic Affairs and Quality Assurance

.....

(Assoc. Prof. Dr. Pornsiri Jongkol)

Dean of Institute of Engineering

สุวิมล เตชะนอก : การดำเนินงานที่เหมาะที่สุดแบบหลายวัตถุประสงค์ของยานยนต์สู่โครงข่ายในระบบจำหน่าย (MULTI-OBJECTIVE OPTIMUM OPERATION OF V2G IN DISTRIBUTION SYSTEM)
อาจารย์ที่ปรึกษา : รองศาสตราจารย์ ดร. กีรติ ชยะกุลคีรี, 217 หน้า.

คำสำคัญ : การดำเนินงานที่เหมาะสมของระบบยานยนต์เชื่อมต่อกริด, การหาค่าเหมาะสมที่สุดที่มีหลายวัตถุประสงค์, ต้นทุนค่าไฟของระบบ, การสูญเสียพลังงานของระบบ, กำลังไฟฟ้าสูงสุดของระบบ, การจำลองมอนติคาร์โล

วิทยานิพนธ์นี้นำเสนอการดำเนินงานที่เหมาะที่สุดแบบหลายวัตถุประสงค์ของยานยนต์ไฟฟ้าทั้งรูปแบบการชาร์จทิศทางเดียว (vehicle-one-grid, V1G) และแบบสองทิศทาง (vehicle-to-grid, V2G) ในระบบจำหน่าย เพื่อลดผลกระทบเชิงลบที่เกิดขึ้นกับระบบอันเนื่องมาจากความต้องการชาร์จยานยนต์ไฟฟ้าที่เพิ่มขึ้น วิทยานิพนธ์นี้เสนอวิธีการหาค่าที่เหมาะสมที่สุดแบบฝูงอนุภาคหลายวัตถุประสงค์ (Multi-objective particle swarm optimization, MOPSO) ร่วมกับเทคนิคเรียงลำดับตามอุดมคติ (The technique for order of preference by similarity to ideal solution, TOPSIS) ในการหาวิธีการดำเนินงานที่เหมาะที่สุดแบบหลายวัตถุประสงค์ของยานยนต์ไฟฟ้าและเป็นวิธีการดำเนินการที่ประนีประนอมระหว่างวัตถุประสงค์ต่าง ๆ ได้อย่างมีประสิทธิภาพ โดยวิทยานิพนธ์นี้ได้พิจารณาแก้ปัญหาการดำเนินงานที่เหมาะที่สุดแบบหลายวัตถุประสงค์ของยานยนต์ไฟฟ้าในรูปแบบการชาร์จทิศทางเดียวและแบบสองทิศทาง 2 สถานการณ์ สถานการณแรกคือการแก้ปัญหาการดำเนินงานที่เหมาะที่สุดแบบหลายวัตถุประสงค์ของยานยนต์ไฟฟ้าที่มีวัตถุประสงค์เพื่อลดต้นทุนค่าไฟของระบบและการสูญเสียพลังงานของระบบพร้อมกัน และสถานการ์ที่สองคือการแก้ปัญหาการดำเนินงานที่เหมาะที่สุดแบบหลายวัตถุประสงค์ของยานยนต์ไฟฟ้าที่มีวัตถุประสงค์เพื่อลดต้นทุนค่าไฟของระบบและกำลังไฟฟ้าสูงสุดของระบบพร้อมกัน โดยทั้งหมดมีการดำเนินงานภายใต้โครงสร้างอัตราค่าไฟฟ้าตามช่วงเวลา (Time-of-Use, TOU) นอกจากนี้ความไม่แน่นอนของพฤติกรรมผู้ใช้ยานยนต์ไฟฟ้าจะถูกพิจารณาโดยการใช้แบบจำลองมอนติคาร์โล (Monte Carlo simulation, MCS) ในการสุ่มพฤติกรรมการชัรถเพื่อสร้างรูปแบบการชาร์จไฟจากระบบของผู้ใช้ยานต์ยนต์ไฟฟ้าที่สมจริงและสะท้อนสภาพการใช้งานจริง

จากผลการจำลองแสดงให้เห็นว่าวิธีการที่นำเสนอสามารถวิธีการที่นำเสนอสามารถหาคำตอบที่สมดุลและประนีประนอมระหว่างวัตถุประสงค์ทั้งสถานการณ์การลดต้นทุนค่าไฟฟ้าและการสูญเสียพลังงาน และสถานการณ์การลดต้นทุนค่าไฟฟ้าและความต้องการพลังไฟฟ้าสูงสุดได้อย่างมีประสิทธิภาพ ทั้งยังมีความยืดหยุ่นและสามารถปรับใช้ได้กับระดับการใช้งาน EV ที่แตกต่าง ซึ่งเป็นประโยชน์ต่อการวางแผนและบริหารจัดการระบบไฟฟ้าในอนาคตที่มีการบูรณาการยานยนต์ไฟฟ้าได้

สาขาวิชาวิศวกรรมไฟฟ้า ลายมือชื่อนักศึกษา .....

ปีการศึกษา 2567 ลายมือชื่ออาจารย์ที่ปรึกษา.....

SUWIMON TECHANOK : MULTI-OBJECTIVE OPTIMUM OPERATION OF V2G IN DISTRIBUTION SYSTEM

THESIS ADVISOR : ASSOC. PROF. KEERATI CHAYAKULKHEEREE, D.Eng., 217 PP.

Keyword : Optimal operation of vehicle-to-grid / Multi-objective optimization / Electricity cost of system / Energy loss of system / Peak power of system /Monte Carlo simulation

This thesis presents a multi-objective optimum operation of electric vehicles (EVs) in both unidirectional charging mode (vehicle-one-grid: V1G) and bidirectional charging mode (vehicle-to-grid: V2G) within power distribution systems, aimed at mitigating the negative impacts caused by the increasing charging demand of EVs. The study proposes the application of Multi-objective Particle Swarm Optimization (MOPSO) in combination with the Technique for Order of Preference by Similarity to Ideal Solution (TOPSIS) to identify the optimal EV operation strategies that effectively balance and compromise among conflicting objectives. The research considers two main scenarios of multi-objective optimization for both V1G and V2G operations. The first scenario focuses on minimizing electricity cost and energy loss simultaneously, while the second scenario aims to minimize electricity cost and peak power demand concurrently. All optimization processes are carried out under a Time-of-Use (TOU) electricity tariff structure. Additionally, to account for the uncertainty of EV user behavior, this thesis applies Monte Carlo Simulation (MCS) to model diverse user activity patterns. The generated charging load profiles reflect realistic EV usage behaviors based on probabilistic distributions. The simulation results demonstrate that the proposed approach effectively identifies balanced and well-compromised solutions between the objectives in both scenarios. These include the minimization of electricity cost and energy loss (MCAL) and the minimization of electricity cost and peak power demand (MCAP). Furthermore, the method shows flexibility and adaptability to different EV usage levels, making it highly beneficial for future planning and management of power systems with increasing EV integration.

School of Electrical Engineering

Academic Year 2024

Student's Signature .....

Advisor's Signature .....

ACKNOWLEDGEMENT

The authors are particularly grateful to the Kittibandit Scholarship at Suranaree University of Technology, for which I am sincerely grateful.

I appreciate my advisor, Assoc. Prof. Dr. Keerati Chayakulkheeree, whose guidance, insightful feedback, and constant encouragement have been instrumental in the completion of this work. Beyond academic advice, I am deeply grateful for the valuable life skills and practical wisdom I have gained from him in my daily life. His mentorship has not only shaped my research abilities but also inspired me to develop discipline, perseverance, and a positive attitude in facing challenges both in my studies and in everyday living. I also extend my sincere thanks to the committee members: Asst. Prof. Dr. Piampoom Sarikprueck, Prof. Dr. Thanatchai Kulworawanichpong, and Asst. Prof. Dr. Tosaphol Ratniyomchai, for their valuable advice, suggestions, and support throughout the thesis evaluation process

Special appreciation is given to my parents for their enduring support, both emotionally and financially. Their belief in me has been a cornerstone of my academic journey. I am deeply grateful for everything they have done for me.

Furthermore, I would like to acknowledge all my lecturers at the School of Electrical Engineering for providing me with foundational knowledge and academic mentorship during my studies. I am also grateful to my friends, seniors, and fellow members of the Energy and Power Engineering Research Group (EPERG), whose collaboration, encouragement, and assistance greatly contributed to this work.

Lastly, I would like to thank the faculty members and administrative staff at Suranaree University of Technology for their support and kind assistance throughout my academic life.

Suwimon Techanok

TABLE OF CONTENTS

Page

TABLE OF CONTENTS (Continued)

Page

TABLE OF CONTENTS (Continued)

Page

TABLE OF CONTENTS (Continued)

Page

TABLE OF CONTENTS (Continued)

Page

LIST OF TABLES

Table **Page**

LIST OF TABLES (Continued)

Table **Page**

LIST OF TABLES (Continued)

Table **Page**

LIST OF FIGURES

Figure **Page**

LIST OF FIGURES (Continued)

Figure **Page**

LIST OF FIGURES (Continued)

Figure **Page**

LIST OF FIGURES (Continued)

Figure **Page**

LIST OF ABBREVIATIONS

BEV	=	Battery electric vehicle
DOD	=	Depth of discharge
EV	=	Electric vehicle
MCS	=	Monte Carlo simulation
MOPSO	=	Multi-objective particle swarm optimization
MDO	=	Multiple Design Option
MOO	=	Multi-Objective Optimization
MOOV1G	=	Multi-objective optimum operation of V1G
MOOV2G	=	Multi-objective optimum operation of V2G
MEC	=	Minimizing electricity cost
MEL	=	Minimizing energy loss
MPP	=	Minimizing peak power demand
NB	=	The total number of buses
NC	=	The total number of cars
OOV1G	=	Optimum operation of V1G
OOV2G	=	Optimum operation of V2G
PSO	=	Particle swarm optimization
GA	=	Genetic algorithm
SOC	=	State of charge
TOU	=	Time of use
TOPSIS	=	Technique for order preference by similarity to Ideal solution

LIST OF NOMENCLATURES

B_{ij}	=	The susceptance on branch *ij*
C_{ep}^{total}	=	The total daily electricity prices
C_{ep}^{h}	=	The total hourly electricity prices
$C_{en,i}^{h}$	=	The electricity energy prices at bus *i* and hour *h*
$C_{Ft,i}^{h}$	=	The electricity fuel adjustment charge prices at bus *i* and hour *h*
$C_{vat,i}^{h}$	=	The electricity value added tax prices at bus *i* and hour *h*
C_{s}^{t}	=	Season coefficient
c_m	=	Electricity consumption in distance (kWh/km)
c_1	=	The cognitive constant (Acceleration coefficients)
c_2	=	The social constant (Acceleration coefficients)
f^l	=	The MVA flow of line *l*
f_{max}^{l}	=	The maximum limit of line *l*
Ft	=	The fuel Adjustment Charge (at the given time)
G_{ij}	=	The conductance on branch *ij*
E_{loss}^{total}	=	The total daily energy losses
P_{chg}	=	Charging power (kWh)
P_{dchg}	=	Discharging power (kWh)
$P_{V1G,i,h}^{total}$	=	The total V1G charging power at bus *i* and hour *h*
$P_{V2G,i,h}^{total}$	=	The total V2G operation power at bus *i* and hour *h*
P_{loss}^{h}	=	The hourly power loss
P_{hh}^{h}	=	The hourly power of the household load
P_{daily}^{peak}	=	The peak power demand of the day
$P_{V1G,i,t}^{n}$	=	The V1G charging power of *n* cars at bus *i* and period *t*
$P_{V1G,i,h}^{n}$	=	The V1G charging power of *n* cars at bus *i* and hour *h*
$P_{V1G,i}^{h,on}$	=	The V1G charging power at bus *i* and hour *h* in on-grid mode

LIST OF NOMENCLATURES (Continued)

$P_{V1G,i}^{h,off}$	=	The V1G charging power at bus *i* and hour *h* in off-grid mode
$P_{V2G,i,t}^{n}$	=	The V2G operation power of *n* cars at bus *i* and period *t*
$P_{V2G,i,h}^{n}$	=	The V2G operation power of *n* cars at bus *i* and hour *h*
$P_{V2G,i}^{h,on}$	=	The V2G operation power at bus *i* and hour *h* in on-grid mode
$P_{V2G,i}^{h,off}$	=	The V2G operation power at bus *i* and hour *h* in off-grid mode
P_{Di}	=	The real power demand at bus *i*
P_{Gi}	=	The real power of the generator at bus *i*
$P_{Gi}^{\min}$	=	The minimum real power of the generator at bus *i*
$P_{Gi}^{\max}$	=	The maximum real power of the generator at bus *i*
$psoc$	=	The total state of charge
p_{dod}	=	Depth of discharge fraction
p_{car}	=	Vehicle usage probability
Q_{Di}	=	The reactive power demand at bus *i*
Q_{Gi}	=	The reactive power of the generator at bus *i*
r_{tou}^{h}	=	The electricity pricing at hour *h*
r_1, r_2	=	The random numbers parameter
SOC_0^n	=	Initial State of charge of *n* cars
$SOC_{\max}^{n}$	=	The maximum state of charge of *n* cars
$SOC_{\min}^{n}$	=	The minimum state of charge of *n* cars
T_{edr}^{n}	=	The time the *n*-th EV departs from its residence
T_{htw}^{n}	=	The duration of time it takes for the *n*-th EV to travel from home to the workplace
T_{eop}^{n}	=	The duration of time the *n*-th EV is parked in the garage at the workplace
T_{ebh}^{n}	=	The duration of time it takes for the *n*-th EV to travel from workplace to the home
$V_{Gi}^{\max}$	=	The maximum generator voltage
$V_{Gi}^{\min}$	=	The minimum generator voltage

LIST OF NOMENCLATURES (Continued)

Vij	=	The voltage of bus *i* and *j*
VAT	=	The value added tax
v_m	=	The average velocity for a private vehicle trip
w	=	The inertia weight
$x_{i,t}^{Pbest}$	=	Personal best
$x_{i,t}^{Gbest}$	=	Global best
Δt	=	Time step length (hr)
δ_{ij}	=	The phase difference of voltages between bus *i* and *j*

CHAPTER I
INTRODUCTION

1.1 General Introduction

The global energy landscape has undergone a substantial transformation over the past decade. Energy demand has grown, creating an urgent need to reduce environmental impacts through a transition toward cleaner technologies. This change has caused many countries to reconsider their energy policies. The rapid adoption of electric vehicles (EVs) is among the most prominent trends. They are considered a key solution for reducing greenhouse gas emissions from the transportation sector. The international energy agency (IEA) reports that nearly 14 million new EVs were registered worldwide in 2023, and electric car sales topped 17 million worldwide in 2024. According to Thailand's EV promotion plan guidelines, the 30@30 policy was introduced to produce zero-emission vehicles (ZEVs) accounting for at least 30% of total vehicle production by 2030. To attain this goal, the government has implemented various support measures, including tax and non-tax incentives, promoting investment in industries related to EVs, and developing infrastructure to support EVs, including promoting smart grid technology.

EVs offer many advantages, such as reduced fossil fuel use, lower emissions, and higher energy efficiency. However, uncoordinated EV charging increases the electrical system's significant challenges. The primary problem is that charging numerous EVs at once raises the electricity demand, particularly during peak hours. This can make it difficult for the system to provide enough power. Furthermore, connecting a large number of electric vehicles to the electricity grid can have critical negative impacts on the distribution system. Therefore, controlling the energy usage from EVs, known as the optimal operation of electric vehicles (OOEV), is very important.

To address these challenges, demand side management (DSM), smart control systems, time-of-use (TOU) tariffs, and vehicle-to-grid (V2G) technology have been proposed. These methods improve EV operation by connecting to the grid. Meanwhile, the complexity of EV user behavior, grid limitations, and other impacts must also be considered. Multi-objective optimization (MOO) is a promising method for OOEV because it can handle competing goals. This method can be applied to unidirectional charging (V1G) and bidirectional energy exchange vehicle-to-grid (V2G) operations.

1.2 Problem Statement

According to the Paris Agreement, which is the solution that many countries are working on, such as net zero emissions, it aims to reduce and limit greenhouse gases in the long term. Supporting the transition from internal combustion engines (ICEs) to EVs is another policy that has been used to achieve this goal because fuel combustion in combustion engines produces carbon dioxide (CO_2), which is part of the greenhouse gas demonstrated that the widespread adoption of EVs will lead to carbon reductions. The forecasts indicate that by 2030, EVs could account for up to 65% of all light car sales worldwide, driven by strong policy support, advancements in battery technology, and market expansion in major regions. Meanwhile, Thailand's 30 at 30 policy has driven almost 100,000 new EVs in 2023 through various incentives and infrastructure development.

The increase in EVs has a substantial negative impact on the distribution system due to the simultaneous connection of a large number of EVs to the electricity grid. This impacts such as energy loss from transmitting large amounts of electricity and effects on grid equipment that may not yet be compatible. The challenges in energy management, if electricity is insufficient to meet the increasing demand, the distribution system operator's (DSO) may need to procure additional power by purchasing electricity from abroad, which leads to increased electricity costs, influenced by global energy prices. From the perspective of solving scheduling issues to minimize the DSO expenses, this aspect is one of the challenging issues. In large scale EV charging, power losses from extensive electricity transmission impose significant challenges that are comparable to other grid impacts.

Therefore, EV integration is a critical strategy for minimizing the negative impact, such as reducing daily electricity cost, energy losses, and peak power demand of the system due to the increasing use of EVs. Smart charging management and V2G technology are one of EV integration, aimed at addressing energy demand and capacity requirements. However, V2G operation may increase losses in the distribution system due to additional bidirectional power flows, so implementing optimal operation strategies is essential to maximize its benefits, mitigate adverse effects on the network, and consider minimizing peak power demand. Therefore, optimally managing the connection of EVs to the power grid is crucial to handling the increase in EVs.

Demand side management (DSM) is an alternative solution to control electricity demand, including the electricity demand for EV charging. Dynamic pricing is important for controlling electricity demands from EV charging and discharging. In Thailand, TOU tariffs are employed to manage electricity demand to reduce demand at peak and stabilize energy consumption as much as possible. The studies from Aljohani et al. (2021) demonstrated that the dynamic real-time demand electricity pricing mechanism can significantly reduce electricity costs. The TOU tariffs can be applied for optimal energy scheduling to reduce system costs and minimizing CO_2 emissions (Gamil et al. ,2022)

To address these challenges, this thesis proposes the application of multi-objective optimization (MOO) by the multi-objective particle swarm optimization (MOPSO) algorithm, which is capable of managing the complex interactions and trade-offs among conflicting objectives in the power system, including minimizing electricity cost (MEC), minimizing energy loss (MEL), and minimizing peak power demand (MPP). The MOPSO was employed to solve the multi-objective optimum operation of V1G (MOOV1G) and the multi-objective optimum operation of V2G (MOOV2G) problems. The proposed approach integrates the TOU tariffs scheme as a dynamic incentive mechanism to encourage EV users to shift their charging behavior toward off-peak hours. The Pareto front is used to represent a set of optimal trade-off solutions among objectives, and this thesis proposed the technique for order of preference by similarity to ideal solution (TOPSIS) method to select the most suitable solution from the non-dominated set after the post-processing phase. Additionally, the EV users' uncertain

behavior is modeled by using the Monte Carlo simulation (MCS) to generate realistic and probabilistic charging profiles. The effectiveness of the proposed method is validated using the modified IEEE 30-bus test system. This integrated framework aims to provide a robust and flexible strategy to address the challenges of optimal EV operation under real-world distribution network conditions.

1.3 Research Objectives

This research aims to explore effective strategies for addressing the impacts caused by the large-scale integration of EVs into power distribution systems. It focuses on the OOEV to MEC, MEL, and MPP. The MOPSO algorithm is applied to solve the MOOV1G and MOOV2G problems under a TOU tariff scheme. The Pareto frontier is used to analyze a balanced trade-off between conflicting objectives. This thesis considers two MOO cases: (1) minimizing MEC and MEL, and (2) minimizing MEC and MPP. Additionally, MCS is used for modeling EVs' behaviour to generate realistic and probabilistic EV charging profiles, to handle the uncertainty in EV user behavior.

The main objectives of this thesis are as follows,

1) To solve the OOEV in the distribution systems to MEC, MEL, and MPP of the systems under dynamic pricing conditions using the TOU tariff.

2) To model the uncertainty in EV user charging behavior and generate realistic EV load profiles using MCS.

3) To solve the MOOV1G and MOOV2G in distribution systems using the MOPSO algorithm, applying the concept of Pareto front to balance multiple objectives.

4) To apply the TOPSIS method to select the best solution from the Pareto front of the MOPSO algorithm.

1.4 Scope and limitations

1.4.1 Scope

The scope of this thesis focuses on solving both the MOOV1G and MOOV2G in distribution systems. The optimization framework is implemented on the modified IEEE 33-bus distribution test system, using realistic household load profiles

from central Thailand. The research applies the MOPSO algorithm under a TOU tariff scheme to solves both the MOOV1G and MOOV2G. Consideration is given to different multi-objective optimization (MOO) problems in two cases: 1) minimizing electricity cost and energy loss (MCAL), and 2) minimizing electricity cost and peak power demand (MCAP). The separation into two cases allows for clearer analysis and interpretation of system behavior under different operational priorities. Furthermore, particle swarm optimization (PSO) and genetic algorithm (GA) are used to solve the single-objective optimal operation of V1G and V2G for comparison with the MOSPO. The Monte Carlo simulation (MCS) will be used to handle the uncertainty of EV user behavior, generating probabilistic and realistic EV charging profiles for the uncontrolled scenarios. These are then compared with optimized operation EV schedules. This thesis considers the following seven cases to compare electricity costs, energy losses, and peak power demand:

1) The base case of the IEEE 33-bus distribution system without EV devices.

2) The modified IEEE 33-bus distribution system includes EV devices with uncontrolled EV charging.

3) The modified IEEE 33-bus distribution system includes EV devices with controlled EV operation (V1G/V2G), considering a single objective of minimizing electricity cost (MEC).

4) The modified IEEE 33-bus distribution system includes EV devices with controlled EV operation (V1G/V2G), considering a single objective of MEL.

5) The modified IEEE 33-bus distribution system includes EV devices with controlled EV operation (V1G/V2G), considering a single objective of MPP.

6) The modified IEEE 33-bus distribution system includes EV devices with controlled EV operation (V1G/V2G), considering a multi-objective to minimize both electricity cost and energy losses (MCAL).

7) The modified IEEE 33-bus distribution system includes EV devices with controlled EV operation (V1G/V2G), considering a multi-objective to minimize both electricity cost and peak power demand (MCAP).

1.4.2 limitations

The limitations of this thesis are detailed as follows:

1) The behavior of all EV users is assumed to be homogeneous. All EVs share the same operating characteristics and follow the same patterns of use and response.

2) The TOU tariff used is based on a predefined pattern and does not reflect real-time market pricing. Additionally, the electricity selling price during discharging in V2G operations is assumed to follow the same TOU tariff as for charging.

3) Battery degradation costs and capacity fade from repeated charging and discharging cycles are not considered.

4) The IEEE 33-bus distribution system used for testing is not modified to reflect grid reconfiguration or support topology changes that might occur in real-time operations.

5. Monthly service charges and peak demand charges are not considered in the electricity cost calculation.

1.5 Conception

The thesis focuses on solving the multi-objective optimum operation of V1G (MOOV1G) and V2G (MOOV2G) to minimize electricity cost (MEC), energy losses (MEL), and peak power demand (MPP). For multi-objective optimization, two cases are formulated: minimizing electricity cost and energy losses (MCAL), and minimizing electricity cost and peak power demand (MCAP). This thesis proposed a significant approach is applies the multi-objective particle swarm optimization combined with the technique for order of preference by similarity to ideal solution (MOPSO-TOPSIS) to select the best solution (final solution) to solve the MOOV1G and MOOV2G problems. The IEEE 33-bus distribution system, combined with actual household load profiles from central Thailand, is used as a test system. The process begins by collecting key input data, including household load profiles, the IEEE 33-bus test system data, and EV parameters. The inputs are used in a MCS to model the uncertain behavior of EV users and generate probabilistic EV charging profiles following the operation of V1G and V2G modeling. These outputs are applied to evaluate the baseline cases, namely

the base case (without EVs) and uncontrolled EV charging, which serve as references for comparison with controlled cases.

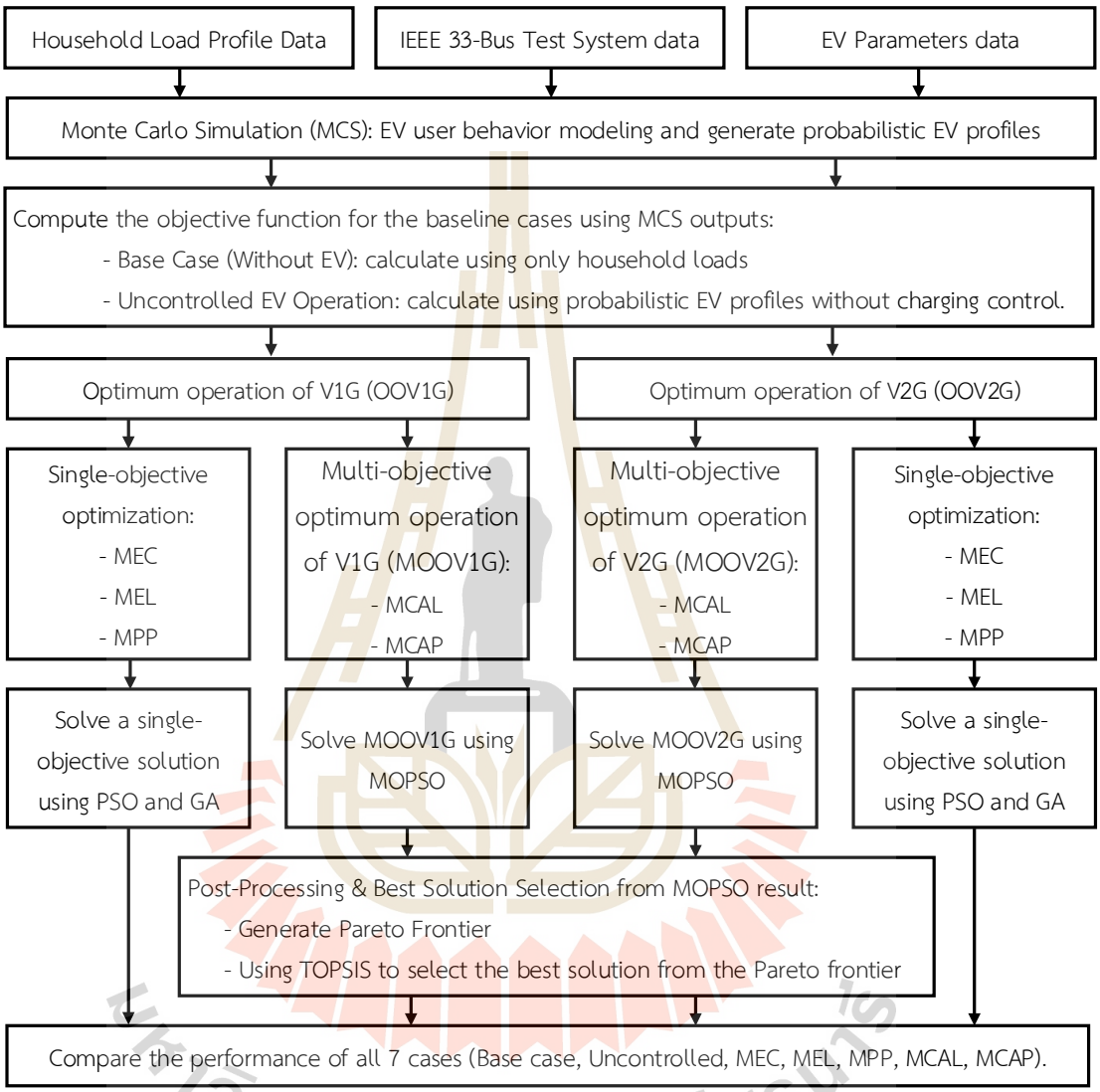

Figure 1.1 The conceptual structure of the proposed framework.

The optimum operation of V1G (OOV1G) and optimum operation of V2G (OOV2G) consider both single-objective optimization and multi-objective optimization. The single-objective cases are solved using two metaheuristic algorithms: PSO and GA. Meanwhile, MOPSO is employed to solve the MOOV1G and MOOV2G problems, to enable performance comparison and demonstrate that a solution from MOPSO can maintain the balance between the multi-objectives. Finally, the performance of all seven simulation cases is compared to evaluate the effectiveness and flexibility of the

proposed optimization method under various operational scenarios. All simulations were performed using MATLAB programming. Figure 1.1 shows the conceptual structure of the proposed thesis.

1.6 Research Benefits

The proposed MOOV1G and MOOV2G using MOPSO can find an effective solution to the optimum operation of EV charging and discharging schedules in the distribution systems. Incorporating a probabilistic model through MCS, the uncertainty of EV user behavior is considered, leading to more realistic and adaptable operation plans. The inclusion of TOU tariffs enhances the flexibility of load management by encouraging off-peak charging. Additionally, the use of the Pareto front and TOPSIS method supports effective decision-making by selecting the most balanced solution among conflicting objectives. The findings solution expected to help DSO reduce electricity costs, energy losses, and peak power demand, while also serving as a reference for developing smart EV integration strategies in real-world grid environments.

1.7 Structure of thesis

This thesis is organized into five chapters, outlined as follows:

Chapter I: This chapter presents the background and significance of the thesis. The challenges arising from large-scale EV integration into power distribution systems. It includes the problem statement, research objectives, scope and limitations, concept of the proposed methodology, and the overall structure of the thesis.

Chapter II: This chapter covers theoretical principles and research on both the V1G and V2G technologies. Including reviews of relevant optimization methods and analyzing the gaps in existing studies. Additionally, it examines current strategies in EV integration, including smart charging, TOU tariff, and DSM, to solve the problem.

Chapter III: This chapter presents a solution to the optimal operation of V1G. The modeling of EV user behavior using MCS to generate realistic load profiles is explained in this chapter. The chapter formulates single-objective and multi-objective

problems aimed at minimizing electricity cost (MEC), energy losses (MEL), and peak power demand (MPP), solved using PSO, GA, and MOPSO under TOU pricing. Furthermore, it explains the post-processing technique, including Pareto front analysis and the use of the TOPSIS method to select the best solution.

Chapter IV: This chapter addresses a solution to the optimal operation of V2G. While much of the MCS model and optimization framework is similar to Chapter 3, it emphasizes the impact of bidirectional power flow and the additional complexity. Moreover, a comparison of algorithm performance through parameter tuning and simulation experiments is presented. And have the demonstration of the flexibility of the proposed multi-objective particle swarm optimization combined with the technique for order of preference by similarity to ideal solution (MOPSO-TOPSIS) approach under varying EV levels.

Chapter V: The final chapter summarizes the significant findings of the research and evaluates the performance of the proposed methods, including a comparison of the results of solving problems of V1G and V2G from the simulation results and analysis.

CHAPTER II
LITERATURE REVIEW

2.1 Introduction

In the past decade, the electrical system has been facing significant challenges due to the increasing use of electric vehicles (EVs), which has rapidly increased the demand for charging energy. Connecting a large number of electric vehicles to the electrical network will have a significant negative impact on the electricity grid system in terms of social, environmental, and economic effects, especially during peak energy demand periods. Therefore, managing EV in both V1G and V2G connections has become a crucial issue that needs to be developed and optimized. The multi-objective optimum operation of V1G (MOOV1) and V2G (MOOV2G) in the distribution systems can address multiple objectives related to the problems arising from the connection of a large number of EVs

2.2 Literature Overview

In the past decade, the challenge of effectively managing electric vehicles (EVs) has garnered significant attention. Many management approaches have been proposed, differing in problem formulation, targeted objectives, and solution methods, as well as considering the operational models of V1G and V2G on different test systems. This section provides a conclusion and an overview of relevant research in the form of tables to demonstrate an overview and gaps in research that have not yet been addressed. The literature review has been divided into two tables: Table 2.1 for research considering V1G operations and Table 2.2 for research considering V2G operations.

Table 2.1 The research considering V1G operations

Reference	Objective	Method	Description
Yihao Wan et al. (2023)	-minimize operation costs and battery degradation in FCS	-Interior point optimizer (IPOPT)	-Tested on a fast EV charging station. -Considered multi-stage degradation of the battery. -No uncertainty in user behavior modelled.
Yisheng An et al. (2023)	-minimize total charging time and improve efficiency	-Earliest Finish Charging (EFC) -Particle Swarm Optimization (PSO)	-Simulated in an urban traffic network with 17 charging stations and 222 charging piles. -Using real-time traffic data to optimize scheduling.
Joy Chandra Mukherjee and Arobinda Gupta (2017)	-maximize total profit and number of PEVs charged	-Distributed offline and online algorithms	-Simulated using city maps of Tokyo and San Francisco, with a 7 × 15 grid and four aggregators collaborating.

Table 2.1 The research considering V1G operations (Continued)

Reference	Objective	Method	Description
Paul Malisani et al. (2023)	-minimize total charging time and improve efficiency	-Branch and Bound algorithm -Pontryagin maximum principle (PMP) -Interior point methods (IPMs)	-Simulated in an urban traffic network with 17 charging stations and 222 charging piles. -Using real-time traffic data to optimize scheduling.
Leehter Yao et al. (2017)	-maximize the number of EVs charged -minimize electricity costs.	-Convex relaxation method	-Using a parking station with 200 charging poles. -Considers both regular and random arrival patterns of EVs.
Techanok and Chayakulkheeree (2024)	-minimize total power loss	-PSO algorithm	-Tested on modified IEEE 30 bus system -No uncertainty in user behavior modeled.
Haojie Zhang et al. (2024)	-minimize peak-to-valley difference in grid load -minimize charging costs	-Genetic Algorithm (GA)	-Tested on a simulation model with 1440 minutes. -Using Monte Carlo method for different EV types.

Table 2.1 The research considering V1G operations (Continued)

Reference	Objective	Method	Description
Mohamed et al. (2022)	-minimize power loss -minimize power consumption -minimize charging costs	-PSO algorithm	-Tested on modified IEEE 31 bus system.
Hongming Yang et al. (2015)	-minimize total distribution costs	-Learnable Partheno-Genetic Algorithm (LPGA)	-Tested on the 36-node and 112-node systems -Considering time-of-use electricity pricing.
Jie Chen et al. (2019)	-minimize total charging cost -minimize load variance of the grid	-Multi-objective Particle Swarm Optimization (MOPSO)	-Tested on IEEE 30 bus system -Considers user preferences and economic factors.
Qi Kang et al. (2017)	-minimize peak-to-valley difference in power load -minimize economic loss for power suppliers.	Weight Aggregation Multi-Objective Particle Swarm Optimization (WA-MOPSO)	-Assume that there are 200,000 charging piles. -Consider the balance between objectives

Table 2.1 The research considering V1G operations (Continued)

Reference	Objective	Method	Description
Yuana Adianto et al. (2022)	-minimize electricity production costs	-PSO algorithm	-Tested on the Java-Bali power system with different EV uptake scenarios. -Using Monte Carlo method for probabilistic modeling
Kalakanti and Rao (2024)	Maximize revenue Maximize quality of service Minimize peak-to-average ratio	Non-dominated Sorting Genetic Algorithm II/III (NSGA-II/III)	-Using a Bayesian model to quantify demand-price probabilistically

Table 2.2 The research considering V2G operations

Reference	Objective	Method	Description
Farshad Rassaei et al. (2015)	-minimizing peak demand	-Distributed Demand Response Algorithm	-Conducted with 1000 users over a 24-hour day-ahead programming scenario. -Assigning random distribution functions for the EVs behaviors.
Xiuyun Wang et al. (2020)	-minimize the total cost -minimize standard deviation of the load curve	-PSO algorithm	-Using a two-stage optimization approach. -Using Monte Carlo simulations to model driving and charging behaviors.
Ahmed Yousuf Saber and Ganesh Kumar Venayagamoorthy (2010)	-minimize operational costs -minimize emissions	-PSO algorithm	-The test system used is 10-unit system with 50,000 gridable vehicles
James J.Q. Yu et al. (2013)	-minimize total system running cost	-Chemical Reaction Optimization (CRO)	-The test system used is a 10-unit system with 50,000 gridable vehicles

Table 2.2 The research considering V2G operations (Continued)

Reference	Objective	Method	Description
Sajjad Ahmadi et al. (2020)	-minimize load variance	-JAYA algorithm	-Tested on IEEE 69 bus system with 110 EVs -The probabilistic model using Monte Carlo
Abdorreza Rabiee et al. (2016)	-minimize operation cost -minimize emissions	-PSO algorithm	-Considers the uncertainties associated with wind and PV powers.
Mahmoud M. Gamil et al. (2022)	-minimization of load generation mismatch -minimize system costs -minimize CO2 emissions	-multi-objective grasshopper optimization algorithm (MOGOA)	-Considers Time of Use (TOU), to adjust load profiles based on electricity pricing.
Alicia Triviño-Cabrera et al. (2019)	-maximize the revenue of EV users	-Mixed-Integer Linear Programming (MILP)	-Uses the IEEE 37-node test feeder as the test system.
Yao et al. (2017)	-maximize renewable energy usage -minimize operational costs	-MILP	-Proposes a real-time optimization scheme for EV charging and discharging.

Table 2.2 The research considering V2G operations (Continued)

Reference	Objective	Method	Description
Shalini Pal and Rajesh Kumar (2018)	-minimize the total energy cost	-MILP	-Considers the day-ahead dynamic prices -Considers incorporates V2G, V2H, and V2N connections.
Qihang Huang et al. (2019)	-minimize system costs	-Power system optimal scheduling model and price elasticity matrix to create a scheduling model for charging and discharging EVs.	-Uses a simulated power grid divided into three dispatch regions, with a total of 12 million EVs. -Uses TOU electricity price
Durgesh Choudhary et al. (2024)	-maximize DSO profit -minimize charging costs -maximize discharging costs	-Metaheuristic optimization -decentralized and centralized pricing strategies	-Proposes pricing strategies for optimizing PEV charging/discharging - Tested on a system with 3,000 PEVs

2.3 V1G in Distribution Systems

EVs involve unidirectional charging, which means that energy is charged from the distribution system to the EV only, without the ability to send energy back to the distribution system like V2G technology.

In V1G charging, an EV charger, which is typically unidirectional, is used. This charger connects to the distribution system, and when charging, energy flows from the distribution system to the charger and into the EV battery in a single direction. A unidirectional charger connected to the power grid and the energy management system (EMS) can help optimize the charging process, such as selecting optimal charging scheduling and using smart charging to adjust power according to energy usage. However, V1G cannot send electricity back to the distribution system.

The continuous growth of EVs presents significant challenges to maintaining the stability of the power system. Many research articles focus on studying optimal V1G charging scheduling and propose different methods to address this solution, adapted to the specific objectives of each problem. Research focused on user objectives, such as Yihao Wan et al. (2023), proposes optimizing the day-ahead scheduling of EV charging to minimize operation costs and battery degradation in fast charging stations (FCS) using the interior point optimizer (IPOPT). An et al. (2023) propose developing an optimal scheduling model for electric vehicle (EV) charging, aiming to improve charging efficiency and reduce charging anxiety among EV users by optimizing the allocation of charging resources in urban areas using the earliest finish charging (EFC) algorithm and a particle swarm optimization (PSO) approach to optimize the scheduling process. The research focused on operator objectives such as Mukherjee and Gupta (2017) propose distributed offline and online algorithms to solve bi-objective charge scheduling optimization problems to maximize the total profit of the aggregators and the total number of PEVs charged. Malisani et al. (2023)used the Branch and Bound algorithm with the pontryagin maximum principle (PMP) and interior point methods (IPMs) for the optimal scheduling for a co-charging parking system to minimize the total charging cost while charging all vehicles to the required battery level. Leehter Yao et al. (2017) propose a convex relaxation method to solve the problem of optimal EV charging scheduling to coordinate EV charging to maximize the number of EVs charged and

minimize electricity costs. In research focused on distribution system operator (DSO) objectives. Techanok & Chayakulkheeree. (2024) discuss how the PSO algorithm can be employed to optimize EV charging scheduling to effectively minimize total power loss of the distribution system, although it does not account for the uncertainty in user charging behavior. multi-objective optimization that aims to minimize power loss, power consumption, and charging costs.). Haojie Zhang et al. (2024) focus on minimizing the peak-to-valley difference in grid load and reducing user charging costs, proposing using genetic algorithms (GA) for optimal scheduling schemes for electric vehicles. Mohamed et al. (2022) propose scheduling of EV charging to enhance both technical and economic aspects of the power system. It minimizes power loss, power consumption, and charging costs. The developed optimal route model for EVs of H. Yang et al. (2015) introduces a learnable partheno-genetic algorithm (LPGA) to solve the proposed EV route optimization to minimize total distribution costs under the TOU price. Chen et al. (2019) introduce the development of a multi-objective scheduling method for optimizing EV charging schedules that aim to minimize the total charging cost for EVs and the load variance of the grid. By considering the factors of charging price, service fees, and user preferences, propose using multi-objective particle swarm optimization (MOPSO) to determine the optimal charging schedule. Q. Kang et al. (2017) proposed an optimal plug-in hybrid electric vehicles (PHEVs) load scheduling with multi-objective aims to minimize potential serious peak-to-valley and minimize economic loss. By proposing the WA-MOPSO algorithm. This algorithm integrates the WA strategy into the MOPSO framework to effectively solve the problem. Yuana Adianto et al. (2021) proposed a novel EV charge scheduling strategy for vertically structured power systems, aiming to minimize the peak-to-valley difference in the system load profile and reduce production costs. The proposed strategy uses a decision-making framework that integrates probabilistic modeling and Monte Carlo simulations. PSO is employed to optimize the scheduled load profile. Furthermore, Kalakanti and Rao (2024) introduced a dynamic pricing strategy for EV charging that formulates the problem as a multi-objective optimization, targeting revenue, service quality, and grid impact. Their method leverages NSGA-II/III for Pareto optimization and

applies a Bayesian model to represent the uncertainty in user demand response to price signals, thus directly addressing user behavior uncertainty.

2.4 V2G in Distribution Systems

V2G (Vehicle-to-Grid) technology allows EVs to operate bidirectionally, unlike V1G which operates in only one direction. The development of V2G not only charges electricity from the distribution system to store in the battery but also the ability to supply electricity back to the distribution system when necessary. This functionality enhances energy efficiency, particularly during peak demand periods or when the grid is unstable.

When V2G begins charging from the grid, the power flow direction is the same as V1G. However, when the distribution system requires additional power during high demand periods, V2G enabled electric vehicles can supply power back to the grid. The power flow direction reverses from the EV battery through a bi-directional charger and into the grid. This process not only helps reduce the load on the power system but also lowers electricity costs in the long term, as users can sell energy back to the grid during high electricity price periods. V2G is an important technology that is being developed to manage electricity on a large scale. It will help support the grid to be more stable and flexible in energy control.

Currently, there is a lot of research focused on developing the use of V2G technology to maximize its benefits to the grid system. The optimal operation of V2G is a complex and challenging issue. Many problem-solving methods and different objectives have been proposed. The use of different algorithms in problem-solving is crucial for finding effective solutions that appropriately meet the set objectives. Rassaei et al. (2015) proposed minimizing peak demand by optimizing EV charging using a distributed demand response (DR) algorithm. The research effectively manages EV charging to reduce peak demand and shape the aggregated demand profile. Moreover, the research investigates the effects of V2G-enabled EVs and the impact of charging and discharging rates on peak demand and the overall systems demand profile. Wang et al. (2020) used a two-stage optimization approach to minimize the total cost and standard deviation of the load curve. The first stage is the joint scheduling of EVs and

thermal power units to create a guiding load curve. The second stage rolling optimization to adjust charging and discharging plans based on real-time data. And using PSO to solve the scheduling problem. Saber and Venayagamoorthy (2010) proposed a method to minimize operational costs and pollution emissions through the scheduling of EV charging and energy distribution. PSO is used to optimize power generation unit allocation and the operation of V2G systems, resulting in a more efficient energy backup capability for the electrical grid. Yu et al. (2013) propose a formulation of the joint scheduling of EV and unit commitment (UC), called EVUC, with the aim of minimizing total system running cost, showing that using chemical reaction optimization (CRO) can effectively optimize this problem. Rabiee et al. (2016) proposed a method, the electrical vehicles are used for peak shaving and load curve using the PSO algorithm to minimize operation cost and minimize emissions in presence of wind and PV powers in the microgrid. Gamil et al. (2022) discussed the multi-objective optimal power scheduling of the residential microgrids considering EV charging and discharging management and demand response programs., utilizing the multi-objective grasshopper optimization algorithm (MOGOA) to solve optimal power scheduling of microgrids through V2G techniques. Three objectives, the first objective is the minimization of load generation mismatch, the second objective is to minimize the system cost, and the third objective is emissions minimization. Triviño-Cabrera et al. (2019) developed a joint routing and scheduling strategy for EVs in smart grids, incorporating V2G to maximize the revenue of EV users while improving the operation of the power network by optimizing the charging and discharging schedules of EVs. This research proposes a mixed-integer linear programming (MILP) problem to optimize the routing and scheduling of EVs. Yao et al. (2017) proposed an optimization of the charging and discharging schedules of EVs to maximize renewable energy usage and minimize operational costs. The study employs MILP to solve the real-time charging optimization problem, considering factors such as dynamic electricity tariffs, solar power generation from the photovoltaic system (PVS), and energy stored in the energy storage system (ESS). Pal and Kumar (2018) proposed an EV scheduling strategy within residential demand response programs to reduce household electricity costs and enhance user flexibility. The strategy incorporates V2G, vehicle-to-home (V2H), and

vehicle-to-neighbor (V2N) connections. A mixed-integer linear programming (MILP) approach is used to solve the EV scheduling problem, aiming to minimize the total daily energy cost. Huang et al. (2019) proposed an optimal scheduling strategy for multiple EV aggregators, considering TOU electricity pricing. The research aims to optimize the charging and discharging schedules of EVs to minimize operational costs. A power system optimal scheduling model is employed, which uses a price elasticity matrix to solve problems. Choudhary et al. (2024) proposed the development of dynamic pricing strategies for managing the charging and discharging of PEVs using a metaheuristic optimization approach to solve the multi-objective problem of maximizing DSO profit, minimize charging costs, and maximize discharging costs. The proposed strategies include decentralized and centralized pricing schemes to optimize the scheduling of charging and discharging, effectively reducing charging costs and enhancing the profit of the V2G system.

2.5 Load Flow Analysis and Loss Calculation

Load flow analysis is a fundamental aspect of power system studies. In this research, the calculation of energy losses in the distribution system is based on the results obtained from load flow analysis. The Newton-Raphson method is employed for solving the load flow problem due to its high accuracy. The loss calculation method is necessary to present the theoretical background of the complex power equations, which form the basis of the load flow analysis and loss evaluation process. The complex power at bus i is given by:

$$S_i = P_i + Q_i = V_i I_i^* \tag{2.1}$$

where S_i is the complex power , P_i is active power, and Q_i is reactive power at bus i . V_i is the voltage at bus i and is the current flowing into bus i . Therefore, the complex power conjugated as equation 2.2.

$$S_i^* = \sum_{i=1}^{NB} V_i^* V_j Y_{ij} \tag{2.2}$$

In a multi-bus system, voltage and current relationships are defined through the bus admittance matrix (Y_{bus}), composed of real and imaginary components:

$$Y_{ij} = G_{ij} + jB_{ij} \tag{2.3}$$

Using the Y_{bus} matrix, power flow equations at bus i can be expressed P_i and Q_i as follows in equations 2.4 and 2.5, respectively.

$$P_i = \sum_{j=1}^{NB} |V_i||V_j| \left[G_{ij} \cos\left(\delta_i - \delta_j\right) + B_{ij} \sin\left(\delta_i - \delta_j\right) \right] \tag{2.4}$$

$$Q_i = \sum_{j=1}^{NB} |V_i||V_j| \left[G_{ij} \sin\left(\delta_i - \delta_j\right) - B_{ij} \cos\left(\delta_i - \delta_j\right) \right] \tag{2.5}$$

These nonlinear equations require iterative numerical methods for solution. The Newton-Raphson method is widely adopted due to its high convergence rate. The method involves constructing the Jacobian matrix, which contains partial derivatives of the power flow equations with respect to the unknowns are the voltage angle (δ) and the voltage magnitude ($|V|$). The general matrix form equation 2.6.

$$\begin{bmatrix} \Delta\delta \\ \Delta|V| \end{bmatrix} = \begin{bmatrix} J_1 & J_2 \\ J_3 & J_4 \end{bmatrix}^{-1} \begin{bmatrix} \Delta P \\ \Delta Q \end{bmatrix} \tag{2.6}$$

The values of δ and $|V|$ are updated iteratively until the mismatches ΔP and ΔQ fall within an acceptable error margin, indicating convergence. The iteration stops when both ΔP and ΔQ are less than or equal to the error threshold of 0.001. Once the voltage magnitude and angle are obtained at each bus, these values are used to compute power loss across the system.

2.6 Research Gaps in Optimal EV Operations

Based on previous research, important gaps exist in the optimal operation of EVs that require further development. This section shows the key research gaps that have not yet been considered. Table 2.3 presents a comparison of previous research, underscoring limitations in considering EV uncertainties, EV operation, dynamic pricing, efficiency improvement methods, and certain multi-objective goals that have not been fully resolved in current research.

To address this gap, this thesis proposes a comprehensive study that considers the operation of both V1G and V2G operational modes under a unified multi-objective optimization framework. The research uses the MOPSO algorithm in combination with the TOPSIS to efficiently identify well-compromised solutions between objectives. Furthermore, single-objective optimization is used for the comparison of the proposed method. This research also incorporates user behavior uncertainty by modeling EV usage through the MCS and the entire optimization process is conducted under a TOU dynamic pricing scheme, providing practical insights into real-world electricity pricing conditions.

Table 2.3 Presents a comparison of previous research

Reference	EV operation (V1G/V2G)	Objective Type	Optimization method.	Dynamic price	User uncertainty
Yihao Wan et al. (2023)	V1G	Single	IPOPT	✘	✘
Yisheng An et al. (2023)	V1G	Single	EFC, PSO	✘	✘
Mukherjee and Gupta (2017)	V1G	Single	Distributed offline and online algorithms	✘	✘

Table 2.3 presents a comparison of previous research (Continued)

Reference	EV operation (V1G/V2G)	Objective Type	Optimization method.	Dynamic price	User uncertainty
Paul Malisani et al. (2023)	V1G	Single	Branch and Bound algorithm, PMP, IPMs	✘	✘
Leehter Yao et al. (2017)	V1G	Single	Convex relaxation method	✘	✓
Techanok and Chayakulkheeree (2024)	V1G	Single	PSO	✘	✘
Haojie Zhang et al. (2024)	V1G	Multi	GA	✘	✓
N. M. M. Mohamed et al. (2022)	V1G	Multi	PSO	✘	✘
Hongming Yang et al. (2015)	V1G	Single	LPGA	TOU pricing	✘
. Jie Chen et al. (2019)	V1G	Multi	MOPSO	✘	✘
Qi Kang et al. (2017)	V1G	Multi	WA-MOPSO	✘	✘
Yuana Adianto et al. (2022)	V1G	Single	PSO	✘	✓

Table 2.3 presents a comparison of previous research (Continued)

Reference	EV operation (V1G/V2G)	Objective Type	Optimization method.	Dynamic price	User uncertainty
Kalakanti and Rao (2024)	V1G	Multi	NSGA-II/III	✓	✓
Farshad Rassaei et al. (2015)	V2G	Single	Distributed Demand Response Algorithm	✗	✓
Xiuyun Wang et al. (2020)	V2G	Single	PSO	✗	✓
Saber and Venayagamoorthy (2010)	V2G	Single	PSO	✗	✗
James J.Q. Yu et al. (2013)	V2G	Multi	CRO	✗	✗
Sajjad Ahmadi et al. (2020)	V2G	Multi	JAYA	✗	✓
Abdorreza Rabiee et al. (2016)	V2G	Single	PSO	✗	✗
Gamil et al. (2022)	V2G	Multi	MOGOA	TOU pricing	✗
Cabrera et al. (2019)	V2G	Single	MILP	✗	✗

Table 2.3 presents a comparison of previous research (Continued)

Reference	EV operation (V1G/V2G)	Objective Type	Optimization method.	Dynamic price	User uncertainty
Yao et al. (2017)	V2G	Single	MILP	✘	✘
Pal and Kumar (2018)	V2G	Single	MILP	electricity prices	✘
Huang et al. (2019)	V2G	Single	Power system optimal scheduling model and price elasticity matrix	TOU tariff	✘
Durgesh Choudhary et al. (2024)	V2G	Multi	Metaheuristic Optimization, decentralized and centralized pricing strategies	Charge and discharge prices	✘
Proposed Framework	V1G & V2G	Multi	-MOPSO-TOPSIS	TOU tariff	✓

CHAPTER III
OPTIMAL OPERATION OF V1G

3.1 Introduction

The increasing penetration of electric vehicles (EVs) in residential areas has introduced new challenges to power distribution systems, particularly when charging is operated in a unidirectional mode or vehicle-one-grid (V1G). Therefore, optimal operation of V1G (OOV1G) becomes a critical strategy. Many studies on optimal EV charging have primarily focused on user benefits-oriented scheduling strategies or have often addressed a single objective function. Therefore, this thesis solves the multi-objective optimum operation of V1G (MOOV1G) problem by considering multi-objective optimization (MOO) in two scenarios: (1) minimizing electricity cost and energy loss (MCAL) simultaneously, and (2) minimizing electricity cost and peak power demand (MCAP) simultaneously. Moreover, the OOV1G problem is also solved using single-objective optimization to provide a comparative analysis.

This chapter presents the methodology and simulation results for the OOV1G. The proposed approach applies multi-objective particle swarm optimization (MOPSO) in combination with the technique for order of preference by similarity to ideal solution (TOPSIS) under a time-of-use (TOU) tariff scheme to identify the most optimal and balanced solutions among conflicting objectives. For comparative analysis, the OOV1G problem is also solved as a single-objective optimization using particle swarm optimization (PSO) and genetic algorithm (GA) to independently minimize electricity cost, energy loss, and peak power demand. The proposed method was tested on the IEEE 33-bus distribution test system. Additionally, incorporates Monte Carlo simulation (MCS) to model the uncertainty in EV user behavior and generate probabilistic EV charging load profiles. The simulation results and discussion in this chapter demonstrate the effectiveness of the proposed method for OOV1G using the MOPSO-TOPSIS on the IEEE 33-bus distribution test system.

3.2 Problem formulation

The formulation of the MOOV1G includes the implementation of the TOU tariff scheme to reflect electricity pricing dynamics; the use of MCS to model the uncertainty of EV user behavior and generate realistic behavior. Moreover, the modeling of V1G operation is used to generate load profiles.

3.2.1 Time of Use (TOU) Tariff for V1G

The TOU rate is an electricity rate that represents the cost of generating power over two periods. Electricity costs are calculated based on the period of electricity usage of the user. The electricity cost is higher during peak hours and lower during off-peak hours, as shown in the figure. 3.1. Implementing the TOU tariff encourages EV users to adjust their charging and discharging times to take advantage of lower rates. In this thesis, the TOU tariff applied is based on the TOU tariff structure used in Thailand.

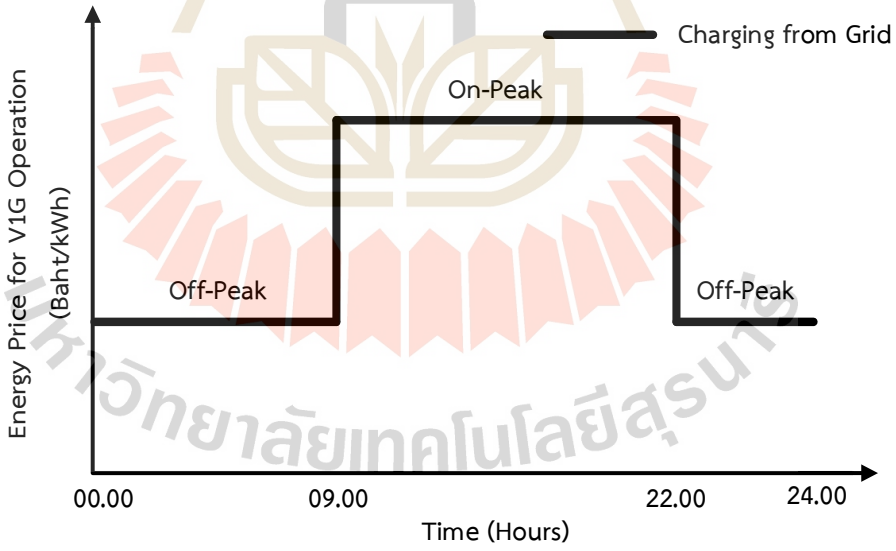

Figure. 3.1 Typical TOU tariff pattern

3.2.2 Monte Carlo Simulation (MCS) for Modeling EV Users' Behavior

The Monte Carlo Method is a statistical technique that uses random sampling to solve complex mathematical and engineering problems, first developed by Stanislaw Ulam and John von Neumann in the 1940s (Metropolis and Ulam, 1949). The name Monte Carlo comes from the famous casino city in Monaco, reflecting the method's reliance on randomness and probability. Monte Carlo simulation (MCS) generates simulated data sets by randomly sampling variables according to specified probability distributions and uses simulated data of random for the estimation or analysis of complex system statistical behaviors. Iqbal et al. (2021) used MCS to generate stochastic EV charging load profiles by randomly simulating, enabling the assessment of the impact of uncertain EV charging demand on the distribution system. Farh et al. (2024) applied MCS to model uncertainty in wind speed and solar irradiance and combined it with a genetic algorithm to optimize the sizing of a hybrid energy system for cost-effectiveness and reliability.

Therefore, this thesis applies MCS to consider the uncertainty in EV user behavior. For the behavior of EV users, MCS is used to address the uncertainty of EV users' behavior. The random variables (r) considered include the time EVs depart from home (T_{edr}), the duration from home to work (T_{htw}), the duration back from work to home (T_{ebh}), and the duration of EVs in a parking lot at work without being connected to the grid (T_{eop}). Additionally, the model considers battery capacity and distance. To generate these random variables, each uncertain parameter is modeled using a probability distribution defined by its means (μ) and standard deviations (σ). The values for these parameters are obtained from real-world EV usage data collected from a parking lot in the city of Livermore, California, USA (Biyouki, Jahromi, and Rashidinejad, 2012). Each random variable is sampled using the truncated normal distribution, which ensures that the randomly generated values stay within practical and realistic limits. The mathematical form of the truncated normal distribution used in this thesis is as follows:

$$f(r,\mu,\sigma,a,b)=\frac{\frac{1}{\sigma}\varphi\left(\frac{r-\mu}{\sigma}\right)}{\varphi\left(\frac{b-\mu}{\sigma}\right)-\varphi\left(\frac{a-\mu}{\sigma}\right)} \tag{3.1}$$

In Equation 3.1, a and b is are the upper and lower bounds for each random variable, and normal distribution function is φ.

Additionally, to assess the flexibility of the modeling approach and evaluate the impact of different probability distributions on the simulation results, this thesis also tests the use of the Weibull distribution as an alternative sampling method. The Weibull distribution is characterized by the probability density function (PDF) as follows in Equation 3.2, which describes the likelihood of r.

$$f(r)=\frac{k}{\lambda}\cdot\left(\frac{r}{\lambda}\right)^{k-1}\cdot e^{-\left(\frac{r}{\lambda}\right)^{k}} \tag{3.2}$$

Where r is the random variable, λ is the scale parameter, and k is the shape parameter. For the Weibull distribution, the shape and scale parameters are crucial as they determine the form and spread of the distribution. For the mean and standard deviation data, a transformation is required to convert these values into corresponding shape and scale parameters. The transformation of the shape and scale are as follows in Equations 3.3 and 3.4, respectively.

$$f(k)=\left[\frac{\sqrt{\Gamma(1+\frac{2}{k})-(\Gamma(1+\frac{1}{k}))^{2}}}{\Gamma(1+\frac{1}{k})}-\frac{\sigma}{\mu}\right]^{2} \tag{3.3}$$

$$\lambda=\frac{\mu}{\Gamma\left(1+\frac{1}{k}\right)} \tag{3.4}$$

Once these random time variables are obtained from the MCS, they serve as inputs to model the EV usage activities of users, as described in Equations. (3.5) - (3.10).

$$\mathbf{ATV}_{\mathbf{day}}^{\mathbf{n}}=[\mathbf{ATV}_{1}+\mathbf{ATV}_{2}+\mathbf{ATV}_{3}+\mathbf{ATV}_{4}+\mathbf{ATV}_{5}], \tag{3.5}$$

$$ATV_1^n = \{1 : T_{edr}^n \text{ -1}\}, \tag{3.6}$$

$$ATV_2^n = \{T_{edr}^n : T_{edr}^n + T_{htw}^n\}, \tag{3.7}$$

$$ATV_3^n = \{T_{edr}^n + T_{htw}^n + 1 : T_{edr}^n + T_{htw}^n + T_{eop}^n\}, \tag{3.8}$$

$$ATV_4^n = \{T_{edr}^n + T_{htw}^n + T_{eop}^n + 1 : T_{edr}^n + T_{htw}^n + T_{eop}^n + T_{ebh}^n\}, \tag{3.9}$$

$$ATV_5^n = \{T_{edr}^n + T_{htw}^n + T_{eop}^n + T_{ebh}^n + 1 : np\}, \tag{3.10}$$

Where, $n = 1, \ldots, NC$ and $t = 1, \ldots, np$.

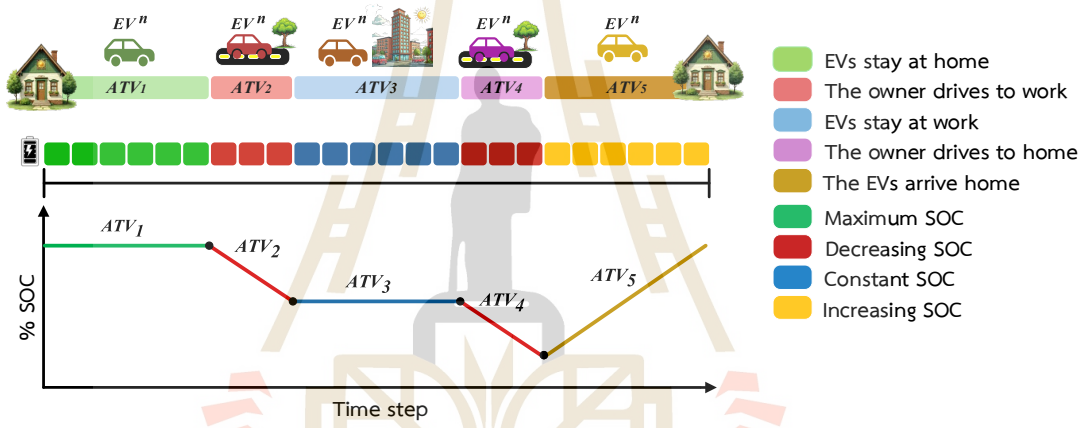

Figure. 3.2 EV user activity model

The EV usage activities of users and their effect on the state of charge (SOC) of the EV across different time steps throughout the day, as shown in Figure 3.2. The EV usage activities of users and their effect on the SOC of the EV across different time steps throughout the day. This thesis assumes that all EVs have the same daily activities (ATV_{day}^n) : staying at home before departing from home (ATV_1^n), commuting to work (ATV_2^n), being parked at the workplace without charging (ATV_3^n), returning to home (ATV_2^n), and staying at home after they arrived home (ATV_5^n).

3.2.3 Operation of V1G Modeling

Based on the results generated from the MCS of daily EV usage patterns, the modeled activities are used to simulate EV charging behavior and generate realistic EV charging load profiles. The modeling of EV operation in this study is adapted and enhanced based on the work of Grahn. (2013). To estimate the electricity consumption

from EV charging and generate the load profile for uncontrolled charging of EVs, it is necessary to calculate the state of charge (SOC). This modeling concept includes increasing the flexibility of the simulation. The initial SOC (SOC_0) is to be defined using a parameter called the percentage of the total state of charge ($psoc$) used to determine the initial SOC relative to the battery's maximum capacity, as shown in the following equation (3.11).

$$SOC_0^n = psoc \times SOC_{\max}^n \tag{3.11}$$

Considering only the charging state, it is assumed that the SOC^t is limited to a minimum depth of discharge (DOD), determined by the fraction p_{dod} and the maximum $SOC_{\max}$ when fully charged, denoted as , as shown in Eq. (3.12).

$$p_{dod}\, SOC_{\min}^n \le SOC_t^n \le SOC_{\max}^n \tag{3.12}$$

The level of SOC changes according to the EV usage activities. It increases from its previous level based on the charging power when the EV is plugged in at home, and it decreases due to energy consumption when the EV is being driven. The energy consumption follows $C^t = c_m C_s^t v_m$. The change of SOC is according to Equation (3.13).

$$SOC_{t+1}^n = \begin{cases} SOC_t^n + P_{chg}\Delta t & , \quad \text{for charging mode} \\ SOC_t^n - C^t \Delta t & , \quad \text{for driving mode} \\ SOC_t^n & , \quad \text{else} \end{cases} \tag{3.13}$$

Where, $n = 1, \ldots, NC$ and $t = 1, \ldots, np$.

The EV load profile $P_{V1G,i,t}^n$ will be equal to or dependent on P_{chg} following the vehicle usage activities at that time, as shown in Equation (3.14). The total EV charging load profile is determined by summing the charging loads of all EVs, as described in Equation (3.15).

$$P_{V1G,i,t}^n = \begin{cases} P_{chg} & , \quad \text{for charging mode} \\ 0 & , \quad \text{else} \end{cases} \tag{3.14}$$

$$P_{V1G,i,t}^{total} = \sum_{n=1}^{NC} P_{V1G,i,t}^n \tag{3.15}$$

Where, $n = 1,\ldots,NC$ and $t = 1,\ldots,np$.

The power EV $P^{n}_{v1G,i,t}$ must be considered hourly in the data analysis to ensure that the information is in line with the objective function, understandable, and adheres to standard procedure. The outcome of changing and discharging the time step from one minute to one hour is displayed in Equation (3.16).

$$P^{total}_{V1G,i,h} = \sum_{n=1}^{NC} P^{n}_{V1G,i,h} \tag{3.16}$$

Where, $n = 1,\ldots,NC$ and $t = 1,\ldots,np$.

3.3 Objective Function

The optimal operation of electric vehicle charging (OOV1G) is formulated as an optimization problem to improve power system performance while minimizing negative impacts caused by increasing EV integration. To ensure that the optimization process adheres to essential system constraints, a penalty-based constraint handling technique is integrated into the objective function formulation. This approach is widely known as the exterior penalty method, in which constraint violations are transformed into additive penalty terms and incorporated into the objective function value. The penalty function is shown in Equation 3.17.

$$PN(P_{V1G,i}) = a_1 \sum_{h=1}^{24} \left[\max(0, P^{h}_{V1G,i} - ub^{h}) + \max(0, lb^{h} - P^{h}_{V1G,i}) \right] + a_2 \left| \sum_{h=1}^{24} P^{h}_{V1G,i} - T \right| \tag{3.17}$$

In the penalty function PN above equation, lb^{h} and ub^{h} are the lower and upper bounds, respectively, that constrain $P^{h}_{V1G,i}$ within permissible operating limits. T represents the total required energy to be delivered to all EVs over the scheduling period. This value is calculated as the sum of the charging power values obtained from the MCS. By enforcing the constraint that the sum of operation EV charging must equal T, the optimization process demonstrates the ability to reshuffle and control the timing of charging while maintaining the same overall demand. This ensures that flexibility is introduced into the charging schedule without altering the total energy consumption. The coefficients a_1 and a_2 are penalty weights that control the severity of the penalties applied for constraint violations. A larger value of these coefficients

enforces stricter adherence to the constraints during the optimization process. This thesis considers three objective functions as follows.

3.3.1 Total electricity cost minimization

The first objective function is to minimize the daily electricity cost incurred from EV charging under a TOU tariff structure. The mathematical of the objective function is as follows in Equation (3.18).

$$\text{Minimize}\, C_{ep}^{total} = \sum_{h=1}^{24} C_{ep}^{h} + PN \tag{3.18}$$

Where the hourly electricity cost can be calculated by:

$$C_{ep}^{h} = \sum_{i}^{NB} C_{en,i}^{h} + C_{Ft,i}^{h} + C_{vat,i}^{h} \tag{3.19}$$

$$C_{en,i}^{h} = (P_{hh,i}^{h} + P_{V1G,i}^{h}) \times r_{tou}^{h} \tag{3.20}$$

$$C_{Ft,i}^{h} = (P_{hh,i}^{h} + P_{V1G,i}^{h}) \times Ft \tag{3.21}$$

$$C_{vat,i}^{h} = \left(C_{en,i}^{h} + C_{Ft,i}^{h}\right) \times VAT \tag{3.22}$$

Where, $i = 1,\ldots,NB$ and $h = 1,\ldots,24$.

3.3.2 Total energy loss minimization

Energy losses in distribution systems occur due to resistance in power lines, particularly when large loads such as EVs are connected. Therefore, the second objective function of the proposed problem is to minimize the energy losses in distribution systems. This objective function can be expressed as below:

$$\text{Minimize}\, E_{loss}^{total} = \sum_{h=1}^{24} P_{loss}^{h} + PN \ , \tag{3.23}$$

Where the hourly loss can be calculated by:

$$P_{loss}^{h} = \sum_{i=1}^{NB} (P_{G,i}^{h} - P_{D,i}^{h}) \ , \tag{3.24}$$

$$P_{D,i}^{h} = P_{hh,i}^{h} + P_{V1G,i}^{h} \ , \tag{3.25}$$

$$P_{loss}^{h} = V_i \sum_{j=1}^{NB} V_j [G_{ij} \cos(\delta_i - \delta_j) + B_{ij} \sin(\delta_i - \delta_j)] \ , \tag{3.26}$$

Where, $i = 1,\ldots,NB$ and $h = 1,\ldots,24$.

3.3.3 Peak power demand minimization

Peak demand periods stress the electrical infrastructure, leading to higher operating costs and grid instability. Therefore, the last objective function is to minimize the peak power demand, as shown in Equation (3.27).

$$\text{Minimize} \quad P_{daily}^{peak} = \max_{h \in \{1,2,\ldots,24\}} \{P_{hh,i}^{h} + \sum_{n=1}^{NC} (P_{V1G,i,n}^{h})\} + PN \tag{3.27}$$

Where, $i = 1,\ldots,NB$, $n = 1,\ldots,NC$, and $h = 1,\ldots,24$.

3.4 Constrains

To solve the MOOV1G under two optimization scenarios, MCAL and MCAP. This study applies both equality and inequality constraints, as described as follows.

3.4.1 Equality constrains

Constraints on MOOV1G in distribution systems following the MCS of EV user behavior can be presented as follows:

$$(pnc \times \sum_{n=1}^{NC} P_{chg,i,n}^{h}) \leq P_{V1G,i}^{h,on} \leq (\sum_{n=1}^{NC} P_{chg,i,n}^{h}), \tag{3.28}$$

$$P_{V1G,i}^{h,off} = 0 \ , \tag{3.29}$$

Where, $i = 1,\ldots,NB$, $n = 1,\ldots,NC$ and $h = 1,\ldots,24$.

The equality constraints, which represent the load flow equations Ghasemi et al. (2015), are as follows:

$$P_{Gi} - P_{Di} - V_i \sum_{j=1}^{NB} V_j [G_{ij} \cos(\delta_i - \delta_j) + B_{ij} \sin(\delta_i - \delta_j)] = 0 \tag{3.30}$$

$$Q_{Gi} - Q_{Di} - V_i \sum_{j=1}^{NB} V_j [G_{ij} \sin(\delta_i - \delta_j) - B_{ij} \cos(\delta_i - \delta_j)] = 0 \tag{3.31}$$

Where, $i = 1,\ldots,NB$, $n = 1,\ldots,NC$ and $h = 1,\ldots,24$.

3.4.2 Inequality constraints

The inequality constraints establish the system's operational bound, as follows. Generator constraints, including voltage, active power, and reactive power at the i^{th} bus, are restricted between their upper and lower bound, as shown:

$$\begin{aligned} |V_{Gi}|^{\min} \le |V_{Gi}| \le |V_{Gi}|^{\max} \\ |P_{Gi}|^{\min} \le |P_{Gi}| \le |P_{Gi}|^{\max} \\ |Q_{Gi}|^{\min} \le |Q_{Gi}| \le |Q_{Gi}|^{\max} \end{aligned} , \quad (3.32)$$

and line flow constraints, which are power flow limits for each line.

$$f_l \le f_l^{\max} \quad (3.33)$$

3.5 Multi-objective optimum operation of V1G (MOOV1G) Using MOPSO

This section presents the multi-objective optimization (MOO) approach for solving the MOOV1G problem using the multi-objective particle swarm optimization (MOPSO) algorithm. The optimization aims to achieve a trade-off between conflicting objectives by generating a Pareto front of non-dominated solutions. Moreover, to select the best solution from the Pareto set, the technique for order of preference by similarity to ideal solution (TOPSIS) method is employed. The fundamentals of Pareto dominance, the structure of the MOPSO algorithm, and the integration of TOPSIS as a post-processing method are described as follows.

3.5.1 Basic Concept of Pareto Dominance

In MOO problems, such as minimizing electricity costs and energy losses, the balance between conflicting objectives is crucial. The concept of Pareto dominance helps find solutions where one objective cannot be improved without worsening another, resulting in a balanced trade-off. A solution that is better in all objectives compared to another is called dominating. This thesis applies the Pareto dominance to MOOV1G solutions, using the MOPSO method introduced first by Coello and Lechuga (2002), which combines the PSO algorithm with MOO. The operation of the Pareto front before entering the MOPSO process is as follows:

Step 1 Initial population creation: A set of potential solutions is generated randomly using the PSO algorithm. In this thesis, the population matrix of the power V1G each hour is shown in Equation (3.34).

$$P_{V1G,i} = [P^1_{V1G,i},\ P^2_{V1G,i},\ ...,\ P^h_{V1G,i}], \tag{3.34}$$

Where, $h = 1,\ldots,24$.

Step 2 Objective functions evaluation: From multiple objective functions $\text{Minimize}: \{f_1(x), f_2(x)\}$, where $f_1(x)$ is the first objective function and $f_2(x)$ is the second objective function. x is a set of potential solutions of objective function following Equation (3.34). Two comprehensive multi-objective frameworks are considered in this thesis.

Scenario 1 solves the MOOV1G problem for minimizing electricity cost and energy loss (MCAL). For this scenario, the first objective function $f_{1,MCAL}(P_{V1G,i})$ is to minimize electricity costs following Equation (3.18) and $f_{2,MCAL}(P_{V1G,i})$ is the second objective function to minimize energy losses following Equation (3.23). The multiple objective functions to MOOV1G for MCAL, as shown in Equation (3.35).

$$\text{Minimize}: \{f_{1,MCAL}(P_{V1G,i}), f_{2,MCAL}(P_{V1G,i})\} \tag{3.35}$$

Scenario 2 solves the MOOV1G problem for minimizing electricity cost and peak power demand (MCAP). For this scenario, the first objective function $f_{1,MCAP}(P_{V1G,i})$ is to minimize electricity costs following Equation (3.18) and $f_{2,MCAP}(P_{V1G,i})$ is the second objective function to minimize peak power demand following Equation (3.27). The multiple objective functions to MOOV1G for MCAP, as shown in Equation (3.36).

$$\text{Minimize}: \{f_{1,MCAP}(P_{V1G,i}), f_{2,MCAP}(P_{V1G,i})\} \tag{3.36}$$

Each solution (fitness values for each particle) is evaluated using multiple objectives to calculate the objective function, which will be used for comparison in the next step.

Step 3 Pareto dominance: In comparing the solutions of this multi-objective problem obtained in Step 2, the concept of Pareto dominance is applied. If solution 1 (x_1) is better than solution 2 (x_2) in every objective function, then solution

1 (x_1) is said to dominate solution 2 (x_2). A solution that is non-dominated by any other solutions is referred to as a Pareto optimal solution.

Step 4 Pareto front: All the Pareto optimal solutions will be used to construct the Pareto front. These solutions represent a balance between the conflicting objectives. MOPSO refines the population of Pareto optimal solutions by using PSO to discover better solutions and then recalculates Pareto dominance to identify any new optimal solutions until the specified convergence criteria are reached.

3.5.2 MOPSO Algorithm

MOPSO is an extension of the original PSO algorithm proposed by Kennedy (1997), which retains the fundamental principles of PSO while integrating the concept of Pareto dominance to handle MOO problems as developed by Lalwani, Singhal, Kumar, and Gupta (2013). Therefore, in each iteration, the equations for velocity and position updates remain as defined in Equations (3.37) and (3.38) respectively. This thesis, w the inertia weight. c_1 and c_2 are acceleration coefficients (cognitive and learning factors). r_1 and r_2 are random numbers uniformly distributed between [0,1].

$$V_{i,t+1} = wV_{i,t} + c_1 r_1 (x_{i,t}^{Pbest} - x_{i,t}) + c_2 r_2 (x_{i,t}^{Gbest} - x_{i,t}) \quad (3.37)$$

$$x_{i,t+1} = x_{i,t} + V_{i,t+1} \quad (3.38)$$

The operation of MOPSO for MOOV1G is an optimization method that extends the classical PSO to handle multiple objectives, which is inspired by the behavior of bird flocks. MOPSO focuses on finding solutions that balance multiple objectives. This process is combined with the concept of the Pareto front. It is initialed by randomly positioned particles in the search space. Each particle i in the swarm represents a potential solution to the optimal V2G operation scheduling problem. In this thesis, the evaluation of each particle depends on the specific multi-objective scenario being considered. Under two optimization scenarios, the first is MCAL, and the second is MCAP. Accordingly, each particle is evaluated based on a pair of objective functions corresponding to the selected scenario. In the MCAL case, particles are evaluated with the objectives of minimizing electricity cost (MEC) and energy loss

(MEL). In the MCAP case, the objectives are minimizing electricity cost (MEC) and peak power demand (MPP). The process then improves with each iteration t by updating the velocity ($V_{i,t}$) and position ($x_{i,t}$) of the particles according to the Equations (3.37) and (3.38), while recording the best position of each particle ($x_{i,t}^{Pbest}$). If a new position is better than the position best, the new position replaces it. The $x_{i,t}^{Gbest}$ is the best position among all particles in the swarm, selected from an external archive of non-dominated solutions using techniques such as crowding distance to ensure diversity in the Pareto front. The main goal of MOPSO is to find Pareto optimal solutions that form the Pareto front. Therefore, the update process considers Pareto dominance to help filter out non-dominated solutions and construct the Pareto front with each iteration until the specified convergence criteria are reached.

The MOPSO algorithm has been developed in Wang et al. (2023) and is called multiple design options-MOPSO (MDO-MOPSO). In this research, the MDO-MOPSO algorithm has adapted to suit the specific characteristics of the problem in this article while still considering the spread of the mean of the crowding distances (quand mean) as convergence criteria according to Equations (3.39) and (3.40).

$$spread = \frac{\mu + \sigma}{\mu + Q\bar{d}} \tag{3.39}$$

$$quand\ mean = \sqrt{\frac{1}{Q}\sum_{k}\bar{d}_k^2} \tag{3.40}$$

Where μ is the parameter, it quantifies whether the extreme values of the Pareto front have changed between two consecutive iterations. σ and $\bar{d}$ are the standard deviation and the arithmetical average of the crowding distances of point k, and Q is the number of points on the Pareto front. Therefore. The iterative process stops when one of the following three conditions is met:

1) The maximum number of iterations is reached.

2) The change in the spread measure falls below a specified relative and absolute tolerance of 10^6.

3) The change in the quadratic means of crowding distances falls below a specified absolute and relative tolerance.

This modified MOPSO algorithm incorporates performance metrics and a post-processing phase for MDO identification. In the post-processing section, a process is conducted to identify the optimal solutions according to predefined criteria. The steps are as follows:

1) Identify the search area for selecting extreme values and conducting trade-off analysis based on the Pareto front.

2) Remove any outliers to ensure only relevant and feasible solutions are considered.

3) Select extreme designs that maximize energy shares, focusing on solutions that provide the best balance between objectives.

4) Calculate key performance indicators (KPIs). KPIs are computed to evaluate and compare the diversity characteristics among the original Pareto front, the enhanced Pareto front, and the selected MDO points. The calculation of KPIs is based on the Manhattan measure. Details of this calculation are presented in (Fioriti, Lutzemberger, Poli, Duenas-Martinez, and Micangel, 2021).

3.5.3 TOPSIS method

The technique for order preference by similarity to Ideal solution (TOPSIS) is a multi-criteria decision-making (MCDM) method designed to identify the best solution from a set of alternatives based on relative closeness to an ideal solution. The concept of TOPSIS is that the optimal alternative should have the shortest distance from the positive ideal solution (PIS) and the farthest distance from the negative ideal solution (NIS). Therefore, TOPSIS makes an effective decision-support tool. For this thesis, TOPSIS is applied to the final step of the post-processing phase to identify the best compromise solution from the Pareto front obtained from solving the MOOV1G. Figure 3.3 illustrates the methodology of the MDO-MOPSO-TOPSIS algorithm for MOOV1G. The TOPSIS method consists of the following steps:

Step 1: Construct the normalized decision matrix. The decision matrix consists of the objective function values of all non-dominated solutions (MDO points) obtained from the Pareto front generated by the MOPSO algorithm. The decision matrix is of MCAL and MCAP scenarios shown following Equations (3.41) and (3.42), respectively. To eliminate the effects of differing units and scales among the objectives,

the objective values in the decision matrix are normalized using the vector normalization method, as shown in equation (3.43).

$$X_{decision} = \left[x_{kf} \right]_{k=1,\ldots,a.\ f=1,2.} = \left[f_{1,MCAL}(P_{V1G,i,k}) \quad f_{2,MCAL}(P_{V1G,i,k}) \right]_{k=1,\ldots,a.} \tag{3.41}$$

$$X_{decision} = \left[x_{kf} \right]_{k=1,\ldots,a.\ f=1,2.} = \left[f_{1,MCAP}(P_{V1G,i,k}) \quad f_{2,MCAP}(P_{V1G,i,k}) \right]_{k=1,\ldots,a.} \tag{3.42}$$

$$r_{kf} = \frac{x_{kf}}{\sqrt{\sum_{k=1}^{a} x_{kf}^2}} \tag{3.43}$$

Where, $k = 1,\ldots,a.$ and $f = 1,2.$ k is the number of solutions on the Pareto front, and a is the total number of solutions on the Pareto front. f is the number of objective functions.

Step 2: Weighted normalized decision matrix. Multiply each normalized value by the corresponding criterion weight to reflect importance. Following this thesis, focus on balancing both the objective functions. Therefore, equal weights are assigned to all objectives in the TOPSIS process. The weighted normalized decision matrix equation is as follows:

$$v_{kf} = w_f \cdot r_{kf} \tag{3.44}$$

Where, $k = 1,\ldots,a.\ , f = 1,2.$

Step 3: Determine the ideal and negative-ideal solutions. This involves identifying the best and worst values for each objective across all alternatives in the weighted normalized decision matrix. For minimization problems, the ideal solution (v_f^+) is the minimum value of each objective function, while the negative-ideal solution (v_f^-) is the maximum value of each objective function . These are calculated using equations (3.45) and (3.46), respectively.

$$v_f^+ = \min(v_{kf}) \tag{3.45}$$

$$v_f^- = \max(v_{kf}) \tag{3.46}$$

Where, $k = 1,\ldots,a.\ , f = 1,2.$

Step 4: Calculate the distance to the ideal and worst solutions. The distance from each alternative to both the ideal and the worst solution is calculated.

D_k^+ is the distance from the weighted normalized value of each alternative to the ideal solution. D_k^- is the distance from the weighted normalized value of each alternative to the worst solution. The calculation follows in Equations (3.47) and (3.48)

$$D_k^+ = \sqrt{\sum_{k=1}^{a}\left(v_{fk} - v_f^+\right)^2} \tag{3.47}$$

$$D_k^- = \sqrt{\sum_{k=1}^{a}\left(v_{fk} - v_f^-\right)^2} \tag{3.48}$$

Where, $k = 1,\ldots,a.\ , f = 1,2.$

Step 5: Calculate the closeness coefficient (C_k). After calculating the distances from each alternative to the ideal and worst solutions, the final step is to calculate the closeness coefficient of each alternative. The alternative with the highest C_k is considered the best compromise solution among all Pareto-optimal solutions. Calculating C_k follows the Equation (3.49).

$$C_k = \frac{D_k^-}{D_k^+ + D_k^-} \tag{3.49}$$

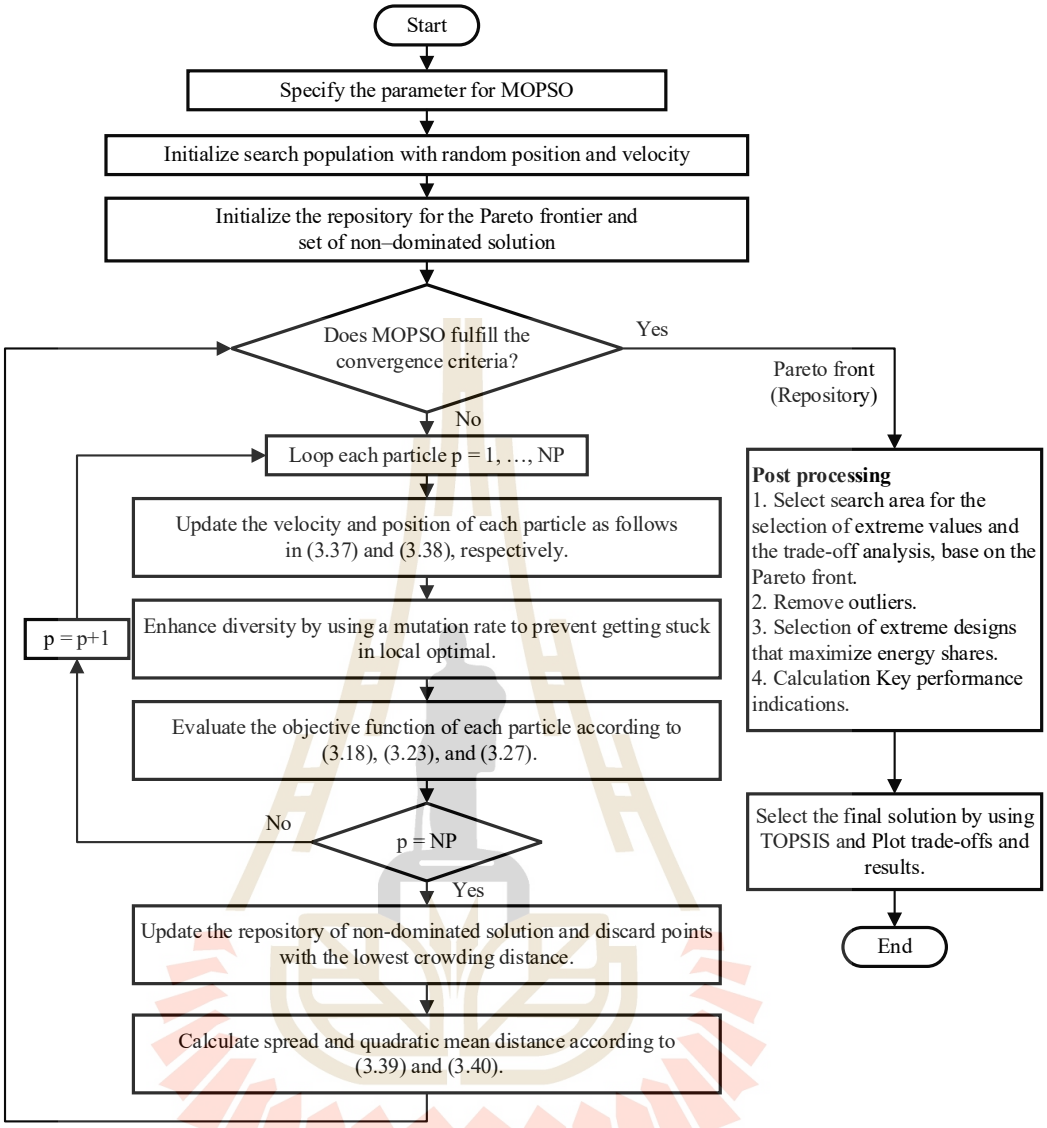

Figure 3.3 The MDO-MOPSO-TOPSIS methodology of MOOV1G

3.6 Simulation Results

This section presents the simulation results for the optimal operation of V1G (OOV1G) in the modified IEEE 33-bus distribution test system with integrated EV load profiles generated by MCS. This chapter focuses on solving MOOV1G using the MOPSO-TOPSIS method under the TOU tariff. The analysis is structured into several cases to comprehensively evaluate the impact of EV charging under different control approaches and optimization objectives. The simulation results have seven cases as follows:

Case 1: Base Case Without EV Charging Devices.

Case 2: Uncontrolled EV Charging Devices in The Modified IEEE 33-Bus Distribution System.

Case 3: Controlled EV Charging Devices in The Modified IEEE 33-bus Distribution System Under Single Objective for Minimizing Electricity Costs (MEC).

Case 4: Controlled EV Charging Devices Under Single Objective for Minimizing Energy Losses (MEL).

Case 5: Controlled EV Charging Devices Under Single Objective for Minimizing Peak Power Demand (MPP).

Case 6: Controlled EV Charging Devices Under Multi-Objective for Minimizing Electricity Cost and Energy Losses (MCAL).

Case 7: Controlled EV Charging Devices Under Multi-Objective for Minimizing Electricity Cost and Peak Power Demand (MCAP).

All simulations were conducted using MATLAB software.

3.6.1 Input Parameter

The MOOV1G using the MOPSO algorithm will be tested on the IEEE 33-bus distribution system, which has been modified from the Baran & Wu model for distribution system planning as shown in Figure 3.4. The information data and information of the IEEE 33-bus distribution system are given in Dolatabadi, Ghorbanian, Siano, and Hatziargyriou (2021). This thesis modifies the IEEE 33-bus distribution test system by integrating EVs at each bus, excluding bus number 1 (the slack bus). The EV charging demand at each bus is proportionally determined based on the base load of that bus in the IEEE 33-bus distribution test system, as shown in Figure 3.5.

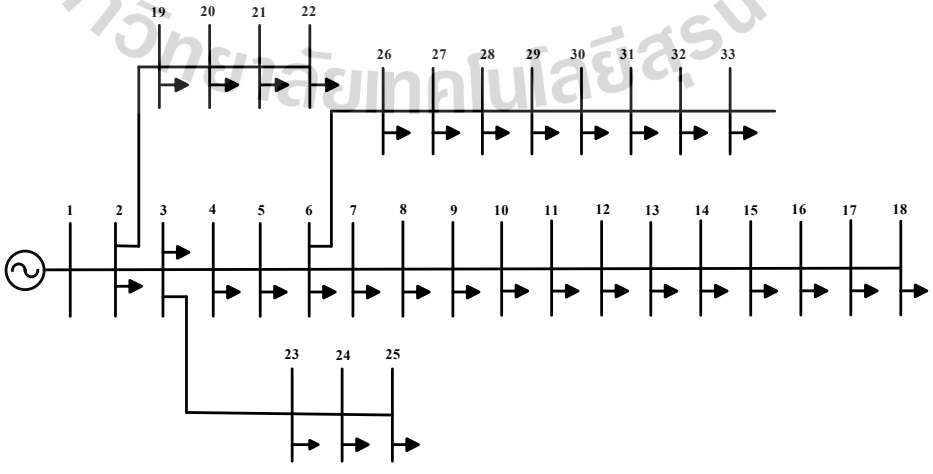

Figure 3.4 The IEEE 33-bus distribution system

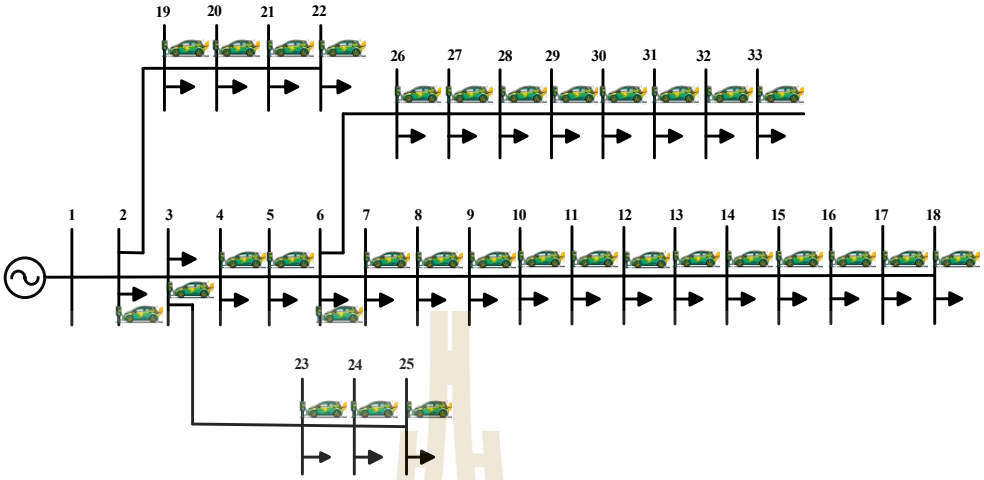

Figure 3.5 The modification IEEE-33 bus distribution system with EV charging devices

The modification of the IEEE 33-bus distribution system by incorporating EV charging devices will be applied in simulation study cases to solve the OOV1G problem in different control approaches and optimization objectives.

In MCS, probability distributions are used to generate random variables. The random variables considered in MCS relate to the uncertain variables' averages and standard deviations displayed in Table 3.1 and the Weibull distribution parameter displayed in Table 3.2. From the vehicle usage behavior obtained by MCS, an uncontrolled EV load profile is generated using input parameters for the EV charging model as shown in Table 3.3. The vehicle model used in this thesis uses the BYD Atto 3. For the calculation of electricity costs in this thesis, use the TOU tariff of Thailand, as indicated in Table 3.4. This thesis considers household consumption at a voltage level lower than 12 kV.

Table 3.1 The Truncated normal parameter for EV behavior modeling

Random variable	Mean (μ)	Variance (σ^2)
T_{edr}	7:15 AM	30 min
T_{htw}	30 min	15 min
T_{eop}	9 h and 20 min	50 min
T_{ebh}	30 min	15 min

Table 3.2 The Weibull distribution parameter for EV behavior modeling

Random variable	Shape ()	Scale ()
T_{edr}	101.1365	437.4548
T_{htw}	9.2793	31.6367
T_{eop}	100.8495	563.1690
T_{ebh}	9.2793	31.6367

Table 3.3 Input parameters of EV charging

	Parameter values
$SOC_{\max}$	60.48 kWh
p_{chg}	3.7 kWh
p_{dod}	0.6
$C_s{}^t$ of Jun-Aug	1.1
v_m	60 km/h
c_m	0.257 kWh/km
Δt	1/60 h
pnc	0.1

Table 3.4 Time of use rate (TOU rate) for type 1 residential households

Voltage level	Energy charge (Bath/kWh)	
	Peak (09:00 a.m. - 10:00 p.m.)	Off-Peak (10:00 p.m. - 09:00 a.m.)
At voltage level 12 – 24 kV	5.1135	2.6037
At voltage level lower than 12 kV	5.7982	2.6369

3.6.2 Case 1: Base Case Without EV Charging Devices

In the base case scenario, the IEEE 33-bus distribution system is without the integration of EV charging devices, as illustrated in Figure 3.4. The load profile applied to represent the household electricity consumption is based on the residential load profile for the central region of Thailand in July, as shown in Figure 3.6. This case serves as the base case to compare the impacts of EV charging integration under different strategies. The simulation results for the base case indicate that the total daily electricity cost of the system is 86.0471 kTHB/day, the total energy loss is 2.045 MWh/day, and the peak power demand reaches 1,144.2832 kW. These values reflect the system's original operating condition without the additional load from EVs, providing a reference for evaluating the effectiveness of optimization strategies under EV integration in scenarios.

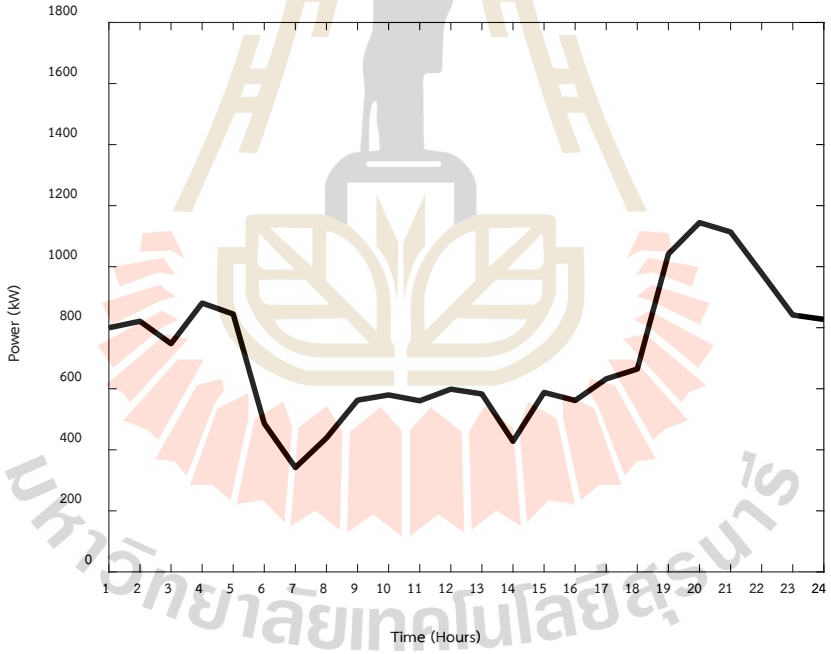

Figure 3.6 The central Thailand load profile for July

3.6.3 Case 2: Uncontrolled EV Charging Devices in The Modified IEEE 33-Bus Distribution System

In this scenario, EVs are integrated into the modified IEEE 33-bus distribution system with uncontrolled EV charging devices. The EV load profile for this case is generated based on user behavior modeled using the MCS. The simulation accounts for variability in EV users' daily routines, including the time of departure from home, duration from home to work, duration from work back home, and the time spent parked at the workplace without being connected to the grid. The random variables using the Truncated normal distribution and Weibull distribution were obtained with 2,000 MCS iterations, and with tested for 30 trials.

The Truncated normal distribution random values were generated using the mean and standard deviation of each variable. Figure 3.7 illustrates the results of 30 iterations for all four random variables using the Truncated normal distribution. Each subplot shows the average line and the selected value closest to the mean. The selected variables were statistically analyzed and visualized in the form of histograms, as shown in Figures 3.8 to 3.11. The convergence of the MCS process, which reflects the stability of Truncated normal distribution random variables after repeated sampling, is shown in Figure 3.12. The Weibull distribution random is defined by shape (k) and scale (λ) parameters, calculated based on the mean and standard deviation of the data. Figure 3.13 displays the 30 trial values for each variable using the Weibull Distribution, along with the average line and the selected value closest to the mean. Figures 3.14 to 3.17 show histograms of the selected values for each variable along with the corresponding PDF curves of the truncated normal distribution. The convergence of the MCS process, which reflects the stability of Weibull distribution random variables after repeated sampling, is shown in Figure 3.18.

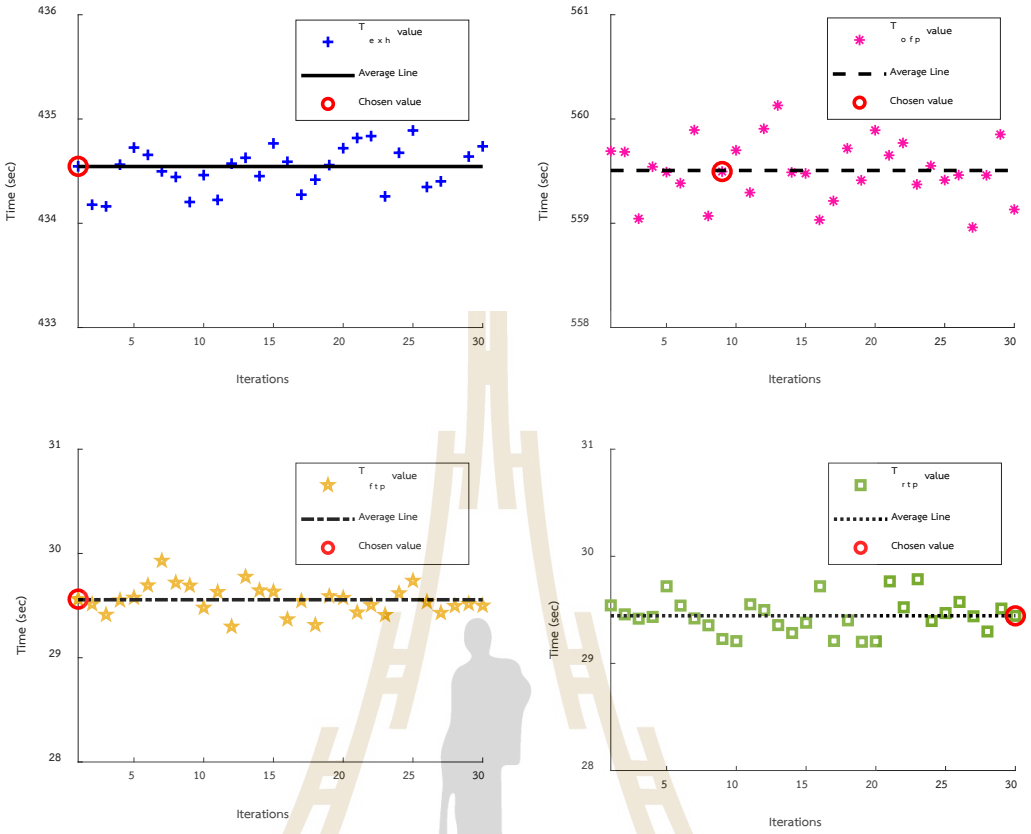

Figure 3.7 Random variable over 30 rials using Truncated normal distribution

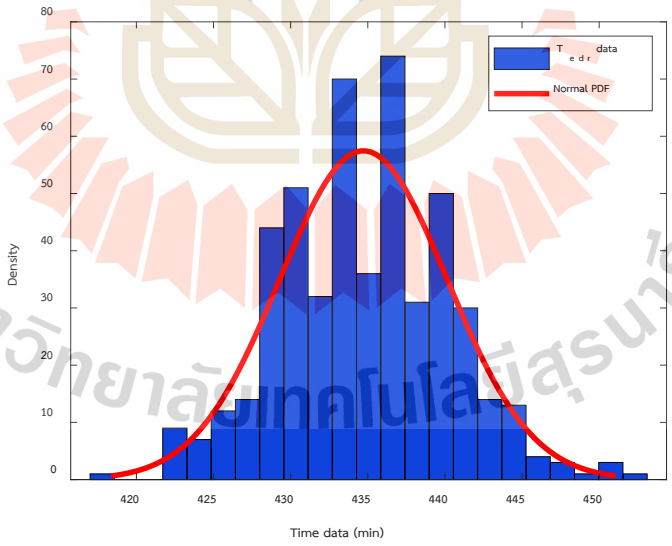

Figure 3.8 The normal PDF of the time EVs depart from home (T_{edr})

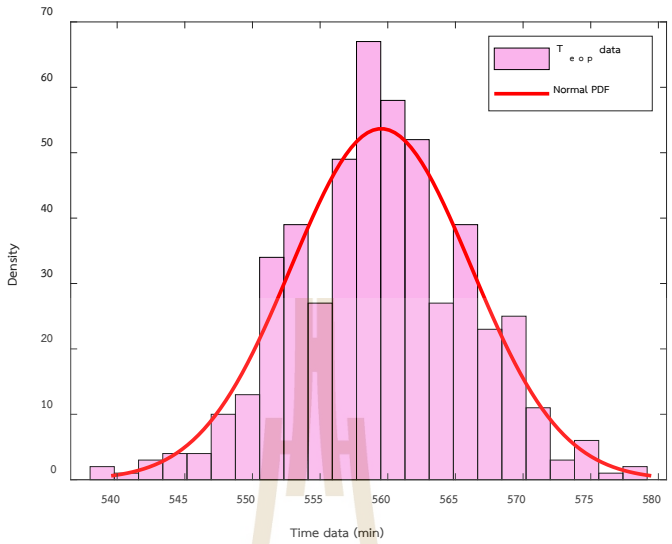

Figure 3.9 The normal PDF of the duration of EVs in a parking lot at work without being connected to the grid (T_{eop})

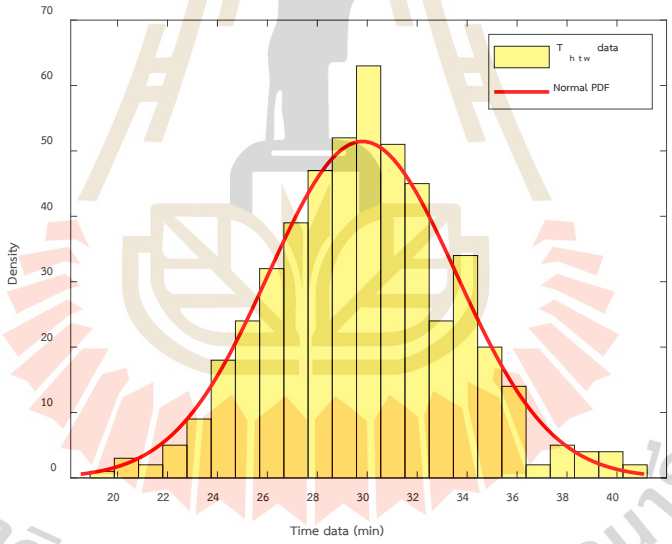

Figure 3.10 The normal PDF of the duration from home to work (T_{htw})

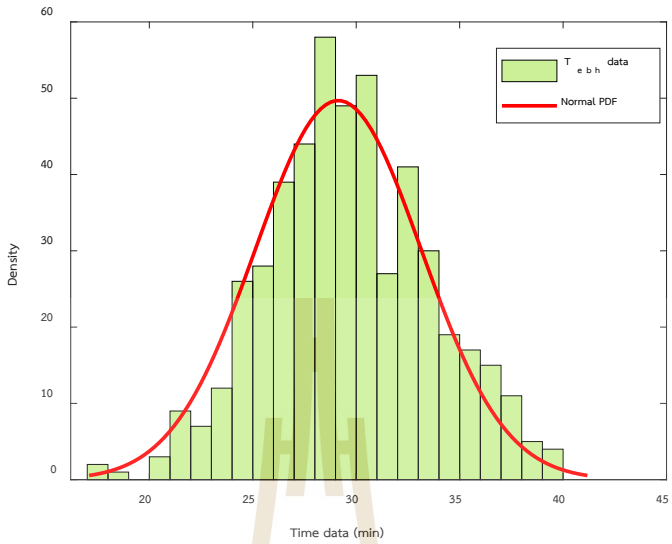

Figure 3.11 The normal PDF of the duration back from work to home (T_{ebh})

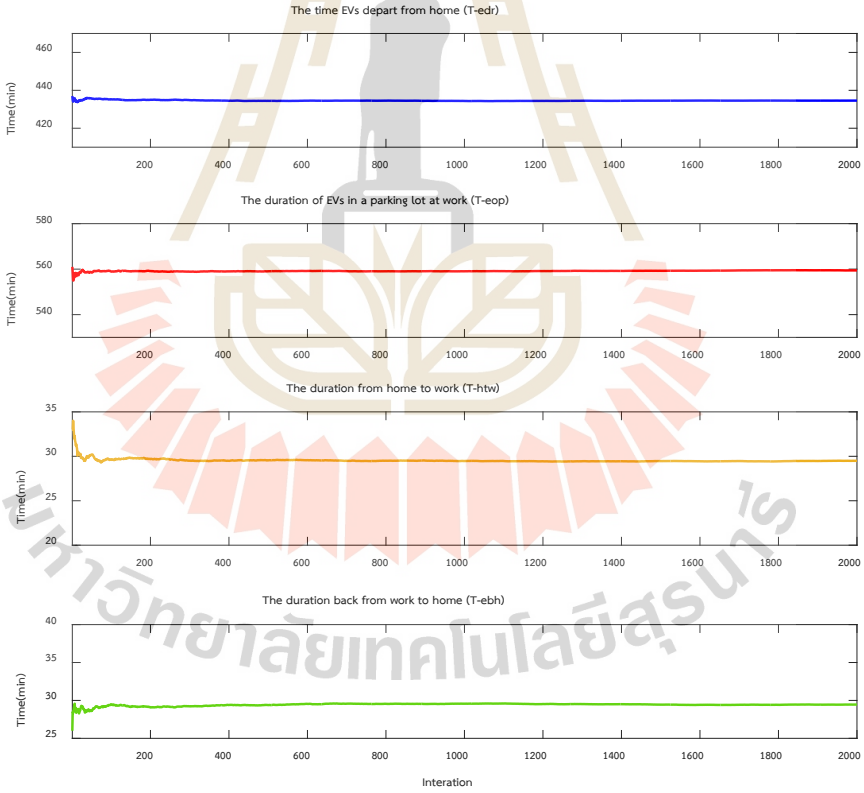

Figure 3.12 The Convergence behavior of random variables generated by MCS using the Truncated normal distribution

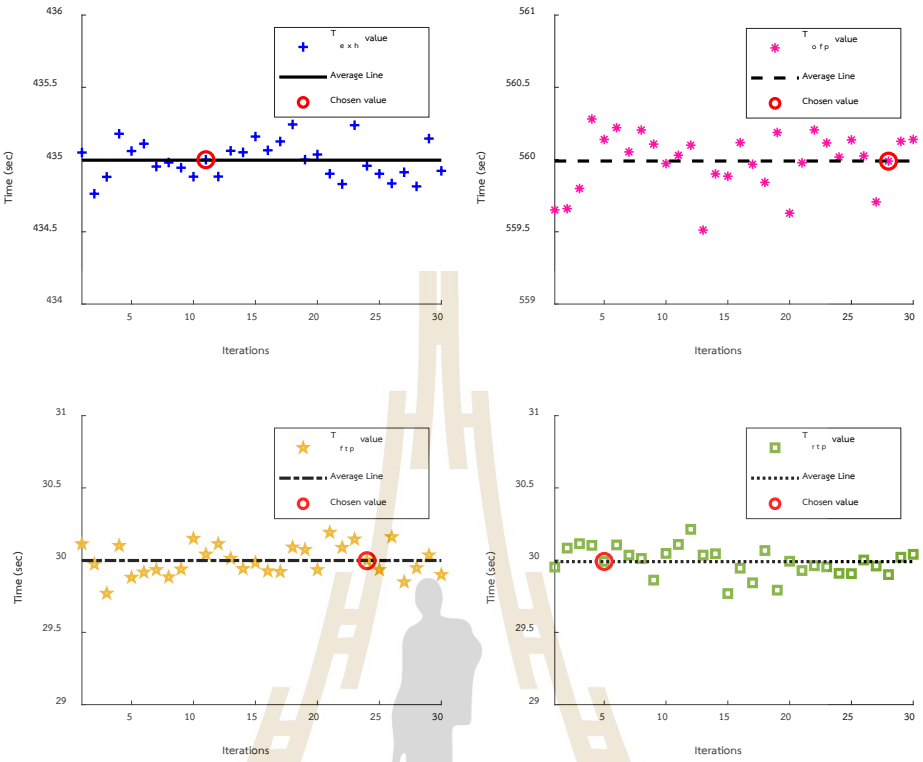

Figure 3.13 Random variable over 30 rials using Weibull Distribution

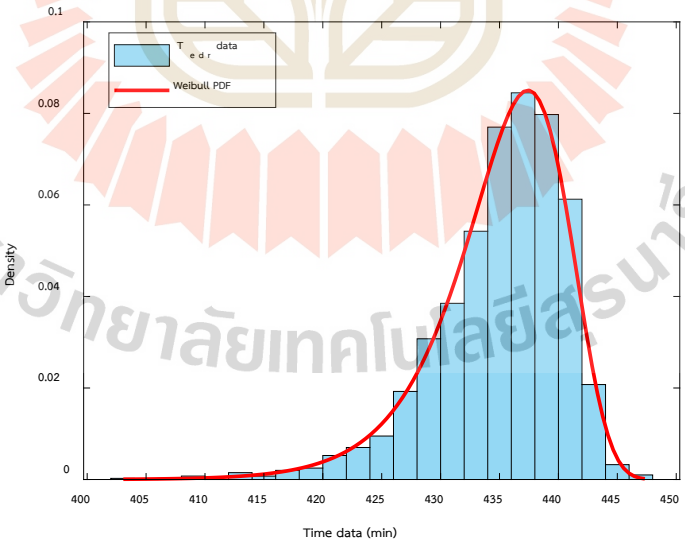

Figure 3.14 The Weibull PDF of the time EVs depart from home (T_{edr})

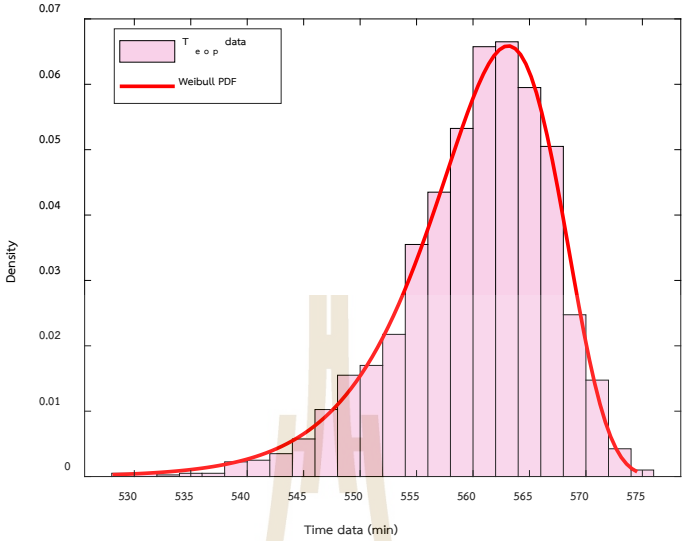

Figure 3.15 The Weibull PDF of the duration of EVs in a parking lot at work without being connected to the grid (T_{eop})

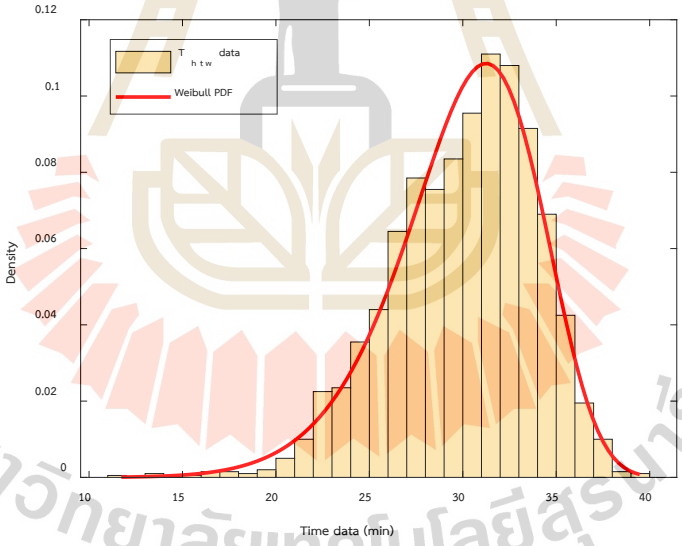

Figure 3.16 The Weibull PDF of the duration from home to work (T_{htw})

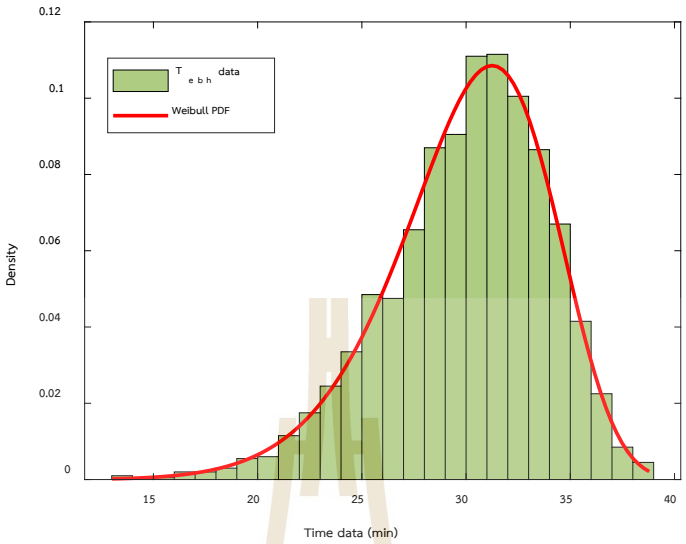

Figure 3.17 The Weibull PDF of the duration back from work to home (T_{ebh})

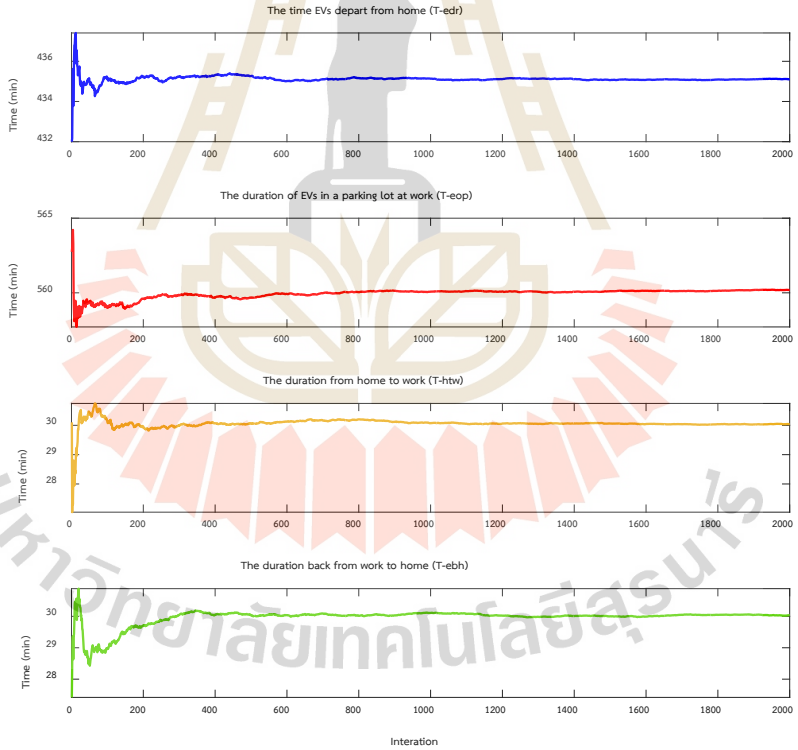

Figure 3.18 The Convergence behavior of random variables generated by MCS using the Weibull distribution

The truncated normal distribution and the Weibull distribution were employed to generate random values for modeling EV user behavior. Each method

was used to perform 30 Monte Carlo trials, and the selected values for each random variable were those closest to their respective means. However, since the random variables used in the activity modeling represent time-based quantities, the final values used in the simulation were rounded to the nearest integers. As a result, the rounded values obtained from both distributions turned out to be identical across all four key variables: departure time, travel time to work, travel time back home, and parking duration at the workplace. Consequently, the resulting daily activity patterns generated using either distribution are the same.

This thesis assumes that EV batteries are fully charged at the beginning of the day before departing from home. During the day, EVs are parked at work but not connected to the grid, meaning no charging or discharging occurs during working hours. The operation of the V1G model for generating uncontrolled load profile EV charging is modeled based on the assumption of 200 EVs per bus, excluding the slack bus. However, the actual number of EVs on each bus is not fixed. Instead, the EV load is proportionally allocated to each bus based on its original base load, with higher load demand receiving a greater share of the EV load. The load profile for EV charging from the operation of the V1G model follows user behavior through the MCS, assuming the percentage of the total state of charge ($psoc$) is equal to $SOC_{\max}$. The simulation result of the operation of the V1G model in generating an uncontrolled EV charging load profile, location status based on user activities, and SOC by considering the time period $np=1440$ minutes is shown in Figure 3.19. Figure 3.19 shows the activity of EV users from MCS, which determines when EVs are at home and available for charging. When EVs arrive home with low SOC causes EV charging, which uncontrolled charging causes a pronounced evening peak in power demand.

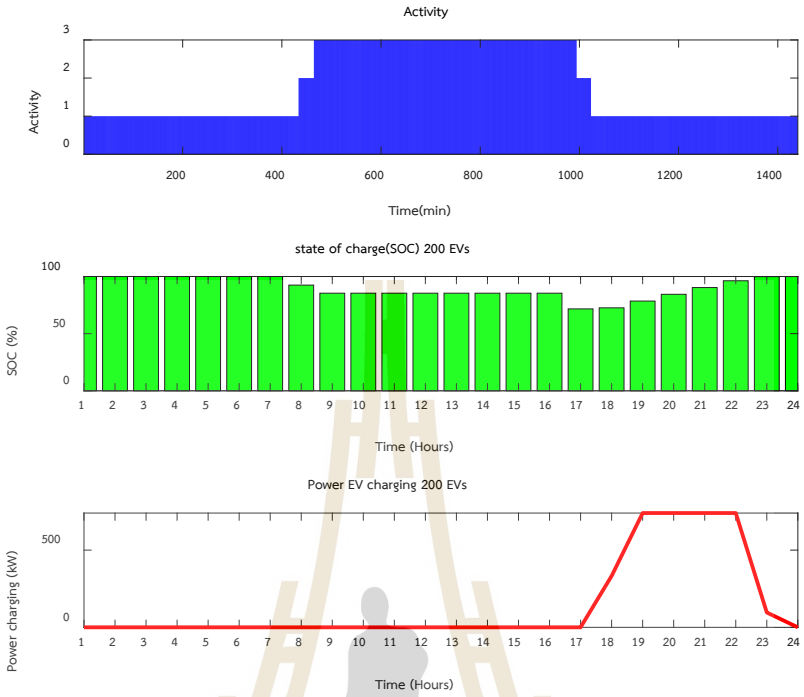

Figure. 3.19 The result from the MCS and the operation of V1G modeling

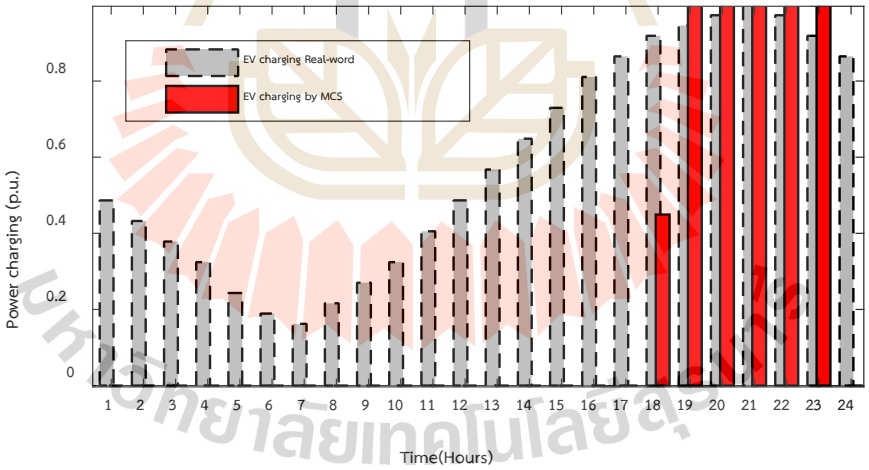

Figure. 3.20 Comparison EV charging load profile of MCS result and real-world data

Figure 3.20 compares the EV charging load profile generated by the MCS with real-world charging data obtained from a Denmark-based study (Andersen, Jacobsen, and Gunkel, 2021). The results demonstrate a strong alignment between the simulated and actual data, particularly in terms of the peak demand period. Notably, both profiles show the highest electricity usage occurring between 8:00 PM and 9:00

PM, indicating the effectiveness of the MCS in modeling realistic EV charging behavior under the given assumptions.

When the load profile from the EV charging model is compared to the systems basic household load profile, the EV charging behavior is found to be consistent with the typical household electricity demand period. This generates an increase in peak electricity demand. Figure 3.21 presents a comparison of the load profiles of case 1 and case 2, illustrating that the charging demand of EVs coincides with the peak periods of general household electricity consumption.

The simulation results show that, under uncontrolled charging, calculating the daily electricity cost for the entire system is 105.6815 kTHB/day, the total daily energy loss is 4.1049 MWh, and peck power demand is 1,884.2832 kW. These results highlight the significant impact of uncoordinated EV charging on both system costs and energy losses, especially when compared to the base case without EVs. As a result, electricity costs, energy losses, and peck power demand increase, as followed by the simulation result. Table 3.5 shows the comparison results of the load profiles and Table 3.6 shows the objective function values.

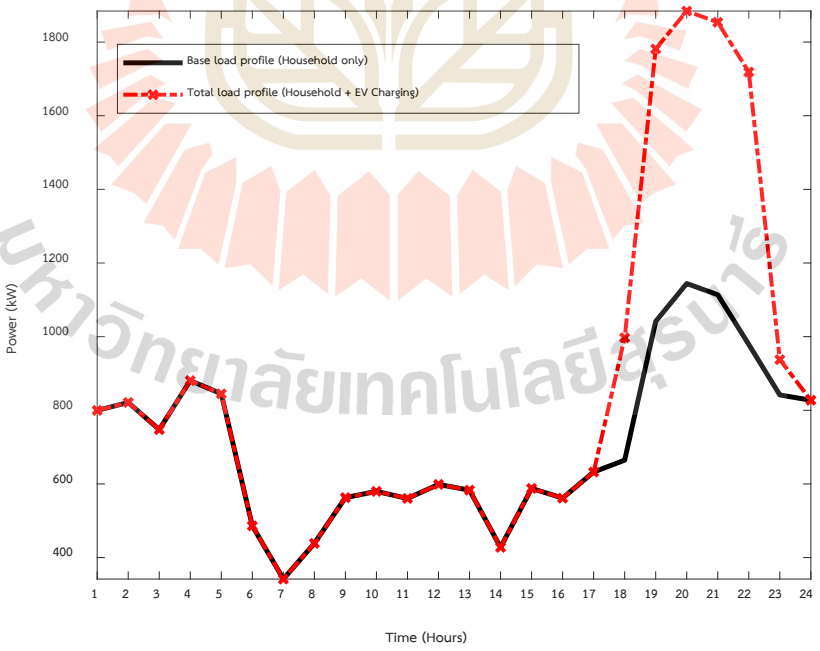

Figure 3.21 Comparison of the load profiles Case 1 and Case 2

Table 3.5 Comparison results of the load profile and objective function value of the IEEE 33-bus distribution system for Case 1 and Case 2

Hours	Power consumption (kW)		
	Case 1	Case 2	
		Power EV charging	Total power load
1	799.720	0	799.72
2	821.242	0	821.24
3	747.64	0	747.64
4	880.72	0	880.72
5	844.678	0	844.68
6	486.02	0	486.03
7	341.71	0	341.71
8	438.65	0	438.65
9	562.76	0	562.76
10	579.72	0	579.72
11	560.58	0	560.58
12	598.66	0	598.66
13	583.04	0	583.04
14	427.85	0	427.85
15	587.92	0	587.92
16	561.53	0	561.53
17	632.37	0	632.37
18	664.62	332.445	997.06
19	1041.43	740.00	1781.42
20	1144.28	740.00	1884.28
21	1113.68	740.00	1853.68
22	978.70	740.00	1718.70
23	841.64	96.015	937.66
24	827.31	0	827.31

Table 3.6 Comparison the objective function value of the IEEE 33-bus distribution system for Case 1 and Case 2

The objective function value	Case Study		
	Case 1	Case 2	
		Power EV charging	Total power load
C_{ep}^{total} (kTHB)	86.0471	19.6344	105.6815
E_{loss}^{total} (MWh)	2.045	2.0599	4.1049
P_{daily}^{peak} (kW)	1,144.2832	740	1,884.2832

3.6.4 Case 3: Controlled EV Charging Devices in The Modified IEEE 33-bus Distribution System Under Single Objective for Minimizing Electricity Costs (MEC)

In this case, the optimal operation of V1G (OOV1G) is under a single-objective optimization. The objective considered in this scenario is MEC for the modified IEEE 33-bus distribution system with a controlled EV charging device. To solve the OOV1G problem, the PSO and GA algorithm determines the optimum operation of EV charging for MEC. Both algorithms are executed separately, with each algorithm being tested for a total of 30 trials. The simulation results are presented as follows in Table 3.7, which shows the objective function values of the maximum, minimum, and average obtained from 30 PSO and GA trials for Case 3. Additionally, the results from across 30 PSO and GA trials are plotted in the Figures. 3.22 and 3.23, respectively. The best result from PSO, determined from the minimum electricity cost across 30 trials, was 98.0490 kTHB/day, with a corresponding energy loss of 5.2211 MWh/day and peak power demand of 1,226.2472 kW. On the other hand, when comparing GA. The best solution from GA has an electricity cost of 98.0510 kTHB/day but resulted in a reduced energy loss of 4.0110 MWh/day and a higher peak demand of 1,370.7270 kW.

The results indicate that both algorithms are effective in minimizing electricity costs under the OOV1G solving. Notably, PSO achieves a slightly lower minimum electricity cost compared to GA, demonstrating its superior performance in electricity cost minimization for this case.

Table 3.7 The result of 30 trials by PSO and GA for Case 3 of the OOV1G

Algorithm	Electricity cost (kTHB/day)			Energy loss (MWh/day)	Peak power demand (kW)
	Max	Avg.	Min	Calculated	Calculated
PSO	98.0493	98.0490	98.0490	5.2211	1,226.2472
GA	98.1602	98.0778	98.051	4.0110	1,370.7270

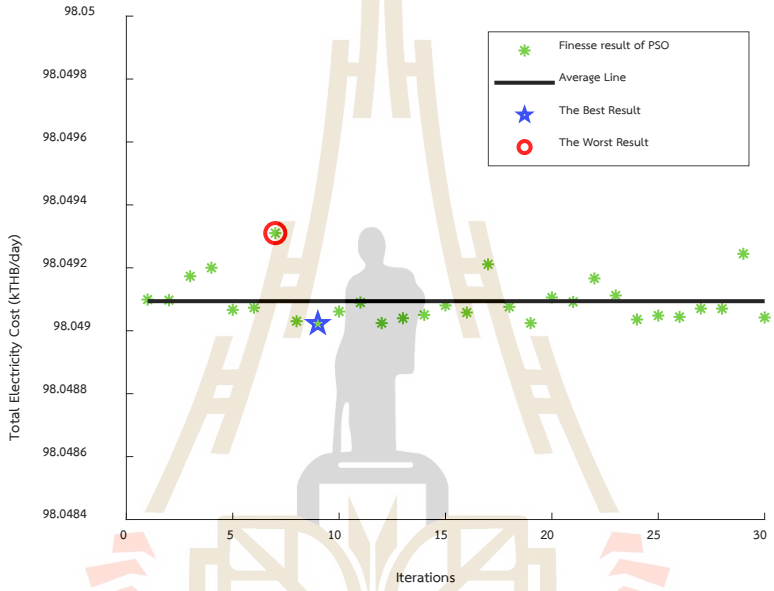

Figure 3.22 The results from 30 trials of PSO for Case 3 of the OOV1G

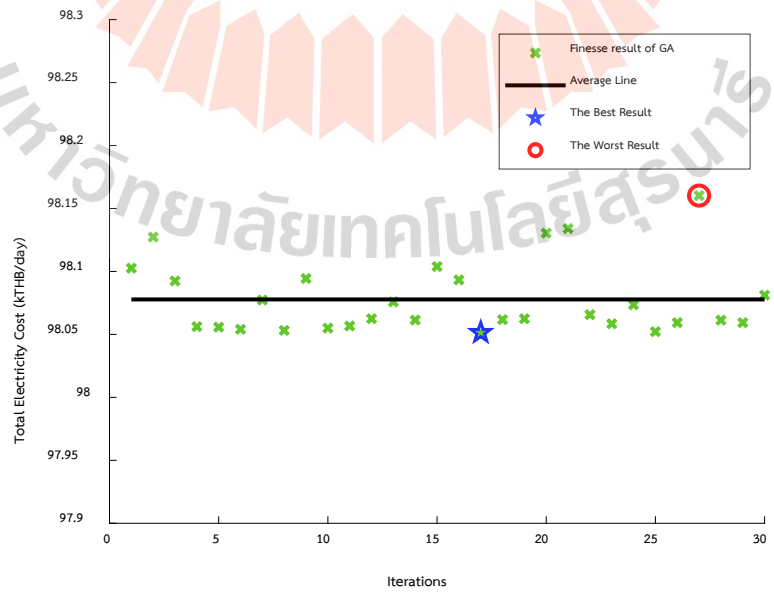

Figure 3.23 The results from 30 trials of GA for Case 3 of the OOV1G

3.6.5 Case 4: Controlled EV Charging Devices Under Single Objective for Minimizing Energy Losses (MEL)

In this case, the OOV1G is under a single-objective optimization. The objective considered in this scenario is MEL for the modified IEEE 33-bus distribution system with a controlled EV charging device. To solve the OOV1G problem, the PSO and GA algorithm determines the optimum operation of EV charging for MEL. Both algorithms are executed separately, with each algorithm being tested for a total of 30 trials. The simulation results are presented as follows in Table 3.8, which shows the objective function values of the maximum, minimum, and average obtained from 30 PSO and GA trials for Case 4. Additionally, the results from across 30 PSO and GA trials are plotted in the Figures. 3.24 and 3.25, respectively. The best result from PSO, determined from the minimum energy loss across 30 trials, was 3.1716 MWh/day, with a corresponding electricity cost of 99.2622 kTHB/day and peak power demand of 1,236.7796 kW. On the other hand, when comparing GA. The best solution from GA has an energy loss of 3.1991 MWh/day, but the electricity cost and peak power demand increased to 99.4714 kTHB/day and 1,339.514 kW, respectively.

The results indicate that both algorithms are effective in minimizing energy loss under the OOV1G solving. Notably, PSO achieves a slightly lower minimum energy loss compared to GA, demonstrating its superior performance in energy loss minimization for this case.

Table 3.8 The result of 30 trials by PSO and GA for Case 4 of the OOV1G

Algorithm	Energy loss (MWh/day)			Electricity cost (kTHB/day)	Peak power demand (kW)
	Max	Avg.	Min	Calculated	Calculated
PSO	3.3569	3.2167	3.1716	99.2622	1,236.7796
GA	3.3331	3.2451	3.1991	99.4714	1,339.5140

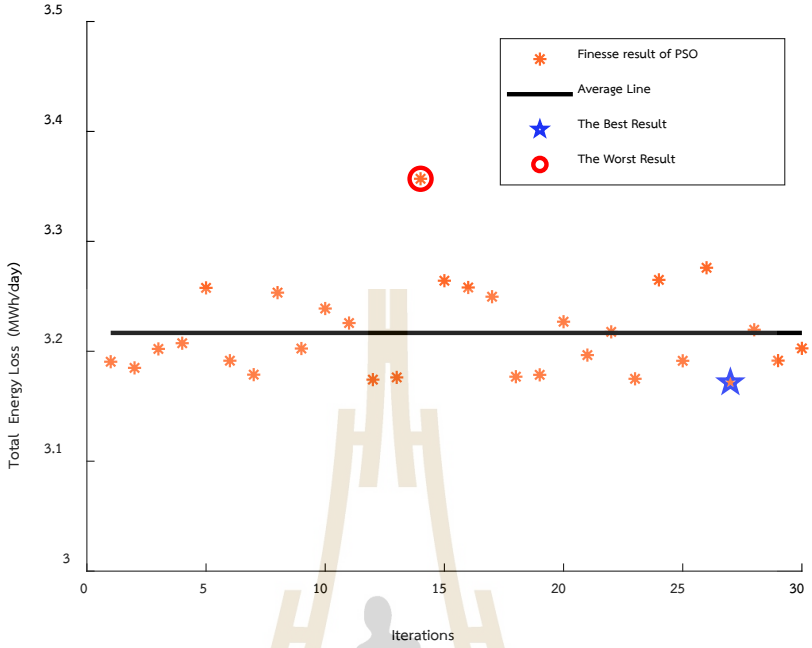

Figure 3.24 The results from 30 trials of PSO for Case 4 of the OOV1G

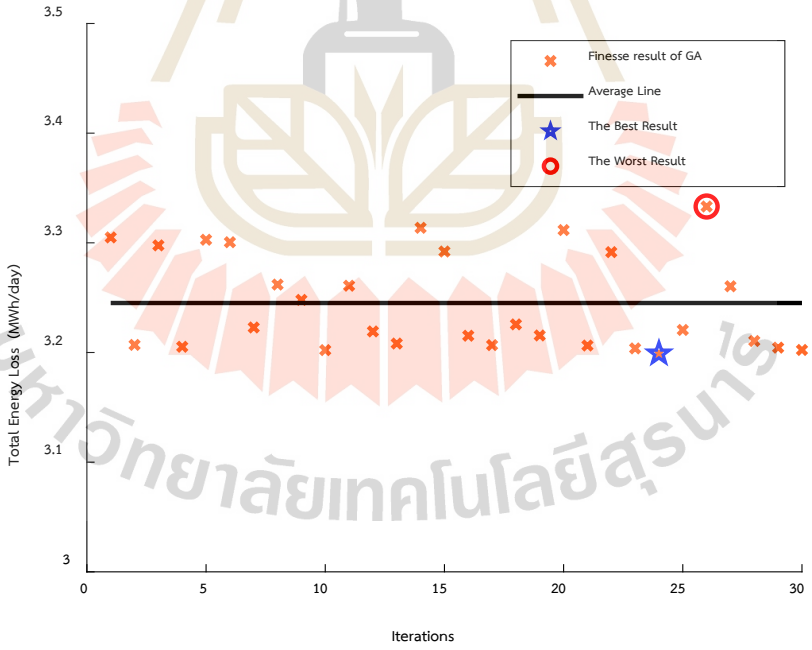

Figure 3.25 The results from 30 trials of GA for Case 4 of the OOV1G

3.6.6 Case 5: Controlled EV Charging Devices Under Single Objective for Minimizing Peak Power Demand (MPP)

In this case, the OOV1G is under a single-objective optimization. The objective considered in this scenario is MPP for the modified IEEE 33-bus distribution system with a controlled EV charging device. To solve the OOV1G problem, the PSO and GA algorithm determines the optimum operation of EV charging for MPP. Both algorithms are executed separately, with each algorithm being tested for a total of 30 trials. The simulation results are presented as follows in Table 3.9, which shows the objective function values of the maximum, minimum, and average obtained from 30 PSO and GA trials for Case 5. Additionally, the results from across 30 PSO and GA trials are plotted in the Figures. 3.26 and 3.27, respectively. The best result from PSO, determined from the minimum peak power demand across 30 trials, was 1,218.28320 kW, with a corresponding electricity cost of 99.3561 kTHB/day and an energy loss of 5.1965 MWh/day. On the other hand, the best solution from GA has a peak power demand of 1,218.2906 kW, and the electricity cost and energy loss reduced to 99.0555 kTHB/day and 5.0380 MWh/day, respectively.

The results indicate that both algorithms are effective in minimizing peak power demand under the OOV1G solving. Notably, PSO achieves a slightly lower minimum peak power demand compared to GA, demonstrating its superior performance in peak power demand minimization for this case.

Table 3.9 The result of 30 trials by PSO and GA for Case 5 of the OOV1G

Algorithm	Peak power demand (kW)			Electricity cost (kTHB/day)	Energy loss (MWh/day)
	Max	Avg.	Min	Calculated	Calculated
PSO	1,218.28328	1,218.28322	1,218.28320	99.3561	5.1965
GA	1,239.81419	1,224.38289	1,218.2906	99.0555	5.038

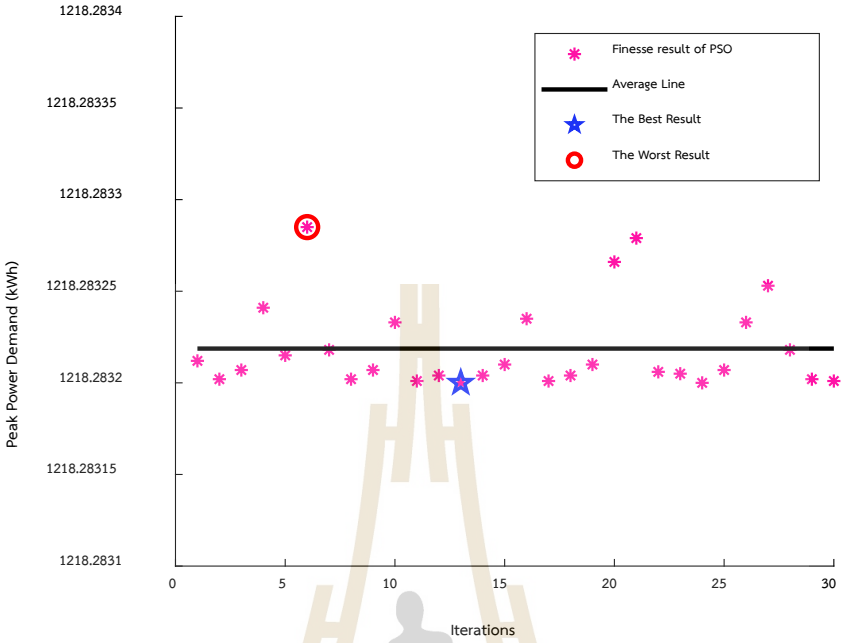

Figure 3.26 The results from 30 trials of PSO for Case 5 of the OOV1G

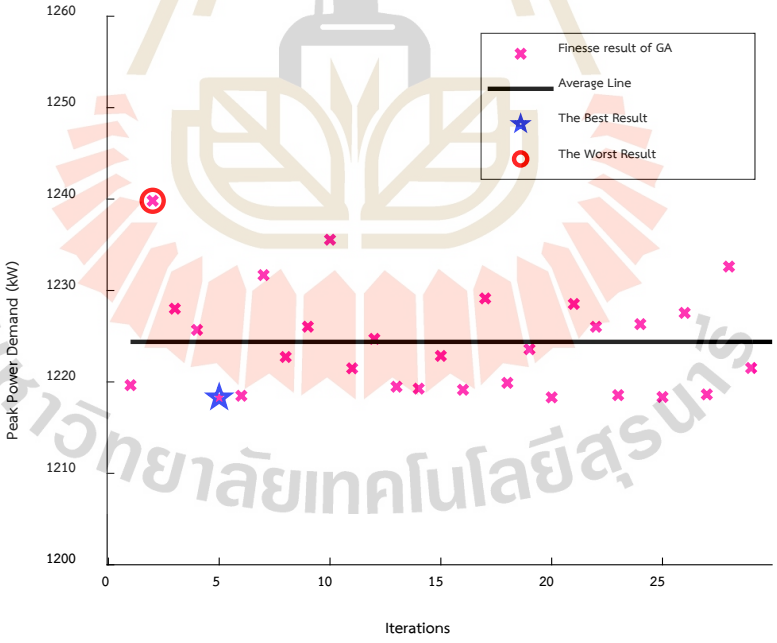

Figure 3.27 The results from 30 trials of GA for Case 5 of the OOV1G

3.6.7 Case 6: Controlled EV Charging Devices Under Multi-Objective for Minimizing Electricity Cost and Energy Losses (MCAL)

In this case, the OOV1G under a multi-objective optimization aimed to MCAL. The multi-objective optimal operation of the V1G (MOOV1G) problem was solved using the proposed MOPSO algorithm, integrated with the TOPSIS method for selecting the best solution from the Pareto front. The MOOV1G solving is under control EV Charging devices on the modified IEEE 33-bus distribution system. The MOPSO algorithm was tested for 30 trials, each generating a Pareto-optimal set. For each run, the TOPSIS method was applied in the post-processing phase to identify the best-compromised solution. The closeness coefficient calculated in TOPSIS was used to evaluate how close each Pareto solution was to the ideal solution.

The simulation results are presented in Table 3.10, which shows the best, average, and worst closeness coefficient values obtained from the 30 trials for Case 6. Additionally, Table 3.10 shows the best objective function from the best solution. The best solution was selected based on the highest closeness coefficient of 0.9818, indicating high proximity to the ideal point and farthest from the worst point. The best solution obtained from the MDO-MOPSO-TOPSIS method across 30 trials, the electricity cost and energy loss were reduced to 99.0428 kTHB/day and 3.1967 MWh/day, and the peak power demand was 1,291.7347 kW.

Table 3.10 The result of 30 trials by MDO-MOPSO-TOPSIS for Case 6 of the OOV1G

	MDO-MOPSO-TOPSIS method			Calculation
Result value	**Closeness Coefficient**	**Electricity cost (kTHB/day)**	**Energy loss (MWh/day)**	**Peak power demand (kW)**
Max	0.9818	99.0428	3.1967	1,291.7347
Avg.	0.9786			
Min	0.9683			

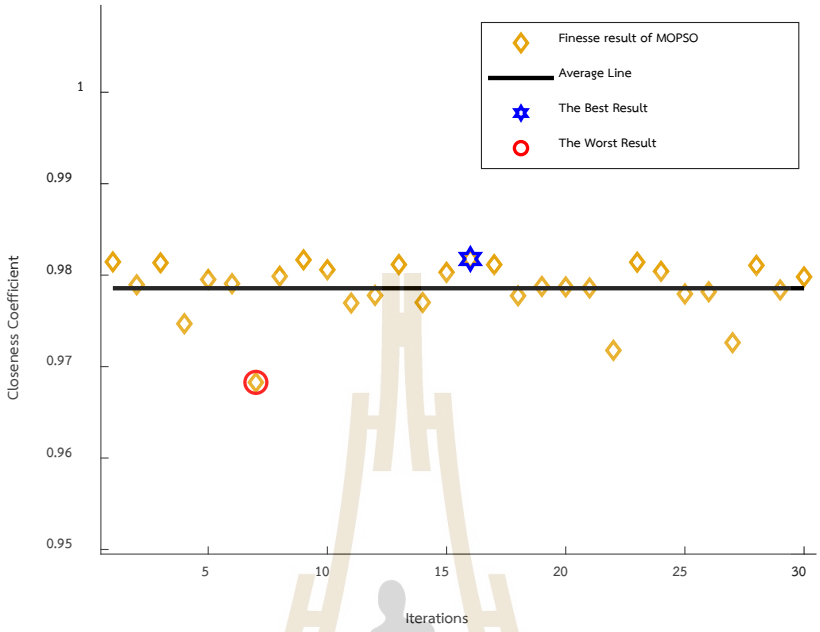

Figure 3.28 The closeness coefficient from 30 trials of MDO-MOPSO-TOPSIS for Case 6 of the OOV1G

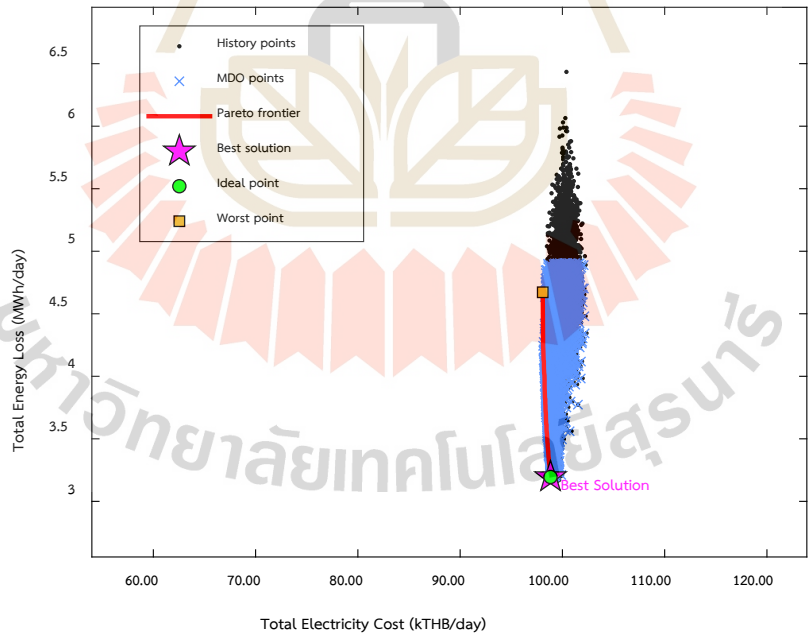

Figure 3.29 The results from MDO-MOPSO for Case 6 of the OOV1G

The closeness coefficient results from across 30 MDO-MOPSO-TOPSIS are illustrated in Figure 3.28. Figure 3.29 plots the MDO-MOPSO result along with the ideal and worst points on the Pareto front of the TOPSIS method. From Figure 3.29,

the history of fitness values evaluated during the MOPSO algorithm process, including optimal and suboptimal solutions, is represented by black points. The blue indicates the MDO solution set selected after post-processing analysis. The red line shows the Pareto front, representing the optimal trade-offs between electricity cost and energy loss. The ideal point, represented by a green circle on the Pareto front, refers to a hypothetical optimal solution where both objective functions, electricity cost and energy loss, achieve their minimum values simultaneously. Although such a point may not be practically attainable, it serves as a benchmark for evaluation. Conversely, the worst point, shown as an orange square, represents the solution with the highest values of both electricity cost and energy loss among all Pareto-optimal solutions. This point indicates the worst but is used as to reference for calculating the relative closeness of each alternative in the TOPSIS method. Figure 3.29 illustrates that the best solution selected by TOPSIS is located at the ideal point, demonstrating a good balance between minimizing electricity cost and energy loss. The simulation result for a combination of MOPSO and TOPSIS in solving the MCAL problem demonstrates effectiveness in maintaining the balance between conflicting objectives of solving the MOOV1G.

3.6.8 Case 7: Controlled EV Charging Devices Under Multi-Objective for Minimizing Electricity Cost and Peak Power Demand (MCAP)

Case 7 presents the results of the MOOV1G under the MCAP scenario, which focuses on minimizing electricity costs and peak power demand. The optimization problem was solved using the proposed MOPSO algorithm, combined with the TOPSIS for selecting the best solution from the Pareto front. This case was applied to a modified IEEE 33-bus distribution system with controlled EV charging devices. The MOPSO algorithm was tested for 30 trials, each generating a Pareto-optimal set. For each run, the TOPSIS method was applied in the post-processing phase to identify the best-compromised solution. The closeness coefficient calculated in TOPSIS was used to evaluate how close each Pareto solution was to the ideal solution.

Table 3.11 The result of 30 trials by MDO-MOPSO-TOPSIS for Case 7 of the OOV1G

MDO-MOPSO-TOPSIS method				Calculation
Result value	Closeness Coefficient	Electricity cost (kTHB/day)	Peak power demand (kW)	Energy loss (MWh/day)
Max	0.9965			
Avg.	0.9169	98.2912	1,223.3531	4.8091
Min	0.9169			

The simulation results are presented in Table 3.11, which shows the best, average, and worst closeness coefficient values obtained from the 30 trials for Case 7. Additionally, Table 3.11 shows the best objective function from the best solution. The best solution was selected based on the highest closeness coefficient of 0.9965, indicating high proximity to the ideal point and farthest from the worst point. The best solution obtained from the MDO-MOPSO-TOPSIS method across 30 trials demonstrates significant improvements in system performance. The electricity cost was reduced to 98.29128 kTHB/day, while the peak power demand decreased to 1,223.3531 kW, and the energy loss was 4.8091MWh/day.

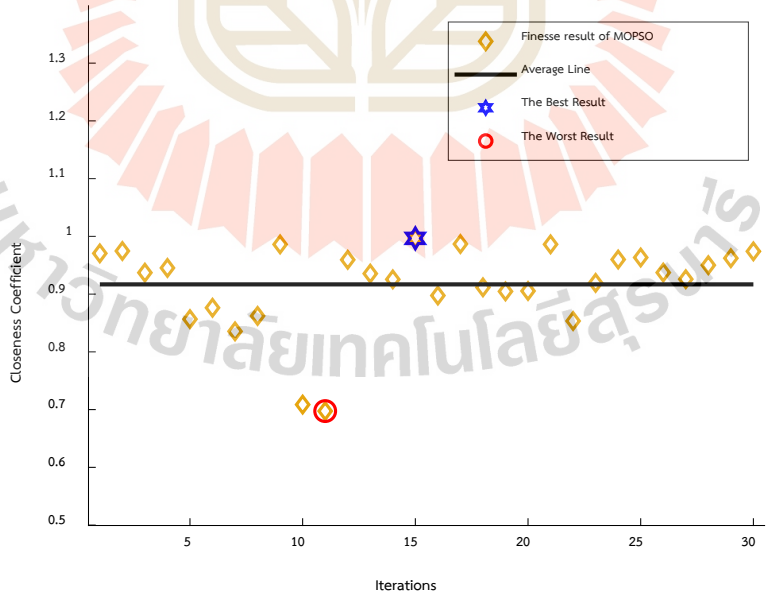

Figure 3.30 The closeness coefficient from 30 trials of MDO-MOPSO-TOPSIS for Case 7 of the OOV1G

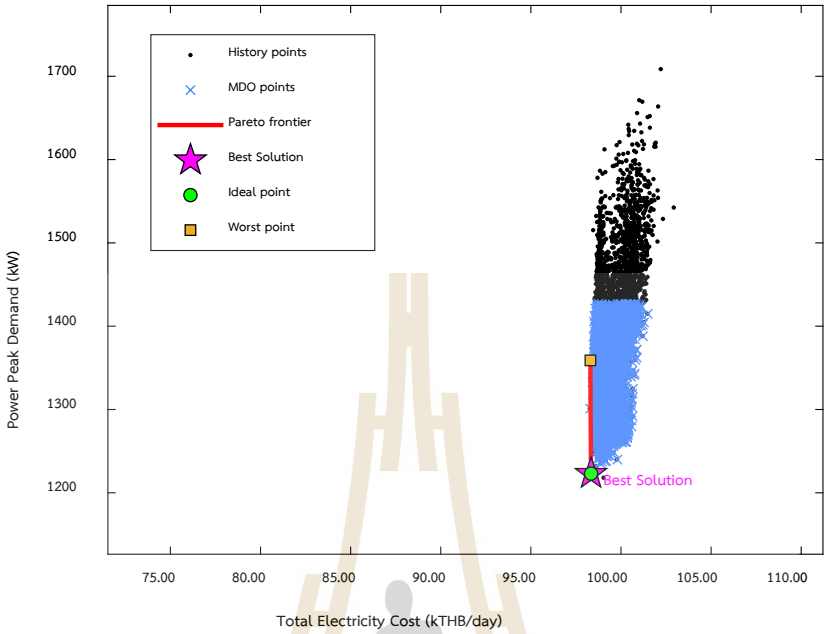

Figure 3.31 The results from MDO-MOPSO for Case 7 of the OOV1G

The closeness coefficient results from across 30 MDO-MOPSO-TOPSIS of Case 7 are illustrated in Figure 3.30. Figure 3.31 plots the MDO-MOPSO result along with the ideal and worst points on the Pareto front of the TOPSIS method. From Figure 3.31, the history of fitness values evaluated during the MOPSO algorithm process, including optimal and suboptimal solutions, is represented by black points. The blue indicates the MDO solution set selected after post-processing analysis. The red line shows the Pareto front, representing the optimal trade-offs between electricity cost and peak power demand. The ideal point, represented by a green circle on the Pareto front, refers to a hypothetical optimal solution where both objective functions, electricity cost and peak power demand, achieve their minimum values simultaneously. Although such a point may not be practically attainable, it serves as a benchmark for evaluation. Conversely, the worst point, shown as an orange square, represents the solution with the highest values of both electricity cost and peak power demand among all Pareto-optimal solutions. This point indicates the worst but is used as to reference for calculating the relative closeness of each alternative in the TOPSIS method. Figure 3.31 illustrates that the best solution selected by TOPSIS is located at the ideal point, demonstrating a good balance between minimizing electricity cost and peak power demand. The simulation result for a combination of MOPSO and TOPSIS

in solving the MCAP problem demonstrates effectiveness in maintaining the balance between conflicting objectives of solving the MOOV1G.

Table 3.12 and Figure 3.32 present the results of the operation of the V1G across six cases, with the modified IEEE 33-bus test distribution system integrating EV charging. The comparison in Table 3.13 clearly demonstrates the fundamental difference between single-objective and multi-objective optimization approaches, where the single-objective result used for comparison is from PSO. Since in the case of single-objective, PSO will give better results than GA. In the single-objective cases, Cases 3, 4, and 5 focus exclusively on MEC, MEL, and MPP, respectively. Focus exclusively on minimizing one specific objective without considering the impact on the other objectives. As a result, while the selected objective achieves its best possible value, the remaining objectives often have higher values. In contrast, the MOPSO-based multi-objective optimization seeks a balance between conflicting objectives. By simultaneously considering two objectives, MCAL or MCAP. The simulation results are in Figure. 3.33 compares the system load profiles, showing that the system with charging control under TOU pricing results in lower on-peak power demand, which helps reduce electricity cost and energy loss, as shown in Figures 3.34 and 3.35.

Table 3.12 Comparison results of the operation of V1G for OOV1G

Hours	Power consumption (kW)					
	Case 2	Case 3 (PSO)	Case 4 (PSO)	Case 5 (PSO)	Case 6 (MOPSO)	Case 7 (MOPSO)
1	0	192.45	249.12	318.38	240.47	232.87
2	0	358.18	133.43	320.16	152.94	400.87
3	0	355.15	194.65	213.03	364.42	348.27
4	0	345.52	191.65	88.99	147.45	207.45
5	0	349.27	217.11	326.63	214.90	302.25
6	0	346.22	435.98	313.04	409.42	406.89
7	0	319.41	739.68	325.11	737.26	266.05
8	0	0.00	0.00	0.00	0.00	0.00
9	0	0.00	0.00	0.00	0.00	0.00
10	0	0.00	0.00	0.00	0.00	0.00
11	0	0.00	0.00	0.00	0.00	0.00
12	0	0.00	0.00	0.00	0.00	0.00
13	0	0.00	0.00	0.00	0.00	0.00
14	0	0.00	0.00	0.00	0.00	0.00
15	0	0.00	0.00	0.00	0.00	0.00
16	0	0.00	0.00	0.00	0.00	0.00
17	0	0.00	0.00	0.00	0.00	0.00
18	332.445	74.00	368.64	351.15	147.45	230.53
19	740.00	74.00	112.43	166.51	147.45	125.69
20	740.00	74.00	92.50	74.00	147.45	82.74
21	740.00	74.00	81.08	90.74	147.45	82.74
22	740.00	182.05	162.91	223.35	147.45	106.38
23	96.015	357.63	195.49	239.78	189.67	284.58
24	0	286.64	213.82	337.62	194.71	311.17

Table 3.13 Comparison the objective function value of the IEEE 33-bus distribution system for OOV1G

The objective function value	Case Study					
	Case 2	Case 3 (PSO)	Case 4 (PSO)	Case 5 (PSO)	Case 6 (MOPSO)	Case 7 (MOPSO)
C_{ep}^{total} (kTHB)	105.6815	98.0490	99.2622	99.3561	99.0428	98.2912
E_{loss}^{total} (MW)	4.1049	5.2211	3.1716	5.1965	3.1967	4.8091
P_{daily}^{peak} (kW)	1,884.283	1,226.247	1,236.780	1,218.283	1,291.735	1,223.353

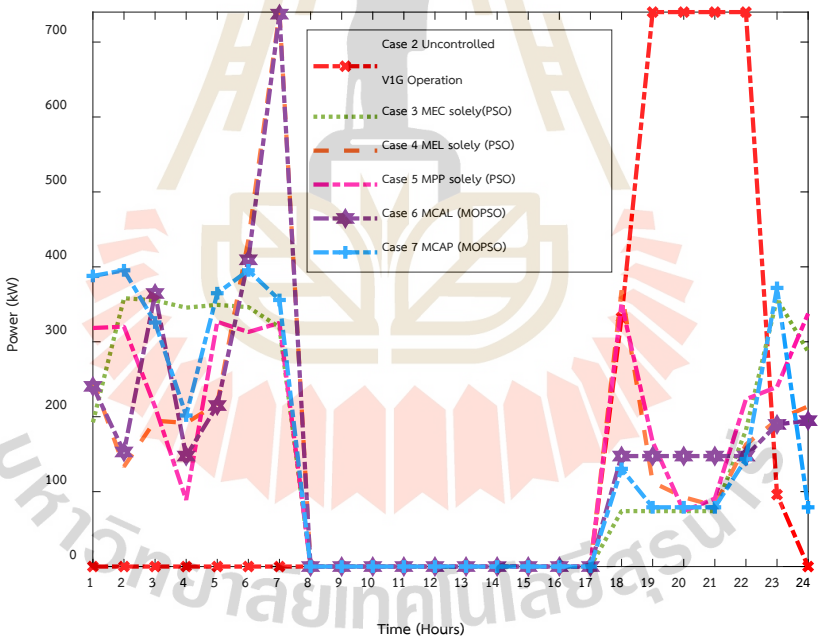

Figure 3.32 Comparison operation of the V1G

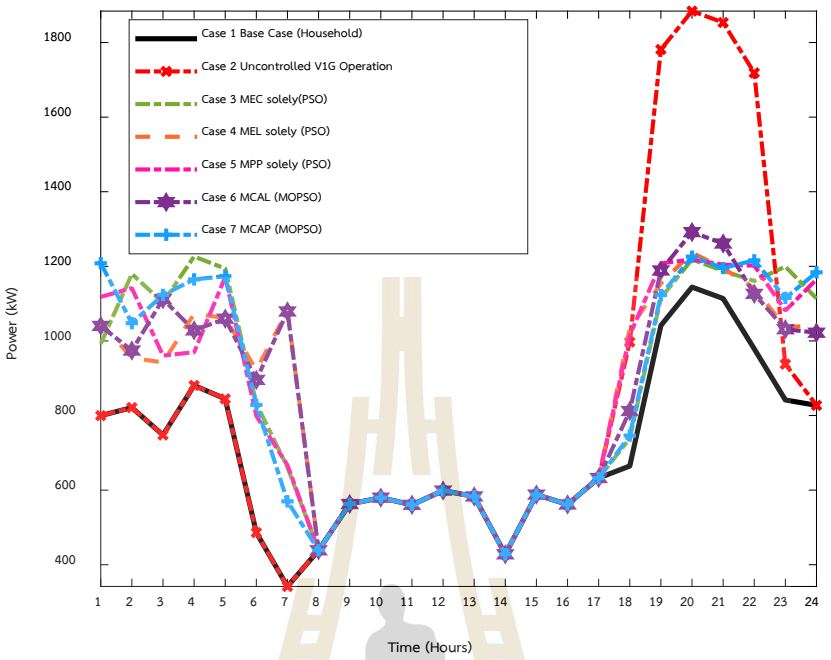

Figure 3.33 Comparison system load profile of the OOV1G

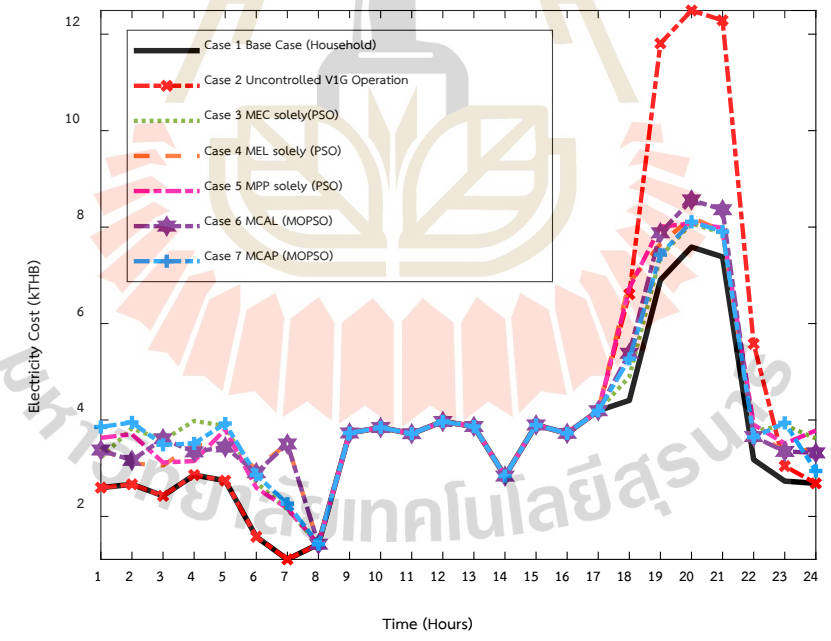

Figure 3.34 Comparison of electricity cost of the OOV1G

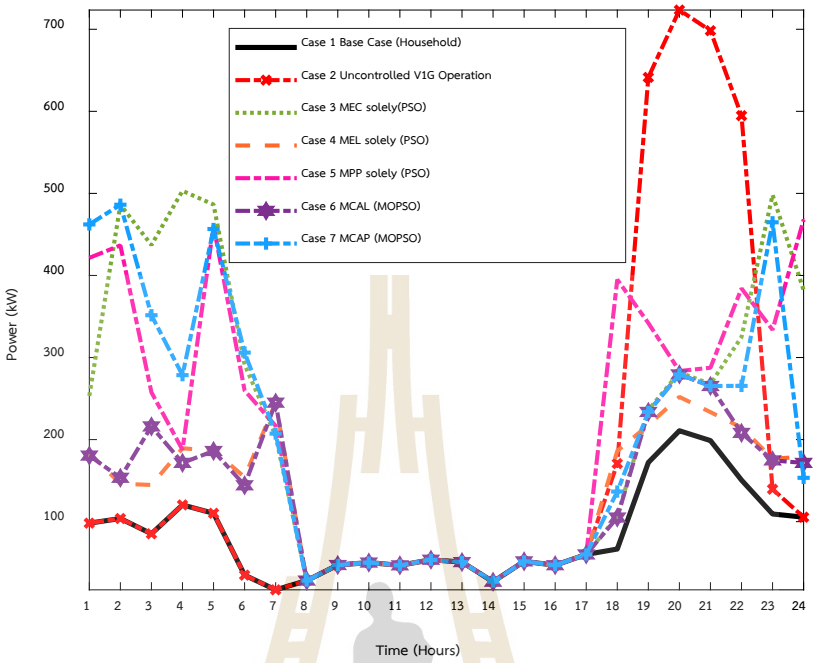

Figure 3.35 Comparison of energy loss of the OOV1G

Figure 3.32 presents the comparison of V1G operations over 24 hours for six cases. The graph shows that in the controlled cases, the proposed method effectively shifts EV charging to off-peak hours where household demand is low, unlike Case 2, where EV charging overlaps with household peak demand. In Cases 4 and 6, a noticeable new peak occurs around hour 7, which results from the system allocating EV charging to this hour due to lower household load. Nevertheless, Case 4 still achieves its objective by effectively reducing energy loss, and Case 6 reduces both energy loss and electricity cost in a balanced manner. Figure 3.33 presents the comparison of total system load profiles across seven cases, combining household load with EV charging demand. When comparing with Case 2, which represents the total load of uncontrolled EV charging combined with household demand, it is clear that the cases with controlled V1G operation significantly reduce the peak power demand of the system. The proposed optimal scheduling effectively shifts EV charging away from household peak demand periods and toward off-peak hours.

The hourly electricity costs for each case are shown in Figure 3.34. The results reveal that in all cases where EV charging is controlled, the total electricity cost of the system is reduced when compared with Case 2. The cost reduction is particularly

evident during peak hours, while a slight increase in cost is observed during off-peak periods due to the shifting of EV charging to lower-cost time intervals. Nevertheless, the total electricity cost in the optimized cases remains higher than that of Case 1 during hours 18-21 due to the modeling constraint that EVs are allowed to charge only at home. This restriction limits the ability to eliminate peak-time consumption, although the scheduling remains aligned with the intended objectives. Figure 3.35 illustrates the hourly energy loss for each case. Among all scenarios, Case 4 achieves the most significant reduction in power losses, followed closely by Case 6, which balances the minimization of both electricity cost and loss. The results confirm that the proposed optimal V1G scheduling is effective in reducing system losses across all controlled cases when compared to the uncontrolled EV charging scenario. The result highlights the advantages of coordinated EV charging in mitigating the adverse effects on distribution system performance.

CHAPTER IV

OPTIMAL OPERATION OF V2G

4.1 Introduction

The unidirectional charging has been widely studied for handling the increasing integration of large-scale EVs into distribution systems, and the implementation of vehicle-to-grid (V2G) technology is emerging as a promising solution to enhance grid flexibility and address the issues arising from large-scale EV charging connections. The bidirectional power flow operation of V2G enables EVs to not only charge energy from the grid but also discharge stored energy back into the system. When the operation of V2G is optimally managed, it can use to distribute energy storage, support renewable energy integration, and reduce peak demand in both transmission and distribution systems. However, the bidirectional nature of V2G introduces new operational challenges. The discharging of EVs back to the grid can increase the total power flow and the overall system losses. For the highest benefits, it is crucial to consider the impact on system losses and peak power demand in the optimization process alongside electricity cost reduction.

This chapter presents the optimal operation of V2G (OOV2G) is investigated using a methodology similar to that presented in Chapter III. The multi-objective optimum operation of V2G (MOOV2G) is formulated to simultaneously minimize electricity cost and energy loss (MCAL), as well as electricity cost and peak power demand (MCAP). The MOOV2G problem will use a multi-objective particle swarm optimization (MOPSO) algorithm combined with the technique for order preference by similarity to ideal solution (TOPSIS) to identify the most balanced solution among multiple conflicting objectives. While the particle swarm optimization (PSO) and genetic algorithm (GA) are used to solve the single-objective optimization for minimizing electricity cost (MEC), energy loss (MEL), and peak power demand (MPP) for comparison. The proposed approach is tested on the IEEE 33-bus distribution test

system, incorporating a Monte Carlo simulation (MCS) to model the uncertainty in EV user behavior and generate probabilistic EV charging and discharging profiles. The results and discussion in this chapter demonstrate the effectiveness of the multi-objective particle swarm optimization combined with the technique for order of preference by similarity to Ideal solution (MOPSO-TOPSIS) method for solving MOOV2G problems in enhancing grid flexibility and supporting renewable integration.

4.2 Problem Introductions

The formulation of the OOV2G follows a similar framework to that of Chapter III. The OOV2G escalates from the framework established in the previous chapter for V1G, with several key extensions to accommodate the bidirectional nature of V2G. In this chapter, the OOV2G problem aims to determine the optimal charging and discharging schedules for EVs. The TOU tariff is used for both charging and discharging operations. While simulating uncontrolled scenarios using the MCS for the stochastic modeling of EV user behavior.

4.2.1 Time of Use (TOU) Tariff for V2G

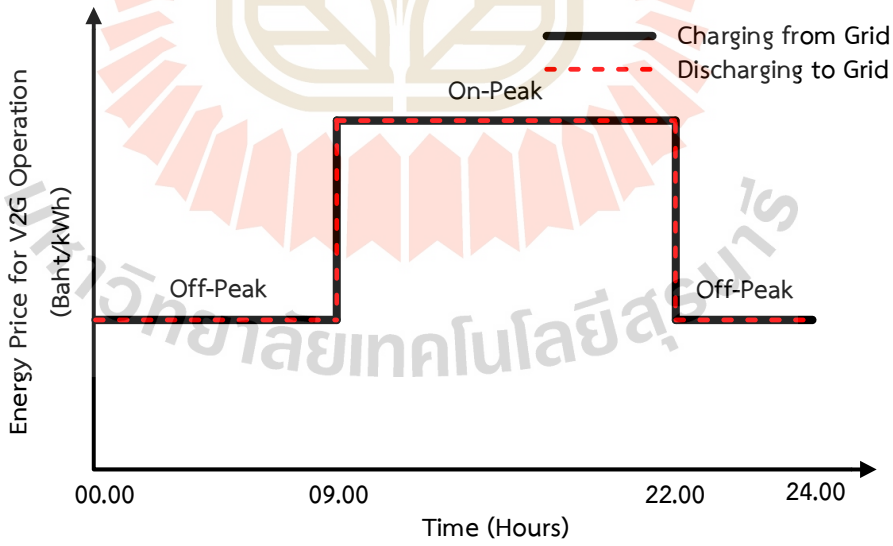

Figure 4.1 TOU Tariff Pattern for V2G Operation

The V2G operation applies the TOU tariff scheme to both charging and discharging operations to solve the OOV2G problem. The TOU tariff reflects the variation in electricity prices throughout the day, encouraging users to shift their energy

consumption and injection according to grid demand. As illustrated in Figure 3.1, the TOU tariff is divided into two main periods: on-peak and off-peak. The on-peak period, typically from 09:00 to 22:00, is characterized by higher electricity prices due to increased demand. Conversely, the off-peak period from 22:00 to 09:00 features lower prices to incentivize energy use and grid support during times of lower demand.

4.2.2 Monte Carlo Simulation (MCS) for Modeling EV Users' Behavior

This chapter applies the same MCS framework as introduced in Section 3.2.2. to account for the uncertainty of EV user behavior in the V2G operation. The MCS is used for the stochastic modeling of EV user behavior to generate realistic and probabilistic EV load profiles for the base case scenario, where no optimal scheduling is applied. The random variables considered in the MCS include the departure time from home (T_{edr}), travel duration to work (T_{htw}), return duration from work to home (T_{ebh}), and the duration that EVs remain parked at the workplace connected to the grid (T_{eop}). Each of the random variables uses the truncated normal distribution to ensure that the sampled values remain within realistic and practical bounds. The mathematical form of the truncated normal distribution and the Weibull distribution used in this thesis is as follows in Equations (3.1) and (3.32), respectively.

The random variables are used to model the EV usage activities as represented in Equations (4.1) - (4.6). The resulting probabilistic EV activities from the MCS are used as input data for the operation of V2G modeling.

$$\mathbf{ATV}_{\mathbf{day}}^{\mathbf{n}} = [\mathbf{ATV}_1 + \mathbf{ATV}_2 + \mathbf{ATV}_3 + \mathbf{ATV}_4 + \mathbf{ATV}_5], \tag{4.1}$$

$$ATV_1^n = \{1 : T_{edr}^n \text{-} 1\}, \tag{4.2}$$

$$ATV_2^n = \{T_{edr}^n : T_{edr}^n + T_{htw}^n\}, \tag{4.3}$$

$$ATV_3^n = \{T_{edr}^n + T_{htw}^n + 1 : T_{edr}^n + T_{htw}^n + T_{eop}^n\}, \tag{4.4}$$

$$ATV_4^n = \{T_{edr}^n + T_{htw}^n + T_{eop}^n + 1 : T_{edr}^n + T_{htw}^n + T_{eop}^n + T_{ebh}^n\}, \tag{4.5}$$

$$ATV_5^n = \{T_{edr}^n + T_{htw}^n + T_{eop}^n + T_{ebh}^n + 1 : np\}, \tag{4.6}$$

Where, $n = 1, \ldots, NC$ and $t = 1, \ldots, np$.

4.2.3 Operation of V2G Modeling

The modeling of the V2G operation in this chapter is adapted and enhanced based on the work of Pia Grahn (2013), as described in section 3.2.3 in Chapter III. Based on the results generated from the MCS of daily EV usage patterns, the modeled activities are used to simulate EV behavior and generate realistic EV charging load profiles. To increase the flexibility of the simulation, the initial state of charge (SOC_0) is defined using a parameter called the percentage of the total state of charge ($psoc$), which represents the initial SOC relative to the battery's maximum capacity. Furthermore, it is assumed that the SOC at each time step is limited by a minimum depth of discharge (DOD), represented by the fraction p_{dod} These constraints are applied as shown in Equations (4.7) and (4.8).

$$SOC_0^n = psoc \times SOC_{\max}^n \tag{4.7}$$

$$p_{dod}\, SOC_{\min}^n \le SOC_t^n \le SOC_{\max}^n \tag{4.8}$$

The level of SOC varies dynamically according to the activities of EV usage under V2G operation. This thesis assumes that EV charging occurs exclusively when the EV parked at home, and discharging occurs exclusively when the EV parked at the workplace. Therefore, the SOC increases when the EV is charged at home locations only and decreases when the EV discharges power back to the grid at the workplace or is being driven. During time steps when the EV is parked without charging or discharging, the SOC remains constant. Specifically, for each time step, the SOC increases based on the charging power, decreases according to the energy discharged to the grid or consumed during driving, and remains unchanged during idle periods. These changes in SOC are computed as shown in Equation (4.9).

$$SOC_{t+1}^n = \begin{cases} SOC_t^n + P_{chg}\Delta t & , \quad \text{for charging mode} \\ SOC_t^n - P_{dchg}\Delta t & , \quad \text{for discharging mode} \\ SOC_t^n - C^t\Delta t & , \quad \text{for driving mode} \\ SOC_t^n & , \quad \text{else} \end{cases} \tag{4.9}$$

Where, $n = 1,\ldots,NC$ and $t = 1,\ldots,np$.

The EV load profile for V2G operation $P_{v2G,i,t}^n$ will be equal to or dependent on P_{chg} and P_{dchg} following the vehicle usage activities at that time, as

shown in Equation (4.10). The total V2G operation load profile is determined by summing both the charging and discharging loads of all EVs, as follows in Equation (4.11).

$$P^{n}_{V2G,i,t} = \begin{cases} P_{chg} & , \text{ for charging mode} \\ P_{dchg} & , \text{ for discharging mode} \\ 0 & , \text{ else} \end{cases} \tag{4.10}$$

$$P^{total}_{V2G,i,t} = \sum_{n=1}^{NC} P^{n}_{V2G,i,t} \tag{4.11}$$

Where, $n = 1,\ldots,NC$ and $t = 1,\ldots,np$.

The power EV $P^{n}_{v2G,i,t}$ must be considered hourly in the data analysis. The outcome of changing and discharging the time step from one minute to one hour is displayed in Eq. (4.12).

$$P^{total}_{V2G,i,h} = \sum_{n=1}^{NC} P^{n}_{V2G,i,h} \tag{4.12}$$

Where, $n = 1,\ldots,NC$ and $t = 1,\ldots,np$.

4.3 Objective Function

The OOV2G is formulated as an optimization problem to enhance power system performance while minimizing the negative impacts of increasing EV integration. While in the OOV1G case, EVs only charge power from the grid for charging. The OOV2G will consider the bidirectional power flow of EVs, allowing both charging and discharging on the grid. To ensure that the solution adheres to system limitations, particularly the total daily energy required and variable bounds, a penalty function is applied in the same manner as the OOV1G formulation in Chapter 3. The penalty term is added to the original objective function when constraint violations occur. This ensures that any infeasible solution is penalized, guiding the search toward feasible and optimal results. The penalty-based formulation for OOV2G is expressed in Equation (4.13), which incorporates both bound constraints and energy equality constraints into the optimization model.

$$PN(P_{V2G,i}) = a_1 \sum_{h=1}^{24} \left[\max(0, P_{V2G,i}^h - ub^h) + \max(0, lb^h - P_{V2G,i}^h) \right] + a_2 \left| \sum_{h=1}^{24} P_{V2G,i}^h - T \right| \quad (4.13)$$

This thesis considers three objective functions as follows.

4.3.1 Total electricity cost minimization

The first objective function is to minimize the daily electricity cost incurred from EV charging and discharging under a TOU tariff structure. In this OOV2G, the same TOU tariff rates are used for charging from the grid and discharging to the grid. The mathematical of the objective function is as follows in Equation (4.14).

$$\text{Minimize } C_{ep}^{total} = \sum_{h=1}^{24} C_{ep}^h + PN \quad (4.14)$$

Where the hourly electricity cost can be calculated by:

$$C_{ep}^h = \sum_i^{NB} C_{en,i}^h + C_{Ft,i}^h + C_{vat,i}^h \quad (4.15)$$

$$C_{en,i}^h = (P_{hh,i}^h + P_{V2G,i}^h) \times r_{tou}^h \quad (4.16)$$

$$C_{Ft,i}^h = (P_{hh,i}^h + P_{V2G,i}^h) \times Ft \quad (4.17)$$

$$C_{vat,i}^h = \left(C_{en,i}^h + C_{Ft,i}^h \right) \times VAT \quad (4.18)$$

Where, $i = 1, \ldots, NB$ and $h = 1, \ldots, 24$.

4.3.2 Total energy loss minimization

The second objective function of the proposed problem is to minimize the energy losses in distribution systems. This objective function can be expressed as below:

$$\text{Minimize } E_{loss}^{total} = \sum_{h=1}^{24} P_{loss}^h + PN \ , \quad (4.19)$$

Where the hourly loss can be calculated by:

$$P_{loss}^h = \sum_{i=1}^{NB} (P_{G,i}^h - P_{D,i}^h) \ , \quad (4.20)$$

$$P_{D,i}^h = P_{hh,i}^h + P_{V2G,i}^h \ , \quad (4.21)$$

$$P_{loss}^{h} = V_i \sum_{j=1}^{NB} V_j [G_{ij} \cos(\delta_i - \delta_j) + B_{ij} \sin(\delta_i - \delta_j)] , \quad (4.22)$$

Where, $i = 1,\ldots,NB$ and $h = 1,\ldots,24$.

4.3.3 Peak power demand minimization

The last objective function is to minimize the peak power demand, as shown in Equation (4.23). For the OOV2G, this objective aims to reduce the peak power demand by defining optimized charging and discharging operations of EVs. The leveraging of bidirectional power flow used in V2G will enable EVs to discharge energy back to the grid during peak periods.

$$\text{Minimize} \quad P_{daily}^{peak} = \max_{h \in \{1,2,\ldots,24\}} \{P_{hh}^{h} + \sum_{i=1}^{NC} (P_{V2G,i}^{h})\} + PN \quad (4.23)$$

Where, $i = 1,\ldots,NB$ and $h = 1,\ldots,24$.

4.4 Constrains

This chapter focuses on managing the increasing electricity demand resulting from EV charging by solving the MOOV2G time. In addressing this MOOV2G issue, solve under two optimization scenarios, MCAL and MCAP. This study applies both equality and inequality constraints, as described as follows.

4.4.1 Equality constrains

Constraints on MOOV2G in distribution systems following the MCS of EV user behavior are increased when operating V2G. This thesis assumes that EV charging occurs only when the EV is at home, and discharging is allowed only when the EV is parked at the workplace. Therefore, the condition when the EV is on the grid at home follows Equation (4.24). When the EV is on the grid at the workplace, the condition follows Equation (4.25). Moreover, in the case where the EV is off-grid, the power of V2G is set to zero, as shown in Equation (4.26).

$$(\sum_{n=1}^{NC} P_{dchg,i,n}^{h}) \le P_{V2G,i}^{h,on} \le (\sum_{n=1}^{NC} P_{chg,i,n}^{h}) , \quad \text{if at home} \quad (4.24)$$

$$(\sum_{n=1}^{NC} P_{dchg,i,n}^{h}) \le P_{V2G,i}^{h,on} \le 0 , \quad \text{if at a parking lot at work} \quad (4.25)$$

$$P_{V2G,i}^{h,off} = 0 \quad , \tag{4.26}$$

Where, $i = 1,\ldots,NB$, $n = 1,\ldots,NC$ and $h = 1,\ldots,24$.

The equality constraints, which represent the load flow equations, are as follows:

$$P_{Gi} - P_{Di} - V_i \sum_{j=1}^{NB} V_j [G_{ij} \cos(\delta_i - \delta_j) + B_{ij} \sin(\delta_i - \delta_j)] = 0 \tag{4.27}$$

$$Q_{Gi} - Q_{Di} - V_i \sum_{j=1}^{NB} V_j [G_{ij} \sin(\delta_i - \delta_j) - B_{ij} \cos(\delta_i - \delta_j)] = 0 \tag{4.28}$$

Where, $i = 1,\ldots,NB$, $n = 1,\ldots,NC$ and $h = 1,\ldots,24$.

4.4.2 Inequality constraints

The inequality constraints establish the system's operational bound, as follows. Generator constraints, including voltage, active power, and reactive power at the i^{th} bus, are restricted between their upper and lower bound, as shown:

$$\begin{aligned} |V_{Gi}|^{\min} \le |V_{Gi}| \le |V_{Gi}|^{\max} \\ |P_{Gi}|^{\min} \le |P_{Gi}| \le |P_{Gi}|^{\max} \\ |Q_{Gi}|^{\min} \le |Q_{Gi}| \le |Q_{Gi}|^{\max} \end{aligned} \quad , \tag{4.29}$$

and line flow constraints,

$$f_l \le f_l^{\max} \tag{4.30}$$

4.5 Multi-objective optimum operation of V2G (MOOV2G) Using MOPSO

The MOOV2G, which aims to optimize multiple objectives, this thesis presents the application of MOPSO to solve the MOOV2G problem. The optimization aims to achieve a trade-off between conflicting objectives by generating a Pareto front of non-dominated solutions. Moreover, to select the best solution from the Pareto set, the technique for order of preference by similarity to ideal solution (TOPSIS) method is employed. The fundamentals of Pareto dominance, the structure of the MOPSO

algorithm, and the integration of TOPSIS as a post-processing method. The methodology is explained in detail in Section 3.5 of Chapter III. However, this chapter applied the MOPSO to the V2G case, utilizing the corresponding V2G model and equations.

4.5.1 Basic Concept of Pareto Dominance

In MOOV2G for both minimizing electricity cost and energy loss (MCAL) and minimizing electricity cost and peak power demand (MCAP), the Pareto dominance is utilized to identify solutions that best balance the trade-offs between conflicting objectives. The basic concept of Pareto dominance is explained in Section 3.5.1 of Chapter III. In this chapter, Pareto dominance is applied to the MOOV2G problem to construct the Pareto front, which represents a set of non-dominated solutions. The process of the Pareto front before applying the MOPSO for MOOV2G is described as follows:

Step 1 Initial population creation: A set of potential solutions is generated randomly using the particle swarm optimization (PSO) algorithm. In this thesis, the population matrix of the power V2G each hour is shown in Eq. (4.31).

$$P_{V2G,i} = [P^1_{V2G,i},\ P^2_{V2G,i},\ ...,\ P^h_{V2G,i}], \tag{4.31}$$

Where, $h = 1,\ldots,24$.

Step 2 Objective functions evaluation: From multiple objective functions $\text{Minimize} : \{f_1(x), f_2(x)\}$, where $f_1(x)$ is the first objective function and $f_2(x)$ is the second objective function. x is a set of potential solutions of objective function following Equation (4.31). Two comprehensive multi-objective frameworks are considered in this thesis.

Scenario 1 solves the MOOV2G problem for MCAL. For this scenario, the first objective function $f_{1,MCAL}(P_{V2G,i})$ is to minimize electricity costs following Equation (4.14) and $f_{2,MCAL}(P_{V2G,i})$ is the second objective function to minimize energy losses following Equation (4.19). The multiple objective functions to MOOV2G for MCAL, as shown in Equation (4.32).

$$\text{Minimize} : \{f_{1,MCAL}(P_{V2G,i}), f_{2,MCAL}(P_{V2G,i})\} \tag{4.32}$$

Scenario 2 solves the MOOV1G problem for MCAP. For this scenario, the first objective function $f_{1,MCAP}(P_{V2G,i})$ is to minimize electricity costs following Equation (4.14) and $f_{2,MCAP}(P_{V2G,i})$ is the second objective function to minimize peak power demand following Equation (4.23). The multiple objective functions to MOOV2G for MCAP, as shown in Equation (4.33).

$$\text{Minimize}: \left\{f_{1,MCAP}(P_{V2G,i}), f_{2,MCAP}(P_{V2G,i})\right\} \quad (4.33)$$

Each solution (fitness values for each particle) is evaluated using multiple objectives to calculate the objective function, which will be used for comparison in the next step.

Step 3 Pareto dominance: In this step, the Pareto dominance is applied to compare the results from solving the MOO problem. Specifically, if one solution performs better than another in all objectives, it is said to dominate the other. Conversely, a solution that is non-dominated by any other solution is considered a Pareto optimal solution or lies on the Pareto front.

Step 4 Pareto front: All the Pareto optimal solutions will be used to construct the Pareto front. These solutions represent a balance between the conflicting objectives. MOPSO refines the population of Pareto optimal solutions by using PSO to discover better solutions and then recalculates Pareto dominance to identify any new optimal solutions until the specified convergence criteria are reached.

4.5.2 MOPSO Algorithm

MOPSO is maintaining the fundamental principles of PSO while incorporating the core concept of Pareto dominance to manage MOO. Therefore, in each iteration, the equations for velocity and position updates remain as defined in Equations (4.34) and (4.35), respectively. This thesis, w the inertia weight. c_1 and c_2 are acceleration coefficients (cognitive and learning factors). r_1 and r_2 are random numbers uniformly distributed between [0,1].

$$V_{i,t+1} = wV_{i,t} + c_1 r_1 (x_{i,t}^{Pbest} - x_{i,t}) + c_2 r_2 (x_{i,t}^{Gbest}{}_{i,t} - x_{i,t}) \quad (4.34)$$

$$x_{i,t+1} = x_{i,t} + V_{i,t+1} \quad (4.35)$$

The operation of MOPSO for MOOV2G is an optimization method that extends the classical PSO to handle multiple objectives, which is inspired by the behavior of bird flocks. MOPSO focuses on finding optimal operation of V2G solutions that balance multiple objectives. This process is combined with the concept of the Pareto front. It is initialed by randomly positioned particles in the search space. Each particle i in the swarm represents a potential solution to the optimal V2G operation scheduling problem. In this thesis, the evaluation of each particle depends on the specific multi-objective scenario being considered. Under two optimization scenarios, the first is MCAL, and the second is MCAP. Accordingly, each particle is evaluated based on a pair of objective functions corresponding to the selected scenario. In the MCAL case, particles are evaluated with the objectives of minimizing electricity cost (MEC) and energy loss (MEL). In the MCAP case, the objectives are minimizing electricity cost (MEC) and peak power demand (MPP). The process then improves with each iteration t by updating the velocity ($V_{i,t}$) and position ($x_{i,t}$)of the particles according to the Equations (4.34) and (4.35), while recording the best position of each particle ($x_{i,t}^{Pbest}$). If a new position is better than the position best, the new position replaces it. The $x_{i,t}^{Gbest}$ is the best position among all particles in the swarm. The main goal of MOPSO is to find Pareto optimal solutions that form the Pareto front. Therefore, the update process considers Pareto dominance to help filter out non-dominated solutions and construct the Pareto front with each iteration until the specified convergence criteria are reached.

The MOPSO algorithm has been developed in H. Wang, et al. (2023) and is called multiple design options-MOPSO (MDO-MOPSO). In this research, the MDO-MOPSO algorithm has adapted to suit the specific characteristics of the problem in this article while still considering the spread of the mean of the crowding distances (quand mean) as convergence criteria according to Equations. (4.36) and (4.37). Fig. 3.3 illustrates the methodology of the MDO-MOPSO algorithm.

$$spread = \frac{\mu + \sigma}{\mu + Q\bar{d}} \tag{4.36}$$

$$quand\ mean = \sqrt{\frac{1}{Q}\sum_{k}\bar{d}_k^2} \tag{4.37}$$

Where μ is the parameter, it quantifies whether the extreme values of the Pareto front have changed between two consecutive iterations. σ and $\overline{d}$ are the standard deviation and the arithmetical average of the crowding distances of point k, and Q is the number of points on the Pareto front.

The iterative process stops when one of the three conditions is met, including limits on iterations and convergence metrics. The modified MOPSO algorithm also incorporates performance metrics and a post-processing phase for identifying MDO (Most Desirable Option) solutions. The detailed procedures of this algorithm, including stopping criteria and post-processing steps, are described in section 3.5.2 of Chapter III.

4.5.3 TOPSIS method

TOPSIS is the final step after obtaining the Pareto front, it is used to select the best compromise solution from the set of Pareto-optimal solutions. For this chapter, TOPSIS is applied during the post-processing phase to identify the best compromise solution from the Pareto frontier obtained from solving the MOOV2G. The detailed procedures of TOPSIS method are described in section 3.5.3 of Chapter III. Figure 4.2 illustrates the methodology of the MDO-MOPSO-TOPSIS algorithm for MOOV2G. The TOPSIS method consists of the following steps:

Step 1: Construct the normalized decision matrix. The decision matrix consists of the objective function values of all non-dominated solutions (MDO points) obtained from the Pareto front generated by the MOPSO algorithm. The decision matrix is of MCAL and MCAP scenarios shown following Equations (4.38) and (439), respectively. To eliminate the effects of differing units and scales among the objectives, the objective values in the decision matrix are normalized using the vector normalization method, as shown in equation (4.40).

$$X_{decision} = \left[x_{kf} \right]_{k=1,\ldots,a.\ f=1,2.} = \left[f_{1,MCAL}(P_{V2G,i,k}) \;\; f_{2,MCAL}(P_{V2G,i,k}) \right]_{k=1,\ldots,a.} \tag{4.38}$$

$$X_{decision} = \left[x_{kf} \right]_{k=1,\ldots,a.\ f=1,2.} = \left[f_{1,MCAP}(P_{V2G,i,k}) \;\; f_{2,MCAP}(P_{V2G,i,k}) \right]_{k=1,\ldots,a.} \tag{4.39}$$

$$r_{kf} = \frac{x_{kf}}{\sqrt{\sum_{k=1}^{a} x_{kf}^2}} \tag{4.40}$$

Where, $k=1,\ldots,a.$ and $f=1,2.$ k is the number of solutions on the Pareto front, and a is the total number of solutions on the Pareto front. f is the number of objective functions.

Step 2: Weighted normalized decision matrix. Following this thesis, focus on balancing both the objective functions. Therefore, equal weights are assigned to all objectives in the TOPSIS process. The weighted normalized decision matrix equation is as follows:

$$v_{kf} = w_f \cdot r_{kf} \tag{4.41}$$

Where, $k=1,\ldots,a.$, $f=1,2.$

Step 3: Determine the ideal and negative-ideal solutions. For minimization problems, the ideal solution (v_f^+) is the minimum value of each objective function, while the negative-ideal solution (v_f^-) is the maximum value of each objective function . These are calculated using equations (4.42) and (4.43), respectively.

$$v_f^+ = \min(v_{kf}) \tag{4.42}$$

$$v_f^- = \max(v_{kf}) \tag{4.43}$$

Where, $k=1,\ldots,a.$, $f=1,2.$

Step 4: Calculate the distance to the ideal and worst solutions. D_k^+ is the distance from the weighted normalized value of each alternative to the ideal solution. D_k^- is the distance from the weighted normalized value of each alternative to the worst solution. The calculation follows in Equations (4.44) and (4.45)

$$D_k^+ = \sqrt{\sum_{k=1}^{a}\left(v_{fk} - v_f^+\right)^2} \tag{4.44}$$

$$D_k^- = \sqrt{\sum_{k=1}^{a}\left(v_{fk} - v_f^-\right)^2} \tag{4.45}$$

Where, $k=1,\ldots,a.$, $f=1,2.$

Step 5: Calculate the closeness coefficient (C_k). The alternative with the highest C_k is considered the best compromise solution among all Pareto-optimal solutions. Calculating C_k follows the Equation (4.46).

$$C_k = \frac{D_k^-}{D_k^+ + D_k^-} \tag{4.46}$$

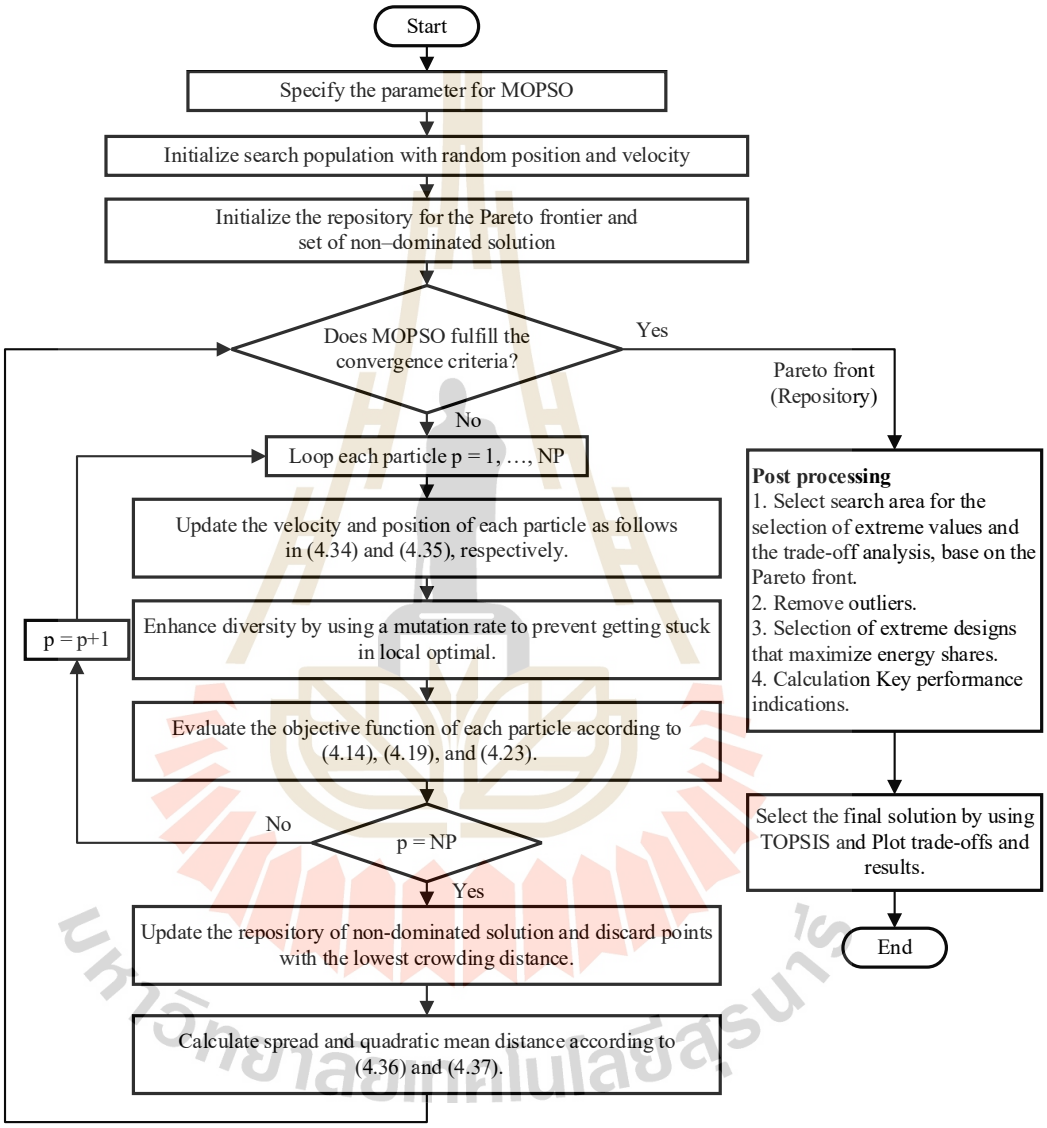

Figure 4.2 The MDO-MOPSO-TOPSIS methodology of MOOV2G

4.6 Simulation Results

This section presents the simulation results for the optimal operation of V2G (OOV2G) in the modified IEEE 33-bus distribution test system with integrated EV load

profiles generated by MCS. This chapter focuses on solving MOOV2G using the MOPSO-TOPSIS method under the TOU tariff. The analysis is structured into several cases to comprehensively evaluate the impact of EV charging under different control approaches and optimization objectives. The simulation results have seven cases as follows:

Case 1: Base Case Without EV Charging Devices.

Case 2: Uncontrolled EV Charging Devices in The Modified IEEE 33-Bus Distribution System.

Case 3: Controlled V2G Operation in The Modified IEEE 33-bus Distribution System Under Single Objective for Minimizing Electricity Costs (MEC).

Case 4: Controlled V2G Operation Under Single Objective for Minimizing Energy Losses (MEL).

Case 5: Controlled V2G Operation Under Single Objective for Minimizing Peak Power Demand (MPP).

Case 6: Controlled V2G Operation Under Multi-Objective for Minimizing Electricity Cost and Energy Losses (MCAL).

Case 7: Controlled V2G Operation Under Multi-Objective for Minimizing Electricity Cost and Peak Power Demand (MCAP).

4.6.1 Sensitivity Analysis of MOPSO Parameters

This section presents a sensitivity analysis of the main parameters of the MOPSO algorithm used to solve the MOOV2G problem under the scenario of minimizing electricity cost and peak power demand (MCAP). The purpose of this analysis is to verify the appropriateness of the parameter values selected in this study.

The parameters analyzed three important fundamental components of the PSO algorithm, including the inertia weight (*w*), cognitive learning factor (c_1), and social learning factor (c_2). The verification parameter is conducted in two parts. The first varying w while keeping c_1 and c_2 fixed. The second is varying c_1 and c_2 while keeping w fixed. Additionally, the random numbers (r) used in the velocity update formula are generated from a uniform distribution in the range [0, 1]. The performance of each parameter setting is evaluated based on four, including the closeness

coefficient (from TOPSIS), electricity cost, peak power demand, and run time. The results of these experiments are summarized in Table 4.1.

Table 4.1 Summary of MOPSO parameter varying results

Value	Parameter varying						
	varying *w*			varying c_1 and c_2			
w	0.1	0.4	1	0.4			
c_1	1			1	2	1	2
c_2	1			1	2	2	1
Result of varying							
Closeness Coefficient	0.8014	0.8091	0.8063	0.8091	0.8009	0.7744	0.7947
Cost (kTHB/day)	88.708	90.355	88.252	90.355	92.087	90.973	91.347
Peak (kW)	1,481.2	1,374.1	1,457.7	1,374.1	1,364.2	1,392.3	1,366.4
Run time (s)	120.819	221.081	149.302	221.081	112.012	178.744	197.583

According to Table 4.1, w = 0.4, c_1 = 1, and c_2 = 1 result in the best overall performance. This configuration had the highest closeness coefficient is 0.8091, indicating that the selected solutions are closest to the ideal point on the Pareto front. Furthermore, the differences in performance metrics across the various parameter combinations are relatively small. The closeness coefficients and objective values do not vary significantly, suggesting that the MOPSO algorithm is robust to moderate changes in these parameters within the tested range. Therefore, this thesis adopts the parameter set w = 0.4, c_1 = 1, and c_2 = 1 for the MOOV2G and MOOV1G problems. For the single-objective optimization cases using PSO and GA, the default parameter settings of each algorithm are adopted to ensure a fair and consistent comparison. The parameter values used in this thesis are summarized in Table 4.2.

Table 4.2 Parameter settings

Parameter value	Algorithm		
	MOPSOP	PSO	GA
w	0.4	0.1-1	0.1-1
c_1	1	1.49	1.49
c_2	1	1.49	1.49
r	[0, 1]	[0, 1]	[0, 1]
Population size	500	100	100
Iterations	100	600	600
Function tolerance	$<10^{-6}$	$<10^{-6}$	$<10^{-6}$

4.6.2 Input Parameter

For the OOV2G in this chapter, the same IEEE 33-bus distribution test system and the modified IEEE 33-bus distribution test system as used in Chapter III for OOV1G are adopted. The IEEE 33-bus distribution test system and the modified IEEE 33-bus distribution test system are shown in Figures 3.4 and 3.5, respectively. The modified IEEE 33-bus distribution test system by integrating EVs at each bus, excluding bus number 1 (the slack bus). The modified IEEE 33-bus distribution system, by incorporating EV charging applied in simulation study cases to solve the OOV2G problem in different control approaches and optimization objectives.

In MCS, probability distributions are used to generate random variables. The random variables considered in MCS relate to the averages and standard deviations of the uncertain variables, as displayed in Table 3.1 and the Weibull distribution parameter displayed in Table 3.2. Parameters used for generating the EV load profile in the uncontrolled case, as shown in Table 3.3. For the calculation of electricity costs in this thesis, use the TOU tariff of Thailand, as indicated in Table 3.4.

4.6.3 Case 1: Base Case Without EV Charging Devices

The base case scenario in this chapter uses the same IEEE 33-bus distribution system without EV charging devices as described in Section 3.6.1 of Chapter III. The load profile applied to represent the household electricity consumption is

based on the residential load profile for the central region of Thailand in July, as shown in Figure 3.6. The simulation results for the base case indicate that the total daily electricity cost is 86.0471 kTHB/day, the total energy loss is 2.045 MWh/day, and the peak power demand reaches 1,144.2832 kW. These results represent the system's original operating condition, serving as a reference for evaluating the impacts of EV integration under various optimization strategies.

4.6.4 Case 2: Uncontrolled V2G Operation in The Modified IEEE 33-Bus Distribution System

This case adopts the same assumptions and modeling methodology as Case 2 in Chapter III, which is the modified IEEE 33-bus distribution system with uncontrolled EV charging devices. The EV load profile used here is derived from the MCS results, incorporating uncertainty in user behavior, including departure times, travel durations, and parking periods. Assume that all EVs are fully charged before leaving home in the morning. During the day, EVs are parked at work but not connected to the grid, meaning no charging or discharging occurs during working hours. This case is under the V2G framework, considered uncontrolled because no grid interaction occurs during the day, making the operation equivalent to uncontrolled V1G. The operation of the V2G model for generating uncontrolled load profile EV charging is modeled based on the assumption of 200 EVs per bus, excluding the slack bus. The simulation result of the operation of the V2G model in generating an uncontrolled EV charging load profile, location status based on user activities, and SOC by considering the time period np=1440 minutes is shown in Figure 3.12. Figure 3.13 presents a comparison of the load profiles of case 1 and case 2.

The simulation results show that, under uncontrolled charging, calculating the daily electricity cost for the entire system is 105.6815 kTHB/day, the total daily energy loss is 4.1049 MWh, and peck power demand is 1,884.2832 kW. In Chapter III, Table 3.5 shows the comparison results of the load profiles and Table 3.6 shows the objective function values.

4.6.5 Case 3: Controlled V2G Operation in The Modified IEEE 33-bus Distribution System Under Single Objective for Minimizing Electricity Costs (MEC)

In this case, the optimal operation of V2G (OOV2G) is under a single-objective optimization. The objective considered in this scenario is MEC for the modified IEEE 33-bus distribution system with a controlled V2G Operation. To solve the OOV2G problem, the PSO and GA algorithm determines the optimum operation of EV charging for MEC. Both algorithms are executed separately, with each algorithm being tested for a total of 30 trials. The simulation results are presented as follows in Table 4.3, which shows the objective function values of the maximum, minimum, and average obtained from 30 PSO and GA trials for Case 3. Additionally, the results from across 30 PSO and GA trials are plotted in the Figures. 4.3 and 4.4, respectively. The best result from PSO, determined from the minimum electricity cost across 30 trials, was 83.5692 kTHB/day, with a corresponding energy loss of 5.9614 MWh/day and peak power demand of 1,716.2567 kW. On the other hand, when comparing GA. The best solution from GA has an electricity cost of 83.9309 kTHB/day, and the energy loss increased to 6.189 MWh/day, but peak demand reduced to 1,703.3678 kW.

The results indicate that both algorithms are effective in minimizing electricity costs under the OOV2G solving. Notably, PSO achieves a slightly lower minimum electricity cost compared to GA, demonstrating its superior performance in electricity cost minimization for this case.

Table 4.3 The result of 30 trials by PSO and GA for Case 3 of the OOV2G

Algorithm	Electricity cost (kTHB/day)			Energy loss (MWh/day)	Peak power demand (kW)
	Max	Avg.	Min	Calculated	Calculated
PSO	84.6377	83.9241	83.5692	5.9614	1716.2567
GA	85.6860	84.3671	83.9309	6.1890	1703.3678

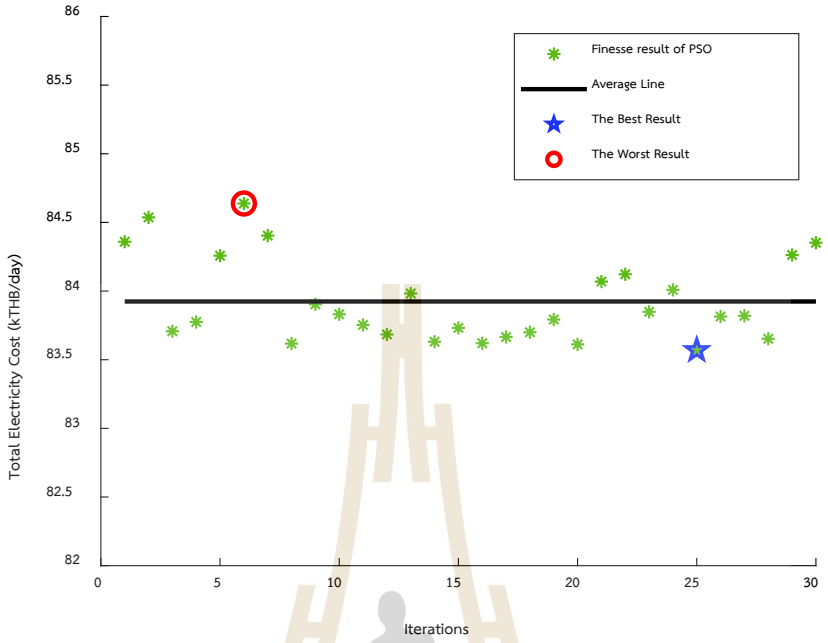

Figure 4.3 The results from 30 trials of PSO for Case 3 of the OOV2G

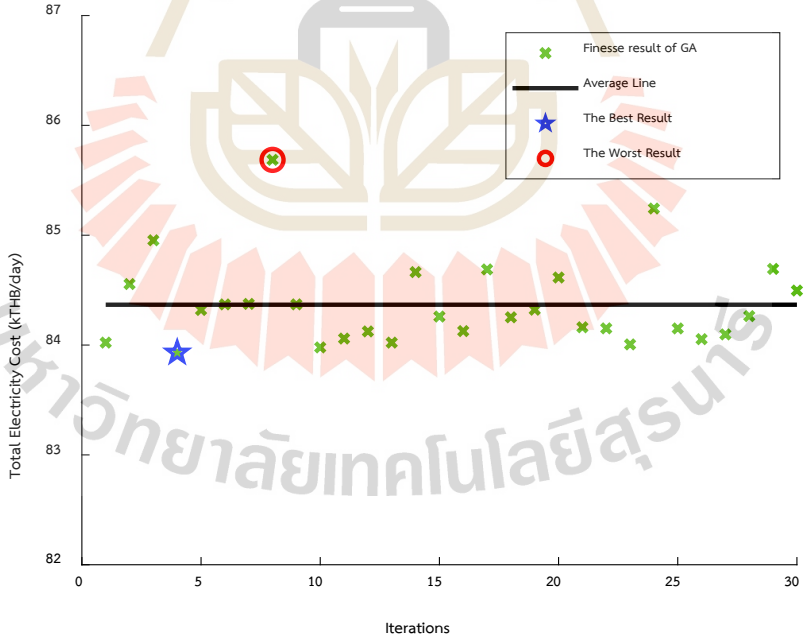

Figure 4.4 The results from 30 trials of GA for Case 3 of the OOV2G

4.6.6 Case 4: Controlled V2G Operation Under Single Objective for Minimizing Energy Losses (MEL)

In this case, the OOV2G is under a single-objective optimization. The objective considered in this scenario is MEL for the modified IEEE 33-bus distribution system with a controlled V2G Operation. To solve the OOV2G problem, the PSO and GA algorithm determines the optimum operation of EV charging for MEL. Both algorithms are executed separately, with each algorithm being tested for a total of 30 trials. The simulation results are presented as follows in Table 4.4, which shows the objective function values of the maximum, minimum, and average obtained from 30 PSO and GA trials for Case 4. Additionally, the results from across 30 PSO and GA trials are plotted in the Figures. 4.5 and 4.6, respectively. The best result from PSO, determined from the minimum energy loss across 30 trials, was 3.2258 MWh/day, with a corresponding electricity cost of 98.3604 kTHB/day and peak power demand of 1,341.2949 kW. On the other hand, when comparing GA. The best solution from GA has an energy loss of 3.4314 MWh/day, and the electricity cost reduced to 97.9874 kTHB/day, but peak power demand increased to 1,396.6688 kW.

The results indicate that both algorithms are effective in minimizing energy loss under the OOV2G solving. Notably, PSO achieves a slightly lower minimum energy loss compared to GA, demonstrating its superior performance in energy loss minimization for this case.

Table 4.4 The result of 30 trials by PSO and GA for Case 4 of the OOV2G

Algorithm	Energy loss (MWh/day)			Electricity cost (kTHB/day)	Peak power demand (kW)
	Max	Avg.	Min	Calculated	Calculated
PSO	3.4060	3.3118	3.2258	98.3604	1341.2949
GA	3.6507	3.5493	3.4314	97.9874	1396.6688

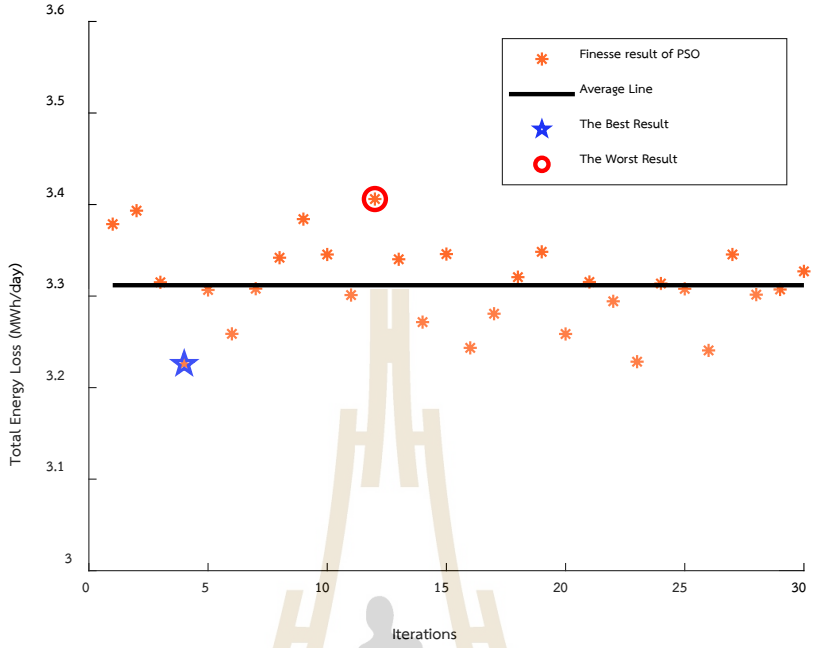

Figure 4.5 The results from 30 trials of PSO for Case 4 of the OOV2G

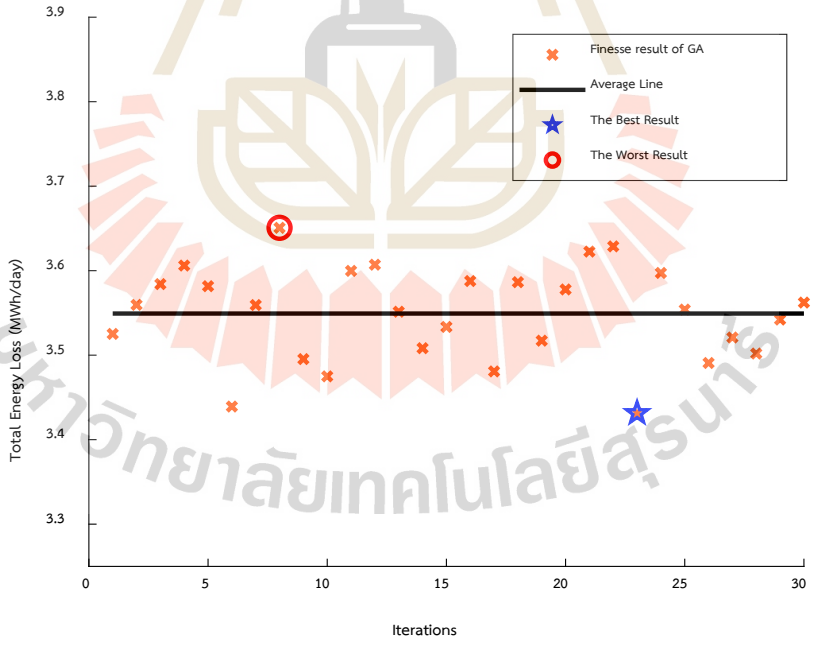

Figure 4.6 The results from 30 trials of GA for Case 4 of the OOV2G

4.6.7 Case 5: Controlled V2G Operation Under Single Objective for Minimizing Peak Power Demand (MPP)

In this case, the OOV2G is under a single-objective optimization. The objective considered in this scenario is MPP for the modified IEEE 33-bus distribution system with a controlled V2G Operation. To solve the OOV2G problem, the PSO and GA algorithm determines the optimum operation of EV charging for MPP. Both algorithms are executed separately, with each algorithm being tested for a total of 30 trials. The simulation results are presented as follows in Table 4.5, which shows the objective function values of the maximum, minimum, and average obtained from 30 PSO and GA trials for Case 5. Additionally, the results from across 30 PSO and GA trials are plotted in the Figures. 4.7 and 4.8, respectively. The best result from PSO, determined from the minimum peak power demand across 30 trials, was 1,218.2832 kW, with a corresponding electricity cost of 96.9743 kTHB/day and an energy loss of 5.0136 MWh/day. On the other hand, the best solution from GA has a peak power demand of 1,218.2895 kW, and the electricity cost and energy loss increased to 97.3778 kTHB/day and 5.5449 MWh/day, respectively.

The results indicate that both algorithms are effective in minimizing peak power demand under the OOV2G solving. Notably, PSO achieves a slightly lower minimum peak power demand compared to GA, demonstrating its superior performance in peak power demand minimization for this case.

Table 4.5 The result of 30 trials by PSO and GA for Case 5 of the OOV2G

Algorithm	Peak power demand (kW)			Electricity cost (kTHB/day)	Energy loss (MWh/day)
	Max	Avg.	Min	Calculated	Calculated
PSO	1,218.2840	1,218.2833	1,218.2832	96.9743	5.0136
GA	1,282.2833	1,254.8672	1,218.2895	97.3778	5.5449

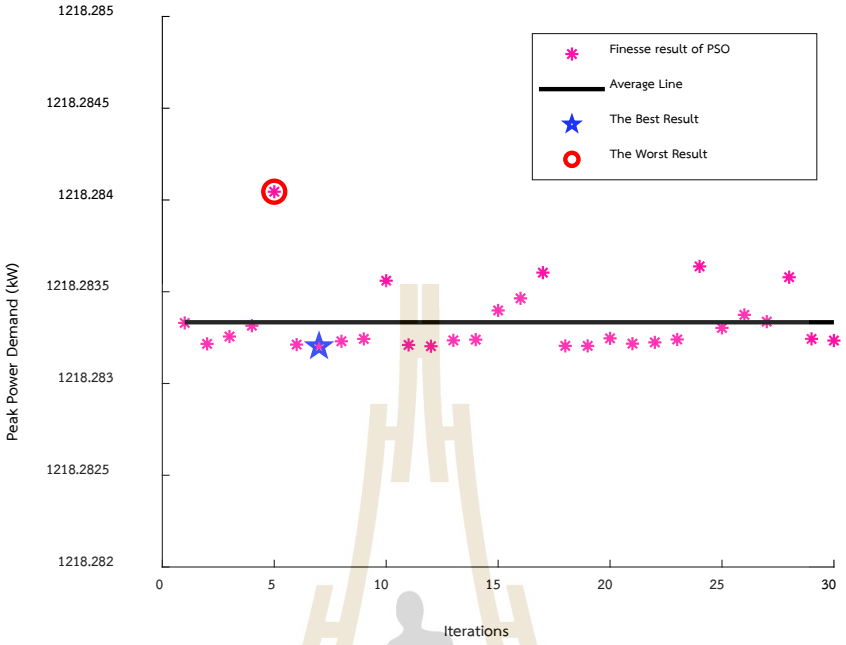

Figure 4.7 The results from 30 trials of PSO for Case 5 of the OOV2G

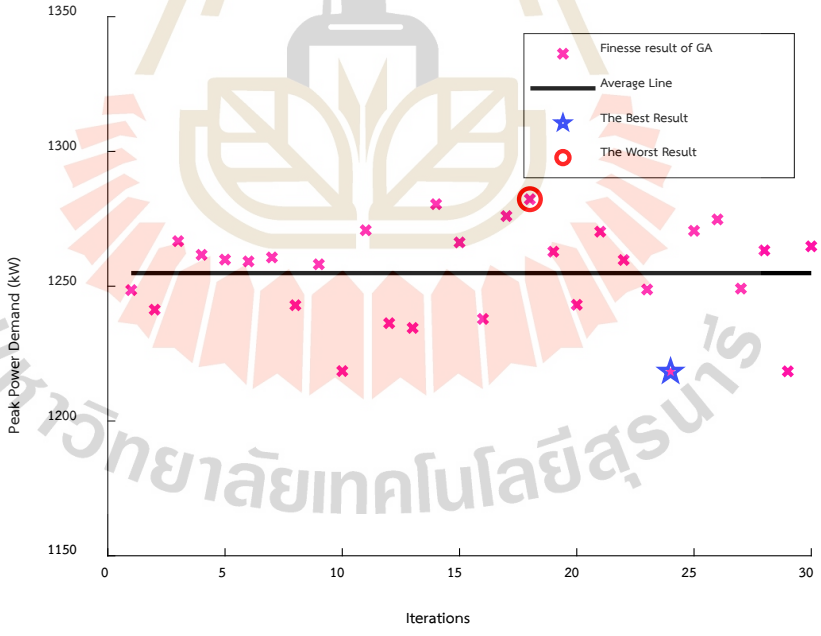

Figure 4.8 The results from 30 trials of GA for Case 5 of the OOV2G

4.6.8 Case 6: Controlled V2G Operation Under Multi-Objective for Minimizing Electricity Cost and Energy Losses (MCAL)

In this case, the OOV2G under a multi-objective optimization aimed to MCAL. The MOOV2G problem was solved using the proposed MOPSO algorithm, integrated with the TOPSIS method for selecting the best solution from the Pareto front. The MOOV2G solving is under control EV charging devices on the modified IEEE 33-bus distribution system. The MOPSO algorithm was tested for 30 trials, each generating a Pareto-optimal set. For each run, the TOPSIS method was applied in the post-processing phase to identify the best-compromised solution. The closeness coefficient calculated in TOPSIS was used to evaluate how close each Pareto solution was to the ideal solution.

The simulation results are presented in Table 4.6, which shows the best, average, and worst closeness coefficient values obtained from the 30 trials for Case 6. Additionally, Table 4.6 shows the best objective function from the best solution. The best solution was selected based on the highest closeness coefficient of 0.8482, indicating high proximity to the ideal point and farthest from the worst point. The best solution obtained from the MDO-MOPSO-TOPSIS method across 30 trials, the electricity cost and energy loss were reduced to 89.3771 kTHB/day and 4.6300 MWh/day, and the peak power demand was 1,717.7204 kW.

Table 4.6 The result of 30 trials by MDO-MOPSO-TOPSIS for Case 6 of the OOV2G

	MDO-MOPSO-TOPSIS method			Calculation
Result value	**Closeness Coefficient**	**Electricity cost (kTHB/day)**	**Energy loss (MWh/day)**	**Peak power demand (kW)**
Max	0.8482	89.3771	4.7055	1,717.7204
Avg.	0.8095			
Min	0.7653			

The closeness coefficient results from across 30 MDO-MOPSO-TOPSIS are illustrated in Figure 4.9. Figure 4.10 plots the MDO-MOPSO result along with the ideal and worst points on the Pareto front of the TOPSIS method. From Figure 4.8, the history of fitness values evaluated during the MOPSO algorithm process, including optimal and suboptimal solutions, is represented by black points. The blue indicates the MDO solution set selected after post-processing analysis. The red line shows the Pareto front, representing the optimal trade-offs between electricity cost and energy loss. The ideal point, represented by a green circle on the Pareto front, refers to a hypothetical optimal solution where both objective functions, electricity cost and energy loss, achieve their minimum values simultaneously. Although such a point may not be practically attainable, it serves as a benchmark for evaluation. Conversely, the worst point, shown as an orange square, represents the solution with the highest values of both electricity cost and energy loss among all Pareto-optimal solutions. This point indicates the worst but is used as to reference for calculating the relative closeness of each alternative in the TOPSIS method. Figure 4.10 illustrates that the best solution selected by TOPSIS is located at the ideal point, demonstrating a good balance between minimizing electricity cost and energy loss. The simulation result for a combination of MOPSO and TOPSIS in solving the MCAL problem demonstrates effectiveness in maintaining the balance between conflicting objectives of solving the MOOV2G.

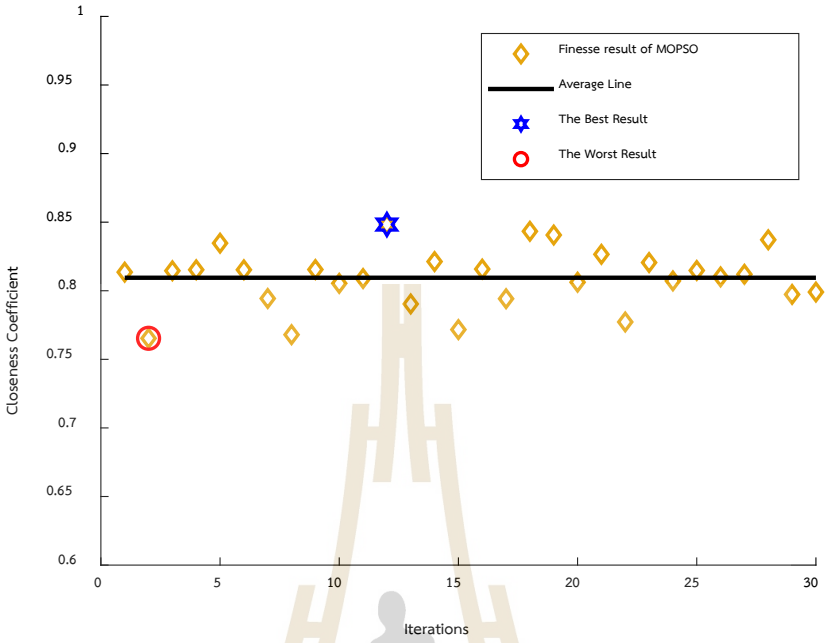

Figure 4.9 The closeness coefficient from 30 trials of MDO-MOPSO-TOPSIS for Case 6 of the OOV2G

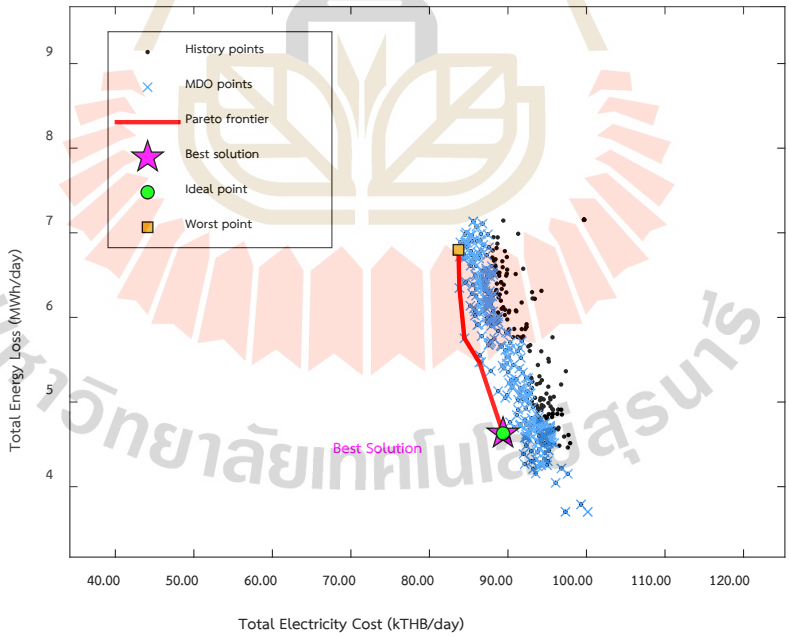

Figure 4.10 The results from MDO-MOPSO for Case 6 of the OOV2G

4.6.9 Case 7: Controlled V2G Operation Under Multi-Objective for Minimizing Electricity Cost and Peak Power Demand (MCAP)

For the MOOV2G problem aiming to minimize both electricity cost and energy loss of Case 6, a key limitation arises from the bidirectional nature of V2G operation. While discharging can help reduce electricity costs, it also increases power flow, leading to higher energy losses. This trade-off makes it difficult to achieve both objectives simultaneously. To address this challenge, this thesis introduces an alternative case that targets the dual objectives of MCAP, offering a more practical and effective optimization strategy under V2G conditions.

Therefore, Case 7 focuses on solving the MOOV2G problem under the MCAP scenario, aiming to minimize both electricity cost and peak power demand. The proposed MOPSO algorithm was employed to generate Pareto-optimal solutions across 30 trials. In each trial, the TOPSIS method was used during the post-processing stage to select the best compromise solution based on the closeness coefficient, which reflects the proximity of each solution to the ideal point. This case was implemented on the modified IEEE 33-bus system with controlled V2G operations.

Table 4.7 The result of 30 trials by MDO-MOPSO-TOPSIS for Case 7 of the OOV2G

	MDO-MOPSO-TOPSIS method			Calculation
Result value	Closeness Coefficient	Electricity cost (kTHB/day)	Peak power demand (kW)	Energy loss (MWh/day)
Max	0.8091			
Avg.	0.7558	90.3547	1,374.0580	5.2815
Min	0.6128			

The simulation results are presented in Table 4.7, which shows the best, average, and worst closeness coefficient values obtained from the 30 trials for Case 7. Additionally, Table 4.7 shows the best objective function from the best solution. The best solution was selected based on the highest closeness coefficient of 0.8091, indicating high proximity to the ideal point and farthest from the worst point. The best

solution obtained from the MDO-MOPSO-TOPSIS method across 30 trials demonstrates significant improvements in system performance. The electricity cost was reduced to 90.3547 kTHB/day, while the peak power demand decreased to 1,374.0580 kW, and the energy loss was 5.2815 MWh/day.

The results of the closeness coefficient from 30 trails of MDO-MOPSO-TOPSIS for Case 7 are shown in Figure 4.11. From Figure 4.12, the history of fitness values evaluated during the MOPSO algorithm process, including optimal and suboptimal solutions, is represented by black points. The blue indicates the MDO solution set selected after post-processing analysis. The red line shows the Pareto front, representing the optimal trade-offs between electricity cost and peak power demand. The ideal point is represented by a green circle on the Pareto front, and the worst point is indicated by an orange square on the Pareto front, which serves as reference indicators in the TOPSIS evaluation. The best-compromised solution selected by TOPSIS from the Pareto front is closest to the ideal point and far from the worst point, indicating an effective trade-off between electricity cost and peak power demand. The simulation result for a combination of MOPSO and TOPSIS in solving the MCAP problem demonstrates effectiveness in maintaining the balance between conflicting objectives of solving the MOOV2G.

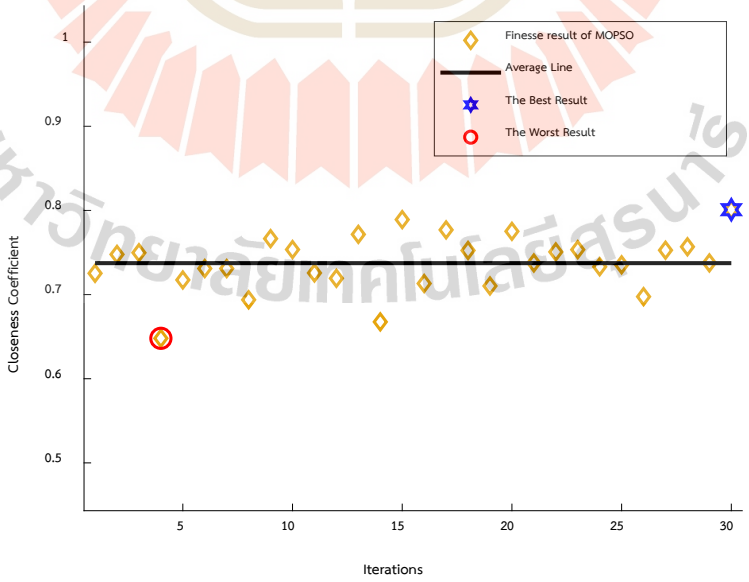

Figure 4.11 The closeness coefficient from 30 trials of MDO-MOPSO-TOPSIS for Case 7 of the OOV2G

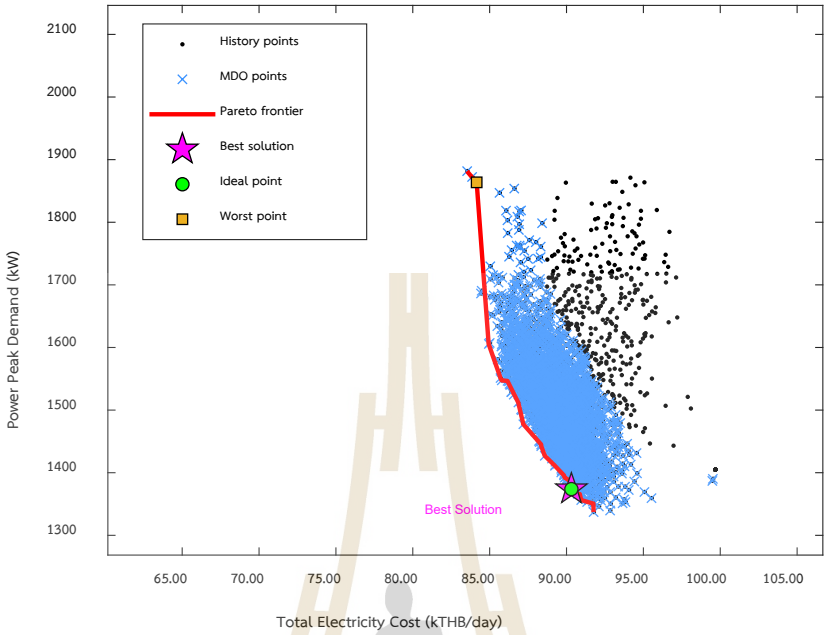

Figure 4.12 The results from MDO-MOPSO for Case 7 of the OOV2G

The results for the operation of V2G, as presented in Table 4.8 and Figure 4.13, show the difference between single-objective and multi-objective optimization approaches for OOV2G. In the single-objective cases (Cases 3, 4, and 5), the PSO algorithm is used for optimization since in the single-objective case, PSO will give better results than GA. Each case focuses exclusively on minimizing one specific objective, MEC, MEL, and MPP, without regard for the impact on the other objectives. As a result, while the targeted objective achieves its lowest value, the other objectives often remain high. Especially the energy loss in the context of V2G EVs not only charge but also discharge power back into the system. This bidirectional energy flow results in an increase in network power flows and leads to elevated energy losses. Observation in Case 4, where the single objective is to minimize energy loss (MEL), the PSO solution results in significantly reduced losses. However, this is achieved by suppressing the discharging operation of V2G during periods when discharging is allowed. The algorithm defines hardly discharge at all, as shown in Table 4.8. The objective value result is shown in Table 4.9. In the case using MOPSO in the MOOV2G cases (Cases 6 and 7), the algorithm simultaneously considers two conflicting objectives. In Case 6, although the electricity cost is significantly reduced, the energy loss remains high due to the intensified power flow caused by V2G discharging. This confirms that MCAL cannot loss

reduction under V2G operation. Therefore, Case 7 is introduced as an alternative that targets electricity cost and peak power demand. In this case, demonstrates MOPSO-TOPSIS capable of providing well-balanced solutions that reduce both electricity cost and peak demand. The simulation results are in Figure. 4.14 compares the system load profiles, showing that the system with charging control under TOU pricing results in lower on-peak power demand, which helps reduce electricity cost and energy loss, as shown in Figures 4.15 and 4.16.

Table 4.8 Comparison results of the operation of V2G for MOOV2G

Hours	Power consumption (kW)					
	Case 2	Case 3 (PSO)	Case 4 (PSO)	Case 5 (PSO)	Case 6 (MOPSO)	Case 7 (MOPSO)
1	0	738.29	296.48	405.85	551.7	571.17
2	0	740	209.7	380.62	409.32	543.05
3	0	739.29	254.33	338.3	533.59	590.25
4	0	736.52	184.4	327.53	739.02	476.8
5	0	730.98	359.12	343.83	406.93	515.94
6	0	732.28	473.63	402.4	590.37	626.82
7	0	739.94	739.95	406.48	606	600.99
8	0	0	0	0	0	0
9	0	-682.28	-2.81	-9.58	-739.02	-241.77
10	0	-695.38	-5	-17.95	-172.3	-388.14
11	0	-601.84	-5.2	-5.67	-409.14	-207.9
12	0	-730.2	-0.31	-18.63	-311.16	-368.34
13	0	-672.01	-6.46	-126.97	-739.02	-550.25
14	0	-697.76	-5.39	-130.42	-300.04	-411.18
15	0	-645.47	-2.22	-26.2	-200.001	-390.12
16	0	-655.66	-12.98	-29.58	-246.16	-575.65
17	0	0	0	0	0	0
18	332.445	415.28	9.99	2.16	336.17	406.42
19	740.00	289.77	130.17	164.69	288.45	326.16
20	740.00	187.79	197.01	74	122.76	194.91
21	740.00	503.07	91.23	102.41	101.75	227.19
22	740.00	737.56	102.88	161.08	739.02	386.56
23	96.015	739.79	181.23	330.5	631.21	532.41
24	0	738.53	198.74	313.64	449.05	523.18

Table 4.9 Comparison the objective function value of the IEEE 33-bus distribution system for OOV2G

The objective function value	Case Study					
	Case 2	Case 3 (PSO)	Case 4 (PSO)	Case 5 (PSO)	Case 6 (MOPSO)	Case 7 (MOPSO)
C_{ep}^{total} (kTHB)	105.6815	83.5692	98.3604	96.9743	89.3771	90.3547
E_{loss}^{total} (MWh)	4.1049	5.9614	3.2258	5.0136	4.7055	5.2815
P_{daily}^{peak} (kW)	1,884.283	1,716.257	1,341.295	1,218.283	1,717.720	1,374.058

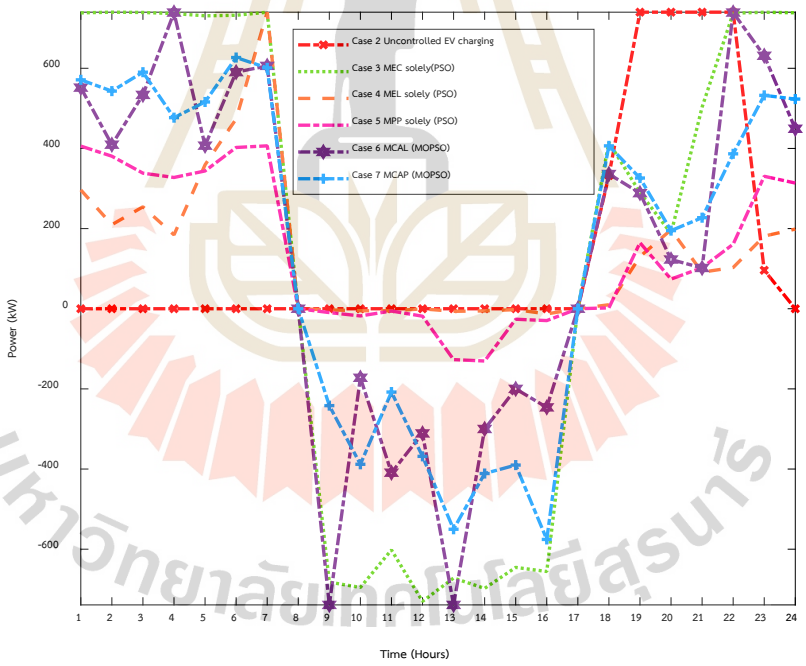

Figure 4.13 Comparison operation of the V2G

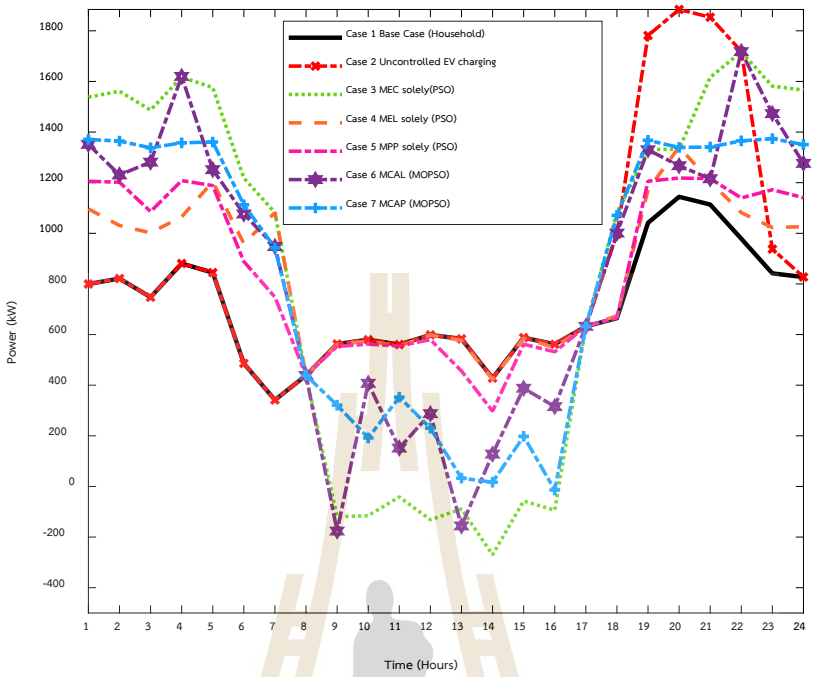

Figure 4.14 Comparison system load profile of the OOV2G

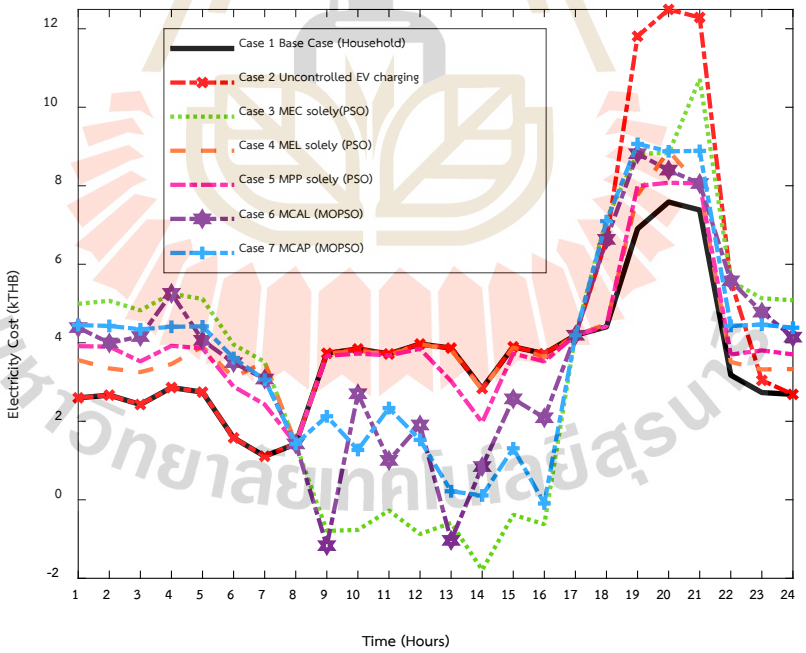

Figure 4.15 Comparison of electricity cost of the OOV2G

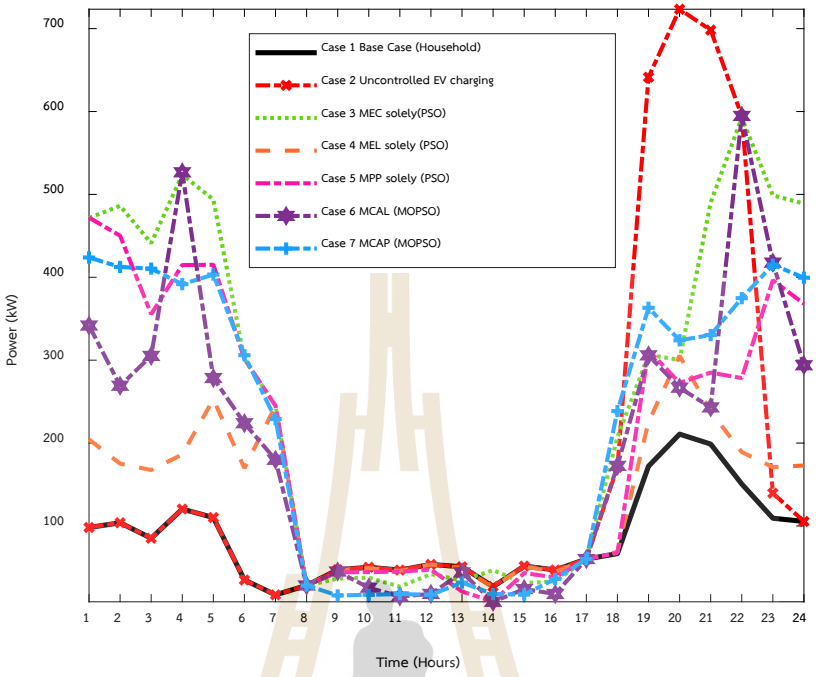

Figure 4.16 Comparison of energy loss of the OOV2G

Figure 4.13 illustrates the comparison of V2G operation profiles across six cases. Case 2 represents the uncontrolled EV charging scenario, in which EVs are charged during peak hours that coincide with the highest levels of household electricity demand. In contrast, Cases 3 through 7 represent optimized V2G operation scenarios based on the proposed method for each case. In these cases, EV charging is shifted to off-peak periods, while discharging is scheduled during working hours, under the assumption that EVs are only allowed to discharge when parked at the workplace. Furthermore, when EV operation load profiles are combined with household load demand, the total system load is illustrated in Figure 4.14. It is observed that during the controlled V2G operations, especially between hours 9 and 16, discharging occurs while EVs are parked at the workplace, supplying power back to the grid. This contributes to a noticeable reduction in overall system demand during that time frame. Among all cases, Case 3 demonstrates the highest discharging activity, resulting in the most significant decrease in total system load during working hours.

Figure 4.15 shows the electricity cost comparison among all cases. It can be observed that controlled V2G operations significantly reduce the overall electricity cost compared to uncontrolled EV charging cases. In several time intervals, especially during

low-demand hours, negative electricity cost values are observed, indicating that the system earns revenue from discharging electricity back to the grid. Among all scenarios, Case 3 achieves the lowest total electricity cost, followed closely by Case 6. However, the results also reveal that excessive discharging can increase system power losses. As shown in Figure 4.16, Case 3 results in the highest energy loss due to the increased bidirectional power flow associated with high discharging activity. This energy loss is even greater than that observed in the uncontrolled scenario. Conversely, Case 4 yields the lowest energy loss, but discharging activities in this case are minimal. These findings indicate that while V2G operation is effective in reducing electricity cost and peak demand, it remains challenging to minimize energy loss together.

4.6.10 Evaluation of MOPSO Flexibility under Different Uncontrolled EV Operation Scenarios

To further evaluate the flexibility and robustness of the proposed MOPSO-TOPSIS approach, this section investigates its performance under different base-case scenarios. Two key aspects are analyzed. The first is varying the number of EVs in the system, and the second is considering an uncontrolled V2G operation model. These evaluations are conducted under the multi-objective optimization scenario for MCAP. The results demonstrate the efficiency and flexibility of the proposed optimization framework in addressing changed and complex system conditions.

4.6.10.1 Varying the Number of EVs

This section presents a case study in which the number of EVs integrated into the modified IEEE 33-bus distribution system is reduced to demonstrate the flexibility and adaptability of the proposed MOPSO algorithm in managing the MOOV2G under changing system conditions. In this scenario, the total number of EVs in each bus is reduced to 100 units, and the initial SOC (SOC_0) for each EV is assumed to be 100% of $SOC_{\max}$, corresponding to a percentage of the total state of charge ($psoc$) equal to 1. The MCS remains the method used to model the uncertainty in EV user behavior, generating stochastic and realistic EV charging profiles based on variables such as departure time, travel duration, and workplace parking time. The impact of reducing the number of EVs alters the resulting uncontrolled EV charging load profile differs from the baseline case (200 EVs). The updated

uncontrolled EV charging is used for comparison with the MOOV2G result in this scenario. The resulting updated uncontrolled load profile is shown in Figure 4.17. Figure 4.18 presents a comparison of the uncontrolled load profiles between the original case of 200 EVs and the reduced case of 100 EVs. The simulation results indicate that in uncontrolled EV charging, the daily electricity cost for the entire system is 95.8486 kTHB/day, the energy loss is 4.1044 MWh/day, and the peak power demand is 1,514.2832 kW.

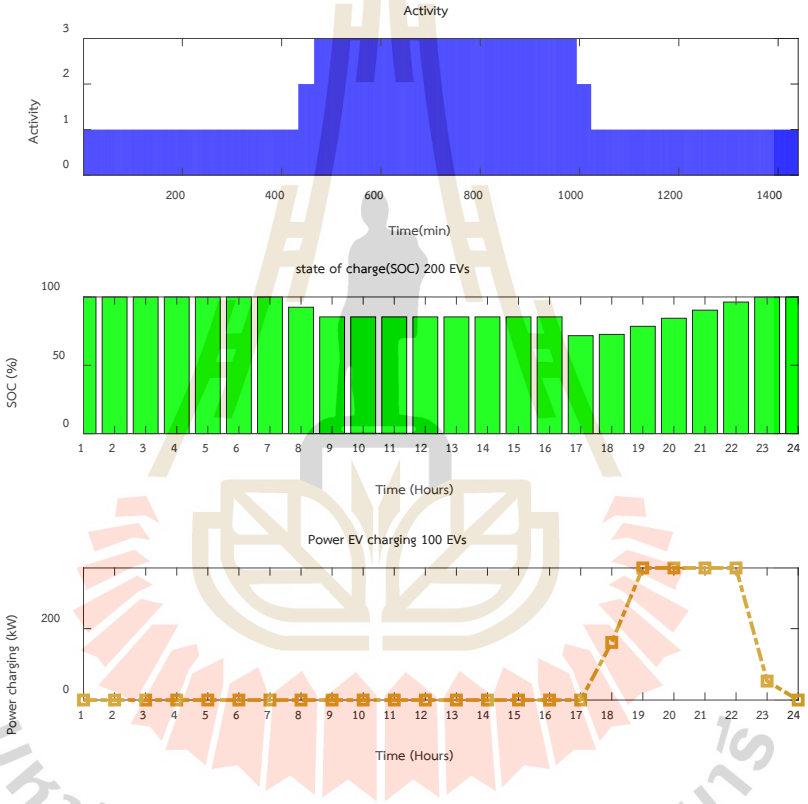

Figure. 4.17 The load profiles EV result of varying EV levels case

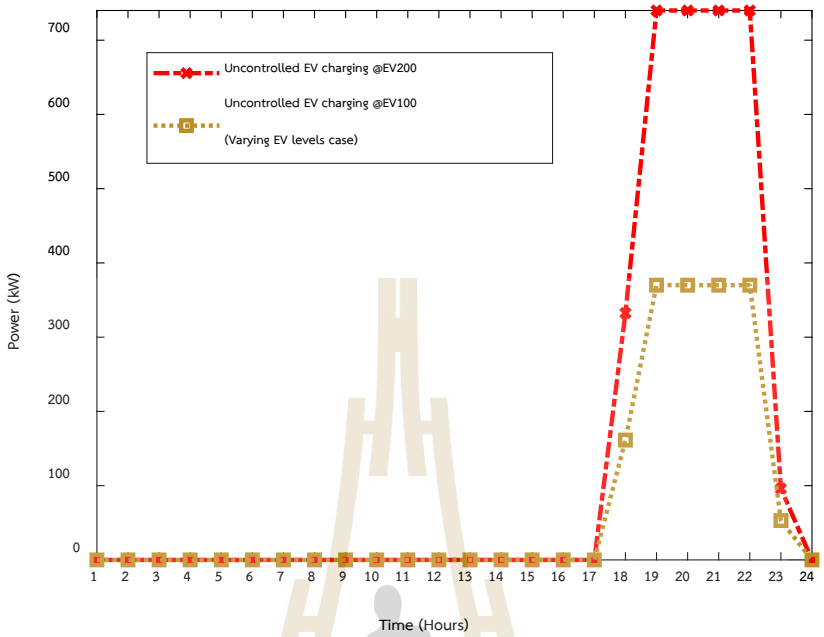

Figure. 4.18 Comparison of uncontrolled EV charging load profiles for 200 and 100 EVs

This case proposed using the MOPSO-TOPSIS to solve the MOOV2G problem under the MCAP scenario. The simulation results of MDO-MOPSO-TOPSIS method are presented in Table 4.10. The best solution was the highest closeness coefficient of 0.9429. The electricity cost was reduced to 86.1352 kTHB/day, while the peak power demand decreased to 1,201.5986 kW, while the energy loss increased to 5.3006 MWh/day. The results of the closeness coefficient from 30 trials are shown in Figure 4.19. Figure 4.20 shows the results from MDO-MOPSO. The simulation result for a combination of MOPSO and TOPSIS in solving the MOOV2G problem demonstrates effectiveness in maintaining the balance between conflicting objectives of the MCAP. Compared to the uncontrolled case, the MOPSO-TOPSIS can find a solution that effectively reduces both electricity cost and peak power demand under low EV integration levels. The comparison of EV operation between the uncontrolled and controlled cases in this scenario is shown in Table 4.11, and Table 4.12 presents the comparison of the objective function values of the IEEE 33-bus distribution system. These findings confirm that the MOPSO-TOPSIS method is a flexible optimization

strategy capable of delivering optimal scheduling solutions for V2G operation under fluctuations in EV quantity.

Table 4.10 The result of 30 trials by MDO-MOPSO-TOPSIS under varying EV levels

	MDO-MOPSO-TOPSIS method			Calculation
Result value	Closeness Coefficient	Electricity cost (kTHB/day)	Peak power demand (kW)	Energy loss (MWh/day)
Max	0.9429			
Avg.	0.8557	86.1352	1,201.5986	5.3006
Min	0.7137			

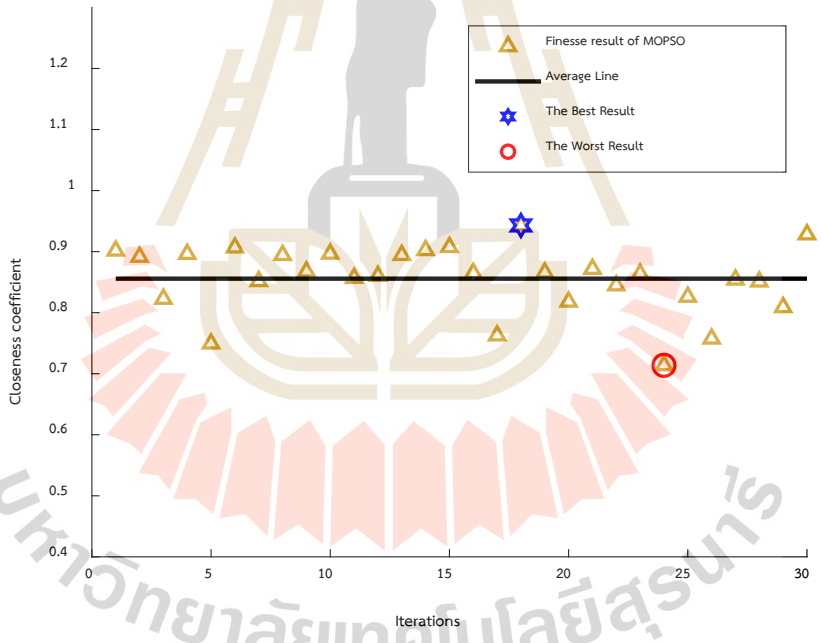

Figure 4.19 The result closeness coefficient from 30 trials under the varying EV levels.

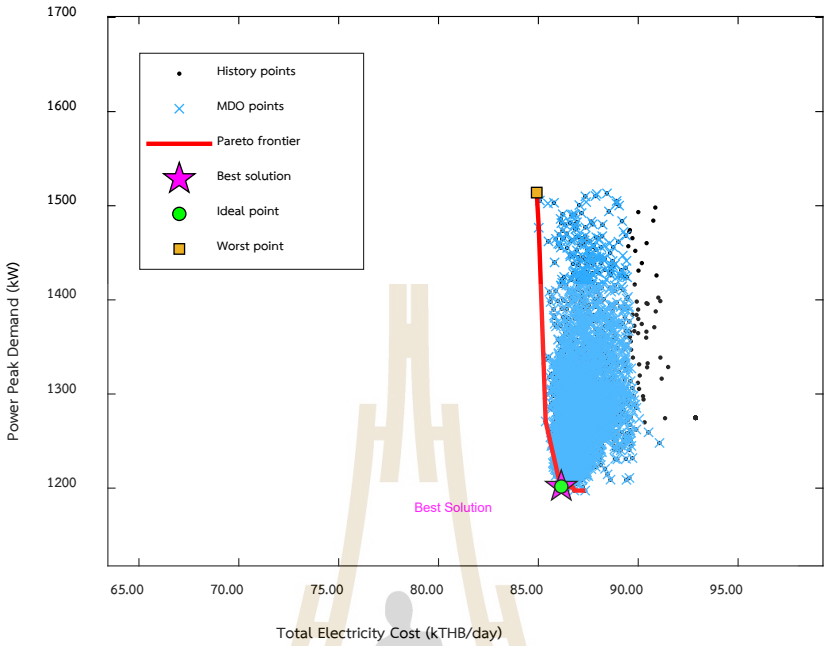

Figure 4.20 The results from MDO-MOPSO for Case varying EV levels

Table 4.11 Comparison results of the operation of V2G for MOOV2G for varying EV levels case

Hours	Power consumption (kW)	
	Uncontrolled EV charging @EV100	MCAP (MOOV2G)
1	0	314.258
2	0	362.764
3	0	356.196
4	0	310.839
5	0	337.991
6	0	335.142
7	0	348.055
8	0	0
9	0	-357.074
10	0	-122.405
11	0	-271.365
12	0	-343.749
13	0	-148.653
14	0	-327.913
15	0	-189.282
16	0	-174.765
17	0	0
18	161.402	52.783
19	370	148.297
20	370	56.587
21	370	77.348
22	370	210.525
23	53.015	359.955
24	0	358.882

Table 4.12 Comparison the objective function value of the IEEE 33-bus distribution system for or varying EV levels case

The objective function value	Case Study	
	Uncontrolled EV charging @EV100	MCAP ()
C_{ep}^{total} (kTHB)	95.8486	86.1352
E_{loss}^{total} (MWh)	4.1044	5.3006
P_{daily}^{peak} (kW)	1,514.2832	1,201.5986

4.6.10.2 Uncontrolled V2G operation model

This section considers the base case of an uncontrolled V2G operation scenario. This study assumed that EVs are allowed to discharge energy to the grid only when parked at the workplace while being connected to the grid. Conversely, charging is permitted only when the EVs are parked at home. The load profile for the uncontrolled V2G operation is generated based on user activity patterns obtained from MCS and follows the operation of the V2G modeling framework described in Section 4.2.3. The resulting load profile for the uncontrolled V2G operation reflects a more realistic representation of EV behavior under bi-directional charging conditions. This uncontrolled V2G load profile, which includes both charging and discharging activities aligned with daily user activity patterns, is shown in Figure 4.21. The comparison between the uncontrolled V2G operation load profile and the uncontrolled EV charging load profile under an equal number of EVs is shown in Figure 4.22. The simulation results indicate that in uncontrolled V2G operation, the daily electricity cost for the entire system is 74.2286 kTHB/day, the energy loss is 4.7975 MWh/day, and the peak power demand is 1,884.2832 kW. When compared to the base case with only household loads and without EV integration in Case 1, the uncontrolled V2G operation scenario results in a lower electricity cost. This is due to increased discharging during periods when EVs are parked at the workplace, which helps reduce the electricity cost of the system. However, the energy loss and peak power demand remain increasing. Moreover, V2G operations still have challenges in effectively

minimizing energy losses. Therefore, this study proposes using the MOPSO-TOPSIS approach to solve the MOOV2G problem to MCAP.

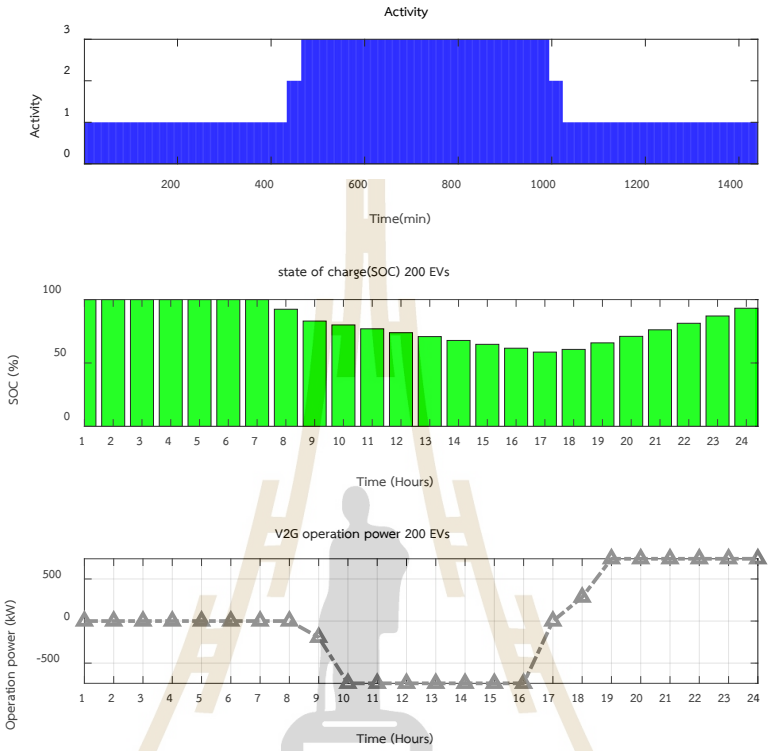

Figure 4.21 The load profiles EV result of uncontrolled V2G operation case

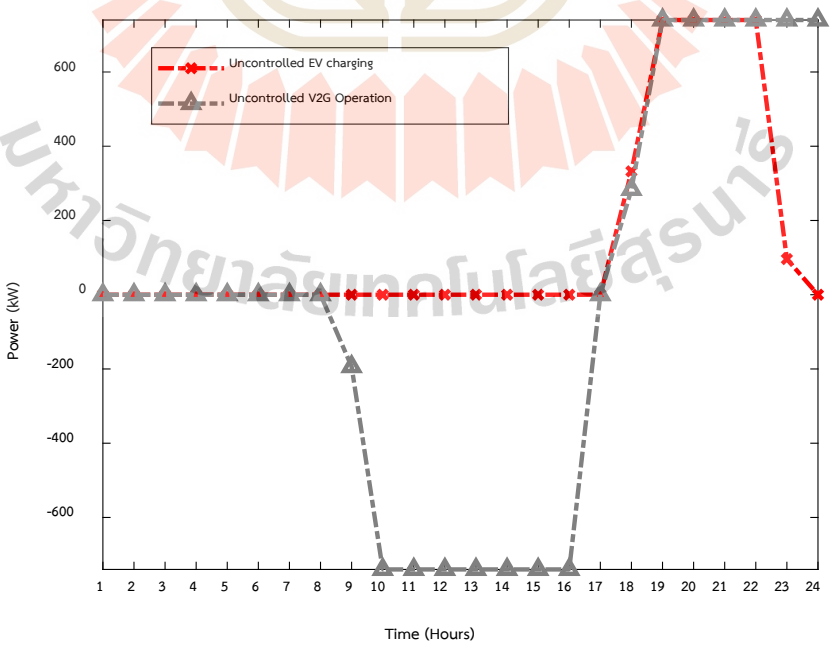

Figure 4.22 Comparison of uncontrolled EV charging and uncontrolled V2G operation

The simulation results obtained from the MDO-MOPSO-TOPSIS method from 30 trials are presented in Table 4.13. The best solution selected by the TOPSIS method is the highest closeness coefficient of 0.8238. This solution reduces the daily electricity cost to 71.3540 kTHB/day and minimizes peak power demand to 1,175.9121 kW. Moreover, the energy loss was reduced to 3.3274 MWh/day. However, energy loss is still higher than without EV integration into the system. Figure 4.23 displays the closeness coefficient from 30 trials. Figure 4.24 shows the results from MDO-MOPSO, and illustrates that the MOPSO-TOPSIS approach successfully selected a solution that effectively maintains a balance between the two conflicting objectives, minimizing electricity cost and peak power demand. Furthermore, the simulation results confirm that the MOOV2G operation using the proposed method remains effective under various uncontrolled V2G operation scenarios. This highlights the capability of the MOPSO-TOPSIS method to maintain optimal performance and flexibility under changed and uncertain conditions. The comparison of EV operation and the objective function values of the IEEE 33-bus distribution system is shown in Tables 4.14 and 4.15, respectively.

Table 4.13 The result of 30 trials by MDO-MOPSO-TOPSIS for uncontrolled V2G base case

	MDO-MOPSO-TOPSIS method			Calculation
Result value	**Closeness Coefficient**	**Electricity cost (kTHB/day)**	**Peak power demand (kW)**	**Energy loss (MWh/day)**
Max	0.8238			
Avg.	0.7366	71.3540	1,175.9121	3.3274
Min	0.6082			

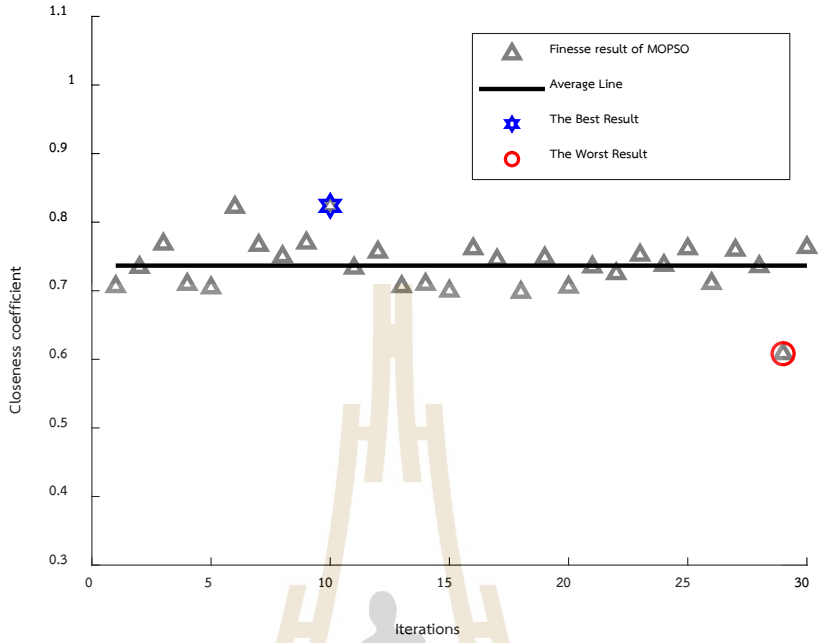

Figure 4.23 The result closeness coefficient from 30 trials for uncontrolled V2G base cases

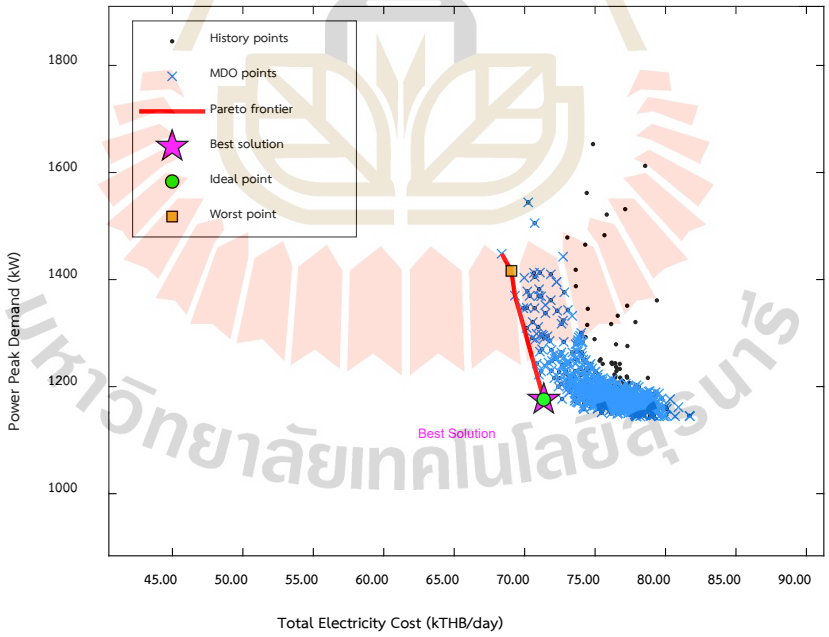

Figure 4.24 The results from MDO-MOPSO for uncontrolled V2G base cases

Table 4.14 Comparison results of the operation of V2G for uncontrolled V2G base case

Hours	Power consumption (kW)		
	Case 1 (Household)	Uncontrolled V2G operation	MCAP (MOPSO)
1	799.720	0	298.757
2	821.242	0	154.258
3	747.64	0	371.872
4	880.72	0	266.725
5	844.678	0	314.523
6	486.02	0	659.267
7	341.71	0	380.372
8	438.65	0	0
9	562.76	-193.695	-414.682
10	579.72	-740	-507.736
11	560.58	-740	-455.719
12	598.66	-740	-699.867
13	583.04	-740	-582.670
14	427.85	-740	-552.769
15	587.92	-740	-498.725
16	561.53	-740	-517.614
17	632.37	0	0
18	664.62	283.667	333.484
19	1041.43	740	128.681
20	1144.28	740	28.221
21	1113.68	740	19.558
22	978.70	740	157.690
23	841.64	740	334.268
24	827.31	740	132.079

Table 4.15 Comparison the objective function value of the IEEE 33-bus distribution system for uncontrolled V2G base case

The objective function value	Case Study		
	Case 1 (Household)	Uncontrolled V2G operation	MCAP (MOPSO)
C_{ep}^{total} (kTHB)	86.0471	74.2286	71.3541
E_{loss}^{total} (MW)	2.045	4.7975	3.3274
P_{daily}^{peak} (kW)	1,144.2832	1,884.2832	1,175.9121

CHAPTER V
CONCLUSION

5.1 Conclusion

This thesis presents a comprehensive study of the OOV1G and OOV2G in distribution systems under both charging and discharging modes. The main objective is to develop an effective optimization framework that minimizes electricity cost, energy losses, and peak power demand in the power distribution network, aiming to minimize an MOO. Consideration is given to different MOO problems in two cases, which are MCAL and MCAP. To achieve this, the modified IEEE 33-bus distribution test system was employed as a simulation environment. A MOPSO algorithm, combined with the TOPSIS decision-making method, was proposed to solve the MOOV1G and MOOV2G, including using the TOU tariff. Additionally, MCS was used to generate realistic EV charging load profiles by modeling user behavior and incorporating uncertainty in daily usage patterns. The proposed framework was tested across seven different operating cases and further validated under varying EV levels and algorithm parameter settings to demonstrate its robustness and flexibility.

Solving the MOOV1G problem by considering MOO in two scenarios, which are MCAL and MCAP. The proposed MOPSO-TOPSIS approach can successfully solve the MOOV1G. When simulation results were compared against uncontrolled EV operation, modeled using the MCS. The results demonstrated that the proposed MOPSO-TOPSIS method effectively achieved the objectives of both MCAL and MCAP, by reducing both objectives and maintaining the balance between conflicting objectives.

For the MOOV2G, the same optimization framework was applied to the bidirectional operation of EVs. While the method successfully minimized electricity costs, especially under the MCAP scenario, it encountered a limitation under the MCAL case. Due to the bidirectional power flow introduced by V2G discharging, energy loss in the system tended to increase, making it difficult to reduce both electricity cost and

energy loss simultaneously. Therefore, the MCAP scenario, which focuses on minimizing electricity cost and peak power demand, was introduced as a more feasible alternative. The results show that the proposed MOPSO-TOPSIS approach remains effective and flexible even under the varying operational complexities of V2G.

Overall, this research successfully achieved its objectives by solving the MOOV1G and MOOV2G problems using the proposed MOPSO algorithm combined with the TOPSIS method to select the best compromise solutions from the Pareto front. The integrated framework demonstrated effectiveness in balancing conflicting objectives under multi-objective optimization. In addition, the uncertainty of EV user behavior was addressed using MCS, which can generate realistic EV load profiles. These profiles were used as a foundation for evaluating and optimizing EV charging strategies in the IEEE 33-bus distribution test system. The proposed methodology has proven to be both robust and adaptable under various operating conditions.

5.2 Suggestions

Based on the findings, this study demonstrates the potential benefits of V1G and V2G operations in effectively reducing electricity costs, energy losses, and peak power demand in the distribution system. These results indicate that the proposed approach can be implemented in the context of Thailand, where EV adoption is increasing and the country is transitioning toward a more sustainable energy future. However, several limitations must be addressed before real-world implementation is feasible. Currently, Thailand's distribution infrastructure is not yet fully equipped to support widespread bidirectional charging. Furthermore, smart energy management systems (EMS), which are essential for implementing optimal charging and discharging schedules, have not been widely deployed across charging stations or home charging. A particularly critical limitation is the issue of user consent and autonomy. Optimal V1G and V2G operations require a degree of centralized control over EV charging and discharging schedules, which may conflict with user preferences. Without appropriate incentives or regulatory frameworks, many users may be unwilling to allow external control of their vehicle's operation.

Therefore, while the research confirms the technical effectiveness of optimized EV operation, its practical implementation in Thailand requires comprehensive development in infrastructure, policy, and user engagement. These elements must be carefully addressed to enable the successful implementation and integration of EVs into the Thai power grid.

REFERENCES

Aljohani, T. M., Ebrahim, A. F., & Mohammed, O. A. (2021). Dynamic Real-Time Pricing Mechanism for Electric Vehicles Charging Considering Optimal Microgrids Energy Management System. IEEE Transactions on Industry Applications, 57(5), 5372-5381. https://doi.org/10.1109/TIA.2021.3099083

Gamil, M., Masrur, H., Muttaqi, K., Huang, Y., Lotfy, M., & Senjyu, T. (2022). Multi-objective Optimal Power Scheduling of A Residential Microgrid Considering V2G and Demand Response Techniques. https://doi.org/10.1109/IAS54023.2022.9939886

Wan, Y., Gebbran, D., Subroto, R., & Dragicevic, T. (2023). Optimal Day-ahead Scheduling of Fast EV Charging Station With Multi-stage Battery Degradation Model.

An, Y., Gao, Y., Wu, N., Zhu, J., Li, H., & Yang, J. (2023, 2023/03/01/). Optimal scheduling of electric vehicle charging operations considering real-time traffic condition and travel distance. Expert Systems with Applications, 213, 118941. https://doi.org/https://doi.org/10.1016/j.eswa.2022.118941

Mukherjee, J. C., & Gupta, A. (2017). Distributed Charge Scheduling of Plug-In Electric Vehicles Using Inter-Aggregator Collaboration. IEEE Transactions on Smart Grid, 8(1), 331-341. https://doi.org/10.1109/TSG.2016.2515849

Malisani, P., Zhu, J., & Pognant-Gros, P. (2023). Optimal Charging Scheduling of Electric Vehicles: The Co-Charging Case. IEEE Transactions on Power Systems, 38(2), 1069-1080. https://doi.org/10.1109/TPWRS.2022.3172286

Yao, L., Damiran, Z., & Lim, W. H. (2017). Optimal Charging and Discharging Scheduling for Electric Vehicles in a Parking Station with Photovoltaic System and Energy Storage System. Energies, 10(4).

Techanok, S., & Chayakulkheeree, K. (2024, 6-8 March 2024). Optimal EV Charging Control for Distribution System Loss Minimization. 2024 12th International Electrical Engineering Congress (iEECON),

Zhang, H., Xu, X., Huang, J., & Rashed, G. (2024). Optimal Scheduling Strategy for Multi-Type Electric Vehicle Charging Based on Improved GA. https://doi.org/10.1109/ICESEP62218.2024.10652221

Mohamed, N. M. M., Sharaf, H. M., Ibrahim, D. K., & El'gharably, A. (2022). Proposed Ranked Strategy for Technical and Economical Enhancement of EVs Charging With High Penetration Level. IEEE Access, 10, 44738-44755. https://doi.org/10.1109/ACCESS.2022.3169342

Yang, H., Yang, S., Xu, Y., Cao, E., Lai, M., & Dong, Z. (2015). Electric Vehicle Route Optimization Considering Time-of-Use Electricity Price by Learnable Partheno-Genetic Algorithm. IEEE Transactions on Smart Grid, 6(2), 657-666. https://doi.org/10.1109/TSG.2014.2382684

Chen, J., Huang, X., Tian, S., Cao, Y., Huang, B., Luo, X., & Yu, W. (2019, 07/16). Electric vehicle charging schedule considering user's charging selection. IET Generation, Transmission & Distribution, 13. https://doi.org/10.1049/iet-gtd.2019.0154

Kang, Q., Feng, S., Zhou, M., Ammari, A. C., & Sedraoui, K. (2017). Optimal Load Scheduling of Plug-In Hybrid Electric Vehicles via Weight-Aggregation Multi-Objective Evolutionary Algorithms. IEEE Transactions on Intelligent Transportation Systems, 18(9), 2557-2568. https://doi.org/10.1109/TITS.2016.2638898

Adianto, Y., Baguley, C., Madawala, U., Hariyanto, N., Suwarno, S., & Kurniawan, T. (2021, 12/21). The Coordinated Operation of Vertically Structured Power Systems for Electric Vehicle Charge Scheduling. Energies, 15, 27. https://doi.org/10.3390/en15010027

Kalakanti, A., & Rao, S. (2024). Dynamic Pricing for Electric Vehicle Charging. https://doi.org/10.48550/arXiv.2408.14169

Rassaei, F., Soh, W. S., & Chua, K. C. (2015). Demand Response for Residential Electric Vehicles With Random Usage Patterns in Smart Grids. IEEE Transactions on Sustainable Energy, 6(4), 1367-1376. https://doi.org/10.1109/TSTE.2015.2438037

Wang, X., Sun, C., Wang, R., & Wei, T. (2020). Two-Stage Optimal Scheduling Strategy for Large-Scale Electric Vehicles. IEEE Access, 8, 13821-13832. https://doi.org/10.1109/ACCESS.2020.2966825

Saber, A. Y., & Venayagamoorthy, G. K. (2010, 2010/02/01/). Intelligent unit commitment with vehicle-to-grid —A cost-emission optimization. Journal of Power Sources, 195(3), 898-911. https://doi.org/https://doi.org/10.1016/j.jpowsour.2009.08.035

Yu, J. J. Q., Li, V. O. K., & Lam, A. Y. S. (2013, 20-23 June 2013). Optimal V2G scheduling of electric vehicles and Unit Commitment using Chemical Reaction Optimization. 2013 IEEE Congress on Evolutionary Computation,

Rabiee, A., Sadeghi, M., Aghaeic, J., & Heidari, A. (2016, 2016/05/01/). Optimal operation of microgrids through simultaneous scheduling of electrical vehicles and responsive loads considering wind and PV units uncertainties. Renewable and Sustainable Energy Reviews, 57, 721-739. https://doi.org/https://doi.org/10.1016/j.rser.2015.12.041

Gamil, M., Masrur, H., Muttaqi, K., Huang, Y., Lotfy, M., & Senjyu, T. (2022). Multi-objective Optimal Power Scheduling of A Residential Microgrid Considering V2G and Demand Response Techniques. https://doi.org/10.1109/IAS54023.2022.9939886

Triviño-Cabrera, A., Aguado, J. A., & Torre, S. d. l. (2019, 2019/05/15/). Joint routing and scheduling for electric vehicles in smart grids with V2G. Energy, 175, 113-122. https://doi.org/https://doi.org/10.1016/j.energy.2019.02.184

Yao, L., Lim, W. H., & Tsai, T. (2017, 01/01). A Real-Time Charging Scheme for Demand Response in Electric Vehicle Parking Station. *IEEE Transactions on Smart Grid, 8*, 52-62. https://doi.org/10.1109/TSG.2016.2582749

Pal, S., & Kumar, R. (2018). Electric Vehicle Scheduling Strategy in Residential Demand Response Programs With Neighbor Connection. IEEE Transactions on Industrial Informatics, 14(3), 980-988. https://doi.org/10.1109/TII.2017.2787121

Huang, Q., Wang, X., Fan, J., Qi, S., Zhang, W., & Zhu, C. (2019, 11-14 June 2019). V2G Optimal Scheduling of Multiple EV Aggregator Based on TOU Electricity Price. 2019 IEEE International Conference on Environment and Electrical Engineering and 2019 IEEE Industrial and Commercial Power Systems Europe (EEEIC / I&CPS Europe),

Choudhary, D., Mahanty, R. N., & Kumar, N. (2024, 2024/06/01/). Plug-in electric vehicle dynamic pricing strategies for bidirectional power flow in decentralized and centralized environment. Sustainable Energy, Grids and Networks, 38, 101317. https://doi.org/https://doi.org/10.1016/j.segan.2024.101317

Metropolis, N., & and Ulam, S. (1949, 1949/09/01). The Monte Carlo Method. Journal of the American Statistical Association, 44(247), 335-341. https://doi.org/10.1080/01621459.1949.10483310

Iqbal, M. N., Kütt, L., Lehtonen, M., Millar, R. J., Püvi, V., Rassõlkin, A., & Demidova, G. L. (2021). Travel Activity Based Stochastic Modelling of Load and Charging State of Electric Vehicles. Sustainability, 13(3).

Farh, H. M. H., Al-Shamma'a, A. A., Alaql, F., Omotoso, H. O., Alfraidi, W., & Mohamed, M. A. (2024, 2024/12/01/). Optimization and uncertainty analysis of hybrid energy systems using Monte Carlo simulation integrated with genetic algorithm. Computers and Electrical Engineering, 120, 109833. https://doi.org/https://doi.org/10.1016/j.compeleceng.2024.109833

Hosseini-Biyouki, M. M., & Zareian Jahromi, M. (2012, 12/01). A combinatorial artificial intelligence real-time solution to the unit commitment problem incorporating V2G. Electrical Engineering, 95, 1-15. https://doi.org/10.1007/s00202-012-0263-5

Grahn, P. (2013). Electric Vehicle Charging Impact on Load Profile. Ph.D. dissertation, Department Electrical Engineering, Royal Institute of Technology, Stockholm, Sweden.

Ghasemi, M., Ghavidel, S., Gitizadeh, M., & Akbari, E. (2015, 2015/02/01/). An improved teaching–learning-based optimization algorithm using Lévy mutation strategy for non-smooth optimal power flow. International Journal of Electrical Power & Energy Systems, 65, 375-384. https://doi.org/https://doi.org/10.1016/j.ijepes.2014.10.027

Coello, C. A. C., & Lechuga, M. S. (2002, 12-17 May 2002). MOPSO: a proposal for multiple objective particle swarm optimization. Proceedings of the 2002 Congress on Evolutionary Computation. CEC'02 (Cat. No.02TH8600),

Kennedy, J. (1997, 13-16 April 1997). The particle swarm: social adaptation of knowledge. Proceedings of 1997 IEEE International Conference on Evolutionary Computation (ICEC '97),

Lalwani, S., Singhal, S., Kumar, R., & Gupta, N. (2013, 08/01). A Comprehensive Survey: Multi-Objective Particle Swarm Optimization (MOPSO) algorithm: Variants and Applications. Transactions on Combinatorics, 2, 89-101.

Wang, H., Shi, M., Xie, P., Lai, C. S., Li, K., & Jia, Y. (2023). Electric Vehicle Charging Scheduling Strategy for Supporting Load Flattening Under Uncertain Electric Vehicle Departures. Journal of Modern Power Systems and Clean Energy, 11(5), 1634-1645. https://doi.org/10.35833/MPCE.2022.000220

Fioriti, D., Lutzemberger, G., Poli, D., Duenas-Martinez, P., & Micangeli, A. (2021, 2021/05/01/). Coupling economic multi-objective optimization and multiple design options: A business-oriented approach to size an off-grid hybrid microgrid. International Journal of Electrical Power & Energy Systems, 127, 106686. https://doi.org/https://doi.org/10.1016/j.ijepes.2020.106686

Dolatabadi, S. H., Ghorbanian, M., Siano, P., & Hatziargyriou, N. D. (2021). An Enhanced IEEE 33 Bus Benchmark Test System for Distribution System Studies. IEEE Transactions on Power Systems, 36(3), 2565-2572. https://doi.org/10.1109/TPWRS.2020.3038030

Andersen, F. M., Jacobsen, H. K., & Gunkel, P. A. (2021, 2021/09/01/). Hourly charging profiles for electric vehicles and their effect on the aggregated consumption profile in Denmark. International Journal of Electrical Power & Energy Systems, 130, 106900. https://doi.org/https://doi.org/10.1016/j.ijepes.2021.106900

APPENDIX

APPENDIX A

Input parameter

Table A.1 Load bus data of IEEE 33-bus distribution test system

Bus	Load (MW)	Load (Mvar)
1	0.00	0
2	0.10	0.06
3	0.09	0.04
4	0.12	0.08
5	0.06	0.03
6	0.06	0.02
7	0.20	0.1
8	0.20	0.1
9	0.06	0.02
10	0.06	0.02
11	0.05	0.03
12	0.06	0.035
13	0.06	0.035
14	0.12	0.08
15	0.06	0.01
16	0.06	0.02
17	0.06	0.02
18	0.09	0.04

Table A.1 Load bus data of IEEE 33-bus distribution test system (continued)

Bus	Load (MW)	Load (Mvar)
19	0.09	0.04
20	0.09	0.04
21	0.09	0.04
22	0.09	0.04
23	0.09	0.05
24	0.42	0.2
25	0.42	0.2
26	0.06	0.025
27	0.06	0.025
28	0.06	0.02
29	0.12	0.07
30	0.20	0.6
31	0.15	0.07
32	0.21	0.1
33	0.06	0.04

Table A.2 Line data of IEEE 33-bus distribution test system

No. Line	From (Bus)	To (Bus)	R (p.u.)	X (p.u.)	f_{max}^{l} (MW)
1	1	2	0.0575	0.0298	5
2	2	3	0.3076	0.1567	5
3	3	4	0.2284	0.1163	5
4	4	5	0.2378	0.1211	5
5	5	6	0.5110	0.4411	5
6	6	7	0.1168	0.3861	5
7	7	8	1.0678	0.7706	5
8	8	9	0.6426	0.4617	5
9	9	10	0.6489	0.4617	2.5
10	10	11	0.1227	0.0406	2.5
11	11	12	0.2336	0.0772	2.5
12	12	13	0.9159	0.7206	2.5
13	13	14	0.3379	0.4448	2.5
14	14	15	0.3687	0.3282	2.5
15	15	16	0.4656	0.3400	2.5
16	16	17	0.8042	1.0738	2.5
17	17	18	0.4567	0.3581	2.5
18	2	19	0.1023	0.0976	2.5
19	19	20	0.9385	0.8457	2.5
20	20	21	0.2555	0.2985	2.5
21	21	22	0.4423	0.5848	2.5
22	3	23	0.2815	0.1924	2.5

Table A.2 Line data of IEEE 33-bus distribution test system (continued)

No. Line	From (Bus)	To (Bus)	R (p.u.)	X (p.u.)	f_{max}^{l} (MW)
23	23	24	0.5603	0.4424	2.5
24	24	25	0.559	0.4374	2.5
25	6	26	0.1267	0.0645	2.5
26	26	27	0.1773	0.0903	2.5
27	27	28	0.6607	0.5826	2.5
28	28	29	0.5018	0.4371	2.5
29	29	30	0.3166	0.1613	2.5
30	30	31	0.608	0.6008	2.5
31	31	32	0.1937	0.2258	2.5
32	32	33	0.2128	0.3308	2.5

Table A.3 Residential Load Profile for Central Thailand in July

Hours	Power consumption (kW)	Power consumption (p.u.)
1	799.7234	0.6989
2	821.2429	0.7177
3	747.639	0.6534
4	880.7245	0.7697
5	844.6797	0.7382
6	486.0253	0.4247
7	341.7095	0.2986
8	438.6506	0.3833
9	562.7579	0.4918
10	579.7174	0.5066
11	560.5811	0.4899
12	598.6628	0.5232
13	583.0363	0.5095
14	427.8459	0.3739
15	587.9189	0.5138
16	561.5341	0.4907
17	632.3694	0.5526
18	664.6177	0.5808
19	1041.423	0.9101
20	1144.283	1.0000
21	1113.682	0.9733
22	978.7002	0.8553
23	841.6437	0.7355
24	827.3081	0.7230

APPENDIX B

Convergence Characteristics of PSO and GA for Sigle-objective optimization

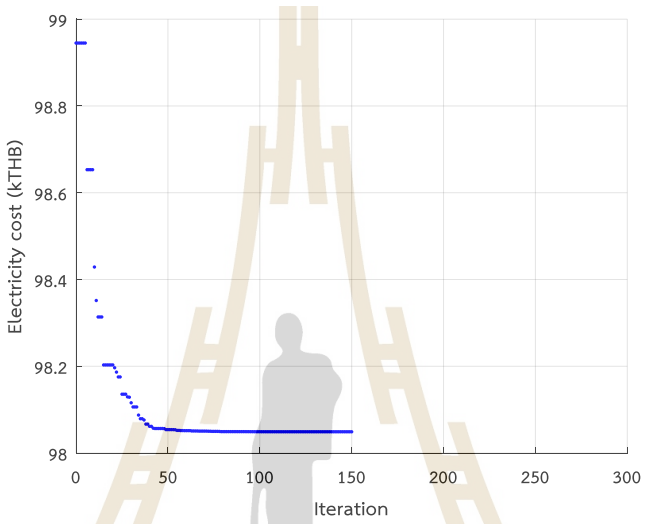

(a)

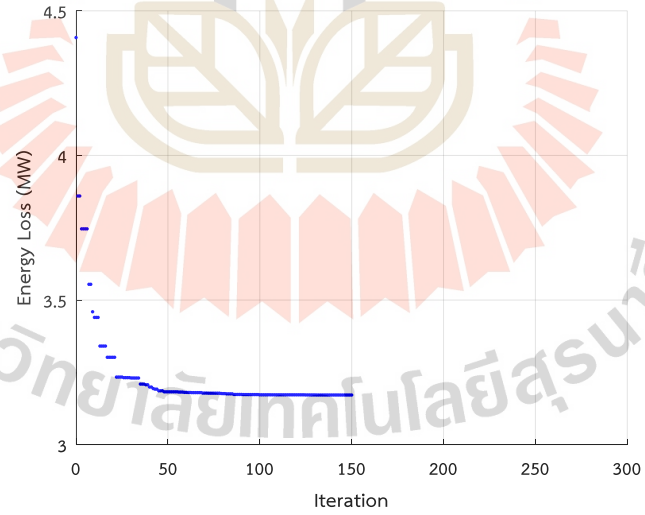

(b)

Figure B.1 PSO Convergence curves for V1G Single-Objective Cases: (a) MEC, (b) MEL, and (c) MPP

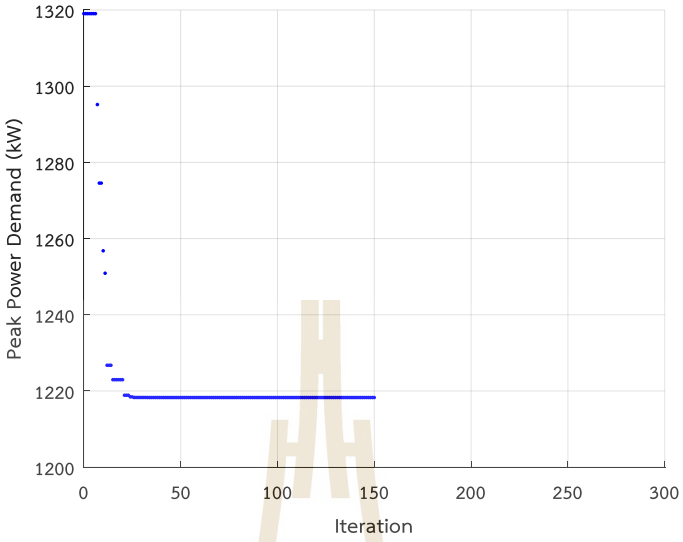

(c)

Figure B.1 PSO Convergence curves for V1G Single-Objective Cases: (a) MEC, (b) MEL, and (c) MPP (continued)

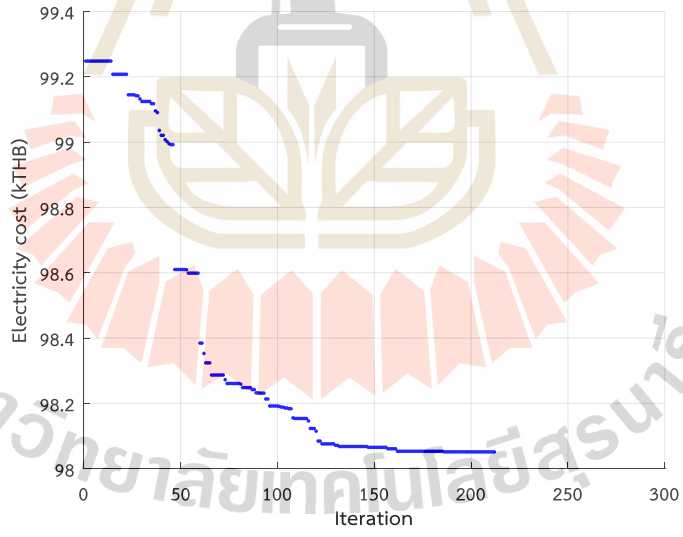

(a)

Figure B.2 GA Convergence curves for V1G Single-Objective Cases: (a) MEC, (b) MEL, and (c) MPP

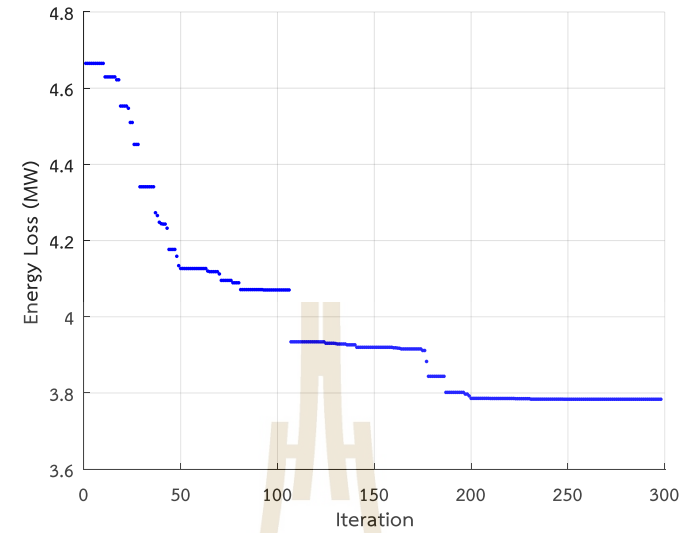

(b)

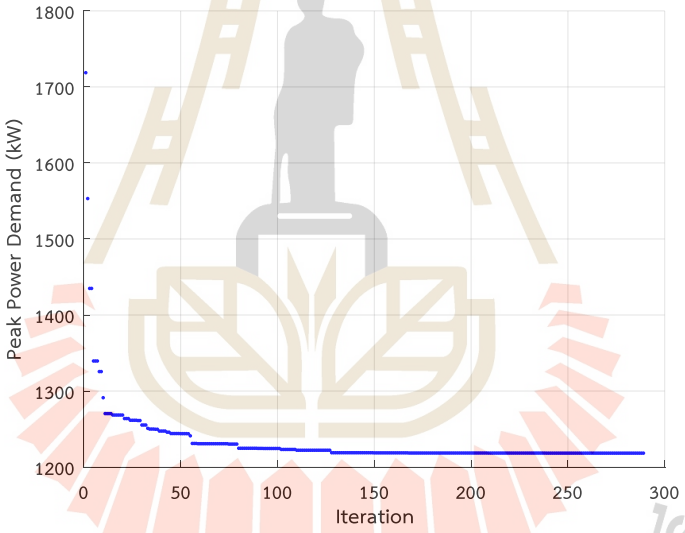

(c)

Figure B.2 GA Convergence curves for V1G Single-Objective Cases: (a) MEC, (b) MEL, and (c) MPP (continued)

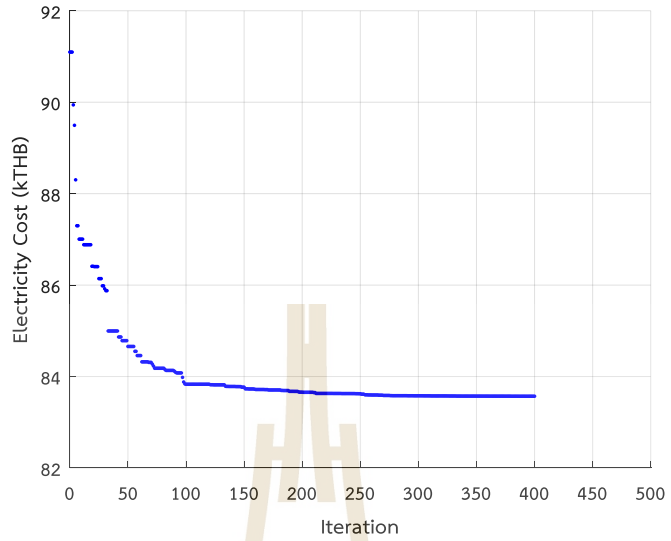

(a)

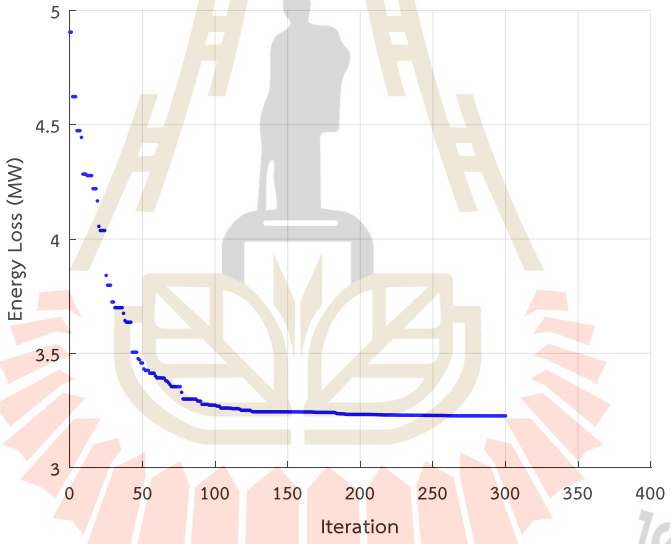

(b)

Figure B.3 PSO Convergence curves for V2G Single-Objective Cases: (a) MEC, (b) MEL, and (c) MPP

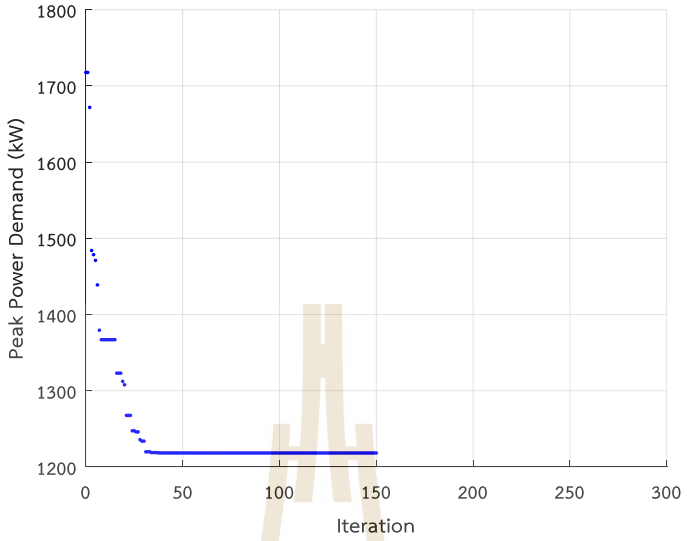

(c)

Figure B.3 PSO Convergence curves for V2G Single-Objective Cases: (a) MEC, (b) MEL, and (c) MPP (continued)

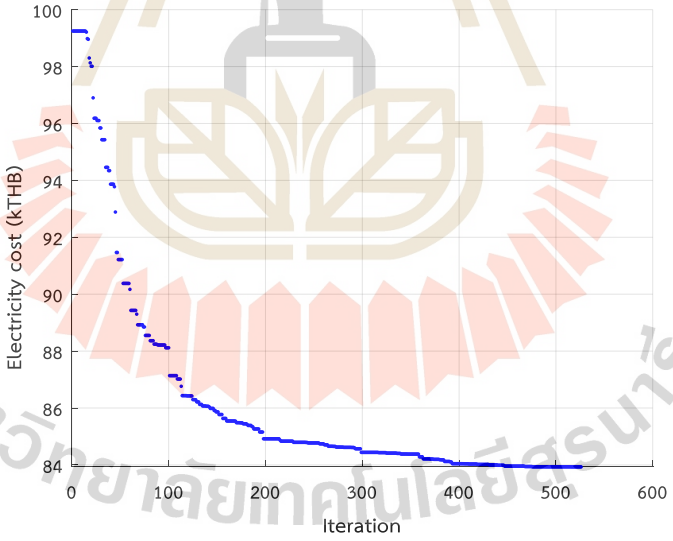

(a)

Figure B.4 GA Convergence curves for V2G Single-Objective Cases: (a) MEC, (b) MEL, and (c) MPP

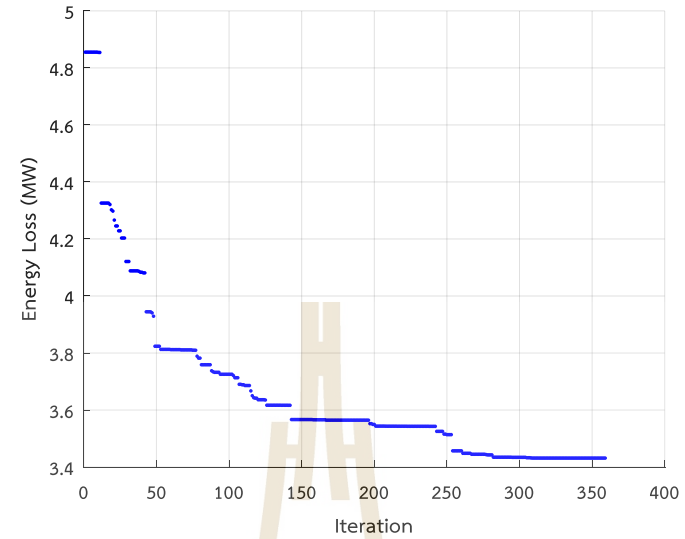

(b)

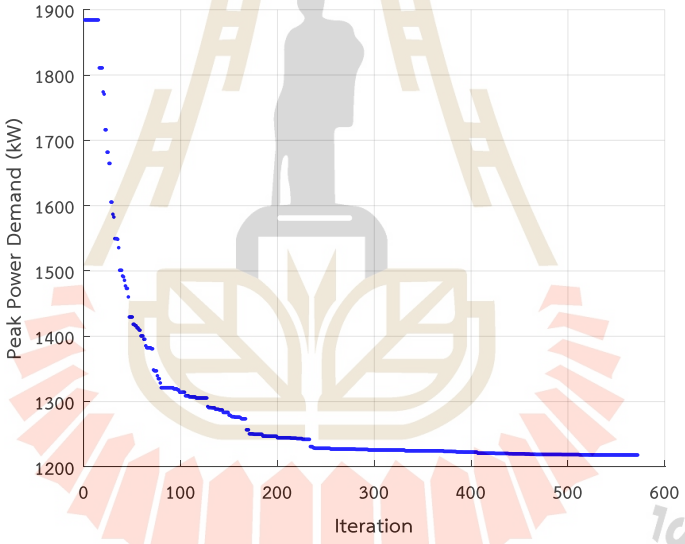

(c)

Figure B.4 GA Convergence curves for V2G Single-Objective Cases: (a) MEC, (b) MEL, and (c) MPP (continued)

APPENDIX C

Hourly Voltage and Power Flow Results of Each Bus

Table C.1 Hourly bus voltage results for the MCAL case from OOV1G

No. Bus	Hourly Bus Voltage (p.u.) Hours				No. Bus	Hourly Bus Voltage (p.u.) Hours			
	1	2	3	4		1	2	3	4
1	1.0000	1.0000	1.0000	1.0000	18	0.9609	0.9677	0.9629	0.9629
2	0.9972	0.9974	0.9969	0.9973	19	0.9967	0.9970	0.9964	0.9968
3	0.9839	0.9852	0.9824	0.9844	20	0.9934	0.9939	0.9928	0.9935
4	0.9769	0.9787	0.9748	0.9775	21	0.9927	0.9933	0.9921	0.9929
5	0.9700	0.9724	0.9673	0.9708	22	0.9921	0.9927	0.9915	0.9923
6	0.9535	0.9569	0.9695	0.9544	23	0.9805	0.9821	0.9788	0.9811
7	0.9505	0.9541	0.9664	0.9514	24	0.9743	0.9763	0.9720	0.9750
8	0.9677	0.9623	0.9624	0.9690	25	0.9712	0.9734	0.9686	0.9719
9	0.9617	0.9669	0.9658	0.9632	26	0.9517	0.9553	0.9676	0.9527
10	0.9662	0.9618	0.9698	0.9678	27	0.9694	0.9532	0.9652	0.9504
11	0.9654	0.9610	0.9688	0.9670	28	0.9696	0.9639	0.9649	0.9606
12	0.9639	0.9697	0.9672	0.9656	29	0.9626	0.9672	0.9675	0.9635
13	0.9681	0.9644	0.9608	0.9700	30	0.9695	0.9643	0.9641	0.9604
14	0.9660	0.9624	0.9685	0.9679	31	0.9657	0.9608	0.9600	0.9666
15	0.9646	0.9612	0.9670	0.9666	32	0.9649	0.9600	0.9691	0.9658
16	0.9633	0.9700	0.9656	0.9653	33	0.9646	0.9698	0.9689	0.9656
17	0.9614	0.9683	0.9635	0.9635					

Table C.1 Hourly bus voltage results for the MCAL case from OOV1G (Continued)

No. Bus	Hourly Bus Voltage (p.u.) Hours				No. Bus	Hourly Bus Voltage (p.u.) Hours			
	5	6	7	8		5	6	7	8
1	1.0000	1.0000	1.0000	1.0000	18	0.9694	0.9620	0.9613	0.9650
2	0.9972	0.9975	0.9968	0.9989	19	0.9967	0.9971	0.9963	0.9987
3	0.9837	0.9857	0.9819	0.9937	20	0.9933	0.9941	0.9927	0.9973
4	0.9766	0.9796	0.9741	0.9910	21	0.9926	0.9936	0.9920	0.9971
5	0.9695	0.9735	0.9663	0.9882	22	0.9920	0.9931	0.9914	0.9968
6	0.9527	0.9594	0.9691	0.9815	23	0.9802	0.9827	0.9781	0.9923
7	0.9696	0.9571	0.9665	0.9803	24	0.9739	0.9772	0.9712	0.9898
8	0.9666	0.9658	0.9619	0.9753	25	0.9708	0.9744	0.9677	0.9886
9	0.9605	0.9605	0.9650	0.9730	26	0.9509	0.9580	0.9673	0.9808
10	0.9650	0.9656	0.9687	0.9709	27	0.9685	0.9560	0.9649	0.9799
11	0.9641	0.9648	0.9677	0.9706	28	0.9685	0.9681	0.9656	0.9757
12	0.9626	0.9635	0.9659	0.9701	29	0.9613	0.9624	0.9691	0.9728
13	0.9667	0.9683	0.9694	0.9678	30	0.9681	0.9698	0.9659	0.9715
14	0.9646	0.9666	0.9671	0.9670	31	0.9642	0.9665	0.9617	0.9700
15	0.9632	0.9653	0.9655	0.9665	32	0.9634	0.9658	0.9609	0.9696
16	0.9619	0.9642	0.9640	0.9660	33	0.9631	0.9656	0.9606	0.9695
17	0.9700	0.9625	0.9619	0.9653					

Table C.1 Hourly bus voltage results for the MCAL case from OOV1G (Continued)

No. Bus	Hourly Bus Voltage (p.u.) Hours				No. Bus	Hourly Bus Voltage (p.u.) Hours			
	9	10	11	12		9	10	11	12
1	1.0000	1.0000	1.0000	1.0000	18	0.9547	0.9533	0.9549	0.9517
2	0.9986	0.9985	0.9986	0.9985	19	0.9983	0.9983	0.9983	0.9982
3	0.9919	0.9916	0.9919	0.9913	20	0.9966	0.9965	0.9966	0.9963
4	0.9883	0.9879	0.9884	0.9875	21	0.9962	0.9961	0.9962	0.9960
5	0.9848	0.9843	0.9849	0.9838	22	0.9959	0.9958	0.9959	0.9956
6	0.9761	0.9754	0.9762	0.9745	23	0.9901	0.9898	0.9902	0.9895
7	0.9745	0.9737	0.9746	0.9728	24	0.9869	0.9865	0.9869	0.9860
8	0.9681	0.9671	0.9682	0.9659	25	0.9853	0.9848	0.9853	0.9843
9	0.9651	0.9640	0.9652	0.9628	26	0.9752	0.9744	0.9753	0.9736
10	0.9624	0.9612	0.9625	0.9599	27	0.9740	0.9732	0.9741	0.9723
11	0.9620	0.9608	0.9621	0.9594	28	0.9686	0.9676	0.9687	0.9665
12	0.9612	0.9600	0.9614	0.9587	29	0.9648	0.9637	0.9649	0.9624
13	0.9584	0.9571	0.9585	0.9556	30	0.9631	0.9619	0.9632	0.9606
14	0.9573	0.9560	0.9575	0.9545	31	0.9611	0.9599	0.9613	0.9585
15	0.9566	0.9553	0.9568	0.9537	32	0.9607	0.9595	0.9609	0.9581
16	0.9560	0.9546	0.9562	0.9531	33	0.9606	0.9593	0.9607	0.9580
17	0.9550	0.9536	0.9552	0.9520					

Table C.1 Hourly bus voltage results for the MCAL case from OOV1G (Continued)

No. Bus	Hourly Bus Voltage (p.u.) Hours				No. Bus	Hourly Bus Voltage (p.u.) Hours			
	13	14	15	16		13	14	15	16
1	1.0000	1.0000	1.0000	1.0000	18	0.9530	0.9659	0.9526	0.9548
2	0.9985	0.9989	0.9985	0.9986	19	0.9983	0.9987	0.9982	0.9983
3	0.9916	0.9939	0.9915	0.9919	20	0.9964	0.9974	0.9964	0.9966
4	0.9879	0.9912	0.9878	0.9883	21	0.9961	0.9971	0.9960	0.9962
5	0.9842	0.9885	0.9841	0.9848	22	0.9958	0.9969	0.9957	0.9959
6	0.9752	0.9820	0.9750	0.9762	23	0.9898	0.9925	0.9897	0.9901
7	0.9735	0.9808	0.9733	0.9745	24	0.9864	0.9901	0.9863	0.9869
8	0.9669	0.9759	0.9666	0.9681	25	0.9847	0.9889	0.9846	0.9853
9	0.9638	0.9737	0.9635	0.9652	26	0.9743	0.9813	0.9741	0.9753
10	0.9610	0.9716	0.9606	0.9624	27	0.9730	0.9804	0.9728	0.9741
11	0.9605	0.9713	0.9602	0.9620	28	0.9674	0.9764	0.9672	0.9687
12	0.9598	0.9708	0.9594	0.9613	29	0.9634	0.9734	0.9631	0.9648
13	0.9568	0.9686	0.9564	0.9585	30	0.9617	0.9722	0.9614	0.9632
14	0.9557	0.9678	0.9553	0.9574	31	0.9597	0.9707	0.9593	0.9612
15	0.9550	0.9673	0.9546	0.9567	32	0.9592	0.9704	0.9589	0.9608
16	0.9543	0.9669	0.9539	0.9561	33	0.9591	0.9703	0.9587	0.9607
17	0.9533	0.9661	0.9529	0.9551					

Table C.1 Hourly bus voltage results for the MCAL case from OOV1G (continued)

No. Bus	Hourly Bus Voltage (p.u.) Hours				No. Bus	Hourly Bus Voltage (p.u.) Hours			
	17	18	19	20		17	18	19	20
1	1.0000	1.0000	1.0000	1.0000	18	0.9689	0.9621	0.9632	0.9535
2	0.9984	0.9979	0.9968	0.9965	19	0.9981	0.9975	0.9963	0.9959
3	0.9908	0.9877	0.9818	0.9801	20	0.9961	0.9949	0.9925	0.9918
4	0.9868	0.9824	0.9738	0.9714	21	0.9957	0.9944	0.9918	0.9910
5	0.9829	0.9771	0.9660	0.9628	22	0.9954	0.9939	0.9911	0.9903
6	0.9730	0.9644	0.9668	0.9618	23	0.9889	0.9851	0.9780	0.9760
7	0.9712	0.9621	0.9633	0.9679	24	0.9852	0.9803	0.9709	0.9683
8	0.9639	0.9524	0.9687	0.9619	25	0.9834	0.9779	0.9674	0.9645
9	0.9606	0.9679	0.9619	0.9645	26	0.9720	0.9631	0.9648	0.9696
10	0.9575	0.9637	0.9656	0.9677	27	0.9707	0.9613	0.9621	0.9667
11	0.9570	0.9631	0.9647	0.9666	28	0.9646	0.9537	0.9605	0.9639
12	0.9562	0.9620	0.9630	0.9648	29	0.9602	0.9683	0.9622	0.9648
13	0.9530	0.9676	0.9665	0.9626	30	0.9583	0.9659	0.9685	0.9608
14	0.9518	0.9660	0.9640	0.9600	31	0.9561	0.9630	0.9642	0.9660
15	0.9510	0.9650	0.9625	0.9583	32	0.9556	0.9623	0.9632	0.9649
16	0.9503	0.9640	0.9610	0.9566	33	0.9555	0.9621	0.9629	0.9646
17	0.9692	0.9625	0.9638	0.9542					

Table C.1 Hourly bus voltage results for the MCAL case from OOV1G (Continued)

No. Bus	Hourly Bus Voltage (p.u.) Hours				No. Bus	Hourly Bus Voltage (p.u.) Hours			
	21	22	23	24		21	22	23	24
1	1.0000	1.0000	1.0000	1.0000	18	0.9564	0.9640	0.9622	0.9630
2	0.9966	0.9970	0.9972	0.9973	19	0.9960	0.9965	0.9968	0.9968
3	0.9806	0.9828	0.9842	0.9843	20	0.9920	0.9929	0.9935	0.9935
4	0.9721	0.9753	0.9773	0.9775	21	0.9913	0.9922	0.9928	0.9929
5	0.9637	0.9679	0.9705	0.9708	22	0.9906	0.9916	0.9923	0.9923
6	0.9633	0.9698	0.9541	0.9545	23	0.9766	0.9792	0.9809	0.9810
7	0.9695	0.9665	0.9511	0.9516	24	0.9691	0.9725	0.9747	0.9749
8	0.9640	0.9627	0.9685	0.9691	25	0.9653	0.9692	0.9717	0.9719
9	0.9667	0.9663	0.9627	0.9633	26	0.9611	0.9679	0.9524	0.9528
10	0.9601	0.9604	0.9673	0.9679	27	0.9683	0.9654	0.9501	0.9505
11	0.9690	0.9695	0.9664	0.9671	28	0.9659	0.9645	0.9603	0.9609
12	0.9673	0.9680	0.9650	0.9657	29	0.9670	0.9666	0.9633	0.9639
13	0.9603	0.9618	0.9693	0.9600	30	0.9631	0.9632	0.9601	0.9608
14	0.9627	0.9695	0.9673	0.9680	31	0.9684	0.9691	0.9664	0.9671
15	0.9610	0.9680	0.9659	0.9667	32	0.9674	0.9682	0.9656	0.9663
16	0.9594	0.9666	0.9646	0.9654	33	0.9671	0.9679	0.9653	0.9661
17	0.9571	0.9646	0.9628	0.9636					

Table C.2 Hourly bus power flow results for the MCAL case from OOV1G

No. line	Hourly Bus Power Flow (MW) Hours				No. line	Hourly Bus Power Flow (MW) Hours			
	1	2	3	4		1	2	3	4
1	3.9878	3.5897	4.4784	3.7732	17	0.0922	0.0832	0.1032	0.0872
2	3.5043	3.1541	3.9361	3.3159	18	0.3701	0.3340	0.4145	0.3501
3	2.4041	2.1644	2.6996	2.2755	19	0.2777	0.2506	0.3110	0.2627
4	2.2641	2.0389	2.5415	2.1429	20	0.1846	0.1666	0.2067	0.1747
5	2.1865	1.9697	2.4534	2.0694	21	0.0923	0.0833	0.1033	0.0873
6	1.1269	1.0152	1.2644	1.0654	22	0.9623	0.8679	1.0784	0.9101
7	0.9204	0.8290	1.0332	0.8701	23	0.8671	0.7821	0.9714	0.8201
8	0.7044	0.6348	0.7900	0.6660	24	0.4317	0.3896	0.4835	0.4084
9	0.6389	0.5760	0.7162	0.6042	25	0.9652	0.8710	1.0808	0.9145
10	0.5741	0.5178	0.6434	0.5430	26	0.9018	0.8137	1.0098	0.8544
11	0.5275	0.4758	0.5911	0.4989	27	0.8378	0.7560	0.9380	0.7937
12	0.4650	0.4195	0.5210	0.4398	28	0.7681	0.6932	0.8600	0.7273
13	0.4009	0.3618	0.4488	0.3792	29	0.6397	0.5773	0.7163	0.6054
14	0.2774	0.2503	0.3106	0.2624	30	0.4319	0.3897	0.4836	0.4085
15	0.2156	0.1946	0.2414	0.2040	31	0.2767	0.2498	0.3098	0.2618
16	0.1538	0.1389	0.1722	0.1455	32	0.0615	0.0555	0.0688	0.0581

Table C.2 Hourly bus power flow results for the MCAL case from OOV1G (Continued)

No. line	Hourly Bus Power Flow (MW) Hours				No. line	Hourly Bus Power Flow (MW) Hours			
	5	6	7	8		5	6	7	8
1	4.0104	3.7847	4.0679	1.4523	17	0.0926	0.0882	0.1168	0.0345
2	3.5245	3.3241	4.4537	1.2741	18	0.3718	0.3538	0.4691	0.1382
3	2.4182	2.2796	3.0525	0.8747	19	0.2790	0.2654	0.3520	0.1036
4	2.2771	2.1484	2.8738	0.8260	20	0.1855	0.1765	0.2340	0.0690
5	2.1987	2.0769	2.7741	0.8005	21	0.0927	0.0882	0.1169	0.0345
6	1.1323	1.0748	1.4330	0.4157	22	0.9668	0.9192	1.2210	0.3579
7	0.9250	0.8775	1.1713	0.3388	23	0.8711	0.8284	1.0997	0.3229
8	0.7077	0.6721	0.8950	0.2605	24	0.4337	0.4127	0.5472	0.1612
9	0.6419	0.6100	0.8111	0.2370	25	0.9706	0.9172	1.2189	0.3567
10	0.5768	0.5484	0.7285	0.2135	26	0.9068	0.8571	1.1388	0.3334
11	0.5299	0.5039	0.6693	0.1962	27	0.8424	0.7965	1.0579	0.3099
12	0.4672	0.4443	0.5899	0.1731	28	0.7720	0.7320	0.9711	0.2855
13	0.4027	0.3833	0.5079	0.1497	29	0.6428	0.6107	0.8097	0.2384
14	0.2786	0.2652	0.3515	0.1036	30	0.4338	0.4128	0.5473	0.1612
15	0.2166	0.2062	0.2732	0.0806	31	0.2780	0.2646	0.3505	0.1035
16	0.1545	0.1471	0.1948	0.0575	32	0.0617	0.0588	0.0778	0.0230

Table C.2 Hourly bus power flow results for the MCAL case from OOV1G (Continued)

No. line	Hourly Bus Power Flow (MW) Hours				No. line	Hourly Bus Power Flow (MW) Hours			
	9	10	11	12		9	10	11	12
1	1.8741	1.9322	1.8667	1.9971	17	0.0443	0.0456	0.0441	0.0471
2	1.6448	1.6959	1.6383	1.7530	18	0.1773	0.1827	0.1766	0.1887
3	1.1292	1.1642	1.1247	1.2034	19	0.1330	0.1370	0.1325	0.1415
4	1.0657	1.0987	1.0615	1.1356	20	0.0886	0.0912	0.0882	0.0942
5	1.0320	1.0638	1.0279	1.0994	21	0.0443	0.0456	0.0441	0.0471
6	0.5347	0.5510	0.5326	0.5692	22	0.4596	0.4735	0.4578	0.4891
7	0.4359	0.4492	0.4342	0.4641	23	0.4146	0.4272	0.4130	0.4412
8	0.3349	0.3451	0.3336	0.3565	24	0.2069	0.2131	0.2061	0.2201
9	0.3045	0.3137	0.3033	0.3241	25	0.4592	0.4733	0.4574	0.4890
10	0.2742	0.2825	0.2731	0.2918	26	0.4292	0.4423	0.4275	0.4570
11	0.2520	0.2596	0.2510	0.2681	27	0.3989	0.4111	0.3974	0.4248
12	0.2223	0.2290	0.2214	0.2365	28	0.3669	0.3781	0.3655	0.3905
13	0.1921	0.1979	0.1914	0.2044	29	0.3062	0.3154	0.3050	0.3258
14	0.1330	0.1370	0.1325	0.1415	30	0.2069	0.2132	0.2061	0.2202
15	0.1034	0.1065	0.1030	0.1100	31	0.1328	0.1368	0.1323	0.1413
16	0.0738	0.0760	0.0735	0.0785	32	0.0295	0.0304	0.0294	0.0314

Table C.2 Hourly bus power flow results for the MCAL case from OOV1G (Continued)

No. line	Hourly Bus Power Flow (MW) Hours 13	14	15	16	No. line	Hourly Bus Power Flow (MW) Hours 13	14	15	16
1	1.9435	1.4158	1.9603	1.8699	17	0.0459	0.0337	0.0462	0.0442
2	1.7059	1.2421	1.7206	1.6411	18	0.1837	0.1348	0.1853	0.1769
3	1.1711	0.8527	1.1812	1.1266	19	0.1378	0.1011	0.1390	0.1327
4	1.1051	0.8053	1.1146	1.0633	20	0.0918	0.0673	0.0925	0.0884
5	1.0700	0.7805	1.0792	1.0297	21	0.0459	0.0337	0.0463	0.0442
6	0.5542	0.4053	0.5589	0.5335	22	0.4763	0.3490	0.4803	0.4586
7	0.4518	0.3303	0.4557	0.4350	23	0.4296	0.3149	0.4332	0.4137
8	0.3471	0.2541	0.3501	0.3342	24	0.2143	0.1572	0.2161	0.2064
9	0.3156	0.2311	0.3182	0.3038	25	0.4761	0.3478	0.4801	0.4582
10	0.2841	0.2082	0.2865	0.2736	26	0.4449	0.3251	0.4487	0.4282
11	0.2611	0.1913	0.2633	0.2514	27	0.4135	0.3022	0.4170	0.3980
12	0.2303	0.1688	0.2322	0.2218	28	0.3803	0.2784	0.3835	0.3661
13	0.1991	0.1460	0.2007	0.1917	29	0.3173	0.2325	0.3199	0.3055
14	0.1378	0.1011	0.1389	0.1327	30	0.2144	0.1573	0.2162	0.2065
15	0.1071	0.0786	0.1080	0.1032	31	0.1376	0.1010	0.1388	0.1325
16	0.0765	0.0561	0.0771	0.0737	32	0.0306	0.0224	0.0308	0.0294

Table C.2 Hourly bus power flow results for the MCAL case from OOV1G (Continued)

No. line	Hourly Bus Power Flow (MW) Hours				No. line	Hourly Bus Power Flow (MW) Hours			
	17	18	19	20		17	18	19	20
1	2.1130	3.0055	4.3564	4.7355	17	0.0497	0.0703	0.0998	0.1079
2	1.8549	2.6393	3.8306	4.1655	18	0.1993	0.2817	0.4010	0.4336
3	1.2734	1.8111	2.6289	2.8589	19	0.1495	0.2114	0.3009	0.3253
4	1.2014	1.7075	2.4736	2.6885	20	0.0995	0.1406	0.2000	0.2162
5	1.1629	1.6513	2.3860	2.5913	21	0.0498	0.0703	0.1000	0.1081
6	0.6017	0.8537	1.2242	1.3266	22	0.5168	0.7314	1.0435	1.1291
7	0.4907	0.6967	1.0006	1.0848	23	0.4661	0.6594	0.9399	1.0167
8	0.3768	0.5342	0.7647	0.8283	24	0.2325	0.3286	0.4677	0.5057
9	0.3425	0.4851	0.6932	0.7503	25	0.5171	0.7317	1.0522	1.1411
10	0.3083	0.4364	0.6226	0.6736	26	0.4832	0.6837	0.9829	1.0659
11	0.2833	0.4010	0.5720	0.6189	27	0.4491	0.6354	0.9128	0.9897
12	0.2499	0.3536	0.5041	0.5454	28	0.4127	0.5836	0.8348	0.9040
13	0.2160	0.3053	0.4341	0.4693	29	0.3442	0.4866	0.6940	0.7509
14	0.1494	0.2112	0.3004	0.3247	30	0.2326	0.3288	0.4678	0.5058
15	0.1162	0.1642	0.2335	0.2524	31	0.1493	0.2109	0.2996	0.3238
16	0.0830	0.1172	0.1665	0.1799	32	0.0332	0.0468	0.0665	0.0719

Table C.2 Hourly bus power flow results for the MCAL case from OOV1G (Continued)

No. line	Hourly Bus Power Flow (MW)				No. line	Hourly Bus Power Flow (MW)			
	Hours					Hours			
	21	22	23	24		21	22	23	24
1	4.6222	4.1275	3.8621	3.8379	17	0.1055	0.0949	0.0893	0.0888
2	4.0654	3.6285	3.3939	3.3725	18	0.4239	0.3811	0.3584	0.3564
3	2.7901	2.4901	2.3287	2.3140	19	0.3181	0.2860	0.2689	0.2674
4	2.6242	2.3438	2.1931	2.1794	20	0.2114	0.1901	0.1788	0.1778
5	2.5300	2.2618	2.1179	2.1048	21	0.1056	0.0950	0.0894	0.0889
6	1.2961	1.1621	1.0910	1.0845	22	1.1036	0.9914	0.9319	0.9265
7	1.0597	0.9495	0.8911	0.8857	23	0.9939	0.8931	0.8397	0.8348
8	0.8094	0.7261	0.6820	0.6780	24	0.4944	0.4445	0.4181	0.4157
9	0.7333	0.6584	0.6186	0.6150	25	1.1146	0.9982	0.9355	0.9298
10	0.6584	0.5915	0.5560	0.5527	26	1.0412	0.9326	0.8740	0.8687
11	0.6049	0.5434	0.5108	0.5079	27	0.9668	0.8662	0.8120	0.8070
12	0.5331	0.4790	0.4504	0.4477	28	0.8834	0.7928	0.7443	0.7398
13	0.4588	0.4127	0.3882	0.3860	29	0.7340	0.6594	0.6197	0.6161
14	0.3175	0.2856	0.2686	0.2671	30	0.4945	0.4447	0.4183	0.4159
15	0.2468	0.2220	0.2088	0.2076	31	0.3166	0.2849	0.2680	0.2665
16	0.1759	0.1583	0.1490	0.1481	32	0.0703	0.0633	0.0595	0.0592

Table C.3 Hourly bus voltage results for the MCAP case from OOV1G

No. Bus	Hourly Bus Voltage (p.u.) Hours				No. Bus	Hourly Bus Voltage (p.u.) Hours			
	1	2	3	4		1	2	3	4
1	1.0000	1.0000	1.0000	1.0000	18	0.9536	0.9508	0.9619	0.9743
2	0.9956	0.9955	0.9961	0.9965	19	0.9948	0.9947	0.9955	0.9959
3	0.9746	0.9740	0.9778	0.9801	20	0.9898	0.9896	0.9910	0.9919
4	0.9636	0.9626	0.9681	0.9714	21	0.9888	0.9886	0.9902	0.9911
5	0.9526	0.9514	0.9586	0.9628	22	0.9880	0.9877	0.9894	0.9904
6	0.9673	0.9654	0.9665	0.9625	23	0.9694	0.9686	0.9732	0.9759
7	0.9631	0.9610	0.9627	0.9689	24	0.9598	0.9587	0.9647	0.9682
8	0.9623	0.9847	0.9647	0.9629	25	0.9549	0.9538	0.9605	0.9644
9	0.9776	0.9748	0.9663	0.9654	26	0.9647	0.9627	0.9641	0.9603
10	0.9686	0.9655	0.9835	0.9685	27	0.9611	0.9691	0.9610	0.9675
11	0.9672	0.9641	0.9823	0.9674	28	0.9670	0.9645	0.9685	0.9657
12	0.9648	0.9616	0.9802	0.9656	29	0.9819	0.9791	0.9696	0.9672
13	0.9553	0.9619	0.9720	0.9833	30	0.9771	0.9743	0.9655	0.9633
14	0.9620	0.9585	0.9691	0.9807	31	0.9712	0.9682	0.9603	0.9686
15	0.9597	0.9561	0.9672	0.9790	32	0.9699	0.9669	0.9842	0.9676
16	0.9576	0.9539	0.9653	0.9773	33	0.9696	0.9665	0.9839	0.9673
17	0.9545	0.9508	0.9627	0.9750					

Table C.3 Hourly bus voltage results for the MCAP case from OOV1G (Continued)

No. Bus	Hourly Bus Voltage (p.u.) Hours				No. Bus	Hourly Bus Voltage (p.u.) Hours			
	5	6	7	8		5	6	7	8
1	1.0000	1.0000	1.0000	1.0000	18	0.9540	0.9727	0.9690	0.9650
2	0.9956	0.9964	0.9971	0.9989	19	0.9949	0.9958	0.9966	0.9987
3	0.9747	0.9795	0.9833	0.9937	20	0.9898	0.9917	0.9932	0.9973
4	0.9637	0.9707	0.9761	0.9910	21	0.9889	0.9910	0.9926	0.9971
5	0.9528	0.9619	0.9689	0.9882	22	0.9880	0.9903	0.9920	0.9968
6	0.9675	0.9622	0.9530	0.9815	23	0.9695	0.9753	0.9797	0.9923
7	0.9632	0.9690	0.9506	0.9803	24	0.9599	0.9675	0.9734	0.9898
8	0.9625	0.9625	0.9671	0.9753	25	0.9551	0.9636	0.9702	0.9886
9	0.9779	0.9647	0.9609	0.9730	26	0.9648	0.9601	0.9513	0.9808
10	0.9690	0.9676	0.9651	0.9709	27	0.9613	0.9673	0.9691	0.9799
11	0.9676	0.9664	0.9642	0.9706	28	0.9670	0.9665	0.9605	0.9757
12	0.9651	0.9644	0.9625	0.9701	29	0.9818	0.9688	0.9644	0.9728
13	0.9557	0.9820	0.9665	0.9678	30	0.9771	0.9652	0.9614	0.9715
14	0.9624	0.9794	0.9644	0.9670	31	0.9712	0.9605	0.9676	0.9700
15	0.9602	0.9776	0.9629	0.9665	32	0.9699	0.9695	0.9668	0.9696
16	0.9580	0.9758	0.9615	0.9660	33	0.9695	0.9692	0.9666	0.9695
17	0.9550	0.9735	0.9696	0.9653					

Table C.3 Hourly bus voltage results for the MCAP case from OOV1G (Continued)

No. Bus	Hourly Bus Voltage (p.u.) Hours				No. Bus	Hourly Bus Voltage (p.u.) Hours			
	9	10	11	12		9	10	11	12
1	1.0000	1.0000	1.0000	1.0000	18	0.9547	0.9533	0.9549	0.9517
2	0.9986	0.9985	0.9986	0.9985	19	0.9983	0.9983	0.9983	0.9982
3	0.9919	0.9916	0.9919	0.9913	20	0.9966	0.9965	0.9966	0.9963
4	0.9883	0.9879	0.9884	0.9875	21	0.9962	0.9961	0.9962	0.9960
5	0.9848	0.9843	0.9849	0.9838	22	0.9959	0.9958	0.9959	0.9956
6	0.9761	0.9754	0.9762	0.9745	23	0.9901	0.9898	0.9902	0.9895
7	0.9745	0.9737	0.9746	0.9728	24	0.9869	0.9865	0.9869	0.9860
8	0.9681	0.9671	0.9682	0.9659	25	0.9853	0.9848	0.9853	0.9843
9	0.9651	0.9640	0.9652	0.9628	26	0.9752	0.9744	0.9753	0.9736
10	0.9624	0.9612	0.9625	0.9599	27	0.9740	0.9732	0.9741	0.9723
11	0.9620	0.9608	0.9621	0.9594	28	0.9686	0.9676	0.9687	0.9665
12	0.9612	0.9600	0.9614	0.9587	29	0.9648	0.9637	0.9649	0.9624
13	0.9584	0.9571	0.9585	0.9556	30	0.9631	0.9619	0.9632	0.9606
14	0.9573	0.9560	0.9575	0.9545	31	0.9611	0.9599	0.9613	0.9585
15	0.9566	0.9553	0.9568	0.9537	32	0.9607	0.9595	0.9609	0.9581
16	0.9560	0.9546	0.9562	0.9531	33	0.9606	0.9593	0.9607	0.9580
17	0.9550	0.9536	0.9552	0.9520					

Table C.3 Hourly bus voltage results for the MCAP case from OOV1G (Continued)

No. Bus	Hourly Bus Voltage (p.u.) Hours				No. Bus	Hourly Bus Voltage (p.u.) Hours			
	13	14	15	16		13	14	15	16
1	1.0000	1.0000	1.0000	1.0000	18	0.9530	0.9659	0.9526	0.9548
2	0.9985	0.9989	0.9985	0.9986	19	0.9983	0.9987	0.9982	0.9983
3	0.9916	0.9939	0.9915	0.9919	20	0.9964	0.9974	0.9964	0.9966
4	0.9879	0.9912	0.9878	0.9883	21	0.9961	0.9971	0.9960	0.9962
5	0.9842	0.9885	0.9841	0.9848	22	0.9958	0.9969	0.9957	0.9959
6	0.9752	0.9820	0.9750	0.9762	23	0.9898	0.9925	0.9897	0.9901
7	0.9735	0.9808	0.9733	0.9745	24	0.9864	0.9901	0.9863	0.9869
8	0.9669	0.9759	0.9666	0.9681	25	0.9847	0.9889	0.9846	0.9853
9	0.9638	0.9737	0.9635	0.9652	26	0.9743	0.9813	0.9741	0.9753
10	0.9610	0.9716	0.9606	0.9624	27	0.9730	0.9804	0.9728	0.9741
11	0.9605	0.9713	0.9602	0.9620	28	0.9674	0.9764	0.9672	0.9687
12	0.9598	0.9708	0.9594	0.9613	29	0.9634	0.9734	0.9631	0.9648
13	0.9568	0.9686	0.9564	0.9585	30	0.9617	0.9722	0.9614	0.9632
14	0.9557	0.9678	0.9553	0.9574	31	0.9597	0.9707	0.9593	0.9612
15	0.9550	0.9673	0.9546	0.9567	32	0.9592	0.9704	0.9589	0.9608
16	0.9543	0.9669	0.9539	0.9561	33	0.9591	0.9703	0.9587	0.9607
17	0.9533	0.9661	0.9529	0.9551					

Table C.3 Hourly bus voltage results for the MCAP case from OOV1G (Continued)

No. Bus	Hourly Bus Voltage (p.u.) Hours				No. Bus	Hourly Bus Voltage (p.u.) Hours			
	17	18	19	20		17	18	19	20
1	1.0000	1.0000	1.0000	1.0000	18	0.9689	0.9627	0.9832	0.9735
2	0.9984	0.9976	0.9968	0.9965	19	0.9981	0.9971	0.9963	0.9959
3	0.9908	0.9860	0.9818	0.9801	20	0.9961	0.9942	0.9925	0.9918
4	0.9868	0.9799	0.9738	0.9714	21	0.9957	0.9936	0.9918	0.9910
5	0.9829	0.9739	0.9660	0.9628	22	0.9954	0.9931	0.9911	0.9903
6	0.9730	0.9596	0.9668	0.9618	23	0.9889	0.9830	0.9780	0.9760
7	0.9712	0.9571	0.9633	0.9679	24	0.9852	0.9776	0.9709	0.9683
8	0.9639	0.9660	0.9687	0.9619	25	0.9834	0.9749	0.9674	0.9645
9	0.9606	0.9608	0.9619	0.9645	26	0.9720	0.9581	0.9648	0.9696
10	0.9575	0.9660	0.9656	0.9677	27	0.9707	0.9561	0.9621	0.9667
11	0.9570	0.9653	0.9647	0.9666	28	0.9646	0.9678	0.9605	0.9639
12	0.9562	0.9640	0.9630	0.9648	29	0.9602	0.9618	0.9622	0.9648
13	0.9530	0.9690	0.9665	0.9826	30	0.9583	0.9690	0.9685	0.9608
14	0.9518	0.9672	0.9640	0.9800	31	0.9561	0.9658	0.9642	0.9660
15	0.9510	0.9660	0.9625	0.9783	32	0.9556	0.9651	0.9632	0.9649
16	0.9503	0.9649	0.9610	0.9766	33	0.9555	0.9648	0.9629	0.9646
17	0.9692	0.9632	0.9838	0.9742					

Table C.3 Hourly bus voltage results for the MCAP case from OOV1G (Continued)

No. Bus	Hourly Bus Voltage (p.u.) Hours				No. Bus	Hourly Bus Voltage (p.u.) Hours			
	21	22	23	24		21	22	23	24
1	1.0000	1.0000	1.0000	1.0000	18	0.9764	0.9765	0.9528	0.9677
2	0.9966	0.9966	0.9956	0.9974	19	0.9960	0.9960	0.9948	0.9970
3	0.9806	0.9805	0.9745	0.9852	20	0.9920	0.9920	0.9898	0.9939
4	0.9721	0.9721	0.9634	0.9787	21	0.9913	0.9913	0.9888	0.9933
5	0.9637	0.9637	0.9524	0.9724	22	0.9906	0.9906	0.9879	0.9927
6	0.9633	0.9635	0.9669	0.9569	23	0.9766	0.9765	0.9692	0.9821
7	0.9695	0.9699	0.9626	0.9541	24	0.9691	0.9690	0.9596	0.9763
8	0.9640	0.9642	0.9617	0.9623	25	0.9653	0.9652	0.9547	0.9734
9	0.9667	0.9670	0.9770	0.9669	26	0.9611	0.9614	0.9642	0.9553
10	0.9601	0.9602	0.9680	0.9618	27	0.9683	0.9686	0.9606	0.9531
11	0.9690	0.9692	0.9666	0.9610	28	0.9659	0.9666	0.9663	0.9639
12	0.9673	0.9674	0.9641	0.9697	29	0.9670	0.9680	0.9810	0.9672
13	0.9603	0.9603	0.9646	0.9644	30	0.9631	0.9642	0.9763	0.9642
14	0.9827	0.9828	0.9613	0.9624	31	0.9684	0.9696	0.9703	0.9607
15	0.9810	0.9811	0.9590	0.9612	32	0.9674	0.9686	0.9690	0.9700
16	0.9794	0.9795	0.9568	0.9700	33	0.9671	0.9683	0.9686	0.9697
17	0.9771	0.9772	0.9538	0.9683					

Table C.4 Hourly bus power flow results for the MCAP case from OOV1G

No. line	Hourly Bus Power Flow (MW) Hours				No. line	Hourly Bus Power Flow (MW) Hours			
	1	2	3	4		1	2	3	4
1	4.6982	4.8616	4.8364	4.0301	17	0.1507	0.1540	0.1327	0.1150
2	4.8947	4.0393	4.1334	4.4231	18	0.6076	0.6213	0.5340	0.4623
3	4.0404	4.1395	3.5192	3.0337	19	0.4560	0.4663	0.4007	0.3469
4	3.7953	3.8876	3.3089	2.8539	20	0.3028	0.3096	0.2662	0.2305
5	3.6526	3.7404	3.1886	2.7521	21	0.1513	0.1547	0.1330	0.1152
6	1.8721	1.9158	1.6387	1.4144	22	1.5857	1.6219	1.3918	1.2039
7	1.5335	1.5696	1.3408	1.1566	23	1.4267	1.4591	1.2529	1.0841
8	1.1669	1.1939	1.0224	0.8831	24	0.7086	0.7246	0.6228	0.5392
9	1.0550	1.0791	0.9254	0.8000	25	1.5943	1.6315	1.3968	1.2099
10	0.9458	0.9673	0.8303	0.7182	26	1.4891	1.5238	1.3048	1.1302
11	0.8688	0.8886	0.7628	0.6599	27	1.3822	1.4142	1.2116	1.0496
12	0.7649	0.7822	0.6719	0.5815	28	1.2631	1.2919	1.1089	0.9608
13	0.6562	0.6707	0.5775	0.5003	29	1.0503	1.0741	0.9228	0.7994
14	0.4541	0.4642	0.3996	0.3462	30	0.7080	0.7239	0.6226	0.5393
15	0.3529	0.3608	0.3106	0.2691	31	0.4526	0.4626	0.3984	0.3452
16	0.2513	0.2568	0.2213	0.1919	32	0.1004	0.1027	0.0884	0.0766

Table C.4 Hourly bus power flow results for the MCAP case from OOV1G (Continued)

No. line	Hourly Bus Power Flow (MW) Hours				No. line	Hourly Bus Power Flow (MW) Hours			
	5	6	7	8		5	6	7	8
1	4.6218	4.5966	4.6587	1.4523	**17**	0.1490	0.1280	0.1078	0.0345
2	4.8276	4.9205	4.0931	1.2741	**18**	0.6007	0.5149	0.4328	0.1382
3	3.9948	3.3724	2.8057	0.8747	**19**	0.4508	0.3864	0.3248	0.1036
4	3.7525	3.1727	2.6425	0.8260	**20**	0.2993	0.2567	0.2159	0.0690
5	3.6114	3.0598	2.5522	0.8005	**21**	0.1496	0.1283	0.1079	0.0345
6	1.8504	1.5771	1.3198	0.4157	**22**	1.5676	1.3413	1.1259	0.3579
7	1.5156	1.2898	1.0782	0.3388	**23**	1.4104	1.2076	1.0143	0.3229
8	1.1535	0.9844	0.8246	0.2605	**24**	0.7005	0.6005	0.5049	0.1612
9	1.0429	0.8914	0.7477	0.2370	**25**	1.5769	1.3416	1.1232	0.3567
10	0.9350	0.8001	0.6717	0.2135	**26**	1.4728	1.2533	1.0495	0.3334
11	0.8589	0.7351	0.6172	0.1962	**27**	1.3671	1.1640	0.9751	0.3099
12	0.7562	0.6477	0.5440	0.1731	**28**	1.2491	1.0671	0.8956	0.2855
13	0.6487	0.5571	0.4688	0.1497	**29**	1.0385	0.8891	0.7470	0.2384
14	0.4490	0.3855	0.3244	0.1036	**30**	0.7000	0.6005	0.5050	0.1612
15	0.3489	0.2996	0.2521	0.0806	**31**	0.4475	0.3844	0.3235	0.1035
16	0.2484	0.2136	0.1798	0.0575	**32**	0.0993	0.0853	0.0718	0.0230

Table C.4 Hourly bus power flow results for the MCAP case from OOV1G (Continued)

No. line	Hourly Bus Power Flow (MW) Hours				No. line	Hourly Bus Power Flow (MW) Hours			
	9	10	11	12		9	10	11	12
1	1.8741	1.9322	1.8667	1.9971	17	0.0443	0.0456	0.0441	0.0471
2	1.6448	1.6959	1.6383	1.7530	18	0.1773	0.1827	0.1766	0.1887
3	1.1292	1.1642	1.1247	1.2034	19	0.1330	0.1370	0.1325	0.1415
4	1.0657	1.0987	1.0615	1.1356	20	0.0886	0.0912	0.0882	0.0942
5	1.0320	1.0638	1.0279	1.0994	21	0.0443	0.0456	0.0441	0.0471
6	0.5347	0.5510	0.5326	0.5692	22	0.4596	0.4735	0.4578	0.4891
7	0.4359	0.4492	0.4342	0.4641	23	0.4146	0.4272	0.4130	0.4412
8	0.3349	0.3451	0.3336	0.3565	24	0.2069	0.2131	0.2061	0.2201
9	0.3045	0.3137	0.3033	0.3241	25	0.4592	0.4733	0.4574	0.4890
10	0.2742	0.2825	0.2731	0.2918	26	0.4292	0.4423	0.4275	0.4570
11	0.2520	0.2596	0.2510	0.2681	27	0.3989	0.4111	0.3974	0.4248
12	0.2223	0.2290	0.2214	0.2365	28	0.3669	0.3781	0.3655	0.3905
13	0.1921	0.1979	0.1914	0.2044	29	0.3062	0.3154	0.3050	0.3258
14	0.1330	0.1370	0.1325	0.1415	30	0.2069	0.2132	0.2061	0.2202
15	0.1034	0.1065	0.1030	0.1100	31	0.1328	0.1368	0.1323	0.1413
16	0.0738	0.0760	0.0735	0.0785	32	0.0295	0.0304	0.0294	0.0314

Table C.4 Hourly bus power flow results for the MCAP case from OOV1G (Continued)

No. line	Hourly Bus Power Flow (MW) Hours				No. line	Hourly Bus Power Flow (MW) Hours			
	13	14	15	16		13	14	15	16
1	1.9435	1.4158	1.9603	1.8699	17	0.0459	0.0337	0.0462	0.0442
2	1.7059	1.2421	1.7206	1.6411	18	0.1837	0.1348	0.1853	0.1769
3	1.1711	0.8527	1.1812	1.1266	19	0.1378	0.1011	0.1390	0.1327
4	1.1051	0.8053	1.1146	1.0633	20	0.0918	0.0673	0.0925	0.0884
5	1.0700	0.7805	1.0792	1.0297	21	0.0459	0.0337	0.0463	0.0442
6	0.5542	0.4053	0.5589	0.5335	22	0.4763	0.3490	0.4803	0.4586
7	0.4518	0.3303	0.4557	0.4350	23	0.4296	0.3149	0.4332	0.4137
8	0.3471	0.2541	0.3501	0.3342	24	0.2143	0.1572	0.2161	0.2064
9	0.3156	0.2311	0.3182	0.3038	25	0.4761	0.3478	0.4801	0.4582
10	0.2841	0.2082	0.2865	0.2736	26	0.4449	0.3251	0.4487	0.4282
11	0.2611	0.1913	0.2633	0.2514	27	0.4135	0.3022	0.4170	0.3980
12	0.2303	0.1688	0.2322	0.2218	28	0.3803	0.2784	0.3835	0.3661
13	0.1991	0.1460	0.2007	0.1917	29	0.3173	0.2325	0.3199	0.3055
14	0.1378	0.1011	0.1389	0.1327	30	0.2144	0.1573	0.2162	0.2065
15	0.1071	0.0786	0.1080	0.1032	31	0.1376	0.1010	0.1388	0.1325
16	0.0765	0.0561	0.0771	0.0737	32	0.0306	0.0224	0.0308	0.0294

Table C.4 Hourly bus power flow results for the MCAP case from OOV1G (Continued)

No. line	Hourly Bus Power Flow (MW) Hours				No. line	Hourly Bus Power Flow (MW) Hours			
	17	18	19	20		17	18	19	20
1	2.1130	3.5191	4.3564	4.7355	17	0.0497	0.0819	0.0998	0.1079
2	1.8549	3.0911	3.8306	4.1655	18	0.1993	0.3287	0.4010	0.4336
3	1.2734	2.1206	2.6289	2.8589	19	0.1495	0.2466	0.3009	0.3253
4	1.2014	1.9985	2.4736	2.6885	20	0.0995	0.1640	0.2000	0.2162
5	1.1629	1.9317	2.3860	2.5913	21	0.0498	0.0820	0.1000	0.1081
6	0.6017	0.9981	1.2242	1.3266	22	0.5168	0.8539	1.0435	1.1291
7	0.4907	0.8148	1.0006	1.0848	23	0.4661	0.7696	0.9399	1.0167
8	0.3768	0.6242	0.7647	0.8283	24	0.2325	0.3834	0.4677	0.5057
9	0.3425	0.5666	0.6932	0.7503	25	0.5171	0.8542	1.0522	1.1411
10	0.3083	0.5094	0.6226	0.6736	26	0.4832	0.7981	0.9829	1.0659
11	0.2833	0.4681	0.5720	0.6189	27	0.4491	0.7416	0.9128	0.9897
12	0.2499	0.4127	0.5041	0.5454	28	0.4127	0.6810	0.8348	0.9040
13	0.2160	0.3561	0.4341	0.4693	29	0.3442	0.5677	0.6940	0.7509
14	0.1494	0.2464	0.3004	0.3247	30	0.2326	0.3835	0.4678	0.5058
15	0.1162	0.1915	0.2335	0.2524	31	0.1493	0.2459	0.2996	0.3238
16	0.0830	0.1367	0.1665	0.1799	32	0.0332	0.0546	0.0665	0.0719

Table C.4 Hourly bus power flow results for the MCAP case from OOV1G (Continued)

No. line	Hourly Bus Power Flow (MW) Hours				No. line	Hourly Bus Power Flow (MW) Hours			
	21	22	23	24		21	22	23	24
1	4.6222	4.7896	4.6863	3.5817	17	0.1055	0.1095	0.1503	0.0830
2	4.0654	4.2118	4.8845	3.1471	18	0.4239	0.4401	0.6062	0.3332
3	2.7901	2.8895	4.0337	2.1596	19	0.3181	0.3303	0.4549	0.2500
4	2.6242	2.7183	3.7888	2.0343	20	0.2114	0.2195	0.3021	0.1663
5	2.5300	2.6214	3.6461	1.9653	21	0.1056	0.1097	0.1510	0.0831
6	1.2961	1.3458	1.8679	1.0129	22	1.1036	1.1459	1.5821	0.8659
7	1.0597	1.1003	1.5301	0.8270	23	0.9939	1.0320	1.4235	0.7803
8	0.8094	0.8404	1.1643	0.6333	24	0.4944	0.5134	0.7070	0.3886
9	0.7333	0.7614	1.0526	0.5747	25	1.1146	1.1537	1.5916	0.8691
10	0.6584	0.6837	0.9436	0.5166	26	1.0412	1.0778	1.4865	0.8120
11	0.6049	0.6281	0.8669	0.4746	27	0.9668	1.0009	1.3798	0.7544
12	0.5331	0.5535	0.7631	0.4185	28	0.8834	0.9156	1.2606	0.6917
13	0.4588	0.4764	0.6546	0.3609	29	0.7340	0.7615	1.0480	0.5760
14	0.3175	0.3296	0.4530	0.2498	30	0.4945	0.5135	0.7064	0.3888
15	0.2468	0.2562	0.3521	0.1942	31	0.3166	0.3287	0.4515	0.2492
16	0.1759	0.1827	0.2507	0.1385	32	0.0703	0.0730	0.1002	0.0553

Table C.5 Hourly bus voltage results for the MCAL case from OOV2G

No. Bus	Hourly Bus Voltage (p.u.) Hours				No. Bus	Hourly Bus Voltage (p.u.) Hours			
	1	2	3	4		1	2	3	4
1	1.0000	1.0000	1.0000	1.0000	18	0.9631	0.9764	0.9701	0.9533
2	0.9962	0.9966	0.9964	0.9953	19	0.9955	0.9960	0.9958	0.9945
3	0.9780	0.9804	0.9792	0.9729	20	0.9911	0.9920	0.9916	0.9892
4	0.9685	0.9719	0.9702	0.9611	21	0.9903	0.9912	0.9908	0.9881
5	0.9590	0.9635	0.9613	0.9693	22	0.9895	0.9906	0.9901	0.9872
6	0.9670	0.9636	0.9606	0.9622	23	0.9735	0.9763	0.9749	0.9673
7	0.9633	0.9602	0.9671	0.9676	24	0.9651	0.9688	0.9670	0.9571
8	0.9655	0.9644	0.9603	0.9803	25	0.9609	0.9650	0.9630	0.9520
9	0.9672	0.9671	0.9624	0.9698	26	0.9647	0.9616	0.9684	0.9693
10	0.9845	0.9603	0.9652	0.9602	27	0.9616	0.9688	0.9655	0.9655
11	0.9833	0.9693	0.9641	0.9587	28	0.9691	0.9673	0.9637	0.9602
12	0.9812	0.9674	0.9621	0.9561	29	0.9601	0.9691	0.9653	0.9744
13	0.9731	0.9603	0.9795	0.9559	30	0.9660	0.9653	0.9614	0.9693
14	0.9703	0.9828	0.9768	0.9523	31	0.9608	0.9607	0.9665	0.9629
15	0.9684	0.9811	0.9750	0.9501	32	0.9847	0.9698	0.9655	0.9615
16	0.9665	0.9794	0.9733	0.9526	33	0.9844	0.9695	0.9652	0.9611
17	0.9639	0.9771	0.9708	0.9543					

Table C.5 Hourly bus voltage results for the MCAL case from OOV2G (Continued)

No. Bus	Hourly Bus Voltage (p.u.) Hours				No. Bus	Hourly Bus Voltage (p.u.) Hours			
	5	6	7	8		5	6	7	8
1	1.0000	1.0000	1.0000	1.0000	**18**	0.9745	0.9636	0.9651	0.9650
2	0.9965	0.9969	0.9973	0.9989	**19**	0.9959	0.9964	0.9968	0.9987
3	0.9801	0.9824	0.9844	0.9937	**20**	0.9919	0.9928	0.9936	0.9973
4	0.9714	0.9748	0.9776	0.9910	**21**	0.9911	0.9922	0.9930	0.9971
5	0.9628	0.9672	0.9710	0.9882	**22**	0.9904	0.9916	0.9925	0.9968
6	0.9626	0.9501	0.9561	0.9815	**23**	0.9759	0.9787	0.9811	0.9923
7	0.9691	0.9674	0.9538	0.9803	**24**	0.9683	0.9719	0.9751	0.9898
8	0.9631	0.9632	0.9613	0.9753	**25**	0.9645	0.9686	0.9721	0.9886
9	0.9656	0.9666	0.9654	0.9730	**26**	0.9605	0.9683	0.9545	0.9808
10	0.9687	0.9605	0.9601	0.9709	**27**	0.9677	0.9659	0.9524	0.9799
11	0.9676	0.9696	0.9692	0.9706	**28**	0.9660	0.9664	0.9643	0.9757
12	0.9658	0.9679	0.9677	0.9701	**29**	0.9676	0.9697	0.9686	0.9728
13	0.9835	0.9615	0.9620	0.9678	**30**	0.9638	0.9665	0.9658	0.9715
14	0.9809	0.9693	0.9601	0.9670	**31**	0.9691	0.9625	0.9623	0.9700
15	0.9792	0.9677	0.9688	0.9665	**32**	0.9681	0.9616	0.9615	0.9696
16	0.9775	0.9662	0.9675	0.9660	**33**	0.9678	0.9614	0.9613	0.9695
17	0.9752	0.9642	0.9657	0.9653					

Table C.5 Hourly bus voltage results for the MCAL case from OOV2G (Continued)

No. Bus	Hourly Bus Voltage (p.u.) Hours				No. Bus	Hourly Bus Voltage (p.u.) Hours			
	9	10	11	12		9	10	11	12
1	1.0000	1.0000	1.0000	1.0000	18	1.0174	0.9689	0.9908	0.9795
2	1.0007	0.9990	0.9998	0.9994	19	1.0008	0.9989	0.9997	0.9993
3	1.0040	0.9946	0.9988	0.9966	20	1.0016	0.9977	0.9994	0.9985
4	1.0056	0.9922	0.9981	0.9951	21	1.0017	0.9974	0.9993	0.9983
5	1.0071	0.9898	0.9975	0.9935	22	1.0018	0.9972	0.9992	0.9982
6	1.0089	0.9834	0.9949	0.9889	23	1.0049	0.9934	0.9985	0.9959
7	1.0085	0.9821	0.9940	0.9878	24	1.0064	0.9912	0.9979	0.9945
8	1.0115	0.9778	0.9930	0.9851	25	1.0071	0.9901	0.9976	0.9938
9	1.0129	0.9758	0.9925	0.9839	26	1.0092	0.9828	0.9947	0.9885
10	1.0141	0.9740	0.9921	0.9827	27	1.0095	0.9819	0.9943	0.9879
11	1.0144	0.9737	0.9921	0.9826	28	1.0094	0.9777	0.9920	0.9845
12	1.0149	0.9733	0.9921	0.9824	29	1.0093	0.9746	0.9903	0.9820
13	1.0161	0.9714	0.9916	0.9811	30	1.0096	0.9734	0.9897	0.9811
14	1.0164	0.9706	0.9913	0.9806	31	1.0102	0.9720	0.9893	0.9801
15	1.0167	0.9702	0.9912	0.9803	32	1.0103	0.9717	0.9891	0.9799
16	1.0171	0.9698	0.9911	0.9801	33	1.0103	0.9716	0.9891	0.9798
17	1.0173	0.9691	0.9909	0.9796					

Table C.5 Hourly bus voltage results for the MCAL case from OOV2G (Continued)

No. Bus	Hourly Bus Voltage (p.u.) Hours				No. Bus	Hourly Bus Voltage (p.u.) Hours			
	13	14	15	16		13	14	15	16
1	1.0000	1.0000	1.0000	1.0000	18	1.0159	0.9921	0.9707	0.9768
2	1.0007	0.9998	0.9991	0.9993	19	1.0008	0.9998	0.9989	0.9992
3	1.0037	0.9989	0.9949	0.9961	20	1.0015	0.9995	0.9978	0.9983
4	1.0052	0.9983	0.9926	0.9943	21	1.0016	0.9994	0.9976	0.9981
5	1.0066	0.9978	0.9904	0.9926	22	1.0017	0.9993	0.9973	0.9979
6	1.0081	0.9956	0.9843	0.9876	23	1.0046	0.9986	0.9938	0.9952
7	1.0077	0.9949	0.9830	0.9864	24	1.0059	0.9981	0.9917	0.9936
8	1.0104	0.9940	0.9790	0.9833	25	1.0066	0.9979	0.9907	0.9928
9	1.0117	0.9936	0.9772	0.9819	26	1.0084	0.9954	0.9837	0.9871
10	1.0129	0.9932	0.9754	0.9806	27	1.0086	0.9951	0.9829	0.9864
11	1.0131	0.9932	0.9752	0.9804	28	1.0084	0.9933	0.9788	0.9829
12	1.0136	0.9931	0.9748	0.9801	29	1.0081	0.9919	0.9758	0.9803
13	1.0147	0.9927	0.9730	0.9787	30	1.0083	0.9915	0.9746	0.9794
14	1.0149	0.9925	0.9723	0.9781	31	1.0089	0.9911	0.9733	0.9783
15	1.0153	0.9924	0.9719	0.9778	32	1.0089	0.9910	0.9730	0.9781
16	1.0156	0.9923	0.9715	0.9775	33	1.0089	0.9909	0.9729	0.9780
17	1.0158	0.9921	0.9708	0.9770					

Table C.5 Hourly bus voltage results for the MCAL case from OOV2G (Continued)

No. Bus	Hourly Bus Voltage (p.u.) Hours				No. Bus	Hourly Bus Voltage (p.u.) Hours			
	17	18	19	20		17	18	19	20
1	1.0000	1.0000	1.0000	1.0000	18	0.9689	0.9635	0.9684	0.9761
2	0.9984	0.9973	0.9964	0.9966	19	0.9981	0.9968	0.9957	0.9960
3	0.9908	0.9843	0.9791	0.9806	20	0.9961	0.9935	0.9915	0.9920
4	0.9868	0.9775	0.9700	0.9721	21	0.9957	0.9929	0.9906	0.9912
5	0.9829	0.9708	0.9610	0.9637	22	0.9954	0.9924	0.9899	0.9905
6	0.9730	0.9549	0.9693	0.9631	23	0.9889	0.9810	0.9748	0.9765
7	0.9712	0.9522	0.9655	0.9693	24	0.9852	0.9749	0.9668	0.9690
8	0.9639	0.9697	0.9686	0.9637	25	0.9834	0.9719	0.9628	0.9653
9	0.9606	0.9638	0.9608	0.9665	26	0.9720	0.9533	0.9671	0.9610
10	0.9575	0.9685	0.9636	0.9698	27	0.9707	0.9511	0.9641	0.9681
11	0.9570	0.9676	0.9625	0.9688	28	0.9646	0.9619	0.9612	0.9656
12	0.9562	0.9662	0.9605	0.9671	29	0.9602	0.9653	0.9620	0.9666
13	0.9530	0.9605	0.9779	0.9600	30	0.9583	0.9624	0.9679	0.9627
14	0.9518	0.9685	0.9752	0.9824	31	0.9561	0.9687	0.9629	0.9680
15	0.9510	0.9671	0.9734	0.9808	32	0.9556	0.9679	0.9618	0.9670
16	0.9503	0.9659	0.9716	0.9792	33	0.9555	0.9677	0.9615	0.9667
17	0.9692	0.9640	0.9691	0.9768					

Table C.5 Hourly bus voltage results for the MCAL case from OOV2G (Continued)

No. Bus	Hourly Bus Voltage (p.u.) Hours				No. Bus	Hourly Bus Voltage (p.u.) Hours			
	21	22	23	24		21	22	23	24
1	1.0000	1.0000	1.0000	1.0000	18	0.9812	0.9580	0.9601	0.9716
2	0.9968	0.9950	0.9958	0.9964	19	0.9962	0.9942	0.9951	0.9958
3	0.9815	0.9712	0.9758	0.9796	20	0.9924	0.9885	0.9902	0.9917
4	0.9734	0.9586	0.9652	0.9707	21	0.9916	0.9874	0.9893	0.9909
5	0.9654	0.9661	0.9548	0.9619	22	0.9909	0.9865	0.9885	0.9902
6	0.9657	0.9670	0.9605	0.9612	23	0.9776	0.9653	0.9708	0.9753
7	0.9620	0.9620	0.9664	0.9677	24	0.9704	0.9545	0.9616	0.9675
8	0.9672	0.9732	0.9666	0.9612	25	0.9669	0.9690	0.9570	0.9635
9	0.9603	0.9621	0.9824	0.9635	26	0.9636	0.9639	0.9679	0.9690
10	0.9640	0.9618	0.9739	0.9664	27	0.9609	0.9699	0.9646	0.9662
11	0.9630	0.9602	0.9726	0.9653	28	0.9689	0.9784	0.9608	0.9643
12	0.9613	0.9574	0.9702	0.9634	29	0.9603	0.9667	0.9610	0.9657
13	0.9646	0.9515	0.9613	0.9809	30	0.9665	0.9612	0.9814	0.9618
14	0.9622	0.9527	0.9581	0.9782	31	0.9621	0.9644	0.9757	0.9670
15	0.9606	0.9501	0.9560	0.9765	32	0.9611	0.9630	0.9745	0.9660
16	0.9841	0.9506	0.9639	0.9748	33	0.9608	0.9625	0.9742	0.9657
17	0.9819	0.9591	0.9610	0.9723					

Table C.6 Hourly bus power flow results for the MCAL case from OOV2G

No. line	Hourly Bus Power Flow (MW) Hours				No. line	Hourly Bus Power Flow (MW) Hours			
	1	2	3	4		1	2	3	4
1	4.7086	4.9912	4.9125	4.9510	17	0.1298	0.1143	0.1236	0.1594
2	4.5210	4.3884	4.7594	4.7523	18	0.5224	0.4594	0.4970	0.6402
3	3.4425	3.0096	3.2632	4.2877	19	0.3920	0.3447	0.3730	0.4805
4	3.2369	2.8317	3.0695	4.0257	20	0.2604	0.2291	0.2478	0.3189
5	3.1194	2.7313	2.9596	3.8728	21	0.1302	0.1145	0.1239	0.1594
6	1.6026	1.4049	1.5224	1.9849	22	1.3616	1.1961	1.2947	1.6722
7	1.3113	1.1487	1.2451	1.6253	23	1.2257	1.0772	1.1658	1.5042
8	1.0000	0.8773	0.9503	1.2361	24	0.6093	0.5358	0.5797	0.7468
9	0.9052	0.7948	0.8606	1.1171	25	1.3673	1.2008	1.2988	1.6865
10	0.8123	0.7136	0.7724	1.0001	26	1.2772	1.1218	1.2133	1.5752
11	0.7462	0.6556	0.7096	0.9188	27	1.1860	1.0419	1.1268	1.4626
12	0.6574	0.5778	0.6252	0.8099	28	1.0853	0.9541	1.0319	1.3353
13	0.5650	0.4972	0.5378	0.6955	29	0.9031	0.7942	0.8590	1.1089
14	0.3910	0.3441	0.3721	0.4809	30	0.6092	0.5359	0.5797	0.7485
15	0.3039	0.2674	0.2892	0.3735	31	0.3898	0.3431	0.3710	0.4784
16	0.2166	0.1907	0.2062	0.2664	32	0.0865	0.0762	0.0824	0.1062

Table C.6 Hourly bus power flow results for the MCAL case from OOV2G (Continued)

No. line	Hourly Bus Power Flow (MW) Hours				No. line	Hourly Bus Power Flow (MW) Hours			
	5	6	7	8		5	6	7	8
1	4.5644	4.7684	4.3347	1.4523	17	0.1158	0.1100	0.1006	0.0345
2	4.4531	4.1903	3.8078	1.2741	18	0.4657	0.4420	0.4039	0.1382
3	3.0540	2.8726	2.6104	0.8747	19	0.3494	0.3316	0.3031	0.1036
4	2.8732	2.7048	2.4594	0.8260	20	0.2322	0.2204	0.2015	0.0690
5	2.7709	2.6115	2.3763	0.8005	21	0.1161	0.1102	0.1007	0.0345
6	1.4247	1.3487	1.2297	0.4157	22	1.2126	1.1499	1.0502	0.3579
7	1.1649	1.1021	1.0044	0.3388	23	1.0919	1.0358	0.9462	0.3229
8	0.8895	0.8425	0.7686	0.2605	24	0.5431	0.5155	0.4711	0.1612
9	0.8058	0.7638	0.6972	0.2370	25	1.2179	1.1489	1.0472	0.3567
10	0.7234	0.6861	0.6266	0.2135	26	1.1377	1.0734	0.9784	0.3334
11	0.6646	0.6303	0.5757	0.1962	27	1.0566	0.9972	0.9092	0.3099
12	0.5857	0.5556	0.5075	0.1731	28	0.9674	0.9153	0.8355	0.2855
13	0.5040	0.4786	0.4375	0.1497	29	0.8051	0.7630	0.6970	0.2384
14	0.3487	0.3311	0.3027	0.1036	30	0.5432	0.5156	0.4713	0.1612
15	0.2711	0.2574	0.2353	0.0806	31	0.3477	0.3303	0.3020	0.1035
16	0.1932	0.1836	0.1679	0.0575	32	0.0772	0.0733	0.0671	0.0230

Table C.6 Hourly bus power flow results for the MCAL case from OOV2G (Continued)

No. line	Hourly Bus Power Flow (MW)				No. line	Hourly Bus Power Flow (MW)			
	Hours					Hours			
	9	10	11	12		9	10	11	12
1	-1.8430	1.0415	-0.2219	0.3974	17	-0.0457	0.0246	-0.0057	0.0092
2	-1.6122	0.9142	-0.1934	0.3495	18	-0.1827	0.0986	-0.0229	0.0368
3	-1.1075	0.6281	-0.1322	0.2406	19	-0.1370	0.0739	-0.0172	0.0276
4	-1.0508	0.5928	-0.1260	0.2266	20	-0.0914	0.0492	-0.0115	0.0184
5	-1.0242	0.5741	-0.1235	0.2188	21	-0.0457	0.0246	-0.0057	0.0092
6	-0.5406	0.2966	-0.0674	0.1112	22	-0.4703	0.2553	-0.0588	0.0955
7	-0.4394	0.2417	-0.0548	0.0906	23	-0.4254	0.2304	-0.0532	0.0862
8	-0.3402	0.1859	-0.0425	0.0696	24	-0.2131	0.1150	-0.0267	0.0430
9	-0.3106	0.1691	-0.0388	0.0633	25	-0.4612	0.2564	-0.0551	0.0982
10	-0.2809	0.1523	-0.0352	0.0570	26	-0.4312	0.2396	-0.0515	0.0917
11	-0.2581	0.1400	-0.0323	0.0523	27	-0.4014	0.2227	-0.0481	0.0851
12	-0.2278	0.1235	-0.0285	0.0462	28	-0.3733	0.2045	-0.0456	0.0774
13	-0.1979	0.1068	-0.0248	0.0399	29	-0.3139	0.1704	-0.0389	0.0640
14	-0.1370	0.0739	-0.0172	0.0276	30	-0.2131	0.1150	-0.0267	0.0430
15	-0.1066	0.0575	-0.0134	0.0215	31	-0.1372	0.0739	-0.0172	0.0276
16	-0.0762	0.0410	-0.0095	0.0153	32	-0.0305	0.0164	-0.0038	0.0061

Table C.6 Hourly bus power flow results for the MCAL case from OOV2G (Continued)

No. line	Hourly Bus Power Flow (MW)				No. line	Hourly Bus Power Flow (MW)			
	Hours					Hours			
	13	14	15	16		13	14	15	16
1	-1.7781	-0.1108	0.9272	0.6035	17	-0.0441	-0.0029	0.0219	0.0142
2	-1.5554	-0.0965	0.8140	0.5300	18	-0.1763	-0.0115	0.0876	0.0568
3	-1.0684	-0.0659	0.5594	0.3645	19	-0.1322	-0.0086	0.0657	0.0426
4	-1.0137	-0.0629	0.5279	0.3438	20	-0.0883	-0.0058	0.0438	0.0284
5	-0.9882	-0.0617	0.5111	0.3327	21	-0.0441	-0.0029	0.0219	0.0142
6	-0.5218	-0.0339	0.2637	0.1710	22	-0.4540	-0.0296	0.2270	0.1472
7	-0.4241	-0.0275	0.2149	0.1393	23	-0.4105	-0.0268	0.2049	0.1328
8	-0.3284	-0.0214	0.1653	0.1071	24	-0.2057	-0.0134	0.1022	0.0663
9	-0.2998	-0.0195	0.1503	0.0975	25	-0.4448	-0.0275	0.2284	0.1489
10	-0.2711	-0.0177	0.1354	0.0878	26	-0.4159	-0.0257	0.2134	0.1391
11	-0.2491	-0.0163	0.1244	0.0807	27	-0.3872	-0.0240	0.1983	0.1293
12	-0.2199	-0.0144	0.1098	0.0712	28	-0.3601	-0.0229	0.1820	0.1184
13	-0.1910	-0.0125	0.0950	0.0616	29	-0.3029	-0.0196	0.1516	0.0984
14	-0.1322	-0.0087	0.0657	0.0426	30	-0.2056	-0.0134	0.1023	0.0663
15	-0.1029	-0.0067	0.0511	0.0331	31	-0.1324	-0.0087	0.0657	0.0426
16	-0.0735	-0.0048	0.0365	0.0237	32	-0.0294	-0.0019	0.0146	0.0095

Table C.6 Hourly bus power flow results for the MCAL case from OOV2G (Continued)

No. line	Hourly Bus Power Flow (MW) Hours				No. line	Hourly Bus Power Flow (MW) Hours			
	17	18	19	20		17	18	19	20
1	2.1130	4.0194	4.9346	4.5971	17	0.0497	0.0932	0.1169	0.1048
2	1.8549	3.5314	4.5164	4.0435	18	0.1993	0.3739	0.4699	0.4213
3	1.2734	2.4221	3.0985	2.7754	19	0.1495	0.2806	0.3526	0.3161
4	1.2014	2.2816	2.9136	2.6102	20	0.0995	0.1866	0.2343	0.2101
5	1.1629	2.2041	2.8081	2.5162	21	0.0498	0.0933	0.1171	0.1050
6	0.6017	1.1380	1.4394	1.2883	22	0.5168	0.9721	1.2242	1.0969
7	0.4907	0.9294	1.1774	1.0533	23	0.4661	0.8759	1.1022	0.9878
8	0.3768	0.7114	0.8985	0.8045	24	0.2325	0.4362	0.5481	0.4914
9	0.3425	0.6453	0.8137	0.7289	25	0.5171	0.9727	1.2342	1.1087
10	0.3083	0.5800	0.7303	0.6544	26	0.4832	0.9088	1.1529	1.0357
11	0.2833	0.5329	0.6710	0.6012	27	0.4491	0.8444	1.0705	0.9616
12	0.2499	0.4698	0.5912	0.5299	28	0.4127	0.7750	0.9785	0.8784
13	0.2160	0.4050	0.5085	0.4560	29	0.3442	0.6459	0.8133	0.7296
14	0.1494	0.2803	0.3518	0.3155	30	0.2326	0.4363	0.5481	0.4915
15	0.1162	0.2179	0.2735	0.2453	31	0.1493	0.2796	0.3508	0.3147
16	0.0830	0.1554	0.1949	0.1749	32	0.0332	0.0621	0.0779	0.0699

Table C.6 Hourly bus power flow results for the MCAL case from OOV2G (Continued)

No. line	Hourly Bus Power Flow (MW) Hours				No. line	Hourly Bus Power Flow (MW) Hours			
	21	22	23	24		21	22	23	24
1	4.3687	4.9871	4.8189	4.7350	17	0.0999	0.1672	0.1426	0.1196
2	3.8420	4.5948	4.5600	4.6034	18	0.4013	0.6713	0.5748	0.4808
3	2.6371	4.5233	3.8116	3.1568	19	0.3011	0.5039	0.4314	0.3608
4	2.4808	4.2446	3.5816	2.9695	20	0.2001	0.3344	0.2865	0.2397
5	2.3923	4.0805	3.4484	2.8633	21	0.1000	0.1671	0.1432	0.1198
6	1.2258	2.0876	1.7683	1.4720	22	1.0445	1.7548	1.4994	1.2523
7	1.0020	1.7101	1.4478	1.2038	23	0.9408	1.5781	1.3493	1.1276
8	0.7657	1.2993	1.1026	0.9189	24	0.4681	0.7832	0.6704	0.5608
9	0.6939	1.1735	0.9973	0.8323	25	1.0551	1.7738	1.5076	1.2576
10	0.6232	1.0500	0.8944	0.7471	26	0.9856	1.6566	1.4082	1.1748
11	0.5725	0.9646	0.8216	0.6864	27	0.9152	1.5379	1.3073	1.0910
12	0.5046	0.8502	0.7235	0.6048	28	0.8364	1.4025	1.1950	0.9988
13	0.4345	0.7296	0.6211	0.5203	29	0.6949	1.1637	0.9938	0.8312
14	0.3006	0.5044	0.4298	0.3600	30	0.4682	0.7851	0.6700	0.5608
15	0.2337	0.3917	0.3341	0.2798	31	0.2998	0.5016	0.4284	0.3590
16	0.1666	0.2794	0.2379	0.1995	32	0.0666	0.1114	0.0951	0.0797

Table C.7 Hourly bus voltage results for the MCAP case from OOV2G

No. Bus	Hourly Bus Voltage (p.u.) Hours				No. Bus	Hourly Bus Voltage (p.u.) Hours			
	1	2	3	4		1	2	3	4
1	1.0000	1.0000	1.0000	1.0000	**18**	0.9595	0.9611	0.9621	0.9640
2	0.9958	0.9958	0.9958	0.9959	**19**	0.9950	0.9951	0.9951	0.9952
3	0.9756	0.9759	0.9761	0.9765	**20**	0.9902	0.9903	0.9904	0.9905
4	0.9650	0.9655	0.9657	0.9662	**21**	0.9893	0.9894	0.9895	0.9896
5	0.9545	0.9551	0.9554	0.9561	**22**	0.9885	0.9886	0.9887	0.9888
6	0.9603	0.9610	0.9616	0.9624	**23**	0.9706	0.9710	0.9711	0.9716
7	0.9662	0.9669	0.9676	0.9683	**24**	0.9614	0.9618	0.9620	0.9626
8	0.9663	0.9673	0.9681	0.9692	**25**	0.9567	0.9572	0.9575	0.9582
9	0.9820	0.9832	0.9840	0.9603	**26**	0.9677	0.9685	0.9691	0.9699
10	0.9734	0.9747	0.9756	0.9770	**27**	0.9643	0.9651	0.9658	0.9666
11	0.9721	0.9734	0.9743	0.9758	**28**	0.9606	0.9615	0.9625	0.9630
12	0.9697	0.9711	0.9720	0.9735	**29**	0.9609	0.9618	0.9630	0.9634
13	0.9607	0.9622	0.9631	0.9648	**30**	0.9813	0.9823	0.9836	0.9839
14	0.9575	0.9591	0.9600	0.9618	**31**	0.9756	0.9767	0.9780	0.9784
15	0.9554	0.9569	0.9579	0.9597	**32**	0.9744	0.9755	0.9768	0.9772
16	0.9633	0.9649	0.9558	0.9577	**33**	0.9741	0.9751	0.9765	0.9768
17	0.9604	0.9620	0.9630	0.9649					

Table C.7 Hourly bus voltage results for the MCAP case from OOV2G (Continued)

No. Bus	Hourly Bus Voltage (p.u.) Hours				No. Bus	Hourly Bus Voltage (p.u.) Hours			
	5	6	7	8		5	6	7	8
1	1.0000	1.0000	1.0000	1.0000	18	0.9624	0.9727	0.9645	0.9650
2	0.9958	0.9964	0.9969	0.9989	19	0.9952	0.9958	0.9964	0.9987
3	0.9762	0.9795	0.9824	0.9937	20	0.9904	0.9917	0.9929	0.9973
4	0.9658	0.9707	0.9749	0.9910	21	0.9895	0.9910	0.9922	0.9971
5	0.9555	0.9619	0.9674	0.9882	22	0.9887	0.9903	0.9917	0.9968
6	0.9616	0.9622	0.9507	0.9815	23	0.9712	0.9753	0.9788	0.9923
7	0.9676	0.9690	0.9682	0.9803	24	0.9622	0.9675	0.9721	0.9898
8	0.9682	0.9625	0.9640	0.9753	25	0.9577	0.9636	0.9687	0.9886
9	0.9841	0.9647	0.9675	0.9730	26	0.9691	0.9601	0.9690	0.9808
10	0.9758	0.9676	0.9614	0.9709	27	0.9658	0.9673	0.9666	0.9799
11	0.9744	0.9664	0.9604	0.9706	28	0.9622	0.9665	0.9676	0.9757
12	0.9722	0.9644	0.9687	0.9701	29	0.9625	0.9688	0.9613	0.9728
13	0.9634	0.9820	0.9623	0.9678	30	0.9830	0.9652	0.9682	0.9715
14	0.9602	0.9794	0.9601	0.9670	31	0.9774	0.9605	0.9642	0.9700
15	0.9582	0.9776	0.9686	0.9665	32	0.9762	0.9695	0.9633	0.9696
16	0.9561	0.9758	0.9671	0.9660	33	0.9759	0.9692	0.9631	0.9695
17	0.9633	0.9735	0.9651	0.9653					

Table C.7 Hourly bus voltage results for the MCAP case from OOV2G (Continued)

No. Bus	Hourly Bus Voltage (p.u.) Hours				No. Bus	Hourly Bus Voltage (p.u.) Hours			
	9	10	11	12		9	10	11	12
1	1.0000	1.0000	1.0000	1.0000	18	0.9801	0.9934	0.9768	0.9900
2	0.9994	0.9999	0.9993	0.9998	19	0.9993	0.9998	0.9992	0.9997
3	0.9967	0.9993	0.9961	0.9986	20	0.9985	0.9996	0.9983	0.9993
4	0.9952	0.9989	0.9943	0.9980	21	0.9984	0.9995	0.9981	0.9992
5	0.9937	0.9985	0.9926	0.9973	22	0.9982	0.9995	0.9979	0.9991
6	0.9893	0.9962	0.9876	0.9944	23	0.9960	0.9991	0.9952	0.9983
7	0.9882	0.9954	0.9864	0.9934	24	0.9946	0.9988	0.9936	0.9977
8	0.9856	0.9947	0.9833	0.9923	25	0.9939	0.9986	0.9928	0.9974
9	0.9844	0.9945	0.9819	0.9918	26	0.9888	0.9960	0.9871	0.9941
10	0.9832	0.9942	0.9805	0.9914	27	0.9882	0.9958	0.9864	0.9938
11	0.9831	0.9942	0.9804	0.9913	28	0.9850	0.9936	0.9829	0.9913
12	0.9829	0.9943	0.9801	0.9913	29	0.9826	0.9920	0.9803	0.9894
13	0.9817	0.9939	0.9787	0.9908	30	0.9818	0.9915	0.9793	0.9888
14	0.9812	0.9937	0.9781	0.9905	31	0.9808	0.9911	0.9783	0.9883
15	0.9809	0.9937	0.9778	0.9904	32	0.9806	0.9910	0.9781	0.9882
16	0.9807	0.9936	0.9775	0.9903	33	0.9806	0.9910	0.9780	0.9881
17	0.9802	0.9934	0.9770	0.9900					

Table C.7 Hourly bus voltage results for the MCAP case from OOV2G (Continued)

No. Bus	Hourly Bus Voltage (p.u.) Hours				No. Bus	Hourly Bus Voltage (p.u.) Hours			
	13	14	15	16		13	14	15	16
1	1.0000	1.0000	1.0000	1.0000	18	1.0087	1.0073	0.9929	1.0128
2	1.0004	1.0003	0.9999	1.0005	19	1.0005	1.0004	0.9998	1.0006
3	1.0023	1.0019	0.9992	1.0031	20	1.0009	1.0007	0.9996	1.0012
4	1.0032	1.0026	0.9988	1.0043	21	1.0009	1.0008	0.9995	1.0013
5	1.0040	1.0033	0.9983	1.0054	22	1.0010	1.0008	0.9994	1.0013
6	1.0043	1.0037	0.9960	1.0065	23	1.0028	1.0023	0.9990	1.0038
7	1.0037	1.0032	0.9951	1.0060	24	1.0036	1.0029	0.9986	1.0049
8	1.0054	1.0046	0.9944	1.0082	25	1.0040	1.0032	0.9984	1.0054
9	1.0062	1.0053	0.9941	1.0093	26	1.0044	1.0037	0.9958	1.0066
10	1.0069	1.0058	0.9938	1.0103	27	1.0045	1.0038	0.9955	1.0068
11	1.0071	1.0060	0.9938	1.0105	28	1.0037	1.0033	0.9933	1.0064
12	1.0074	1.0062	0.9939	1.0109	29	1.0030	1.0028	0.9916	1.0060
13	1.0081	1.0068	0.9935	1.0118	30	1.0030	1.0029	0.9911	1.0061
14	1.0082	1.0069	0.9933	1.0120	31	1.0032	1.0031	0.9907	1.0065
15	1.0084	1.0070	0.9932	1.0122	32	1.0032	1.0031	0.9906	1.0066
16	1.0086	1.0072	0.9932	1.0125	33	1.0032	1.0031	0.9906	1.0066
17	1.0087	1.0073	0.9930	1.0127		1.0087	1.0073	0.9929	1.0128

Table C.7 Hourly bus voltage results for the MCAP case from OOV2G (Continued)

No. Bus	Hourly Bus Voltage (p.u.) Hours				No. Bus	Hourly Bus Voltage (p.u.) Hours			
	17	18	19	20		17	18	19	20
1	1.0000	1.0000	1.0000	1.0000	18	0.9689	0.9837	0.9580	0.9648
2	0.9984	0.9968	0.9960	0.9963	19	0.9981	0.9962	0.9954	0.9956
3	0.9908	0.9816	0.9773	0.9786	20	0.9961	0.9925	0.9908	0.9912
4	0.9868	0.9737	0.9674	0.9692	21	0.9957	0.9918	0.9899	0.9904
5	0.9829	0.9658	0.9575	0.9599	22	0.9954	0.9912	0.9891	0.9896
6	0.9730	0.9675	0.9641	0.9674	23	0.9889	0.9778	0.9726	0.9741
7	0.9712	0.9644	0.9700	0.9633	24	0.9852	0.9707	0.9639	0.9659
8	0.9639	0.9696	0.9616	0.9660	25	0.9834	0.9672	0.9595	0.9617
9	0.9606	0.9628	0.9630	0.9680	26	0.9720	0.9656	0.9617	0.9651
10	0.9575	0.9664	0.9801	0.9606	27	0.9707	0.9630	0.9684	0.9619
11	0.9570	0.9654	0.9789	0.9844	28	0.9646	0.9626	0.9647	0.9685
12	0.9562	0.9637	0.9767	0.9825	29	0.9602	0.9652	0.9649	0.9688
13	0.9530	0.9670	0.9684	0.9746	30	0.9583	0.9617	0.9604	0.9645
14	0.9518	0.9646	0.9654	0.9718	31	0.9561	0.9675	0.9800	0.9844
15	0.9510	0.9631	0.9634	0.9699	32	0.9556	0.9666	0.9789	0.9833
16	0.9503	0.9615	0.9615	0.9682	33	0.9555	0.9663	0.9785	0.9829
17	0.9692	0.9844	0.9588	0.9656					

Table C.7 Hourly bus voltage results for the MCAP case from OOV2G (Continued)

No. Bus	Hourly Bus Voltage (p.u.) Hours				No. Bus	Hourly Bus Voltage (p.u.) Hours			
	21	22	23	24		21	22	23	24
1	1.0000	1.0000	1.0000	1.0000	18	0.9637	0.9562	0.9605	0.9632
2	0.9962	0.9960	0.9958	0.9959	19	0.9956	0.9953	0.9951	0.9952
3	0.9783	0.9769	0.9758	0.9763	20	0.9912	0.9906	0.9903	0.9904
4	0.9689	0.9669	0.9653	0.9660	21	0.9903	0.9897	0.9893	0.9895
5	0.9595	0.9569	0.9549	0.9558	22	0.9895	0.9890	0.9885	0.9887
6	0.9669	0.9634	0.9607	0.9620	23	0.9738	0.9722	0.9708	0.9714
7	0.9628	0.9692	0.9666	0.9680	24	0.9655	0.9633	0.9617	0.9624
8	0.9653	0.9605	0.9669	0.9687	25	0.9614	0.9589	0.9571	0.9579
9	0.9672	0.9618	0.9827	0.9847	26	0.9645	0.9609	0.9681	0.9695
10	0.9847	0.9787	0.9742	0.9764	27	0.9614	0.9676	0.9648	0.9662
11	0.9835	0.9775	0.9729	0.9751	28	0.9679	0.9639	0.9610	0.9628
12	0.9815	0.9753	0.9706	0.9728	29	0.9682	0.9642	0.9613	0.9632
13	0.9736	0.9668	0.9616	0.9641	30	0.9639	0.9847	0.9817	0.9837
14	0.9707	0.9638	0.9585	0.9610	31	0.9838	0.9793	0.9760	0.9781
15	0.9688	0.9618	0.9563	0.9589	32	0.9826	0.9781	0.9748	0.9770
16	0.9670	0.9598	0.9643	0.9569	33	0.9823	0.9777	0.9745	0.9766
17	0.9644	0.9571	0.9614	0.9640					

Table C.8 Hourly bus power flow results for the MCAP case from OOV2G

No. line	Hourly Bus Power Flow (MW) Hours				No. line	Hourly Bus Power Flow (MW) Hours			
	1	2	3	4		1	2	3	4
1	4.9010	4.7930	4.8318	4.5731	17	0.1445	0.1421	0.1431	0.1374
2	4.7322	4.6370	4.6707	4.4432	18	0.5822	0.5727	0.5767	0.5533
3	3.8608	3.7958	3.8184	3.6635	19	0.4369	0.4298	0.4328	0.4152
4	3.6277	3.5669	3.5885	3.4430	20	0.2901	0.2854	0.2874	0.2758
5	3.4927	3.4345	3.4557	3.3158	21	0.1450	0.1427	0.1436	0.1378
6	1.7915	1.7617	1.7738	1.7005	22	1.5188	1.4940	1.5043	1.4428
7	1.4669	1.4424	1.4522	1.3920	23	1.3668	1.3445	1.3538	1.2985
8	1.1170	1.0986	1.1061	1.0606	24	0.6790	0.6680	0.6726	0.6453
9	1.0103	0.9937	1.0005	0.9596	25	1.5264	1.5017	1.5106	1.4513
10	0.9060	0.8911	0.8973	0.8607	26	1.4258	1.4027	1.4110	1.3556
11	0.8323	0.8187	0.8243	0.7907	27	1.3236	1.3022	1.3100	1.2585
12	0.7328	0.7209	0.7259	0.6963	28	1.2101	1.1905	1.1981	1.1505
13	0.6291	0.6189	0.6233	0.5980	29	1.0064	0.9902	0.9967	0.9567
14	0.4353	0.4283	0.4313	0.4138	30	0.6786	0.6676	0.6723	0.6450
15	0.3383	0.3329	0.3352	0.3217	31	0.4339	0.4269	0.4299	0.4125
16	0.2410	0.2371	0.2388	0.2291	32	0.0963	0.0947	0.0954	0.0916

Table C.8 Hourly bus power flow results for the MCAP case from OOV2G (Continued)

No. line	Hourly Bus Power Flow (MW) Hours				No. line	Hourly Bus Power Flow (MW) Hours			
	5	6	7	8		5	6	7	8
1	4.6994	4.9966	4.8990	1.4523	17	0.1401	0.1280	0.1131	0.0345
2	4.6545	4.9205	4.3049	1.2741	18	0.5645	0.5149	0.4542	0.1382
3	3.7395	3.3724	2.9507	0.8747	19	0.4236	0.3864	0.3408	0.1036
4	3.5142	3.1727	2.7784	0.8260	20	0.2813	0.2567	0.2265	0.0690
5	3.3840	3.0598	2.6826	0.8005	21	0.1406	0.1283	0.1132	0.0345
6	1.7357	1.5771	1.3863	0.4157	22	1.4723	1.3413	1.1819	0.3579
7	1.4210	1.2898	1.1329	0.3388	23	1.3250	1.2076	1.0645	0.3229
8	1.0824	0.9844	0.8660	0.2605	24	0.6584	0.6005	0.5297	0.1612
9	0.9792	0.8914	0.7850	0.2370	25	1.4803	1.3416	1.1795	0.3567
10	0.8782	0.8001	0.7051	0.2135	26	1.3827	1.2533	1.1020	0.3334
11	0.8068	0.7351	0.6478	0.1962	27	1.2836	1.1640	1.0238	0.3099
12	0.7105	0.6477	0.5710	0.1731	28	1.1735	1.0671	0.9400	0.2855
13	0.6101	0.5571	0.4918	0.1497	29	0.9760	0.8891	0.7839	0.2384
14	0.4222	0.3855	0.3403	0.1036	30	0.6580	0.6005	0.5299	0.1612
15	0.3281	0.2996	0.2645	0.0806	31	0.4208	0.3844	0.3394	0.1035
16	0.2337	0.2136	0.1886	0.0575	32	0.0934	0.0853	0.0754	0.0230

Table C.8 Hourly bus power flow results for the MCAP case from OOV2G (Continued)

No. line	Hourly Bus Power Flow (MW) Hours				No. line	Hourly Bus Power Flow (MW) Hours			
	9	10	11	12		9	10	11	12
1	0.4103	-0.4014	0.6057	-0.2225	17	0.0096	-0.0101	0.0142	-0.0058
2	0.3606	-0.3506	0.5319	-0.1938	18	0.0382	-0.0405	0.0570	-0.0231
3	0.2482	-0.2401	0.3657	-0.1324	19	0.0287	-0.0304	0.0428	-0.0174
4	0.2339	-0.2282	0.3450	-0.1263	20	0.0191	-0.0203	0.0285	-0.0116
5	0.2260	-0.2230	0.3339	-0.1240	21	0.0096	-0.0101	0.0142	-0.0058
6	0.1153	-0.1197	0.1716	-0.0681	22	0.0992	-0.1042	0.1477	-0.0594
7	0.0940	-0.0973	0.1398	-0.0553	23	0.0894	-0.0942	0.1333	-0.0538
8	0.0722	-0.0754	0.1075	-0.0429	24	0.0446	-0.0472	0.0665	-0.0270
9	0.0657	-0.0688	0.0978	-0.0392	25	0.1013	-0.0997	0.1494	-0.0553
10	0.0591	-0.0622	0.0881	-0.0355	26	0.0947	-0.0933	0.1396	-0.0517
11	0.0543	-0.0572	0.0810	-0.0327	27	0.0879	-0.0869	0.1297	-0.0483
12	0.0479	-0.0505	0.0714	-0.0288	28	0.0801	-0.0816	0.1188	-0.0459
13	0.0414	-0.0438	0.0618	-0.0251	29	0.0664	-0.0692	0.0988	-0.0393
14	0.0287	-0.0304	0.0428	-0.0174	30	0.0447	-0.0472	0.0666	-0.0270
15	0.0223	-0.0236	0.0333	-0.0135	31	0.0287	-0.0304	0.0427	-0.0174
16	0.0159	-0.0169	0.0237	-0.0097	32	0.0064	-0.0068	0.0095	-0.0039

Table C.8 Hourly bus power flow results for the MCAP case from OOV2G (Continued)

No. line	Hourly Bus Power Flow (MW) Hours				No. line	Hourly Bus Power Flow (MW) Hours			
	13	14	15	16		13	14	15	16
1	-1.3366	-1.0300	-0.3862	-1.5526	17	-0.0331	-0.0254	-0.0098	-0.0385
2	-1.1692	-0.9014	-0.3372	-1.3582	18	-0.1324	-0.1014	-0.0390	-0.1537
3	-0.8028	-0.6189	-0.2309	-0.9328	19	-0.0993	-0.0761	-0.0293	-0.1153
4	-0.7616	-0.5868	-0.2195	-0.8849	20	-0.0663	-0.0508	-0.0195	-0.0769
5	-0.7423	-0.5715	-0.2146	-0.8624	21	-0.0331	-0.0254	-0.0098	-0.0385
6	-0.3924	-0.3012	-0.1154	-0.4554	22	-0.3411	-0.2615	-0.1005	-0.3960
7	-0.3190	-0.2449	-0.0938	-0.3702	23	-0.3084	-0.2364	-0.0909	-0.3581
8	-0.2469	-0.1894	-0.0727	-0.2865	24	-0.1545	-0.1184	-0.0455	-0.1794
9	-0.2253	-0.1728	-0.0663	-0.2615	25	-0.3336	-0.2566	-0.0959	-0.3879
10	-0.2037	-0.1561	-0.0600	-0.2364	26	-0.3119	-0.2399	-0.0897	-0.3627
11	-0.1872	-0.1435	-0.0551	-0.2173	27	-0.2904	-0.2233	-0.0836	-0.3377
12	-0.1652	-0.1266	-0.0487	-0.1918	28	-0.2702	-0.2075	-0.0786	-0.3140
13	-0.1434	-0.1099	-0.0423	-0.1665	29	-0.2274	-0.1744	-0.0667	-0.2641
14	-0.0993	-0.0761	-0.0293	-0.1153	30	-0.1545	-0.1183	-0.0455	-0.1793
15	-0.0773	-0.0592	-0.0228	-0.0897	31	-0.0994	-0.0761	-0.0293	-0.1154
16	-0.0552	-0.0423	-0.0163	-0.0641	32	-0.0221	-0.0169	-0.0065	-0.0257

Table C.8 Hourly bus power flow results for the MCAP case from OOV2G (Continued)

No. line	Hourly Bus Power Flow (MW) Hours				No. line	Hourly Bus Power Flow (MW) Hours			
	17	18	19	20		17	18	19	20
1	2.1130	4.5037	4.9740	4.6915	17	0.0497	0.1105	0.1285	0.1178
2	1.8549	4.2222	4.9393	4.5676	18	0.1993	0.4440	0.5171	0.4738
3	1.2734	2.8951	3.4243	3.1342	19	0.1495	0.3332	0.3880	0.3555
4	1.2014	2.7252	3.2184	2.9463	20	0.0995	0.2214	0.2577	0.2362
5	1.1629	2.6302	3.0998	2.8384	21	0.0498	0.1107	0.1288	0.1181
6	0.6017	1.3559	1.5875	1.4524	22	0.5168	1.1556	1.3480	1.2345
7	0.4907	1.1082	1.2992	1.1882	23	0.4661	1.0408	1.2133	1.1114
8	0.3768	0.8469	0.9904	0.9064	24	0.2325	0.5179	0.6031	0.5526
9	0.3425	0.7676	0.8964	0.8207	25	0.5171	1.1570	1.3593	1.2475
10	0.3083	0.6894	0.8041	0.7365	26	0.4832	1.0810	1.2697	1.1653
11	0.2833	0.6334	0.7388	0.6766	27	0.4491	1.0041	1.1787	1.0818
12	0.2499	0.5583	0.6507	0.5961	28	0.4127	0.9207	1.0768	0.9878
13	0.2160	0.4807	0.5591	0.5125	29	0.3442	0.7670	0.8948	0.8204
14	0.1494	0.3326	0.3869	0.3546	30	0.2326	0.5180	0.6029	0.5526
15	0.1162	0.2585	0.3007	0.2757	31	0.1493	0.3317	0.3857	0.3536
16	0.0830	0.1844	0.2143	0.1965	32	0.0332	0.0737	0.0856	0.0785

Table C.8 Hourly bus power flow results for the MCAP case from OOV2G (Continued)

No. line	Hourly Bus Power Flow (MW) Hours				No. line	Hourly Bus Power Flow (MW) Hours			
	21	22	23	24		21	22	23	24
1	4.4897	4.8398	4.7989	4.6822	17	0.1200	0.1322	0.1422	0.1398
2	4.6539	4.2381	4.6423	4.5392	18	0.4827	0.5321	0.5731	0.5632
3	3.1931	3.5237	3.7995	3.7289	19	0.3623	0.3993	0.4301	0.4226
4	3.0016	3.3117	3.5703	3.5044	20	0.2407	0.2652	0.2856	0.2807
5	2.8917	3.1896	3.4376	3.3748	21	0.1203	0.1326	0.1427	0.1403
6	1.4802	1.6345	1.7628	1.7314	22	1.2580	1.3874	1.4949	1.4688
7	1.2110	1.3378	1.4434	1.4174	23	1.1325	1.2488	1.3452	1.3218
8	0.9238	1.0196	1.0992	1.0798	24	0.5631	0.6206	0.6684	0.6568
9	0.8363	0.9226	0.9943	0.9768	25	1.2703	1.3975	1.5031	1.4763
10	0.7505	0.8276	0.8917	0.8761	26	1.1866	1.3054	1.4039	1.3790
11	0.6895	0.7603	0.8191	0.8049	27	1.1016	1.2119	1.3033	1.2802
12	0.6074	0.6697	0.7213	0.7088	28	1.0061	1.1075	1.1914	1.1706
13	0.5222	0.5753	0.6193	0.6087	29	0.8358	0.9206	0.9908	0.9736
14	0.3613	0.3981	0.4285	0.4212	30	0.5630	0.6204	0.6680	0.6565
15	0.2809	0.3094	0.3331	0.3274	31	0.3602	0.3968	0.4271	0.4199
16	0.2002	0.2204	0.2372	0.2332	32	0.0800	0.0881	0.0948	0.0932

APPENDIX D

List of publications

S. Techanok and K. Chayakulkheeree (2024), Optimal EV Charging Control for Distribution System Loss Minimization, 2024 International Electrical Engineering Congress (iEECON2024), Pattaya, Thailand.

S. Techanok and K. Chayakulkheeree (2024), Multi-Objective Optimization of EV Charging for Cost and Loss Minimization Under TOU Tariff, Advances in Technology Innovation.

2024 International Electrical Engineering Congress (iEECON 2024)
March 6-8, 2024, Pattaya Chonburi, THAILAND

Optimal EV Charging Control for Distribution System Loss Minimization

Suwimon Techanok **Keerati Chayakulkheeree**
School of Electrical Engineering
Institute of Engineering, Suranaree University of Technology
Nakhonratchasima, Thailand
E-mail: suwimontechanok@gmail.com, keerati.ch@sut.ac.th

***Abstract*— This paper proposes the methodology for optimal EV charging scheduling (OEVCS) using particle optimization (PSO). The goal of this work is to minimize the total energy losses of the distribution system. The proposed PSO-based OEVCS was tested by the IEEE 33-bus system with modifications to include the charging load of the EVs. Simulation results show that the proposed EV charging scheduling method can minimize the total daily system energy losses.**

***Keywords*— optimal EV charging scheduling, particle swarm optimization, total system loss minimization.**

NOMENCLATURE

NB	: The total number of buses
PN	: The penalty factor.
$P_{total,loss}$	: The total daily power loss (kW)
$P_{total,EV}$	: The total power charging (kW)
P^{h}_{loss}	: The hourly power loss (kW)
P^{h}_{EV}	: The hourly power of charging (p.u.)
P^{hon}_{EV}	: The power in hours of charging (p.u.)
P^{hoff}_{EV}	: The power in hours of not charging (p.u.)
Vi	: The voltage of bus *i* (p.u.)
G_{ij}	: The conductance on branch *ij*
$V_{i,h}$	: The hourly voltage magnitude of bus-*i*
$V_{j,h}$	: The hourly voltage magnitude of bus-*j*
θ_{ij}	: The load angle difference between bus *i* and *j* in radian
EV_{ch}	: The matrix of EV charging

I. INTRODUCTION

At present, global warming is an environmental problem that countries around the world are paying attention to and are committed to solving the problem of increasing global temperatures. The increase in greenhouse gases in the atmosphere is one of the causes of this. Carbon dioxide is one element of the greenhouse effect. The primary causes of it are human activities, such as using fuel, operating machinery, and operating cars. As a result, a number of governments have taken measures to reduce carbon dioxide emissions. One way to reduce carbon dioxide emissions is by supporting the transition from internal combustion engines (ICE) to electric vehicles (EVs). Due to EVs do not emit carbon dioxide. Research suggests that by 2030, EVs can cut CO2 emissions by 28% [1].

As a result of many campaigns to encourage the use of EVs [2], the use of EVs has greatly increased. Therefore, the demand for electrical energy is also increasing. The grid is negatively impacted by the connection of an increasing number of EVs to the grid, as follows; (1) Impact on system losses: The transmission of large amounts of electrical energy causes additional electrical losses in the systems. (2) Harmonic impact: EV chargers are power electronic devices. Switching on electronic equipment can affect the power quality of the grid and may lead to equipment damage. (3) Effects of phase and voltage imbalance: Charging of massive electric vehicles causes high voltage within the network. Causes a phase imbalance from charging EVs with single-phase alternating current. (4) Stability impact: Charging EVs results in increased energy demand on the grid.

This results in a decrease in the stability of the electrical network system. Therefore, the increase in EVs results in large load shifts. It has a significant effect on the network system. As the quantity of EVs increases and the preference of owners to charge their vehicles during peak hours, there is a greater demand for electrical energy than usual. Causes more power loss than before. It is also apparent that the increasing number of EVs directly threatens grid stability. For consumers' charging EV behavior, it can generally be assumed that users will charge their EVs at home immediately after returning from work. This is the demand for charging electrical energy at the same time as the demand for normal electrical energy use, causing the demand for electrical energy during peak periods to increase. The network system may become unstable due to higher peak demand and sudden load changes. Increased energy losses result in inefficient electrical transmission and distribution systems. This causes a reduction in the quantity of power available to consumers. Electrical transmission lines are inefficient. This results in lower quality and reliability of power supply, as well as having a negative impact on the financial performance of utilities [3]. For this reason, the charging time of electric vehicles must be properly managed to minimize energy loss.

The optimal electric vehicle charging time and the impact of EV loads on the distribution system have therefore been prominent research topics in the last decade. For instance, the authors in [4] suggest that improving the charging duration of EVs with the use of genetic algorithms can reduce the home load's peak-valley differential. The authors in [5] propose a method to minimize the total daily charge cost by using mixed integer linear programming (MILP) to determine the optimal charging scheduling. Further, the author in [6] has suggested a scheduling approach that incorporates

979-8-3503-8359-1/24/$31.00 ©2024 IEEE

2024 International Electrical Engineering Congress (iEECON 2024)
March 6-8, 2024, Pattaya Chonburi, THAILAND

charge and discharge control with EV path planning. A mixed integer linear programming (MILP) model is enhanced to improve the low-cost charging benefit of EVs. This model increases EV charging efficiency while simultaneously optimizing the load on the power grid. In addition, [7] has suggested using mixed integer nonlinear programming to reformulate an ideal V2G scheduling model to increase the effectiveness of EV dispatching.

Although many researchers proposed mathematical optimization methods, such as genetic algorithms, mixed integer linear programming, and mixed integer nonlinear programming, to effectively optimize the EV charging schedule, there are a limited number of studies that aim to minimize system losses. The proposed problem formulation is a highly nonlinear optimization problem. Therefore, it is a limitation for using classical or deterministic optimization methods such as linear programming.

Therefore, this paper proposes using a PSO to solve the optimal EV charging scheduling problem, to minimize the total power loss of the system from large and sudden load changes. The proposed algorithm is tested on an IEEE 33-bus distribution system [8] connected to EV loads. The load profile of the northeastern region of Thailand and the EV load profile in [9]. The simulation results show that the proposed method can effectively minimize the daily system energy losses.

The remaining sections of the paper is structured as follows: The formulation of the OEVCS problem was covered in Section II. The PSO approach for resolving the OEVCS is presented in Section III. In section IV presents and discusses the simulation results of the proposed PSO-OEVCS using the IEEE 33-bus system. The conclusion is the last section.

II. Problem Formulation

In this paper, the OEVCS problem formulation is to determine the charging schedule that minimizes the total system daily loss. The total daily loss of the system over the course of a day can be calculated by summing up the power loss incurred during each hour throughout the day, as in (1).

$$P_{total,loss} = \sum_{h=1}^{h=24} P^{h}_{loss} \,, \qquad (1)$$

Where the hourly loss can be calculated by:

$$P^{h}_{loss} = \sum_{i=1}^{NB} \sum_{\substack{j=1 \\ j \neq 1}}^{NB} G_{ij} \left[(V_{i,h})^2 + (V_{j,h})^2 - 2V_{i,h}V_{j,h} \cos(\theta_{ij}) \right],$$

$$for \;\; i,j = 1, ..., \mathrm{NB} \,, \; h = 1, \ldots, 24 \,. \qquad (2)$$

A. Objective functions

The objective of the scheduling algorithm is to find the optimal EV charging time interval to minimize daily total system power losses. Mathematically, the power loss minimization problem can be formulated as follows:

$$\text{minimize} \;\; P_{total,loss} = \sum_{h=1}^{h=24} P^{h}_{loss} + PN \,, \qquad (3)$$

subject to the following constraints:

$$0 < P^{h_{on}}_{EV,\,p.u.} < 1 \;\; , \qquad (4)$$

$$P^{h_{off}}_{EV,\,p.u.} = 0 \;\; , \qquad (5)$$

$$\sum_{h=1}^{h=24} P^{h}_{EV} = P_{total,EV} \,, \quad h = 1, \ldots, 24. \qquad (6)$$

Equation (3) represents the objective function to be minimized. From the behavior of EV owners who mostly charge their vehicles immediately after returning home and stop charging when leaving for work. Therefore, it is determined that there is no charging during the h_{off} period, as shown in (5). Therefore, every remaining hour (h_{on}) is determined to have the EV charged, with the charging power in per unit (p.u.) as shown in (4). While (6) establishes a link between hourly charging power and total charging power.

III. PSO Based OEVCS

Kennedy and Eberhart [10] proposed the PSO as a population-based optimization method. Using a population of particles, the PSO approach finds the best solution. Each particle is a potential solution to the problem. PSO is essentially created by simulating bird flocking in two dimensions [11].

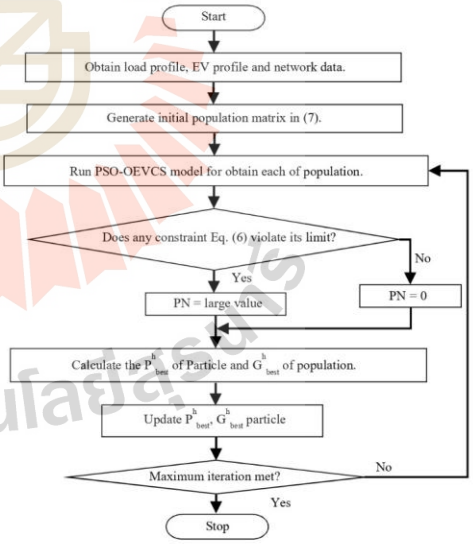

Fig. 1 Computation procedure of the PSO-based OEVCS.

2024 International Electrical Engineering Congress (iEECON 2024)
March 6-8, 2024, Pattaya Chonburi, THAILAND

The PSO algorithm begins by randomly creating particles in the function domain search space. The population matrix of the EVs charging energy each hour, as shown in (7), is used to acquire the EVs charged each hour value obtained from the charging schedule by PSO. The objective function is to minimize the daily power loss of the system in (3). The position in the EV_{ch} of the best fitness returned for a specific particle is P^{h}_{best}. The position in the EV_{ch} of the best fitness returned for the entire swarm is G^{h}_{best}. The computational procedure is illustrated in Fig. 1.

$$EV_{ch}=\left[P^{1}_{EV}, \ldots, P^{h}_{EV} \ldots, P^{24}_{EV}\right], \quad (7)$$

$$h = 1, \ldots, 24$$

IV. Simulation Results

In this section, we focus on the effect of EV charge scheduling by PSO on the total energy loss of the electrical system over the course of a day. Figure 2 displays the modified IEEE 33-bus distribution system under study, which includes EV charging on each bus. The load profile of the northeastern region of Thailand is used as the system base load, as shown in Fig. 3. Based on the charging habits of electric vehicle owners who charge after coming home and off-charge when leaving for work. Therefore, in this simulation, electric cars are not charged in hours 7–16 and are charged in the remaining hours.

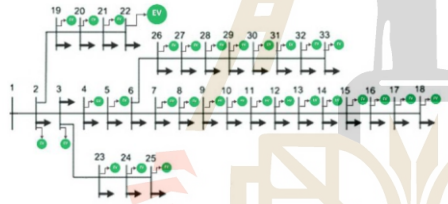

Fig. 2 The modified IEEE 33-bus distribution test system with EV charging.

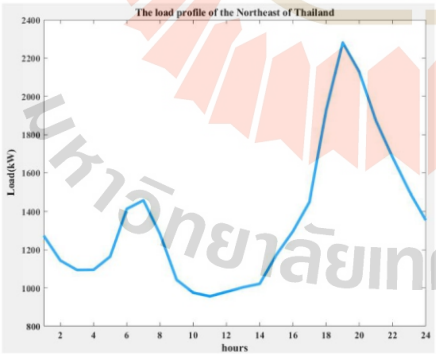

Fig. 3 System base load profile.

In this article, two case studies will be considered, as follows:

A. *Case I: IEEE 33-bus distribution system with Uncontrolled EV charging.*

In Case I, it is a simulation test of results on the IEEE 33-bus distribution system under study with EV charging. In this case, there is no control over the charging. The EV load profile is based on the user's basic charging behavior, according to [8]. As a result, PSO isn't using the optimal charging schedule.

The simulation results showed that the system was without charging control. The total daily system energy losses will be 10,054.34 kW.

B. *Case II: The IEEE 33-bus distribution system with Controlled EV charging.*

In Case II, the charging schedule is optimized using PSO. To minimize the total daily system energy losses per day, a new EV load profile will be obtained from the charging scheduling by PSO result, as shown in Table I (the adjusted EV load profile shown in Table I is the average value obtained from the calculation by PSO for 30 trials.).

The outcomes of the simulation demonstrate that the system has regulated charging. The total daily system energy loss will be 8,107.18 kW. Figure 4 represents the convergence plot of the suggested total daily system energy loss value for Case II.

TABLE I. EV LOAD PROFILE AND TOTAL DAILY SYSTEM POWER LOSSES RESULTS OF IEEE 33-BUS SYSTEM

Hour	Power consumption (p.u.)	
	Case I	Case II
	$P_{Uncontrolled\ ch}$ (p.u.)	$P_{controlled\ ch}$ (p.u.)
1	0.576923077	0.655359241
2	0.384615385	0.69284192
3	0.307692308	0.706330417
4	0.230769231	0.709446676
4	0.192307692	0.687877491
6	0.173076923	0.595910022
7	0	0
8	0	0
9	0	0
10	0	0
11	0	0
12	0	0
13	0	0
14	0	0
15	0	0
16	0	0
17	0.615384615	0.580212928
18	0.769230769	0.463772578
19	0.942307692	0.400388115
20	0.961538462	0.409415789
21	1	0.47795148
22	0.769230769	0.534180498
23	0.615384615	0.575878624
24	0.576923077	0.625818835
$P_{total,loss}$ (kW)	**10,054.34**	**8,107.18**

2024 International Electrical Engineering Congress (iEECON 2024)
March 6-8, 2024, Pattaya Chonburi, THAILAND

From the simulation results, as shown in Table 1, it will be seen that when using PSO By improving the charging time of EVs from Case I to Case II, the power during peak hours will decrease. As a result, the system's overall power loss is reduced.

TABLE II. THE MINIMUM, AVERAGE, AND MAXIMUM DAILY ENERGY LOSS OF THE SYSTEM FROM 30 TRIAL SOLUTIONS OF MODIFIED IEEE 33-BUS SYSTEM (CAES II)

	PSO-OEVCS		
DAILY ENERGY LOSSES (kW)	Min.	Avg.	Max.
	8,106.03	8,107.18	8,109.02

Table II and Fig. 5. illustrate the results from 30 trials of the proposed method. The daily energy losses of the system of the minimum and maximum solutions are 8,106.03 kW and 8,109.02 kW respectively. The average daily energy loss of the system from 30 trials is 8,107.18 kW.

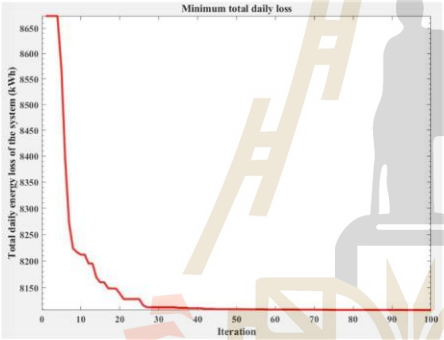

Fig. 4 The convergence plot of the proposed OEVCS for Case II.

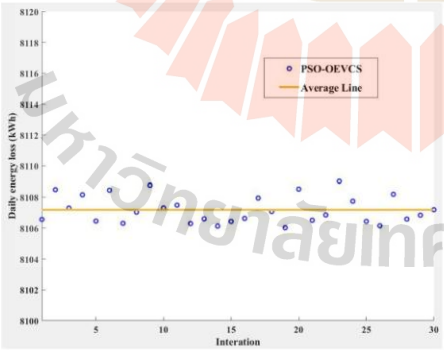

Fig. 5 The results from 30 trials of PSO-OEVCS for Case II.

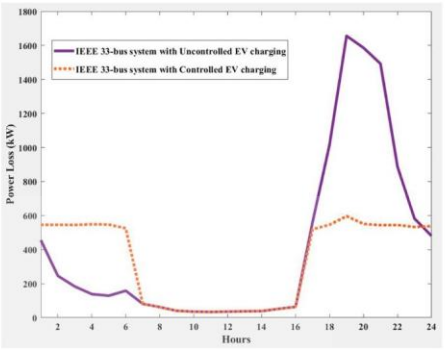

Fig. 6 The comparison of power loss between IEEE 33-bus with Uncontrolled EV charging and IEEE 33-bus with Controlled EV charging.

According to the simulation results, Figure 6 displays the results of comparing the hourly power losses of Case I and Case II. It is evident that the system with controlled EV charging will minimize power losses during peak hours. Compared to the system with uncontrolled charging.

V. CONCLUSION

In this paper, the use of PSO for optimal EV charging scheduling is proposed to minimize the total system power losses. According to simulation results on the IEEE 33-bus distribution system with EV charging, the proposed algorithm resulted in the most suitable electric vehicle charging schedule. In addition, the system peak demand can be substantially reduced, leading to ultimately reduction in the total system loss.

ACKNOWLEDGMENTS

We want to thank Suranaree University of Technology for their invaluable support over the course of our project.

REFERENCES

[1] Adnan, N., Md Nordin, S., bin Bahruddin, M.A. and Ali, M., " How trust can drive forward the user acceptance to the technology? in-vehicle technology for autonomous vehicle", Transp. Res. A 118, pp. 819–836, October 2018.

[2] IEA. All rights reserved, "Policies to promote electric vehicle deployment International Energy", Global EV Outlook 2021 pp. 42–61, 2021.

[3] Vincent Kwame Osei-Appiah1and Jones Lewis Arthur, "Managing System Losses to Improve Energy Efficiency within the Electricity Company of Ghana (ECG) Limited", Smart Grid and Renewable Energy, no.13, pp. 121–136, 2022.

[4] Ruoyun Hu, Qi Ding, Qingjuan Wang, Yifan Wang and Taoyi Qi, "Optimal Charging Scheduling for Household Electric Vehicles under TOU Prices", ICEEPE , no.5, pp. 994–999, 2022.

[5] Alireza Aliakbari and Vahid Vahidinasab, "Optimal Charging Scheduling of Solar Plugin Hybrid Electric Vehicles Considering On-the-Road Solar Energy Harvesting", Smart Grid Conference , no.10, pp. 1–6, 2020.

[6] Alicia Triviño-Cabrera, José A. Aguado and de la Torre S., "Joint routing and scheduling for electric vehicles in smart grids with V2G", Energy, vol.175, pp. 113–122, May 2019.

[7] Song Guo, Zejing Qiu, Chupeng Xiaoa , Hui Liao, Yuping Huang, Ting Lei, Dan Wu and Qian Jiang, "A multi-level vehicle-to-grid optimal scheduling approach with EVeconomic dispatching model", Energy Report, vol.7, pp. 23-37, November 2021.

[8] Meera P.S. and S. Hemamalini, "Optimal Siting of Distributed Generators in a Distribution Network using Artificial Immune System", IJECE, vol. 7, pp. 641649, April 2017.

[9] Jairo Quirós-Tortós, Luis (Nando) Ochoa and Timothy Butler, "How Electric Vehicles and the Grid Work Together", IEEE power & energy magazine, no2, pp. 64-76, December 2018.

[10] J.Kennedy, " The Particle Swarm Social Adaptation of Knowledge", IEEE International Evolutionary Computation ICEC 97, Indianapolis, USA, pp. 303 – 308, 1997.

[11] S. Sivasubramani, A K Chakraborty and P.K.Chattopadhyay, "Active Power Loss Minimization With FACTS Devices Using SA/PSO Techniques", International Conference on Power Systems, pp. 1 – 5, December 2009.

Biography

Ms. Suwimon Techanok received her B.Eng in EE (First Class Honors) from Suranaree University of Technology, Thailand, in 2023. She is currently pursuing M.Eng in EE at School of Electrical Engineering, Institute of Engineering, Suranaree University of Technology. Her research interests currently focuses on power system analysis and optimum charging of electric vehicle.

Assoc. Prof. Dr. Keerati Chayakulkheeree received his B.Eng in EE from King Mongkut Institute of technology ladkrabang, Thailand, in 1955, M.Eng and D.Eng degrees in Electric Power System Management from Asian Institute of technology, in 1999 and 2004, respectively. His primary areas of research interest include smart grid, power system protection, optimization, AI applications in power systems, and related fields.

Advances in Technology Innovation

Multi-Objective Optimization of EV Charging for Cost and Loss Minimization Under TOU Tariff

Suwimon Techanok, Keerati Chayakulkheeree*

Abstract

This study proposes an optimal electric vehicle (EV) charging (OEVC) management methods to minimize electricity costs and energy losses in the distribution system, which arise from the growing demand for EV charging. a multi-objective particle swarm optimization (MOPSO) algorithm is used to solve the OEVC multi-objective optimization (MOO). Additionally, the time-of-use (TOU) tariff is used to coordinate between the distribution system operator and EV users, which can help increase the efficiency of the charging schedule. Monte Carlo Simulation (MCS) is used to model virtual EV user behavior and create EV charging load profiles. The proposed MOPSO-based OEVC approach is verified on the modified IEEE 33-bus distribution test system, using MATLAB software, under both uncontrolled and controlled charging case studies. The simulation results demonstrate that the proposed method optimizes EV charging efficiently, achieving reductions of approximately 7.60% in electricity costs and 28.73% in energy losses compared to the uncontrolled charging case.

Keywords: optimal EV charging (OEVC), multi-objective optimization (MOO), electricity cost minimization, energy loss minimization, time-of-use (TOU) tariff

1. Introduction

Global warming poses a critical threat to ecosystems and human well-being. Many countries aim to achieve net zero emissions (NZE) as the solution under the Paris Agreement, with a key strategy being the transition from internal combustion engines (ICEs) to electric vehicles (EVs). Fuel combustion in ICEs is a major source of CO_2, and studies indicate that widespread EV adoption can reduce emissions by up to 20% [1-2]. Under the most ambitious scenarios, EVs could account for up to 65% of all light car sales globally by 2030, driven by strong policy support, advancements in battery technology, and market expansion in major regions. This projection aligns with the NZE by 2050 Scenario outlined in the Global EV Outlook 2024 [3].

However, the rapid increase in EV adoption also presents significant challenges for electricity grid management. As EV users typically charge their vehicles after returning home, this coincides with peak electricity demand from other daily activities, leading to elevated peak electricity loads. Without proper planning, this can result in significant negative impacts on the grid, such as voltage instability, increased power losses, and transformer overloading. For instance, studies [4] analyzing the impact of uncoordinated EV charging on grid performance, have shown that peak demand can increase by up to 53%. To address these challenges, implementing strategies such as smart charging, time-of-use (TOU) tariffs, and vehicle-to-grid (V2G) technology is crucial for ensuring the sustainable integration of EVs into the energy system [5]. Fig. 1 demonstrates the impact of EV charging on the load profile.

* Corresponding author. E-mail address: keerati.ch@sut.ac.th

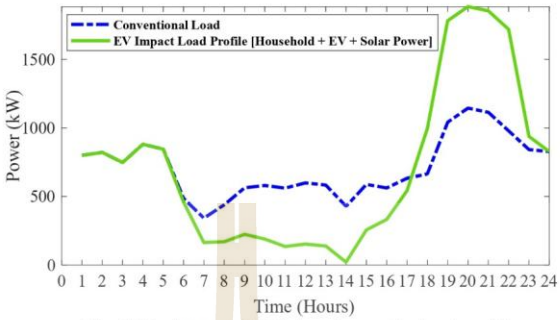

Fig. 1 The impact of EV charging on the load profile

Consequently, many studies are being conducted to find the management approaches to the rapid increase in EV numbers within the electricity system. In [5], an efficient and accurate predictive model for EV charging demand is proposed, specifically designed for use in the management and planning of urban transportation infrastructure. In [6], the authors propose sequential heuristic (SH) and global heuristic (GH) approaches to solve the optimal EV charging (OEVC) scheduling problem to minimize charging costs. In [7-8], centralized EV scheduling problems are proposed to minimize grid load imbalance through valley filling. In [9], the optimization of EV charging and discharging primarily aims to decrease energy costs by shifting loads to low-cost periods and regulating power system demand more efficiently.

Various algorithms have been studied and developed to optimize charging scheduling. Heuristic rule-based algorithms have been proposed in [10-11] to handle a variety of scheduling challenges considering variables such as the number of instances, the available limitations, and computational, including the scheduling of EV charging sessions at charging stations while solving an optimal power flow problem. However, heuristic rules are applied to problems with a small number of decision variables and lower computational complexity.

In contrast, metaheuristic algorithms are better suited for handling complicated problems, especially when it comes to scheduling optimization and power system challenges. In [12], the crow search algorithm (CSA) is used to optimize the energy control system and minimize operating costs. In [13], the focus is on minimizing the peak-to-valley difference in grid load and reducing user charging costs, proposing the use of genetic algorithms (GA) for optimal scheduling schemes for electric vehicles. In [14], the particle swarm optimization (PSO) algorithm can be employed to optimize EV charging scheduling to effectively minimize power loss, although it does not account for the uncertainty in user charging behavior. However, in [15], the uncertain behavior of EVs using a Markov decision process, with optimal charging management achieved through the bounded real-time dynamic programming (BRTDP) algorithm. In [16], GA and monte carlo simulation (MCS) are used to minimize distributed generators' investment costs. Adjusting EV users' charging behavior is crucial for optimizing charging schedules for maximum efficiency.

Demand side management (DSM) is an alternative solution for controlling electricity demand, including the demand for EV charging. DSM has been successfully applied in large-scale buildings through various demand response programs, such as real-time demand reduction, load shifting, and energy efficiency enhancement, as demonstrated in real-world case studies proposed in [5]. Dynamic pricing is important for managing conflicting energy demands from EV charging. In [17], it was demonstrated that the dynamic real-time demand electricity pricing mechanism can significantly reduce electricity costs. The TOU considered in [18] was applied for optimal energy scheduling to reduce system costs and minimize CO_2 emissions, utilizing the multi-objective grasshopper optimization algorithm (MOGOA). Meanwhile, [19] introduced a model developed using the learnable partheno-genetic algorithm (LPGA) to determine the optimal EV routes to minimize total distribution costs under the TOU framework.

However, MOGOA is still a relatively new algorithm with limited development and improvements, and LPGA is susceptible to becoming caught in local optima in the absence of a well-thought-out methodology. By contrast, multi-objective particle swarm optimization (MOPSO) is a widely used algorithm with several improved versions, making it highly effective for solving specific problems. MOPSO also has a strong capability to explore solution spaces efficiently and avoid local optima while offering flexibility in various applications. In [20], MOPSO has been used to optimize the power flow. Many studies focus on solving multi-objective scheduling problems, such as [21-22] minimizing grid load imbalance and focusing on reducing EV users' charging prices.

However, many studies primarily target reducing costs for the benefit of EV users. From the perspective of solving scheduling issues to minimize the distribution system operator's (DSO) expenses, this aspect is one of the most challenging issues. In large-scale EV charging, power losses from extensive electricity transmission impose significant challenges that are comparable to other grid impacts. Insufficient electricity to meet rising demand may also force the DSO to procure additional power, often from international sources, which could elevate costs due to fluctuating global energy prices. Moreover, both escalating costs and rising power losses have substantial and interconnected impacts on the grid's sustainability.

Therefore, both issues should be considered simultaneously in any comprehensive optimization strategy. The study in [5] focuses on developing a predictive model to accurately forecast EV charging demand by leveraging advanced deep learning techniques, primarily emphasizing long-term planning and resource allocation for charging station operators. However, it does not address the critical challenges associated with large-scale EV integration into the power grid, such as increased power losses and higher operational costs for DSOs. Meanwhile, this study aims to address this gap by focusing on optimizing EV charging to minimize both electricity costs and energy loss in the distribution system for the benefit of the DSO.

Based on the discussion above, this study proposes an integrated approach for OEVC that uses the MOPSO algorithm to minimize electricity costs and energy losses, achieving a balanced optimization between both objectives. In the methodology presented in this article, dynamic pricing is incorporated by integrating a TOU tariff as a representative example of price-based demand response actively used in Thailand in conjunction with MOPSO. Moreover, the versatility of MOPSO allows adaptation to other pricing schemes, which provides a flexible framework for diverse market conditions. While accounting for the uncertainty in the user charging behavior, the MCS generates EV load profiles based on actual usage data. The proposed MOPSO-based OEVC algorithm was tested on the IEEE 33-bus distribution system using the central Thailand household load profiles. The simulation results show that the proposed OEVC method effectively minimizes electricity costs and energy losses compared to charging profiles generated by MCS.

This study is structured as follows: Section 2 addresses the OEVC problem formulation, Section 3 presents the MOPSO method for solving the OEVC, Section 4 presents the simulation results and discusses the results of the MOPSO base OEVC, and Section 5 presents the conclusions.

2. Problem Formulation

In this section, objective functions are formulated to minimize electricity costs and energy losses. The MCS is used to model EV user behavior and handle the variability resulting from EV user behavior uncertainty. This part will also cover the TOU tariff, which is a time-based program that encourages response to the OEVC scheduling.

2.1. Time of Use (TOU) Tariff

The TOU rate is an electricity rate that represents the cost of generating power over two periods. Electricity costs are calculated based on the user's electricity usage period. As shown in Fig. 2, electricity costs during peak hours (from 9:00 AM to 10:00 PM) are higher than those during off-peak hours (from 10:00 PM to 9:00 AM). Implementing the TOU tariff encourages EV users to adjust their charging times to take advantage of the lower rates.

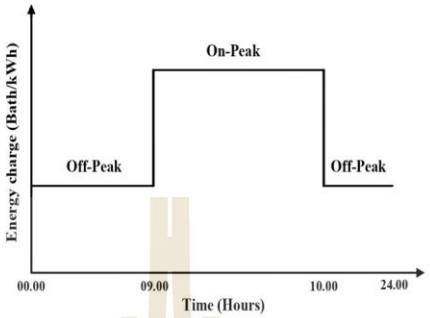

Fig. 2 Typical TOU tariff pattern

2.2. The probabilistic modeling of the EV user's behavior

For the behavior of EV users, MCS is applied to address the uncertainty of EV users' behavior. The random variables considered include the time at which EVs depart from home (T_{edr}), the duration from home to work (T_{htw}), the duration back from work to home (T_{ebh}), and the duration EVs are parked at work without being connected to the grid (T_{eop}). Additionally, the model considers battery capacity and distance. The probability distributions and parameter values used for these variables were derived from empirical studies on real-world EV user behavior in European countries, which investigated travel patterns, parking durations, and charging preferences. These findings provided the basis for determining the means and standard deviations for each parameter, as presented in Table 1 from [23]. The lower and upper bounds of random variables are 0-24 hours. Fig. 3 illustrates the EV user activity model generated using MCS. This model creates an EV charging load profile, which is combined with the household load profile. These inputs and network data are provided to the MOPSO algorithm to solve the OEVC.

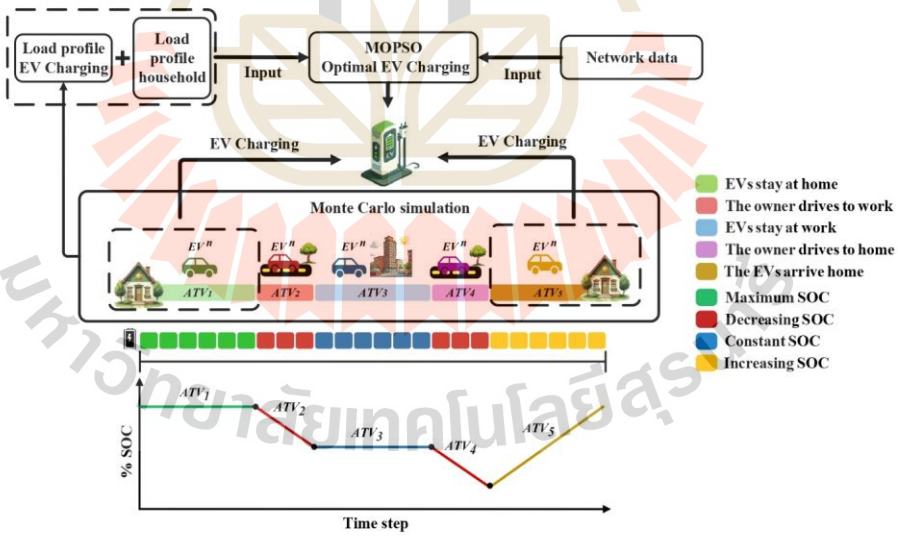

Fig. 3 Framework of MOPSO-based OEVC with probabilistic EV user activity model

Once these random time variables are obtained from the MCS, they serve as inputs to model the EV usage activities of users. The model for EV usage activities is based on the assumption that EVs are primarily used for commuting within urban areas, where they only travel from home to work and do not account for regional variations in user behavior or external factors

such as traffic conditions or weather. Therefore, the activities of EV users include the time of departure from home, the time of return to home, the travel duration, and the duration of parking without charging, as described in Eqs. (1)–(6).

$$ATV_{day}^{n} = [ATV_1^n + ATV_2^n + ATV_3^n + ATV_4^n + ATV_5^n], \tag{1}$$

$$ATV_1^n = \{1 : T_{edr}^n - 1\}, \tag{2}$$

$$ATV_2^n = \{T_{edr}^n : T_{edr}^n + T_{htw}^n\}, \tag{3}$$

$$ATV_3^n = \{T_{edr}^n + T_{htw}^n + 1 : T_{edr}^n + T_{htw}^n + T_{eop}^n\}, \tag{4}$$

$$ATV_4^n = \{T_{edr}^n + T_{htw}^n + T_{eop}^n + 1 : T_{edr}^n + T_{htw}^n + T_{eop}^n + T_{ebh}^n\}, \tag{5}$$

$$ATV_5^n = \{T_{edr}^n + T_{htw}^n + T_{eop}^n + T_{ebh}^n + 1 : np\}, \tag{6}$$

$$for\ n = 1,\ldots,NC, t = 1,\ldots,np$$

where, ATV_{day}^n represents the daily activities of the n^{th} EV usage. The n^{th} EVs stay at home before leaving for work in activity ATV_1^n. ATV_2^n is the owner who drives the n^{th} EVs to work. The user of the n^{th} EV parks the EVs at work without connecting to the grid by ATV_3^n is the activity in which the user of the n^{th} EV parks the EV at work without connecting to the grid. The owner, ATV_4^n takes the n^{th} EVs home. Lastly, ATV_5^n represents the owner of the n^{th} EVs after they get home from work.

In order to estimate the electricity consumption from EV charging and create the load profile for uncontrolled charging of EVs, it is necessary to calculate the state of charge (SOC). Based on the assumption that EV usage begins in the morning after overnight charging, it is initially considered that the battery is fully charged, as indicated in Eq. (7) [24]. Considering only the charging state, it is assumed that the SOC^t is limited to a minimum depth of discharge (DOD), determined by the fraction P_{dod} and the maximum SOC when fully charged, denoted as SOC_{max}, as shown in Eq. (8).

$$SOC_0^n = SOC_{\max}^n \tag{7}$$

$$p_{dod}\ SOC_{\min}^n \le SOC_t^n \le SOC_{\max}^n \tag{8}$$

The level of SOC changes according to EV usage activities. It increases when the EV is charged at home and decreases when the user drives the EV. For the time step of the SOC at time increases from its initial state according to the charging power when the EV is charged. It decreases according to the energy consumption when the EV is driven, as calculated in Eq. (9).

$$SOC_{t+1}^n = \begin{cases} SOC_t^n + P_c \Delta t, & for charging\ mode \\ SOC_t^n - C^t \Delta t, & for driving\ mode \\ SOC_t^n, & else \end{cases} \tag{9}$$

$$for\ n = 1,\ldots,NC, t = 1,\ldots,np$$

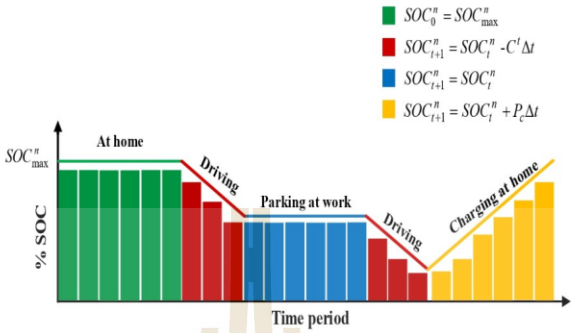

Fig. 4 The SOC varies over time under different EV charging strategies

Fig. 4 illustrates the SOC profiles of an EV under different charging strategies across key activity periods, including staying at home, driving to work, parking at work without charging, EV driving back home, and charging at home. Each segment reflects the change in SOC based on the corresponding activities, where SOC decreases during driving, remains constant while parked at work, and increases when charging at home, following Eqs. (7)-(9).

The EV charging load profile $P^n_{ev,i,t}$ will be equal to or dependent on P_c following the vehicle usage activities at that time initially, as shown in Eq. (10). The total EV charging load profile is determined by summing the charging loads of all EVs, as described in Eq. (11).

$$P^n_{ev,i,t} = \begin{cases} P_c & , for charging mode \\ 0, & else \end{cases} \tag{10}$$

$$P^{total}_{ev,i,t} = \sum_{n=1}^{NC} P^n_{ev,i,t} \tag{11}$$

$$for\ n = 1,\ldots,NC, t = 1,\ldots,np$$

The power EV charging $P^n_{ev,i,t}$ must be taken into account hourly in the data analysis to ensure that the information is in line with the objective function, understandable, and adheres to standard procedure. The outcome of changing the time step from one minute to one hour is displayed in Eq. (12).

$$P^{total}_{ev,i,h} = \sum_{n=1}^{NC} P^n_{ev,i,h} \tag{12}$$

$$for\ n = 1,\ldots,NC, h = 1,\ldots,24$$

2.3. Objective functions

This research focuses on managing the increasing electricity demand resulting from EV charging by searching for the OEVC time with two objectives. The first objective is to reduce electricity costs, and the second is to minimize energy losses in the system. The objective functions of the electricity cost minimization problem are presented in Eq. (13) and the energy loss minimization problem is presented in Eq. (14).

$$Minimize\ C^{total}_{ep} = \sum_{h=1}^{24} C^h_{ep} \tag{13}$$

$$Minimize\, E_{loss}^{total} = \sum_{h=1}^{24} P_{loss}^{h} \tag{14}$$

where the hourly electricity cost can be calculated by:

$$C_{ep}^{h} = \Sigma_{i=1}^{NB} C_{en,i}^{h} + C_{Ft,i}^{h} + C_{vat,i}^{h} \tag{15}$$

$$C_{en,i}^{h} = (P_{hh,i}^{h} + P_{ev,i}^{h}) \times r_{tou}^{h} \tag{16}$$

$$C_{Ft,i}^{h} = (P_{hh,i}^{h} + P_{ev,i}^{h}) \times Ft \tag{17}$$

$$C_{vat,i}^{h} = \left(C_{en,i}^{h} + C_{Ft,i}^{h}\right) \times VAT \tag{18}$$

$$for\, i = 1,\ldots,NB, h = 1,\ldots,24$$

The hourly loss can be calculated using Eqs. (19)-(20), the equations are referred from the load flow equations in [25].

$$P_{loss}^{h} = \Sigma_{i=1}^{NB} P_{G,i}^{h} - (P_{hh,i}^{h} + P_{ev,i}^{h}) \tag{19}$$

$$P_{loss}^{h} = V_i \sum_{j=1}^{NB} V_j [G_{ij} \cos(\delta_i - \delta_j) + B_{ij} \sin(\delta_i - \delta_j)] \tag{20}$$

$$for\ i = 1,\ldots,NB, h = 1,\ldots,24$$

2.4. Constraints

According to the MCS of EV user behavior, EVs are not charged from the moment they leave home until they return. Thus, $P_{ev,i}^{h,on}$ represents the charging power at the time h at bus i when the EV is charging, with its value ranging between a maximum, the total power charge of all EVs at bus i, and the minimum is a percentage of the total number of cars (*pnc*). While $P_{ev,i}^{h,off}$ indicates the total power charge at the time h at bus i when the EV is not charging, which equals 0. According to Eqs. (21)-(22).

$$(pnc \times \Sigma_{n=1}^{NC} P_{c,i,n}^{h}) \le P_{ev,i}^{h,on} \le (\Sigma_{n=1}^{NC} P_{c,i,n}^{h}), \tag{21}$$

$$P_{ev,i}^{h,off} = 0, \tag{22}$$

$$for\, i = 1,\ldots,NB, n = 1,\ldots,NC, h = 1,\ldots,24$$

The equality constraints, which represent the load flow equations, are as follows in Eqs. (23)-(24)[25].

$$P_{Gi} - P_{Di} - V_i \sum_{j=1}^{NB} V_j [G_{ij} \cos(\delta_i - \delta_j) + B_{ij} \sin(\delta_i - \delta_j)] = 0 \tag{23}$$

$$Q_{Gi} - Q_{Di} - V_i \sum_{j=1}^{NB} V_j [G_{ij} \sin(\delta_i - \delta_j) - B_{ij} \cos(\delta_i - \delta_j)] = 0 \quad (24)$$

$$for\, i = 1,\ldots,NB, h = 1,\ldots,24$$

The inequality constraints establish the system's operational bound, as follows. Generator constraints, including voltage, active power, and reactive power at the i^{th} bus, are restricted between their upper and lower bounds, as shown in

$$\begin{aligned} |V_{Gi}|^{\min} \le |V_{Gi}| \le |V_{Gi}|^{\max} \\ |P_{Gi}|^{\min} \le |P_{Gi}| \le |P_{Gi}|^{\max} \\ |Q_{Gi}|^{\min} \le |Q_{Gi}| \le |Q_{Gi}|^{\max} \end{aligned}, \quad (25)$$

Transformer tap settings are confined within specified limits, as detailed in

$$T_i^{\min} \le T_i \le T_i^{\max}, \quad (26)$$

Shunt compensations are subject to their respective limits, as outlined in

$$Q_{ci}^{\min} \le Q_{ci} \le Q_{ci}^{\max}, \quad (27)$$

and line flow constraints in

$$f_l \le f_l^{\max} \quad (28)$$

3. Multi-Objective Particle Swarm Optimization (MOPSO)

In this section, the MOPSO algorithm designed for the problem considered in this article is discussed. Furthermore, the concept of Pareto dominance, which is important for the operation of MOPSO for handling multi-objective optimization (MOO) problems, is explained.

3.1. Basic Concept of Pareto Dominance

Problem-solving with multiple objectives, as presented in this article, targets reducing electricity costs and minimizing energy losses. Therefore, it requires carefully balancing conflicting goals. The Pareto dominance concept is applied to analyze and solve the MOO problem. The Pareto dominance helps identify solutions in which an improvement in one objective cannot be achieved without causing a deterioration in another. In other words, if a solution x_1 is better than a solution x_2, then the solution x_1 is said to be the dominating one. Thus, the set of non-dominated solutions, which is known as the Pareto frontier, naturally represents a balanced trade-off between the two objectives.

Coello and Salazar Lechuga were among the first to extend the PSO algorithm to handle multi-objective problems by incorporating the principle of Pareto dominance. The key advancements include using an external repository to store and update non-dominated solutions and employing a leader selection mechanism based on Pareto criteria. These modifications guide the swarm toward less crowded regions of the objective space, promoting diversity and ensuring that the final set of

solutions maintains a balanced trade-off between minimizing electricity costs and reducing energy losses. This method is known as MOPSO [26].

3.2. MOPSO algorithm

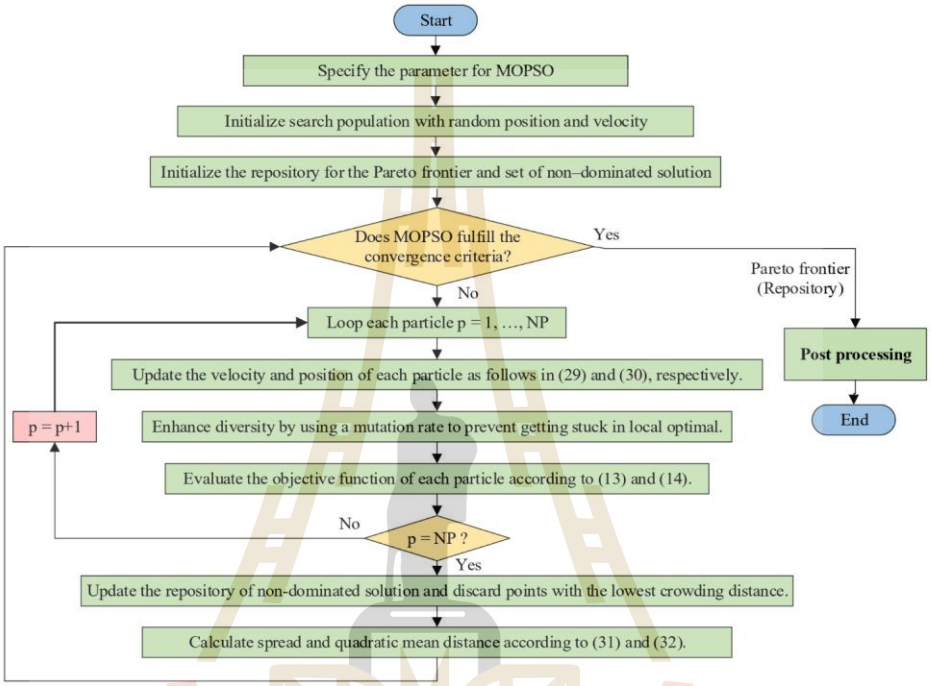

Fig. 5 The proposed MOPSO-based OEVC computational procedure

MOPSO is an extension of the PSO concept, maintaining the fundamental principles of PSO while incorporating the core concept of Pareto dominance to manage MOO [27-28]. Therefore, in each iteration, the equations for velocity and position updates remain as defined in Eqs. (29)-(30), respectively. $V_{i,t}$ is the velocity at iteration t and $V_{i,t+1}$ is the updated velocity at iteration $t+1$ of particle i. $x_{i,t}$ is position at iteration t, and $x_{i,t1}$ is the updated position at iteration $t+1$ of particle i. w is the inertia weight. Parameters c_1 and c_2 are the cognitive constant and the social constant respectively. r_1 and r_2 are the random numbers uniformly distributed between 0 and 1. $x_{i,t}^{Pbest}$ is the best position of particle i at an iteration. This is the best solution that the particle has found till the current iteration. $x_{i,t}^{Gbest}$ is the global best position across all particles up to the current. This is the non-dominated solution or best solution found by the swarm.

$$V_{i,t+1} = wV_{i,t} + c_1 r_1 (x_{i,t}^{Pbest} - x_{i,t}) + c_2 r_2 (x_{i,t}^{Gbest} - x_{i,t}) \tag{29}$$

$$x_{i,t+1} = x_{i,t} + V_{i,t+1} \tag{30}$$

The MOPSO algorithm has been developed and detailed in [29] and is called the multiple design option (MDO)-MOPSO. In this research, the MDO-MOPSO algorithm has adapted to suit the specific characteristics of the problem in this article while still considering the spread and the mean of the crowding distances (quand mean) as convergence criteria according to Eqs. (31)-(32). Fig. 5 illustrates the methodology of the MDO-MOPSO algorithm.

$$spread = \frac{\mu + \sigma}{\mu + Q\bar{d}} \tag{31}$$

$$quand\ mean = \sqrt{\frac{1}{Q}\sum_{k} d_k^2} \tag{32}$$

where μ is the parameter that quantifies whether the extreme values of the Pareto frontier have changed between two consecutive iterations. σ and $\bar{d}$ are the standard deviation and the arithmetical average of the crowding distances of point k, and Q is the number of points on the Pareto frontier. This modified version of the MOPSO algorithm integrates performance metrics and includes a post-processing step to identify MDO. The iterative process stops when one of the following three conditions. The first is when the maximum number of iterations is reached. The second is that the change in the spread measure falls below a specified relative and absolute tolerance of, or the final, the change in the quadratic mean of crowding distances falls below a specified absolute and relative tolerance.

In the post-processing section, a process is conducted to identify the optimal solutions according to predefined criteria. The steps are as follows:

(1) Identify the search area for selecting extreme values and conducting trade-off analysis based on the Pareto frontier.
(2) Remove any outliers to ensure only relevant and feasible solutions are considered.
(3) Select extreme designs that maximize energy shares, focusing on solutions that provide the best balance between objectives.
(4) Calculate key performance indicators (KPIs). KPIs are computed to evaluate and compare the diversity characteristics among the original Pareto frontier, the enhanced Pareto frontier, and the selected MDO points. The calculation of KPIs is based on the Manhattan measure. Details of this calculation are presented in [29].
(5) Plot the trade-offs and results to visually assess and compare the final solutions.

4. Simulation Results and Discussion

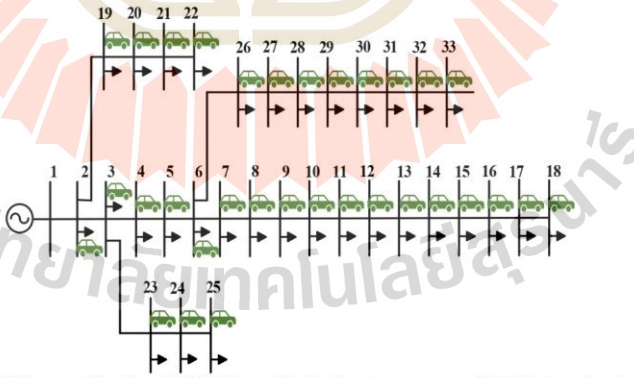

Fig. 6 The modification IEEE 33-bus distribution test system with EV charging devices

This section discusses the simulation of a system modified from the IEEE 33-bus distribution test system by adding EV connections at each bus, as shown in Fig. 6. According to this research study, the OEVC scheduling controls the increasing demand for electricity to minimize electricity costs and energy losses in the system. The MOPSO algorithm is used for OEVC scheduling, and the simulation is performed with MATLAB software.

4.1. IEEE 33-bus distribution system without EV charging device

The IEEE 33-bus distribution system is used as the base system for this study, as shown in Fig. 6. In the base case, the simulation is performed without connecting any EV charging devices to the system, while other cases include EV charging devices. The load profile used as the system's base load for households is the central Thailand load profile for July, as shown in Fig. 7. This case study contrasts the outcomes of the OEVC scheduling for objective functions of different purposes.

4.2. IEEE 33-Bus distribution system with EV charging device

The IEEE 33-bus distribution system with the integration of EV charging devices, as shown in Fig. 6. This system is used for the simulation under uncontrolled and controlled charging conditions. For the controlled scenario, three case studies are presented to assess and compare the performance of the proposed algorithm in solving the OEVC problem.

4.2.1. Uncontrolled EV charging devices

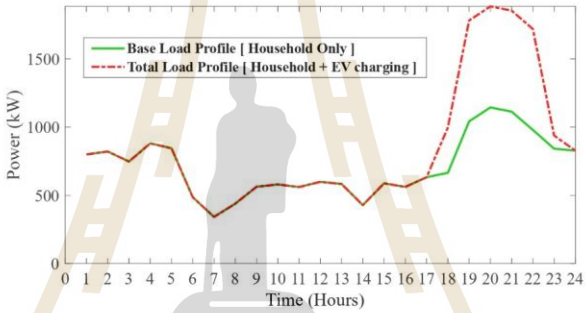

Fig. 7 The Load Profiles of the System without and with EV Charging

IEEE 33-bus distribution system with EV charging device, as shown in Fig. 6. EV charging input parameters are as in [24] and the BYD Atto 3 model, as shown in Table 2. The load profile for EV charging follows user behavior as suggested by the MCS, which is shown in Fig. 7. The uncontrolled EV charging load profile, location status based on user activities and SOC by considering the time period $np = 1440$ minutes, is shown in Fig. 8. Simulation results indicate that without controlling EV charging, the daily electricity cost for the entire system is 105.6815 kTHB/kWh, and the daily energy loss is 6.16 MWh.

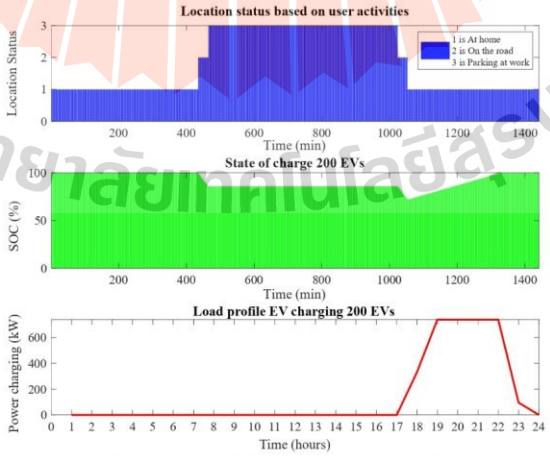

Fig. 8 Uncontrolled EV charging simulation

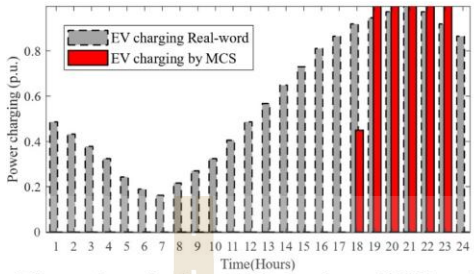

Fig. 9 Comparison of real-world EV charging and MCS results

Fig. 9 presents the comparison of the EV charging load profile from the MCS and the real-world EV charging data from the Denmark study [30]. The outcomes indicate that the load profile generated by the MCS agrees with the real-world data. In particular, the peak electricity demand is close to real-world values and occurs between 8:00 PM and 9:00 PM.

Table 1 Mean and variance of EV usage patterns

Random variable	Mean (μ)	Variance (σ^2)
T_{edr}	7:15 AM	30 min
T_{htw}	30 min	15 min
T_{eop}	9 h and 20 min	50 min
T_{ebh}	30 min	15 min

Table 2 Input parameters of EV charging

Parameter values	
SOC_{max}	60.48 kWh
P_c	3.7 kWh
p_{dod}	0.6
$C_s{}^t$ of Jun-Aug	1.1
v_m	60 km/h
c_m	0.257 kWh/km
Δt	1/60 h
pnc	0.1

4.2.2. Controlled EV charging devices

In this article, household consumption at a voltage level lower than 12 kV is used, using the TOU pricing of Thailand as indicated in Table 3. In this study, the OEVC scheduling is proposed in three case studies to assess the effectiveness of optimal charging planning, including using the algorithms differently to solve the problem. The three case studies are as follows:

Table 3 Time of Use rate (TOU rate) for type 1 residential households

Voltage level	Energy charge (Bath/kWh)	
	Peak (09:00 a.m.-10:00 p.m.)	Off-Peak (10:00 p.m.-09:00 a.m.)
At voltage level 12 – 24 kV	5.1135	2.6037
At voltage level lower than 12 kV	5.7982	2.6369

(1) Case I: Single objective for minimizing Electricity cost

In this case, the PSO and GA determine the OEVC scheduling, considering the single objective function of minimizing the electricity cost of the system. The result of the PSO achieved a minimum daily electricity cost of 96.92823 kTHB, leading to a daily energy loss of 5.4966 MWh. In comparison, the result of the GA produced a minimum daily electricity cost of 98.1728 kTHB, leading to a daily energy loss of 5.5542 MWh. Across 30 trials in this case, the resulting averages of PSO and GA were 97.1056 kTHB and 98.4532 kTHB.

(2) Case II: Single objective for minimizing Energy losses

In this case, the PSO and GA determine the OEVC scheduling, considering the single objective function of minimizing the energy loss of the system. The result of the PSO achieved a minimum daily energy loss of 4.0900 MWh, leading to a daily

electricity cost of 97.752 kTHB. In comparison, the result of the GA produced a minimum daily energy loss of 4.208 MWh, leading to a daily electricity cost of 100.442 kTHB. Across 30 trials in this case, the resulting average of PSO and GA was 4.3195 MWh and 4.3560 MWh.

(3) Case III: Multi-objective for minimizing Electricity cost and Energy losses

The MOPSO will be used to determine the OEVC scheduling in this case, considering both the objective function that minimizes electricity cost and minimizes energy loss. The results of the MOPSO indicate that in the system with controlled charging, the daily electricity cost for the entire system is 97.651 kTHB, and the daily energy loss is 4.39 MWh.

Table 4 Objective function values from 30 trials by PSO and GA (Case I and Case II)

Objective function values	Case studies			
	Case I		Case II	
	Electricity cost (kTHB)		Energy loss (MWh)	
Algorithm	PSO	GA	PSO	GA
Max	99.3399	101.8907	4.8523	4.5714
Avg.	97.6148	099.5013	4.3196	4.3560
Min	96.2823	098.1728	4.0900	4.2085

Table 4 and Fig. 10 show the results of the objective function values of the maximum, minimum, and average obtained from 30 PSO and GA trials for case I and case II. The comparison of the performance of PSO and GA for Case I and II, as shown in Fig. 10(a) and Fig. 10(b). Each figure includes the results of 30 trials, showing the average trend line across trials, with the best result marked by a red diamond and the worst result marked by a black circle. The simulation results show that PSO is better than GA in both cases, with the PSO achieving a minimum daily electricity cost of 96.2823 kTHB and a minimum daily energy loss of 4.09 MWh. The EV charging scheduling results by PSO and GA for case I and case II are the minimum electricity cost and energy loss obtained from the simulation results for 30 trials, as indicated in Table 5.

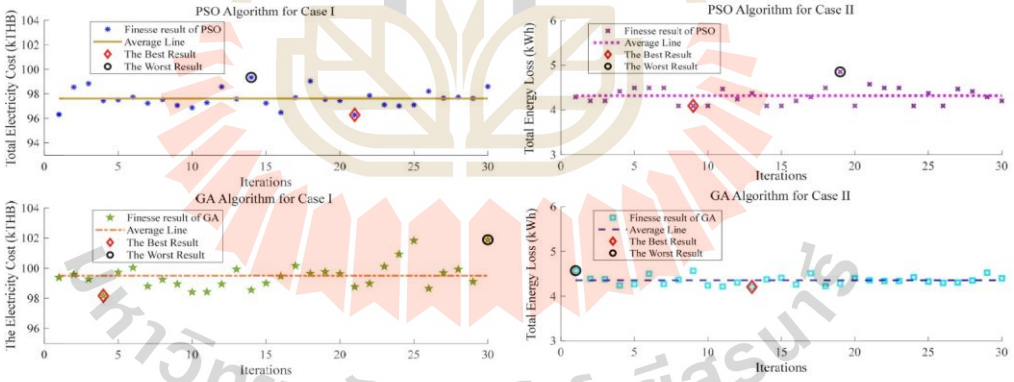

(a) Case I (b) Case II

Fig. 10 The results from 30 trials of the PSO and GA algorithm

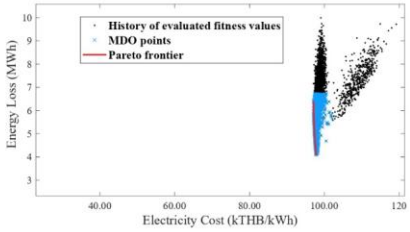

Fig. 11 Pareto Frontier of the proposed MOPSO-based OEVC

Fig. 11 shows the results from MDO-MOPSO for case III. The history of fitness values evaluated during the MOPSO process, including optimal and suboptimal solutions, is represented by black points. The blue points indicate the MDO solution set selected after post-processing analysis. The red line shows the Pareto frontier, representing the optimal trade-offs between electricity cost and energy loss. The most suitable set of solutions is derived from the Pareto frontier after further filtering using a diversity criterion based on crowding distance and a post-processing step that retains only the solutions within a predefined tolerance. This process indicates that the final solutions reflect a balanced trade-off between minimizing electricity costs and reducing energy losses.

Table 5 EV load profiles and minimum objective function values for the IEEE 33-Bus system

Hours	Power consumption (kWh)					
	Uncontrolled charging	Controlled charging				
		Case I		Case II		Case III
		PSO	GA	PSO	GA	MOPSO
1	0	229.40	331.27	231.58	265.42	296.96
2	0	346.16	173.09	221.73	106.09	282.31
3	0	379.73	468.63	255.62	089.09	221.05
4	0	459.64	225.38	194.35	133.60	143.07
5	0	570.91	224.49	211.49	187.90	241.65
6	0	138.92	105.90	373.12	652.74	372.80
7	0	222.69	249.58	740	408.66	675.08
8	0	0	0	0	0	0
9	0	0	0	0	0	0
10	0	0	0	0	0	0
11	0	0	0	0	0	0
12	0	0	0	0	0	0
13	0	0	0	0	0	0
14	0	0	0	0	0	0
15	0	0	0	0	0	0
16	0	0	0	0	0	0
17	0	0	0	0	0	0
18	332.445	103.23	074.66	292.30	382.40	135.02
19	740.000	080.39	074.66	121.54	076.07	138.28
20	740.000	074.01	074.66	074.69	369.62	138.72
21	740.000	074.00	108.62	088.67	175.42	135.02
22	740.000	122.09	339.17	150.63	155.40	222.82
23	096.015	132.41	482.71	212.92	226.21	203.80
24	0	454.92	455.67	219.86	159.88	181.92
C_{ep}^{total} (kTHB)	105.682	96.2823	98.1728	97.752	100.442	97.651
E_{loss}^{total} (MWh)	6.16	5.4966	5.5542	4.0900	4.2085	4.3917

Table 5 presents the results of EV charging scheduling in the three cases compared to uncontrolled EV charging schedules. The results of all three cases show that optimized charging schedules reduce electricity costs and energy loss. In case I, the best result among PSO and GA is a daily electricity cost of 96.922 kTHB, but the energy loss remains relatively high at 5.4966 MWh. In case II, the best result among PSO and GA is a daily energy loss of 4.0900 MWh, but the electricity cost remains relatively high at 97.752 kTHB. The obtained solution in case III is the OEVC. It achieves a daily electricity cost of 97.651 kTHB and an energy loss of 4.3917 MWh. Cases I and II, which consider minimizing a single objective function, using the PSO and GA, achieve the minimum value for that specific objective function. However, the values for the other objective function are higher. Furthermore, the PSO shows slightly superior performance compared to GA.

Conversely, OEVC scheduling with MOPSO considers the balance between the two objective functions in that the results for the obtained objective values are not minimum. But these are the optimal results for both objectives. Therefore, the electricity cost and energy loss values in case III fall between cases I and II. The comparison of the EV load profile, electricity

cost, and energy loss for each hour is shown in Fig. 12. The simulation results in Fig. 12(a) compare the system load profiles, showing that the system with charging control under TOU pricing results in lower on-peak energy demand, which helps reduce electricity costs and energy loss, as shown in Fig. 12(b) and Fig. 12(c).

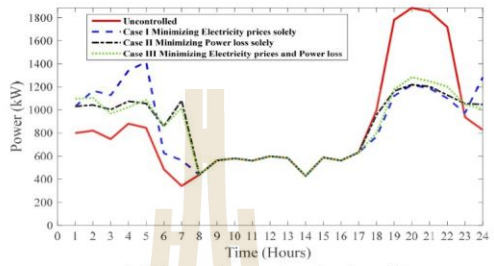

(a) Comparison system load profile

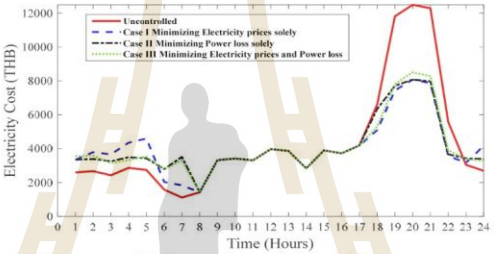

(b) Comparison of electricity cost

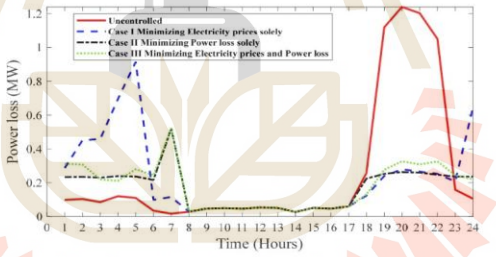

(c) Comparison of power loss

Fig. 12 Comparison of results from all cases

5. Conclusions

This study proposed a method for OEVC that uses the MOPSO algorithm to solve the multi-objective optimization problem. The goal is to minimize electricity costs and energy losses in the system caused by the large increase in EVs. MCS is used to model the uncertain behavior of EV usage. Additionally, a TOU tariff was used to promote OEVC. The experiments were conducted using MATLAB software and tested on the IEEE 33-bus distribution system. According to the simulation results, the conclusion is given below.

(1) MCS has effectively modeled the uncertain behavior of EV users, which can create realistic EV charging load profiles. This shows that the energy demand during peak periods increases, leading to higher electricity costs and energy losses.

(2) The MOPSO algorithm is designed to explore a balanced set of solutions using the Pareto frontier. This approach enables it to effectively address the multi-objective challenge of OEVC by reducing both electricity costs and energy losses. However, MOPSO cannot minimize either aim to the lowest possible level because it operates with the Pareto frontier, which focuses on balancing both objectives without allowing one to outperform the other.

In the future, improvements might include adaptive tuning of parameters, combining MOPSO with other techniques, or using real-time data to boost specific performance while still maintaining the overall balance.

Acknowledgment

The authors sincerely want to thank the Suranaree University of Technology for their invaluable support throughout the project.

Abbreviations and Symbols

BEV	Battery Electric Vehicle	P_{Di}	The real power demand at bus *i*
DOD	Depth of Discharge	P_{Gi}	The real power of the generator at bus *i*
EV	Electric Vehicle	$P_{Gi}^{\min}$	The minimum real power of the generator at bus *i*
MOPSO	Multi-Objective Particle Swarm Optimization	$P_{Gi}^{\max}$	The maximum real power of the generator at bus *i*
MDO	Multiple Design Option	Q_{Di}	The reactive power demand at bus *i*
MOO	Multi-Objective Optimization	Q_{Gi}	The reactive power of the generator at bus *i*
NB	The total number of buses	$Q_{ci}^{\min}$	The minimum shunt VAR compensator
NC	The total number of cars	$Q_{ci}^{\max}$	The maximum shunt VAR compensator
PSO	Particle Swarm Optimization	r_{tou}^{h}	The electricity pricing at hour *h*
SOC	State of Charge	SOC_0^n	Initial State of charge of *n* cars
TOU	Time of Use	$SOC_{\max}^n$	The maximum state of charge of *n* cars
B_{ij}	The susceptance on branch *ij*	$SOC_{\min}^n$	The minimum state of charge of *n* cars
C_{ep}^{total}	The total daily electricity prices	T_{edr}^n	The time the *n*-th EV departs from its residence
C_{ep}^{h}	The total hourly electricity prices	T_{hhw}^n	The duration of time it takes for the *n*-th EV to travel from home to the workplace
$C_{en,i}^{h}$	The electricity energy prices at bus *i* and hour *h*	T_{eop}^n	The duration of time the *n*-th EV is parked in the garage at the workplace
$C_{Ft,i}^{h}$	The electricity fuel adjustment charge prices at bus *i* and hour *h*	T_{ebh}^n	The duration of time it takes for the *n*-th EV to travel from workplace to the home
$C_{vat,i}^{h}$	The electricity value added tax prices at bus *i* and hour *h*	$T_i^{\min}$	The minimum transformer tap settings
f^l	The MVA flow of line *l*	$T_i^{\max}$	The maximum transformer tap settings
f_{max}^l	The maximum limit of line *l*	Vij	The voltage of bus *i* and *j*
Ft	The fuel Adjustment Charge (at the given time)	VAT	The value-added tax
G_{ij}	The conductance on branch *ij*	δ_{ij}	The phase difference of voltages between bus *i* and *j*
E_{loss}^{total}	The total daily energy losses	C_s^t	Season coefficient
$P_{ev,i,h}^{total}$	The total charging power at bus *i* and hour *h*	c_m	Electricity consumption in distance (kWh/km)
$P_{ev,i,h}^{n}$	The charging power of *n* cars at bus *i* and hour *h*	P_c	Charging power (kWh)
P_{loss}^{h}	The hourly power loss	p_{dod}	Depth of discharge fraction
P_{hh}^{h}	The hourly power of the household load	p_{car}	Vehicle usage probability
$P_{ev,i,n}^{h,on}$	The charging power of *n* cars at bus *i* that is charging	Δt	Time step length (hr)
$P_{ev,i,n}^{h,off}$	The charging power of *n* cars at bus *i* that is not charging	v_m	The average velocity for a private vehicle trip

Conflicts of Interest

The authors declare no conflict of interest.

References

[1] Y. Ou, N. Kittner, S. Babaee, S. J. Smith, C. G. Nolte, and D. H. Loughlin, "Evaluating Long-Term Emission Impacts of Large-Scale Electric Vehicle Deployment in the US Using a Human-Earth Systems Model," Applied Energy, vol. 300, article no. 117364, 2021.

[2] C. Hofer, G. Jäger, and M. Füllsack, "Large Scale Simulation of CO2 Emissions Caused by Urban Car Traffic: An Agent-Based Network Approach," Journal of Cleaner Production, vol. 183, pp. 1–10, 2018.

[3] IEA, "Global EV Outlook 2024," https://www.iea.org/reports/global-ev-outlook-2024, 2024.

[4] H. Shareef, M. M. Islam, and A. Mohamed, "A Review of the Stage-of-the-Art Charging Technologies, Placement Methodologies, and Impacts of Electric Vehicles," Renewable and Sustainable Energy Reviews, vol. 64, pp. 403–420, 2016.

[5] R. Gunasekaran, M. B., A. S., P. K. Pareek, S. Gupta, and A. Shukla, "Prediction of Electric Vehicle Charging Demand Using Enhanced Gated Recurrent Units with RKOA Based Graph Convolutional Network," Discover Applied Sciences, vol. 6, article no. 605, 2024.

[6] J. Varga, G. R. Raidl, and S. Limmer, "Computational Methods for Scheduling the Charging and Assignment of an On-Site Shared Electric Vehicle Fleet," IEEE Access, vol. 10, pp. 105786–105806, 2022.

[7] H. Wang, M. Shi, P. Xie, C. S. Lai, K. Li, and Y. Jia, "Electric Vehicle Charging Scheduling Strategy for Supporting Load Flattening under Uncertain Electric Vehicle Departures," Journal of Modern Power Systems and Clean Energy, vol. 11, no. 5, pp. 1634–1645, 2023.

[8] B. Sun, Z. Huang, X. Tan, and D. H. K. Tsang, "Optimal Scheduling for Electric Vehicle Charging with Discrete Charging Levels in Distribution Grid," IEEE Transactions on Smart Grid, vol. 9, no. 2, pp. 624–634, 2018.

[9] M. Aurangzeb, A. Xin, S. Iqbal, S. Habib, M. U. Jan, H. U. Rehman, et al., "Decentralized Based Advance Optimized Scheduling Scheme to Charge and Discharge the Electric Vehicles," Proceedings of 2022 5th International Conference on Energy Conservation and Efficiency, IEEE Press, pp. 1–7, 2022.

[10] Y. Wan, D. Gebbran, R. K. Subroto, and T. Dragičević, "Optimal Day-Ahead Scheduling of Fast EV Charging Station with Multi-Stage Battery Degradation Model," IEEE Transactions on Energy Conversion, vol. 39, no. 2, pp. 872–883, 2024.

[11] G. Tsaousoglou, J. S. Giraldo, P. Pinson, and N. G. Paterakis, "Fair and Scalable Electric Vehicle Charging under Electrical Grid Constraints," IEEE Transactions on Intelligent Transportation Systems, vol. 24, no. 12, pp. 15169–15177, 2023.

[12] A. Tetuko, Subiyanto, and M. A. Malik, "An Optimal Energy Control System for Campus Microgrid Using Crow Search Algorithm Considering Economic Dispatch," Advances in Technology Innovation, vol. 8, no. 4, pp. 303–312, 2023.

[13] H. Zhang, X. Xu, J. Huang, and G. I. Rashed, "Optimal Scheduling Strategy for Multi-Type Electric Vehicle Charging Based on Improved GA," Proceedings of 2024 6th International Conference on Energy Systems and Electrical Power, IEEE Press, pp. 1383–1386, 2024.

[14] S. Techanok and K. Chayakulkheeree, "Optimal EV Charging Control for Distribution System Loss Minimization," Proceedings of 2024 12th International Electrical Engineering Congress, IEEE Press, pp. 1–5, 2024.

[15] Y. Wu, J. Zhang, A. Ravey, D. Chrenko, and A. Miraoui, "Real-Time Energy Management of Photovoltaic-Assisted Electric Vehicle Charging Station by Markov Decision Process," Journal of Power Sources, vol. 476, article no. 228504, 2020.

[16] Z. Liu, F. Wen, and G. Ledwich, "Optimal Siting and Sizing of Distributed Generators in Distribution Systems Considering Uncertainties," IEEE Transactions on Power Delivery, vol. 26, no. 4, pp. 2541–2551, 2011.

[17] T. M. Aljohani, A. F. Ebrahim, and O. A. Mohammed, "Dynamic Real-Time Pricing Mechanism for Electric Vehicles Charging Considering Optimal Microgrids Energy Management System," IEEE Transactions on Industry Applications, vol. 57, no. 5, pp. 5372–5381, 2021.

[18] M. M. Gamil, H. Masrur, K. M. Muttaqi, Y. Huang, M. E. Lotfy, and T. Senjyu, "Multi-Objective Optimal Power Scheduling of a Residential Microgrid Considering V2G and Demand Response Techniques," Proceedings of 2022 IEEE Industry Applications Society Annual Meeting, IEEE press, pp. 1–5, 2022.

[19] H. Yang, S. Yang, Y. Xu, E. Cao, M. Lai, and Z. Dong, "Electric Vehicle Route Optimization Considering Time-of-Use Electricity Price by Learnable Partheno-Genetic Algorithm," IEEE Transactions on Smart Grid, vol. 6, no. 2, pp. 657–666, 2015.

[20] Z. Huang, K. Wang, C. Cao, and Z. Mu, "Multi-Objective Optimal Power Flow Considering Small-Signal Stability Based on MOPSO," Proceedings of 2022 4th International Conference on Electrical Engineering and Control Technologies, IEEE Press, pp. 419–423, 2022.

[21] Maigha and M. L. Crow, "Electric Vehicle Scheduling Considering Co-Optimized Customer and System Objectives," IEEE Transactions on Sustainable Energy, vol. 9, no. 1, pp. 410–419, 2018.

[22] J. Chen, X. Huang, S. Tian, Y. Cao, B. Huang, X. Luo, et al., "Electric Vehicle Charging Schedule Considering User's Charging Selection from Economics," IET Generation, Transmission & Distribution, vol. 13, no. 15, pp. 3388–3396, 2019.

[23] S. Ahmadi, H. P. Arabani, D. A. Haghighi, J. M. Guerrero, Y. Ashgevari, and A. Akbarimajd, "Optimal Use of Vehicle-to-Grid Technology to Modify the Load Profile of the Distribution System," Journal of Energy Storage, vol. 31, article no. 101627, 2020.

[24] P. Grahn, "Electric Vehicle Charging Impact on Load Profile," Ph.D. dissertation, School of Electrical Engineering, Royal Institute of Technology, Stockholm, Sweden, 2013.

[25] M. Ghasemi, S. Ghavidel, M. Gitizadeh, and E. Akbari, "An Improved Teaching–Learning-Based Optimization Algorithm Using Lévy Mutation Strategy for Non-Smooth Optimal Power Flow," International Journal of Electrical Power & Energy Systems, vol. 65, pp. 375–384, 2015.

[26] C. A. C. Coello and M. S. Lechuga, "MOPSO: A Proposal for Multiple Objective Particle Swarm Optimization," Proceedings of the 2002 Congress on Evolutionary Computation, IEEE Press, vol. 2, pp. 1051–1056, 2002.

[27] J. Kennedy, "The Particle Swarm: Social Adaptation of Knowledge," Proceedings of 1997 IEEE International Conference on Evolutionary Computation, IEEE Press, pp. 303–308, 1997.

[28] S. Lalwani, S. Singhal, R. Kumar, and N. Gupta, "A Comprehensive Survey: Multi-Objective Particle Swarm Optimization (MOPSO) Algorithm: Variants and Applications," Transactions on Combinatorics, vol. 2, no. 1, pp. 39–101, 2013.

[29] D. Fioriti, G. Lutzemberger, D. Poli, P. Duenas-Martinez, and A. Micangeli, "Coupling Economic Multi-Objective Optimization and Multiple Design Options: A Business-Oriented Approach to Size an Off-Grid Hybrid Microgrid," International Journal of Electrical Power & Energy Systems, vol. 127, article no. 106686, 2021.

[30] F. M. Andersen, H. K. Jacobsen, and P. A. Gunkel, "Hourly Charging Profiles for Electric Vehicles and Their Effect on the Aggregated Consumption Profile in Denmark," International Journal of Electrical Power & Energy Systems, vol. 130, article no. 106900, 2021.

BIOGRAPHY

Miss Suwimon Techanok was born on October 7, 2000, in Bangkok, Thailand. She received her Bachelor of Engineering degree in Electrical Engineering from Suranaree University of Technology in 2023. In 2024, she began her graduate studies in the Master of Engineering Program in Electrical Engineering at the Graduate School of Engineering, Suranaree University of Technology. Her academic interests include power systems, electric vehicle (EV) integration, and the application of metaheuristic optimization techniques in distribution system operations.

During her graduate studies, she served as a teaching assistant for courses related to power systems and load flow analysis. This role enhanced her skills in academic coordination, communication, and instructional support. She also presented her research at the International Electrical Engineering Congress (iEECON 2024), gaining valuable experience in professional academic communication.

She is passionate about contributing to the advancement of smart grid technology and sustainable energy infrastructure in Thailand, and she aspires to continue working in this field to support national distribution development goals.